Investigating the influence of nanoparticle-mediated FOXJ1 messenger RNA delivery on human bronchial epithelial cell differentiation

Rafaela Konstantinidi

Inflammation, Repair and Development Section

National Heart and Lung Institute

Faculty of Medicine

Imperial College London

A thesis submitted to Imperial College London for the degree of Doctor of Philosophy

2024

Statement of Originality

I hereby declare that the work described in this thesis was performed by myself, with the following exceptions. Poly (β-amino ester) synthesis and nuclear magnetic resonance characterisation was performed by Leigh-Anne Gavin, National Heart and Lung Institute, Imperial College London. Paraffin embedding, sectioning and histological staining (haematoxylin and eosin and periodic acid-Schiff) of air-liquid interface culture inserts was performed by Lorraine Lawrence, Imperial College London, Histology Core Facility. Transmission electron microscopy was performed by Dr Andrew Rogers at the Royal Brompton Hospital, London. I further declare that the intellectual content of this thesis is result of my own work and all sources have been appropriately referenced.

Copyright Declaration

The copyright of this thesis rests with the author. Unless otherwise indicated, its contents are licensed under a Creative Commons Attribution-Non Commercial-No Derivatives 4.0 International Licence (CC BY-NC-ND). Under this licence, you may copy and redistribute the material in any medium or format on the condition that; you credit the author, do not use it for commercial purposes and do not distribute modified versions of the work. When reusing or sharing this work, ensure you make the licence terms clear to others by naming the licence and linking to the licence text. Please seek permission from the copyright holder for uses of this work that are not included in this licence or permitted under UK Copyright Law.

Acknowledgements

First and foremost, I extend my heartfelt thanks to my supervisors, Dr Asha Patel, Dr Laura Yates, Prof Sejal Saglani, and Prof Clare Lloyd, for their invaluable guidance, mentorship, and support during my doctoral journey. Their expertise, insightful feedback, and constant encouragement contributed to my development as a scientist. I appreciate their patience, commitment, and the time they invested to nurture my research skills and academic growth.

I would also like to express my sincere gratitude to the NHLI Foundation for awarding me a fully funded PhD scholarship. This scholarship was not only essential for my financial support but also allowed me to become part of the dynamic academic community within NHLI. My thanks extend to my Early-Stage Assessment and Late-Stage Review examiners, Prof Eric Alton and Prof Terry Tetley. Their constructive feedback has greatly enhanced the quality of my work. Special acknowledgement goes to Lorraine Lawrence for her exceptional histology support, Dr Andrew Rogers for his electron microscopy expertise, and Gill Martin for her efficient management of our orders.

I am thankful to both past and present members of the Patel group for their invaluable support, company, and help in the lab. Special thanks to Skye Quinn for her friendship and enlightening conversations, and to Leigh-Anne Gavin for her significant contributions in polymer synthesis.

Thanks to the IRD community for fostering a friendly and conducive research and learning environment. My fellow PhD colleagues have been a source of inspiration and support throughout this journey, and I am grateful for their presence.

My heartfelt gratitude goes to my family - my parents, brother, grandparents, and friends - for their unwavering belief in me and their continuous support throughout this academic endeavour. Your love and encouragement have been my driving force.

Last but not least, my deepest thanks go to my partner, Panagiotis. You have been my strength when I had none. Your understanding, belief, and support have been my guiding lights. Sharing the tears, the laughter, and every twist and turn of this rollercoaster journey with you has been invaluable. I could not have done it without you.

Abstract

Synthetic messenger RNA (mRNA) presents a promising tool for transient expression of any protein of interest, when efficiently delivered to target cells. Culturing primary human bronchial epithelial cells (HBECs) at air-liquid interface (ALI) results in a pseudostratified differentiated epithelium that closely resembles the cellular architecture found in the human airway. This model provides a powerful tool for studying HBEC biology and manipulating gene expression to modulate differentiation. However, the impact of synthetic mRNA delivery on epithelial differentiation and barrier integrity remains unclear. This thesis first aimed to establish non-viral mRNA transfection of primary HBECs and investigate the impact of reporter mRNA delivery on HBEC differentiation and integrity at ALI. In Chapter 3, formulations of poly (β-amino ester) (PBAE), a cationic polymer known for its gene delivery capabilities, were optimised for efficient reporter mRNA delivery to submerged primary HBECs. Transfection of primary HBECs with reporter mRNA prior to air exposure did not hinder their differentiation or barrier integrity at ALI. Building on these findings, Chapter 4 explored the impact of delivering a physiologically relevant mRNA encoding the transcription factor (TF), Forkhead box J1 (FOXJ1), on HBEC integrity and differentiation at ALI. PBAE-mediated FOXJ1 mRNA delivery successfully induced the expression of FOXJ1 downstream genes involved in ciliogenesis. FOXJ1 mRNA transfected cells maintained at ALI for 28 days exhibited differentiation, epithelial integrity, and cilia ultrastructure comparable to non-transfected controls. Finally, Chapter 5 investigated PBAE modifications to enhance mRNA transfection efficiency in HBEC ALI cultures. A novel peptide-modified PBAE, DD90-Gly-Sar, improved mRNA transfection of day 7 and 14 HBEC ALI cultures. Overall, this thesis demonstrates the potential of PBAE-mediated mRNA delivery to primary HBECs and the utility of mRNA-encoded TF as a platform technology for modulating HBEC differentiation in ALI, opening new avenues for investigating gene function implicated in airway diseases.

Table of Contents

Statement of Originality **2**
Copyright Declaration **3**
Acknowledgements **4**
Abstract **5**
Table of Contents **6**
List of Figures **13**
List of Tables **17**
List of Abbreviations **18**
1 Introduction **22**
1.1 Human airway epithelium **23**
1.1.1 Function 23
1.1.2 Cellular composition and functional diversity 23
1.1.2.1 Basal cells *24*
1.1.2.2 Club cells *25*
1.1.2.3 Ciliated cells *25*
1.1.2.4 Goblet cells *26*
1.1.2.5 Rare epithelial cell types *26*
1.1.3 Dysfunction of airway epithelium in chronic airway diseases 27
1.2 Ciliogenesis and FOXJ1 ..... **29**
1.2.1 Cilium structure and function 29
1.2.2 FOXJ1 31
1.2.3 Ciliary dysfunction 33
1.2.3.1 Inherited disorders *33*
1.2.3.2 Environmental factors *34*
1.2.3.3 Chronic lung diseases associated with ciliary dysfunction *34*
1.2.4 Manipulating ciliogenesis and FOXJ1 expression 36
1.3 mRNA **39**
1.3.1 General overview 39
1.3.2 *In vitro* transcribed (IVT) mRNA 41
1.3.3 mRNA encoded TFs as a platform for understanding and directing cell fate 43
1.3.3.1 mRNA encoded TFs: versatile tools for cellular reprogramming *44*
1.3.3.2 mRNA encoded TFs: versatile tools for transdifferentiation *45*
1.3.3.3 Emerging potential of mRNA encoded TFs in disease modulation *46*

1.4 Recapitulating the airway epithelium *in vitro*.....47
1.4.1 Traditional primary cell culture 48
1.4.2 Air-liquid interface (ALI) culture.....48
1.4.3 Organoids.....49
1.4.4 Lung-on-a-chip 49
1.5 Non-viral mRNA delivery systems 50
1.5.1 Lipid-based vectors 51
1.5.2 Polymers 52
1.5.3 Exosomes 55
1.5.4 Hybrid delivery materials.....55
1.6 Hypothesis and aims 57
2 Materials & Methods 58
2.1 Primary HBECs 59
2.2 Cell lines 59
2.3 Cell culture 59
2.3.1 Cell maintenance, passaging and cryopreservation 59
2.3.2 Air-liquid Interface culture of primary HBECs.....60
2.4 Histology processing of ALI transwell inserts.....62
2.4.1 Agarose-embedding of ALI inserts.....62
2.4.2 Paraffin embedding, sectioning and histological stains.....62
2.4.3 Imaging 62
2.5 Transmission Electron Microscopy (TEM) 62
2.6 Functional assessment of primary HBECs in ALI culture 63
2.6.1 Transepithelial electrical resistance (TEER) 63
2.6.2 Permeability assay 64
2.7 PBAE synthesis and characterisation 64
2.7.1 Linear PBAE synthesis.....64
2.7.2 Branched PBAE synthesis 65
2.7.3 Peptide-modified PBAE synthesis.....65
2.7.3.1 DD90-Ala-Lys & DD90-Ala-Ala.....65
2.7.3.2 DD90-Ala-Gly & DD90-Gly-Sar 65
2.7.4 Proton Nuclear Magnetic Resonance (^{1}H NMR).....66
2.8 Non-viral mRNA transfection of cell lines, submerged and ALI cultured primary HBECs.....66

2.9 Non-viral vector/mRNA particles characterisation 70
2.9.1 Dynamic Light Scattering (DLS) 70
2.9.2 mRNA encapsulation efficiency assay 70
2.9.3 Gel electrophoresis 71
2.10 Biological assays 71
2.10.1 Luminescence assay & luciferase protein quantification 71
2.10.2 Cytotoxicity assay 72
2.10.3 Cell viability assay 72
2.10.4 Protein quantification 73
2.11 Gene expression analysis 73
2.11.1 Cell harvesting & RNA isolation 73
2.11.2 cDNA synthesis 73
2.12 Characterisation of peptide transporter 2 in primary HBECs 76
2.12.1 Uptake of Ala-Lys-AMCA dipeptide 76
2.12.2 Exposure to Cefadroxil 76
2.13 Immunofluorescence 76
2.13.1 Fixation 76
2.13.2 Immunofluorescence staining 76
2.13.2.1 Submerged cells on 8-well chamber slides 76
2.13.2.2 Primary HBECs cultured at ALI (wholemount) 77
2.13.3 Image acquisition and quantification 77
2.14 Statistical Analysis 79
3 Results I - Evaluating reporter mRNA delivery to primary HBECs using non-viral vectors and its impact on epithelial integrity and differentiation 80
3.1 Introduction 81
3.1.1 PBAEs for mRNA delivery to the lung 81
3.1.2 Optimising formulations of non-viral vectors to improve *in vitro* performance 81
3.1.3 ALI culture model 83
3.1.4 Gene delivery to ALI cultures 83
3.1.5 Hypothesis and aims 84
3.2. Results 85
3.2.1 Synthesis of branched DD90-118 based PBAE 85
3.2.2 Branched PBAE mediates effective delivery of FLuc mRNA to 16HBE and A549 cell lines 86
3.2.3 Determining the optimal DMSO concentration of dissolved PBAEs for transfection of 16HBE cells 88

3.2.4 Reporter mRNA transfection does not affect tight junction integrity in 16HBE confluent monolayers 90
3.2.5 Branched PBAE formulation affects mRNA condensation and encapsulation efficiency 92
3.2.6 Branched PBAE polymer mediates effective delivery of FLuc mRNA to primary HBECs 94
3.2.7 Branched PBAE formulation affects PBAE/mRNA polyplexes size and zeta potential 96
3.2.8 Assessing the consistency of optimised branched PBAE formulation across two different PBAE batches 99
3.2.9 Primary HBECs retain their basal cell phenotype 24 hours after transfection with reporter mRNA 100
3.2.10 Differentiation of primary HBECs at ALI 101
3.2.11 Submerged primary HBECs demonstrate higher mRNA transfection efficiency than HBECs cultured at ALI for 7 days 104
3.2.12 Integrity of HBECs cultured at ALI remains intact after reporter mRNA transfection 108
3.2.13 Epithelial differentiation at ALI is successful following reporter mRNA transfection 111
3.3 Discussion 114
3.4 Conclusion 120
4 Results II - Investigating the influence of mRNA encoded FOXJ1 delivery on differentiation of human bronchial epithelial cells 121
4.1 Introduction 122
4.1.1 Motile cilia in airway epithelium 122
4.1.2 Multiciliated cell differentiation 123
4.1.3 FOXJ1 is a master regulator of ciliogenesis 124
4.1.4 Manipulation of FOXJ1 expression in primary HBECs *in vitro* 125
4.1.5 Hypothesis and aims 126
4.2 Results 127
4.2.1 Selection of supplier for ordering synthetic FOXJ1 mRNA 127
4.2.2 Functionality of synthetic FOXJ1 mRNA on 16HBE cells 128
4.2.3 Submerged primary HBECs can be transfected with mRNA-encoded FOXJ1 132
4.2.4 FOXJ1 mRNA transfection induces ciliogenesis transcriptional program in submerged primary HBECs 140
4.2.5 Characterisation of FOXJ1 mRNA/non-viral vector formulations 142

4.2.6 Primary HBECs transfected with FOXJ1 encoded mRNA formed a confluent monolayer and were maintained at ALI culture for 28 days 144
4.2.7 FOXJ1 supplementation mediates induction of FOXJ1-downstream genes involved in ciliogenesis before air-exposure 146
4.2.8 Impact of FOXJ1 supplementation on epithelial morphology 148
4.2.9 Impact of FOXJ1 supplementation on epithelial integrity 153
4.2.10 Impact of FOXJ1 supplementation on epithelial differentiation 155
4.2.11 Impact of FOXJ1 supplementation on transcriptional network of ciliated cell differentiation and cilia ultrastructure 160
4.3 Discussion 164
4.4 Conclusion 173
5 Results III – Investigating PBAE design for improved mRNA delivery to bronchial epithelium 174
5.1 Introduction 175
5.1.1 Barriers in gene delivery to ALI-cultured HBECs 175
5.1.2 Modifying PBAEs 175
5.1.2.1 Molecular weight/chain length modification 175
5.1.2.2 End group modification 176
5.1.3 Harnessing peptide transporter for targeted polyplex internalisation and mRNA transfection 177
5.1.4 Hypothesis and aims 178
Hypothesis **..... 178**
Aims **..... 178**
5.2 Results 179
5.2.1 Synthesis of linear PBAEs 179
5.2.2 Evaluation of transfection efficiency and cytotoxicity of linear PBAEs in submerged primary HBECs 180
5.2.3 Size characterisation of linear PBAE/mRNA polyplexes 182
5.2.4 Expression of PEPT2 in submerged and ALI-cultured primary HBECs 184
5.2.5 Functional activity of peptide transporter (PEPT2) in submerged and ALI-cultured primary HBECs 185
5.2.6 Synthesis of peptide-modified PBAEs 186
5.2.7 Screening of peptide-modified polymers on 16HBE cells 186
5.2.8 Characterisation of DD90-Gly-Sar and DD90-Ala-Lys polymers 188
5.2.8.1 mRNA binding and encapsulation efficiency 188
5.2.8.2 Size and zeta potential measurements 190

5.2.9 Transfection efficiency and cytotoxicity of peptide-modified polymers on submerged primary HBECs 191
5.2.10 Chemically conjugated dipeptides on PBAEs facilitate functional delivery of reporter mRNA to submerged primary HBECs 193
5.2.11 Investigation of peptide-modified PBAE-mediated reporter mRNA uptake and translation in submerged primary HBECs 194
5.2.12 Investigating the effect of PEPT2 transporter blockage on peptide-modified PBAEs uptake 196
5.2.12.1 Effect of cefadroxil pre-incubation on Ala-Lys-AMCA uptake 196
5.2.12.2 Impact of cefadroxil pre-incubation on peptide-modified PBAE transfection efficiency in primary HBECs 197
5.2.12.3 Transfection efficiency of peptide-modified PBAEs in cefadroxil-containing media 199
5.2.12.4 Impact of pre-transfection with peptide-modified PBAEs on Ala-Lys-AMCA dipeptide uptake by submerged primary HBECs 201
5.2.13 Analysis of transfection efficiency and cytotoxicity across two different DD90-Gly-Sar polymer batches 202
5.2.14 Transfection efficiency of DD90-Gly-Sar in primary HBEC ALI cultures 203
5.3 Discussion 206
5.4 Conclusion 213
6 Final discussion 214
6.1 Synopsis of thesis outcomes 215
6.2 Optimised PBAE formulation enables efficient mRNA transfection of submerged primary HBECs 216
6.3 HBEC integrity and differentiation is unaffected following reporter mRNA transfection 217
6.4 mRNA-mediated FOXJ1 protein expression in HBECs induces the expression of downstream genes involved in ciliogenesis 218
6.5 FOXJ1 mRNA transfection maintains integrity, differentiation, and cilia ultrastructure of HBEC ALI cultures 219
6.6 Novel peptide-modified PBAE, DD90-Gly-Sar, enhances reporter mRNA transfection of HBEC ALI cultures 221
6.7 Future directions 223
6.8 Concluding remarks 224

7 References 225

8 Appendix I: FOXJ1 sequence 272

9 Appendix II: Conference presentations arising from this thesis 273

10 Appendix III: Validation of immunofluorescence staining with secondary antibody only controls 274

List of Figures

Figure 1.1 Cellular composition of the airway epithelium.....24
Figure 1.2 Simplified structural overview of motile cilia. 31
Figure 1.3 Predicted FOXJ1 transcriptional network. 33
Figure 1.4 Exogenous mRNA as a tool for transient protein expression. 40
Figure 1.5 Structural elements of IVT mRNA.....43
Figure 3.1 Synthesis schematic of branched poly (β-amino ester) (PBAE). 85
Figure 3.2 Transfection efficiency of branched poly (β-amino ester) (PBAE) on 16 human bronchial epithelial (16HBE) and A549 lung alveolar epithelial cell lines. 87
Figure 3.3 Optimal dimethyl sulfoxide (DMSO) concentration of dissolved branched poly (β-amino ester) (PBAE). 89
Figure 3.4 Impact of reporter mRNA transfection on permeability and tight junction integrity of 16 human bronchial epithelial (16HBE) confluent monolayers. 91
Figure 3.5 Agarose gel electrophoresis retardation assay.....93
Figure 3.6 mRNA encapsulation efficiency of branched poly (β-amino ester) PBAE formulations. 94
Figure 3.7 Transfection efficiency and cytotoxicity of branched poly (β-amino ester) (PBAE) formulations on submerged primary human bronchial epithelial cells (HBECs). 95
Figure 3.8 Size characterisation of branched poly (β-amino ester) (PBAE) formulations complexed with mRNA.....98
Figure 3.9 Zeta potential characterisation of branched poly (β-amino ester) (PBAE) formulations complexed with mRNA. 98
Figure 3.10 Batch-to batch consistency of the optimal branched PBAE formulation.....100
Figure 3.11 Expression of keratin 5 (KRT5) in submerged primary human bronchial epithelial cells (HBECs) following reporter mRNA transfection. 101
Figure 3.12 Culture of primary human bronchial epithelial cells (HBECs) at air-liquid interface (ALI). 103
Figure 3.13 Ultrastructural analysis of primary human bronchial epithelial cell (HBEC) air liquid interface (ALI) cultures through transmission electron microscopy (TEM). 103
Figure 3.14 Cy5-tagged GFP mRNA transfection of submerged primary human bronchial epithelial cells (HBECs). 105
Figure 3.15 Cy5-tagged GFP mRNA transfection of primary human bronchial epithelial cells (HBECs) cultured at air liquid interface (ALI) for 7 days. 108
Figure 3.16 Assessment of epithelial barrier integrity and tight junction morphology in human bronchial epithelial cells (HBECs) cultured at air liquid interface (ALI) following reporter mRNA transfection. 111

Figure 3.17 Assessment of epithelial differentiation in human bronchial epithelial cells (HBECs) cultured at air liquid interface (ALI) following reporter mRNA transfection. 113
Figure 4.1 Performance of reporter FLuc mRNA from four different commercial suppliers following non-viral transfection in 16HBE cells. 128
Figure 4.2 Transfection efficiency of synthetic FOXJ1 mRNA in 16HBE cells.....131
Figure 4.3 Expression of FOXJ1 and two downstream genes following FOXJ1 mRNA transfection in 16HBE cells. 131
Figure 4.4 Expression of FOXJ1 following FOXJ1 mRNA transfection in submerged primary HBECs. 134
Figure 4.5 Expression of FOXJ1 following FOXJ1 mRNA and reporter mRNA transfection in submerged primary HBECs. 135
Figure 4.6 Transfection efficiency of synthetic FOXJ1 mRNA in submerged primary HBECs. 137
Figure 4.7 FOXJ1 expression following control mRNA transfections in submerged primary HBECs. 138
Figure 4.8 Cytotoxicity of FOXJ1 mRNA transfected submerged primary HBECs. 139
Figure 4.9 FOXJ1-mediated expression of ciliogenesis genes in submerged primary HBECs following non-viral FOXJ1 mRNA transfection. 142
Figure 4.10 Characterisation of FOXJ1 mRNA/non-viral vector formulations.....144
Figure 4.11 Primary HBECs transfected with FOXJ1 mRNA formed a confluent monolayer and cultured at ALI. 146
Figure 4.12 Induction of FOXJ1 downstream genes following FOXJ1 mRNA transfection in primary HBECs before air-exposure. 147
Figure 4.13 Overall morphology and thickness of epithelial layers remain unaffected following FOXJ1 mRNA transfection in primary HBECs cultured at ALI. 150
Figure 4.14 Transmission electron microscopic (TEM) assessment of ultrastructural changes in non-transfected and FOXJ1 mRNA transfected human bronchial epithelial cell air-liquid interface cultures over time. 151
Figure 4.15 Transmission electron microscopic (TEM) assessment of ultrastructural changes in non-transfected and FOXJ1 mRNA transfected human bronchial epithelial cell air-liquid interface cultures over time. 152
Figure 4.16 Transmission electron microscopic (TEM) assessment of ultrastructural changes in FOXJ1 mRNA transfected human bronchial epithelial cell air-liquid interface culture at day 7 post-ALI.....153
Figure 4.17 Epithelial integrity is unaffected following FOXJ1 mRNA transfection in primary HBECs cultured at ALI. 155

Figure 4.18 Expression of epithelial differentiation markers is unaffected following FOXJ1 mRNA transfection in primary HBECs cultured at ALI. 158
Figure 4.19 Epithelial differentiation is not influenced following FOXJ1 mRNA transfection in primary HBECs cultured at ALI. 160
Figure 4.20 Impact of FOXJ1 supplementation on ciliogenesis transcriptional network following FOXJ1 mRNA transfection in primary HBECs cultured at ALI. 163
Figure 4.21 Transmission electron microscopic (TEM) assessment of cilia ultrastructure in non-transfected and FOXJ1 mRNA transfected human bronchial epithelial cell air-liquid interface cultures. 163
Figure 5.1 Synthesis schematic of linear poly (β-amino ester) (PBAE). 179
Figure 5.2 Transfection efficiency and cytotoxicity of linear poly (β-amino esters) (PBAEs), DD90-118 1.2 and DD90-118 1.05, in primary human bronchial epithelial cells (HBECs). .181
Figure 5.3 Size of linear poly (β-amino esters) (PBAE)/mRNA polyplexes formed by complexing linear PBAEs DD90-118 1.2 and DD90-118 1.5 with Firefly Luciferase (FLuc) mRNA. 183
Figure 5.4 Expression of peptide transporter (PEPT2) in primary human bronchial epithelial cells (HBECs). 185
Figure 5.5 Concentration-dependent uptake of Ala-Lys-AMCA dipeptide by submerged and air liquid interface (ALI)-cultured primary human bronchial epithelial cells (HBECs). 185
Figure 5.6 Modification of linear poly (β-amino esters) (PBAEs) with dipeptides. 186
Figure 5.7 Transfection efficiency and cytotoxicity of peptide-modified peptide-modified poly (β-amino esters) (PBAEs) in 16 human bronchial epithelial (16HBE) cells. 188
Figure 5.8 mRNA binding and encapsulation efficiency of peptide-modified poly (β-amino esters) (PBAEs). 189
Figure 5.9 Size and zeta potential of peptide-modified PBAE/mRNA polyplexes. 191
Figure 5.10 Transfection efficiency and cytotoxicity of peptide-modified poly (β-amino esters) (PBAEs) in submerged primary human bronchial epithelial cells (HBECs). 192
Figure 5.11 Chemically conjugated dipeptides on poly (β-amino esters) (PBAEs) facilitate delivery of mRNA to primary human bronchial epithelial cells (HBECs). 193
Figure 5.12 Reporter mRNA uptake and translation in submerged primary human bronchial epithelial cells (HBECs) using peptide-modified poly (β-amino esters) (PBAEs). 196
Figure 5.13 Inhibition of Ala-Lys-AMCA uptake by Cefadroxil in submerged primary human bronchial epithelial cells (HBECs). 197
Figure 5.14 Assessing the impact of Cefadroxil pre-incubation on transfection efficiency and cytotoxicity of peptide-modified poly (β-amino esters) (PBAEs) in submerged primary human bronchial epithelial cells (HBECs). 198

Figure 5.15 Impact of Cefadroxil on transfection efficiency and cytotoxicity in submerged primary bronchial epithelial cells (HBECs) using peptide-modified poly (β-amino esters) (PBAEs). 200
Figure 5.16 Competitive binding assay of PEPT2 transporter with peptide-modified poly (β-amino esters) (PBAEs). 202
Figure 5.17 Comparison of transfection efficiency and cytotoxicity between two batches of DD90-Gly-Sar polymers in primary human bronchial epithelial cells (HBECs).....203
Figure 5.18 Transfection of primary human bronchial epithelial cells (HBECs) grown at air liquid interface (ALI) with peptide-modified poly (β-amino ester) (PBAE) DD-90-Gly-Sar. ..205

List of Tables

Table 2.1 Donor information for primary human bronchial epithelial cells. 59
Table 2.2 Cell culture media for cell lines and primary HBECs (submerged & ALI). 61
Table 2.3 Monomers used for PBAE synthesis. 66
Table 2.4 Commercial mRNAs used in transfection experiments.....67
Table 2.5 PBAE formulations.....68
Table 2.6 cDNA synthesis reactions. 74
Table 2.7 Thermal cycler conditions for cDNA synthesis.....74
Table 2.8 Reaction set-up for qPCR. 75
Table 2.9 Human TaqMan™ gene expression assays. 75
Table 2.10 Thermal cycler conditions for qPCR. 75
Table 2.11 Antibodies used for immunofluorescence staining experiments. 78
Table 3.1 Summary of statistical analysis of mRNA uptake and mRNA translation in submerged primary HBECs following reporter mRNA transfection. 106
Table 4.1 Summary of statistical analysis of FOXJ1 transfection efficiency in submerged primary HBECs. 137
Table 4.2 Summary of statistical analysis of cytotoxicity in submerged primary HBECs following FOXJ1 mRNA transfection.....139

List of Abbreviations

90	4-(2-Aminoethyl) morpholine (backbone amine)
118	1,5 diamino 2 methylpentane (end cap amine)
16HBE	16 human bronchial epithelial
1H NMR	Proton Nuclear Magnetic Resonance
3D	Three-dimensional
5moU	5-methoxyuridine
ACTB	Actin beta
Ala-Ala	L-alanyl-L-alanine
Ala-Gln	Alanyl-glutamine
Ala-Lys	Alanyl-lysine hydrochloride
ALI	Air-liquid interface
Alk5	Activin receptor-like kinase 5
ApoE	Apolipoprotein E
ARCA	Anti-reverse cap analogue
CDH1	Cadherin 1
cDNA	complementary DNA
CETN2	Centrin 2
CF	Cystic fibrosis
CFTR	Cystic fibrosis transmembrane conductance regulator
COPD	Chronic obstructive pulmonary disease
COVID-19	Coronavirus disease 2019
CRISPR/Cas9	Clustered regularly interspaced short palindromic repeats-CRISPR-associated protein 9
CSE	Cigarette smoke extract
CXCL-8	C-X-C motif chemokine ligand
Cy5-GFP	Cyanine 5-tagged Green Fluorescent Protein
d6-DMSO	Deuterated dimethyl sulfoxide
DD	Bisphenol A glycerolate (diacrylate)
DEUP1	Deuterosome assembly protein 1
DLS	Dynamic Light Scattering
DMSO	Dimethyl sulfoxide
DNA	Deoxyribonucleic acid
DNAH11	Dynein axonemal heavy chain 11
DNALI1	Dynein axonemal light intermediate chain 1

DOPE	1,2-dioleoyl-sn-glycero-3-phosphoethanolamine
DOTMA	1,2-di-O-octadecenyl-3-trimethylammonium-propane
DSPC	Distearoyl-sn-glycero-3-phosphocholine
DYNC2H1	Dynein cytoplasmic 2 heavy chain 1
EFHC1	EF-hand domain C-terminal containing 1
EGFR	Epidermal growth factor receptor
ELF	Epithelial lining fluid
ELISA	Enzyme-linked immunosorbent assay
EMT	Epithelial-to-mesenchymal transition
FDA	Food and Drug Administration
FITC	Fluorescein isothiocyanate
FLuc	Firefly Luciferase
FOXA3	Forkhead box A3
FOXJ1	Forkhead box protein J1
GFP	Green Fluorescent Protein
GLuc	Gaussia Luciferase
Gly-Sar	Glycyl-sarcosine
GM-CSF	Granulocyte-macrophage colony-stimulating factor
GMNC	Geminin coiled-coil domain containing protein 1
H&E	Haematoxylin and eosin
HBECs	Human bronchial epithelial cells
HIV	Immunodeficiency virus
IFT	Intraflagellar transport
IL-25/33/1β/6/8/13	Interleukin-25/33/1β/6/8/13
IRD	Inflammation, Repair and Development
IVT	*In vitro* transcribed
KRT5	Keratin 5
L2000	Lipofectamine 2000
LDH	Lactate dehydrogenase
LNPs	Lipid nanoparticles
m1A	N1-methylguanosine
m5C	5-methylcytidine
m6A	N6-methyladenosine
MCIDAS	Multicilin
MDA5	Melanoma differentiation-associated gene 5
MHRA	Medicines and Healthcare products Regulatory Agency

mRNA	Messenger ribonucleic acid
MUC5AC	Mucin 5AC
MUC5B	Mucin 5B
MYB	Myeloblastosis
MYOD	Myogenic determination protein 1
MYOG	Myogenin
NaOAc	Sodium acetate buffer
NEBs	Neuroepithelial bodies
NGF	Nerve growth factor
OCLN	Occludin
OM-PBAE	Oligopeptide modified poly (β-amino ester)
ORF	Open reading frame
PAMPs	Pathogen-associated molecular patterns
PAS	Periodic acid-Schiff
PBAE	Poly (β-amino ester)
PBS	Phosphate buffered saline
PCD	Primary ciliary dyskinesia
PDMS	Polydimethylsiloxane
PEG	Polyethylene glycol
PEI	Polyethyleneimine
PEPT2	Peptide transporter 2
PFA	Paraformaldehyde
PRRs	Pattern recognition receptors
qPCR	Quantitative polymerase chain reaction
RFX	Regulatory factor X
RIG-I	Retinoic acid-inducible gene I
RSPH9	Radial spoke head component 9
RVG	Rabies virus glycoprotein
SARS-CoV-2	Severe acute respiratory syndrome coronavirus 2
SCGB1A1	Secretoglobin family 1A member 1
siRNA	Small interfering RNA
SLC15	Solute carrier 15
SLC15A2	Solute carrier family 15 member 2
SP-B	Surfactant protein-B
SPAG6	Sperm associated antigen 6
SPDEF	Sam-pointed domain-Ets-like factor

TALENs	Transcription activator-like effector nucleases
TAS2R	Taste receptor type 2
TEER	Transepithelial electrical resistance
TEKT1	Tektin 1
TEM	Transmission Electron Microscopy
TF	Transcription factor
TGF-β	Transforming growth factor-β
Th2	T helper type 2
TJP1	Tight junction protein 1
TLRs	Toll-like receptors
TNF-α	Tumor necrosis factor
TP63	Tumour protein 63
TRPM5	Transient receptor potential cation channel subfamily M member 5
TSLP	Thymic stromal lymphopoietin
TUBA1A	Tubulin alpha 1a
UTR	Untranslated region
ZFNs	Zinc finger nucleases
ZO-1	Zonula occludens-1
Ψ	Pseudouridine

1 Introduction

1.1 Human airway epithelium

1.1.1 Function

The human airway epithelium is a complex and dynamic tissue that serves as the first line of defence in the respiratory system. It protects the lungs from inhaled pathogens, environmental contaminants, and foreign particles by forming a physical barrier maintained by a network of specialised cell junctions[1–4]. These junctions, including tight junctions, adherens junctions, gap junctions and desmosomes, selectively regulate the paracellular transport of ions and molecules between cells, ensuring the integrity of the barrier[5,6]. Beyond its physical barrier function, the airway epithelium is equipped with a diverse array of defence mechanisms[7], including the expression of pattern recognition receptors (PRRs), such as Toll-like receptors (TLRs)[8,9], and intracellular viral sensors [retinoic acid-inducible gene I (RIG-I) receptors, and melanoma differentiation-associated gene 5 (MDA5)][10–12]. These receptors play a pivotal role in detecting pathogen-associated molecular patterns (PAMPs), which are molecules found on the surface of pathogens. Recognition of PAMPs subsequently lead to epithelial cells initiating an immune response. When activated, these receptors induce the production and release of various pro-inflammatory cytokines and chemokines that orchestrate the recruitment and activation of immune cells into the airways to combat pathogens[13–16]. Additionally, the airway epithelium produces antiviral substances, including interferons, nitric oxide, β-defensins, and lactoferrin, which are important in immune responses[17–20]. The combined actions of these innate immune receptors, pro-inflammatory cytokines, and antiviral substances underscore the airway epithelium's critical role in protecting the respiratory tract against pathogens and other foreign particles.

1.1.2 Cellular composition and functional diversity

The respiratory tract is a complex system organised into distinct regions with specialised function. The upper respiratory tract includes the nasal cavity, pharynx, and larynx, while the lower respiratory tract consists of the trachea, bronchi, bronchioles, and the respiratory zone (alveoli). The conducting airways, which extend from the trachea to the bronchioles, are lined with a pseudostratified columnar epithelium. This epithelium, unlike its stratified counterparts with distinct layers, creates the illusion of multiple layers due to the presence of tall, columnar cells and shorter, basal cells[21]. Although all cells are anchored to the basement membrane, only the taller cells reach the apical surface, generating the appearance of a multi-layered structure. This specialised arrangement allows for a diverse cellular population, including basal cells, club cells, ciliated cells, and goblet cells, each with crucial roles in maintaining a healthy respiratory system[22–24] (Figure 1.1). Importantly, the cellular composition of this

epithelium differs between humans and mice, highlighting the need to consider species-specific variations when studying lung function.

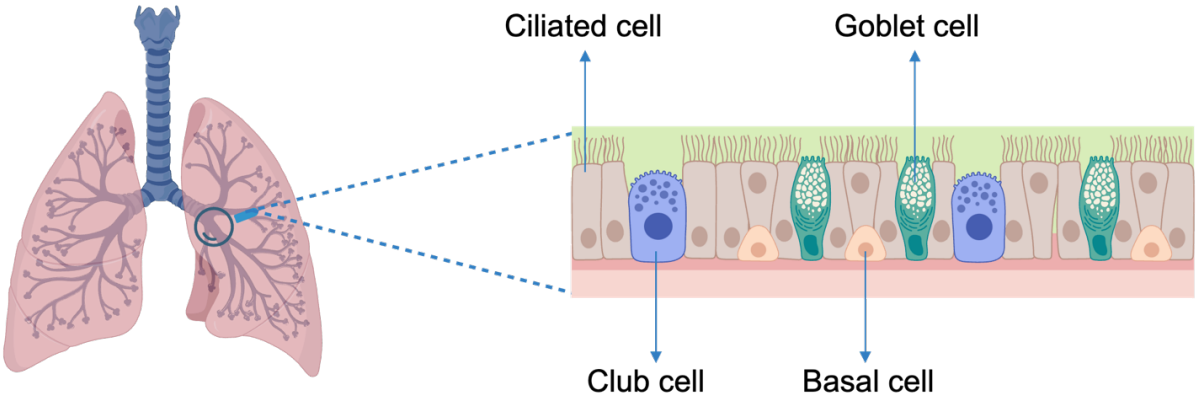


Figure 1.1 Cellular composition of the airway epithelium.
Snapshot of proximal airway epithelium's cellular structure, highlighting the arrangement of basal cells, ciliated cells, goblet cells and club cells. Figure created with Biorender.com.

1.1.2.1 Basal cells

Basal progenitor cells, recognised as cuboidal cells, are tightly anchored to the basement membrane[25]. These cells reside throughout the human respiratory tract, from the trachea to the small conducting airways, while in mice, they are primarily concentrated in the proximal airways (trachea and main bronchi)[26,27]. Characterised by the expression of proteins keratin 5 and 14 (KRT5, KRT14), and the transcription factor tumour protein 63 (TP63)[28], they make up 6-30% of the airway epithelium[29]. They play a critical role in maintaining respiratory homeostasis, especially by repairing damage to the epithelial lining[28]. They act as the primary stem cell population, capable of both self-renewal and differentiation into various epithelial cell types, including ciliated, secretory and goblet cells[30,31]. This ability to self-renew and differentiate allows basal cells to perform two vital functions: maintaining the epithelial barrier's homeostasis and facilitating its repair after injury[32–35]. Recent research has unveiled the heterogeneity of basal progenitor cells, revealing at least two distinct transcriptional subgroups within human airways[25,36]. One group appears to function as stem cell progenitors, crucial for renewal and regeneration, while the other may be more inclined towards luminal differentiation, contributing to the functional diversity of the respiratory epithelium[37].

1.1.2.2 Club cells

Club cells, formerly known as Clara cells, are epithelial cells with a dome-shaped morphology. In humans, they are predominantly found in the bronchioles, constituting around 10% of the airway epithelium[38,39]. In contrast, mouse lungs have a broader distribution of club cells, lining not only the bronchioles but also the trachea and bronchi[26,27]. Their differentiation is regulated by the transforming growth factor-β (TGF-β) receptor, activin receptor-like kinase 5 (Alk5)[40]. Similar to basal cells, club cells exhibit regenerative capabilities, playing a critical role in epithelial repair[41]. They can differentiate into both ciliated and goblet cells, helping to restore the integrity of the airway epithelium after injury. Moreover, they demonstrate the unique ability to dedifferentiate back into basal cells in response to basal cell loss or injury[42,43]. This plasticity highlights the dynamic nature of the respiratory epithelium and its capacity for regeneration and repair. Beyond their role in cellular regeneration, club cells also have a secretory function. They secrete surfactant proteins, along with a range of specific proteins essential for maintaining the structural integrity and functional properties of the airway epithelial lining fluid. This secretory activity is often characterised by the expression of secretoglobin family 1A member 1 (*SCGB1A1*), which encodes uteroglobin, a protein abundantly present in the airway epithelial lining fluid (ELF) and known for its anti-inflammatory and immunosuppressive capabilities[44–46].

1.1.2.3 Ciliated cells

Columnar ciliated cells, which are the most prevalent cell type in the airway epithelium, play a crucial role in maintaining respiratory health. These cells are critical to airway homeostasis, facilitating the removal of trapped particles and pathogens from the lungs. This function is achieved through mucociliary clearance, a process whereby cilia located on the apical surface of these cells beat in a coordinated manner to expel undesired substances[47]. The differentiation of ciliated cells from their progenitors (basal cells or club cells) is governed by a complex transcriptional network. In the absence of Notch signalling, airway progenitors differentiate into ciliated cells under the guidance of the master regulator geminin coiled-coil domain containing protein 1 (*GMNC*)[48]. *GMNC* triggers a cascade involving various components such as multicilin (*MCIDAS*), deuterosome assembly protein 1 (*DEUP1*), and transcription factors *E2F4/5* and myeloblastosis (*MYB*), which control centriole biogenesis and assembly of cilia[49–52]. Moreover, a transcriptional network led by forkhead box protein J1 (FOXJ1) transcription factor (TF) activates the transcription and assembly of ciliary proteins, inducing basal cell progenitors to fully differentiate into ciliated cells[53,54]. This will be discussed in greater detail in Chapter 4.

1.1.2.4 Goblet cells

Goblet cells, the primary mucus-producing cells in the airways, are crucial for maintaining airway function. In humans, they are more prevalent in the proximal epithelium. In contrast, mouse lungs have a sparser distribution of goblet cells throughout their airways[26,27]. They synthesise and secrete a complex mixture of mucins, electrolytes, fluids, metabolites, and antimicrobial proteins, collectively known as mucus[48]. The most abundant mucins are mucin 5AC (MUC5AC) and mucin 5B (MUC5B). Mucus, in collaboration with cilia, forms a protective barrier against inhaled pathogens and particles. It also supports mucociliary clearance, aiding the removal of trapped particles through the action of cilia. Goblet cells originate from basal and club cells. Their differentiation involves complex signalling pathways. Increased Notch signalling suppresses the expression of *TP63* and *GMNC*, while it activates Sam-pointed domain-Ets-like factor (*SPDEF*)[48]. *SPDEF* along with the forkhead box A3 (*FOXA3*) TF orchestrates a transcriptional network that drives goblet cell differentiation, mucin synthesis, and packaging[55].

1.1.2.5 Rare epithelial cell types

Recent progress in cell biology and single-cell sequencing has unveiled rare epithelial cell types within the respiratory tract. These cells are distinctive, each with unique functions, and they represent less than 1% of all human airway epithelial cells[56,57]. Among these, tuft cells, previously referred to as brush cells, are characterised by their elongated microvilli and a chemosensory tuft on their surface. They function as chemosensors, detecting environmental irritants and pathogens through taste receptors like bitter taste receptor type 2 (TAS2R) and transient receptor potential cation channel subfamily M member 5 (TRPM5)[7,58,59]. When activated, tuft cells release various signalling molecules, including neurotransmitters such as acetylcholine, and cytokines like interleukin-25 (IL-25) and thymic stromal lymphopoietin (TSLP), thereby modulating immune responses, mucus production, and neural signalling in the airways[7,59,60]. Another rare epithelial cell type is the ionocyte, crucial for regulating ion transport and maintaining airway hydration[61]. These cells express the cystic fibrosis transmembrane conductance regulator (CFTR)[62]. Additionally, pulmonary neuroendocrine cells are vital for airway homeostasis and response to injury or infection, releasing neuropeptides that modulate immune cell recruitment[63,64]. These cells can also form neuroepithelial bodies (NEBs), acting as progenitor cells for the airway epithelium and contributing to epithelial repair and regeneration[65].

1.1.3 Dysfunction of airway epithelium in chronic airway diseases

As discussed in sections 1.1.1 and 1.1.2, the airway epithelium is crucial for pulmonary defence, where its structure, differentiation, and functional integrity play a key role in maintaining lung health. Dysfunction of the airway epithelium is linked to various chronic airway diseases, such as asthma, chronic obstructive pulmonary disease (COPD), and cystic fibrosis (CF).

Asthma is a chronic respiratory disease characterised by airway inflammation, airway hyperresponsiveness, and reversible airflow obstruction. In asthma, the airway epithelium undergoes significant structural changes, known as remodelling. These include goblet cell hyperplasia[66,67] and excessive deposition of extracellular matrix[68,69]. Inflammation is a key feature of asthma, driven by both innate and adaptive type 2 immune responses. These responses are activated following exposure of airways to various environmental factors such as allergens, pollutants, and microbes[70]. The airway epithelium is central to the pathogenesis of asthma as it releases various cytokines and chemokines, often termed 'alarmins' following inhalation of foreign particles and/or pathogens. These include IL-33, TSLP and IL-25[71]. Increased levels of IL-33 and TSLP have been identified in the bronchoalveolar lavage fluid of asthma patients[72]. A key feature of asthma is the impaired function of the epithelial barrier, often associated with abnormalities in the proteins that form tight junctions between cells. This impairment enhances the susceptibility of asthmatic airways to allergens and other triggers, exacerbating the condition[73–75]. The interplay of these factors – structural changes in the airways, activation of immune responses, and barrier dysfunction – collectively contribute to the complexity and severity of asthma symptoms.

COPD, currently the third leading cause of death worldwide, is characterised by irreversible airflow obstruction[76]. COPD mainly arises from two conditions: chronic bronchitis, involving long-term bronchial inflammation, and emphysema, marked by damage to the alveoli[77]. Cigarette smoking is the primary cause of COPD, although genetic predisposition and environmental factors also play significant roles[78]. COPD induces changes in the cell composition of the pseudostratified respiratory epithelium[79]. There is an increase in the number of basal stem cells[80], which exhibit impaired functionality and altered gene expression[81–83]. Additionally, COPD leads to an increase in the number of goblet cells and a decrease in the number of ciliated cells[84–87]. Inflammation plays a crucial role in the progression of COPD[88]. Inhaled irritants, such as cigarette smoke, activate epithelial cells to release various inflammatory mediators. These include tumour necrosis factor (TNF)-α, IL-1β, IL-6, IL-8, and granulocyte-macrophage colony-stimulating factor (GM-CSF)[89]. Elevated levels of these mediators have been detected in the sputum of COPD patients[90–92]. Furthermore,

COPD compromises the physical barrier function of the airway epithelium. This is characterised by reduced expression of tight junction proteins, such as zonula occludens-1 (ZO-1) and occludin (OCLN), and adherens junction proteins like E-cadherin[93,94]. These changes result in diminished junctional integrity and increased epithelial permeability, thereby exacerbating the severity of the condition.

CF is a genetic disorder caused by mutations in the gene encoding the CFTR protein. This protein functions as a chloride channel, vital for maintaining the balance of salt and water on epithelial surfaces. Dysfunction of the CFTR protein leads to a cascade of pulmonary complications, with the production of dehydrated mucus being a primary concern[95,96]. This arises due to reduced transport of water and chloride ions onto the airway surface, which subsequently impairs the mucociliary clearance mechanism. The impaired mucociliary clearance in CF facilitates bacterial colonization, resulting in recurrent lung infections[97,98]. Additionally, the differentiation of the CF airway epithelium is altered, characterised by an increase in goblet cells and a decrease in ciliated cells[99,100]. Furthermore, the epithelial barrier function is compromised in individuals with CF, as evidenced by abnormalities in tight junction proteins[101,102]. These abnormalities lead to increased permeability, making the epithelium more susceptible to external pathogens.

Bronchiectasis is a chronic condition characterised by the irreversible dilation and damage of the bronchi and bronchioles[103,104]. This damage leads to accumulation of mucus and compromised mucociliary clearance, which can cause recurrent infections, coughing, and shortness of breath. The condition can result from various underlying causes, including infections, immune system disorders, and conditions that affect cilia function, such as CF[105]. Moreover, bronchiectasis can coexist with other chronic airway diseases like COPD and asthma, complicating diagnosis, and management[106].

Chronic lung diseases pose a major health burden as they are among the leading causes of severe illness and mortality[107]. A common driver across many of these conditions, irrespective of age of onset or cause, is the dysfunction of the airway epithelium. This includes dysregulated differentiation, compromised barrier function and impaired mucociliary clearance. Current treatment strategies primarily focus on symptom management, using steroids for airway inflammation and bronchodilators for obstruction. While these approaches are effective, they do not address the underlying pathogenic processes. Targeting the dysregulated differentiation of airway epithelial cells and manipulating gene expression in pathways involved in airway epithelium dysfunction represents a ground-breaking shift in research. This strategy lays the groundwork for exploring how candidate genes contribute to the development of airway diseases and for developing therapeutic interventions aimed at

repairing or reversing these dysfunctions. This approach holds promise for the development of novel therapies that directly target the molecular causes of these diseases, potentially preventing their onset, slowing their progression, and ultimately resolving airway diseases.

In addition to epithelial barrier dysfunction, ciliary dysfunction, characterised by a range of defects that impair the functionality of cilia on ciliated cells is linked to many lung diseases. This dysfunction contributes to impaired mucociliary clearance, resulting in secondary infections, chronic cough, and compromised lung function.

1.2 Ciliogenesis and FOXJ1

1.2.1 Cilium structure and function

Cilia, resembling hair-like projections, are microtubule-based organelles that extend from the surface of many eukaryotic cells. They are broadly classified into two types based on their distinct structures and functions: motile and non-motile (primary) cilia. Motile cilia, found in the respiratory tract, are essential for mucociliary clearance[108–110] (section 1.1.2.3). They also play a key role in moving cerebrospinal fluid through the brain's ventricular system, aiding in the transport of nutrients and waste[111]. In mammalian fallopian tubes, motile cilia assist in the transport of egg cells from the ovary to the uterus, crucial for fertilisation[112]. Furthermore, motile cilia in embryonic nodal cells are vital for establishing left-right body asymmetry, an important aspect of development in bilateral animals[109,113,114]. In contrast, non-motile cilia primarily act as sensory organelles, functioning as antennas that collect information from the surrounding environment[115,116]. Most vertebrate cells possess a single, non-motile primary cilium that detects and responds to various stimuli, including chemical, thermal, and mechanical signals[117–119]. These signals are integrated into complex signalling pathways, influencing diverse cellular responses. For example, photoreceptor cells in the retina utilise non-motile cilia to detect light and initiate the process of vision[120].

At the core of the cilium's structure is the axoneme, a cylindrical arrangement of microtubules extending from the base to the tip of the cilium. Motile cilia are characterised by a '9+2' arrangement, consisting of nine pairs of double microtubules surrounding a central pair of single microtubules (Figure 1.2). In contrast, non-motile cilia usually display a '9+0' arrangement, which lacks the central pair of microtubules. Radial spokes, which extend from the central pair of microtubules to the peripheral microtubule doublets, are critical for maintaining the structural integrity of the axoneme and the coordinated movement of cilia. The basal body, originating from the mother centriole, forms the foundation of the cilium. It features a barrel-like structure composed of nine sets of triplet microtubules, along with subdistal

appendages that anchor the basal body to the plasma membrane, and distal appendages that aid in axoneme formation. During axoneme growth, two microtubules from each triplet extend to create the doublet microtubules. The ciliary rootlet, an extension of the basal body, anchors the cilium to the cytoskeleton. Within the axoneme of a motile cilium, inner and outer dynein arms act as molecular motors, driving the beating motion of the cilium. These dynein motors, along with kinesin motors, form tracks for the transport of other proteins within the cilium[121,122]. The dynein arms generate the force needed for microtubules to slide against each other, causing the characteristic bending and whip-like motion of motile cilia. Intraflagellar transport (IFT) is crucial for distributing components within the cilium, with kinesin facilitating forward movement towards the ciliary tip (anterograde IFT) and dynein facilitating backward movement towards the cell body (retrograde IFT). The cilium has its own membrane, which is enveloped by the cell's adjacent membrane[123].

Ciliogenesis, the formation of cilia, is controlled by a complex network of signalling pathways. This process initiates when the mother centriole migrates to the cell periphery, transforming into the basal body, which acts as the cilium's structural anchor[124,125]. Once at the cell periphery, the basal body forms a stable connection within the plasma membrane, laying the groundwork for cilium development. The basal body serves as a microtubule organising centre, guiding the growth of the axonemal microtubules by utilising tubulin subunits as building blocks. The elongation of these microtubules is crucial for the expansion of cilium to its appropriate length. IFT is vital for ciliogenesis. This bidirectional mechanism, involving motor proteins complexes, is responsible for shuttling protein complexes to and from the tip of the cilium. IFT is essential for the precise delivery and assembly of ciliary components, ensuring the cilium's structural and functional integrity.

The transcriptional network that regulates ciliated cell differentiation in the airways is extensively discussed in Chapter 4. This network consists of a complex array of TFs and signalling molecules, orchestrating the expression of proteins crucial for ciliogenesis.

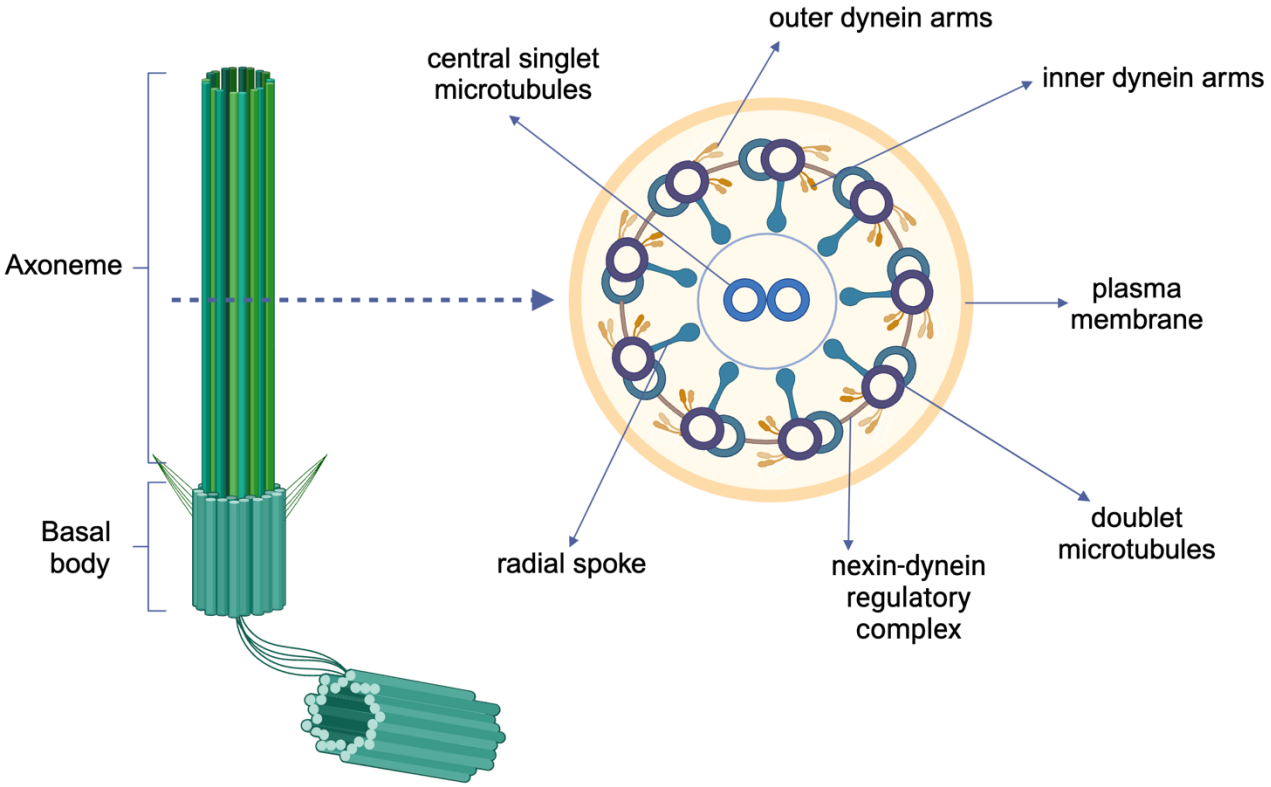


Figure 1.2 Simplified structural overview of motile cilia.

The schematic provides a guide to the architecture of motile cilia, starting from the basal body, which serves as the foundational structure of the cilium. A cross-sectional view shows the axonemal arrangement. Key features include the 9+2 arrangement, characterised by nine microtubule doublets and a central pair of microtubule singlets. Motor proteins (outer and inner dynein arms) together with radial spokes generate the wave-like beating of motile cilia. Nexin linkers, connecting the microtubules doublets, are crucial for maintaining the structural integrity and coordinated movement of cilium. Figure created with Biorender.com.

1.2.2 FOXJ1

FOXJ1, a member of the Forkhead box family of TFs, is characterised by its 'forkhead box' or 'winged helix' DNA-binding domain. As a TF, FOXJ1 binds to specific DNA sequences, regulating the transcription of various target genes. FOXJ1 activity plays a critical role in various cellular functions, with ciliogenesis receiving the most extensive research attention[126]. FOXJ1 is predominantly expressed in ciliated cells located in the respiratory tract[127], central nervous system[128], reproductive tract[129], and embryonic kidney[130].

FOXJ1 emerges as a key regulator in the development of motile cilia, driving the transcription of genes crucial for motile ciliated cell differentiation[131–141]. Its expression serves as a reliable indicator of cells destined to become motile ciliated cells[142]. The process of ciliogenesis begins with a commitment phase prior to FOXJ1 activation. P73, a member of the p53 protein family,

directly regulates FOXJ1 and is vital for ciliated cell formation[143]. FOXJ1 activation facilitates the trafficking of basal bodies to the apical membrane, setting the stage for axoneme growth[141].

The role of FOXJ1 in ciliogenesis is not limited to basal body anchoring. It orchestrates a complex transcriptional network that directly or indirectly controls numerous genes involved in ciliary formation, structure, and movement (Figure 1.3). FOXJ1 induces the expression of basal body components, structural proteins, motor proteins, accessory axonemal proteins, and IFT proteins[144]. The transcriptional network regulated by FOXJ1 will be discussed in Chapter 4.

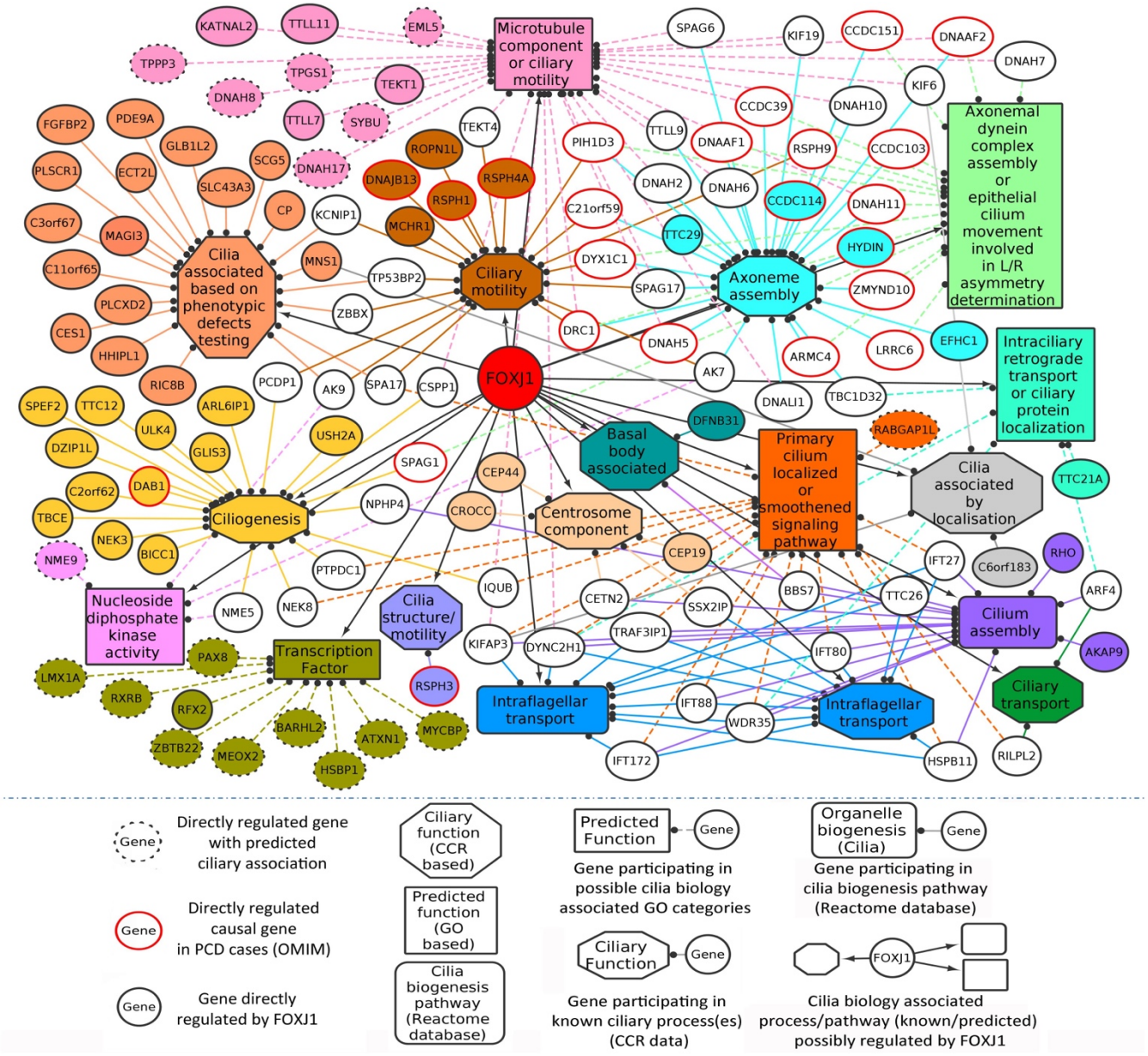


Figure 1.3 Predicted FOXJ1 transcriptional network.

The diagram illustrates the complex network regulated by Forkhead box J1 (FOXJ1), a key transcription factor involved in ciliary assembly and motility. It illustrates how FOXJ1 directly or indirectly regulates several genes, each organised according to their specific functions. The network map provides insights into the gene regulation pathways and interactions under the influence of FOXJ1, highlighting its pivotal role in ciliary dynamics. Figure adapted from Mukherjee *et al.*[591]

1.2.3 Ciliary dysfunction

1.2.3.1 Inherited disorders

Cilia play a crucial role in maintaining lung health by facilitating mucociliary clearance. However, defects in ciliary structure or function can disrupt this process, leading to severe lung disorders, including primary ciliary dyskinesia (PCD)[145]. PCD is a genetic disorder resulting from mutations in genes that encode ciliary proteins essential for the structure and assembly of motile cilia[146]. These mutations can impact the axonemal structure, ciliary assembly, or IFT. Often in PCD, the outer dynein arms, crucial for the rhythmic beating of cilia, are impaired[147–149]. This can result in immotile cilia, disrupting mucociliary clearance and hindering the removal of mucus and debris form the airways.

Malfunctioning cilia in the airways lead to impaired mucociliary clearance, a condition with significant consequences. It causes chronic respiratory symptoms, severely reducing the quality of life of affected individuals[150]. Poor mucociliary clearance creates an environment conducive to recurrent bacterial infections, increasing the risk of pneumonia, persistent cough, and complications such as rhinosinusitis, nasal polyps, and congestion[151–159]. Over time, these persistent airway challenges, coupled with mucus plugging and recurrent infections, can lead to progressive airway obstruction and bronchiectasis[160–162].

Loss of the FOXJ1 gene causes situs inversus, a condition where internal organs are mirrored, and impairs mucociliary clearance [163,164]. Mutations in FOXJ1 have been linked to motile ciliopathies, a group of diseases characterised by hydrocephalus, chronic destructive airway disease, and abnormal left/right body asymmetry, as reported in several studies[165–167]. CF is not classified as a ciliopathy; nevertheless, individuals with CF often experience ciliary dysfunction. This phenomenon arises from various factors, including dehydration of the epithelial surface, increased mucus viscosity, and impaired mucociliary clearance, all linked to dysfunctional chloride channels[168]. While the primary cause of compromised mucociliary clearance in CF is the abnormal viscosity of airway mucus, electron microscopy studies have revealed various ciliary abnormalities in this context, including missing cilia regions and cilia lacking inner dynein arms[169].

1.2.3.2 Environmental factors

Respiratory tract infections can adversely affect ciliary function, leading to acquired, impaired mucociliary clearance[170,171]. Pathogens impair ciliary function through various mechanisms, such as decreasing cilia beat frequency, disrupting cilia coordination, and inducing ciliary dyskinesia[170,172]. For example, lung samples from patients infected with respiratory syncytial virus have shown epithelial damage, loss of cilia, and reduced expression of FOXJ1[170], findings that are also observed in mouse models[170]. Similarly, severe acute respiratory syndrome coronavirus 2 (SARS-CoV-2) infection has been shown to cause ciliary damage, characterised by loss of axoneme, disorientation of basal bodies, and diminished FOXJ1 expression[173].

Chronic exposure to cigarette smoke significantly affects the airway epithelium, causing basal cell hyperplasia and excessive mucus production. It also leads to structural and functional abnormalities in ciliated cells and increases the permeability of the airway epithelial barrier[174–177]. Cigarette smoke generates oxidative stress in the lungs, disrupting normal cellular differentiation and function. This oxidative stress is linked to the activation of the epidermal growth factor receptor (EGFR) in human lung cells[177–180]. Upon exposure to cigarette smoke, ciliated cells release EGF, promoting the transformation of basal cells into a squamous phenotype and inhibiting ciliated cell differentiation[177]. Cigarette smoke exposure damages ciliated cells, resulting in various abnormalities such as reduced cilia count and irregular nuclei. In healthy smokers, airways exhibit shorter motile cilia compared to non-smokers[176,181]. This damage is more pronounced in smokers with respiratory diseases like COPD, where structural ciliary defects are observed[182,183]. Smokers also experience impaired mucociliary clearance, further affecting lung function[184]. However, research on the impact of smoking on motile cilia beating is inconclusive, with studies presenting conflicting evidence regarding cilia beat frequency in healthy and diseased smokers compared to non-smokers[182].

1.2.3.3 Chronic lung diseases associated with ciliary dysfunction

Ciliary dysfunction is a key feature of chronic lung diseases, including asthma[185]. Electron microscopy studies of epithelial samples obtained from both paediatric and adult asthma patients reveal significant damage to ciliated cells, characterised by cilia loss and structural abnormalities[186]. This damage contributes to the decreased mucociliary clearance efficiency observed in asthma patients compared healthy individuals[187]. The severity of asthma correlates with the extent of these ciliary defects; those with moderate to severe asthma have more dyskinetic and immotile cilia, as well as lower ciliary beat frequency than healthy individuals[187,188]. Severe asthma cases show even more pronounced ciliary disorientation,

depletion, and microtubule abnormalities, distinguishing them from both healthy controls and mild asthma patients[188]. In asthmatic airways, IL-13, a cytokine associated with T helper type 2 (Th2) immune response, is found at elevated levels[187]. This cytokine promotes goblet cell differentiation while reducing the number of ciliated cells and the number of cilia per cell[189]. IL-13 also interacts with ezrin, affecting basal body numbers[187,189], and can reduce or halt ciliary beat frequency by suppressing FOXJ1 expression[189].

The mechanisms underlying COPD are complex and not fully understood. Key contributors include the impaired function of airway epithelial cells due to cigarette smoke and environmental pollutants. These factors lead to shortening of motile cilia, promotion of epithelial cell death, and increased goblet cell count, resulting in elevated mucus production[190–193]. These changes adversely affect the lung's mucociliary clearance, diminishing its ability to expel pathogens and particles, potentially leading to chronic or recurrent infections that exacerbate the disease[193,194].

Lung cancer, the leading cause of cancer-related deaths globally[195], often starts with changes in the airway epithelium, influenced by environmental factors and genetic mutations. The role of cilia in lung cancer is not yet fully understood. Initial findings suggest that individuals with ciliopathies rarely develop lung cancer, indicating that cilia dysfunction may not increase the risk of developing cancer[196]. However, recent studies show downregulation of ciliated cell differentiation genes like *FOXJ1* and *DNAI1* in basal cell-high adenocarcinoma, which may contribute to epithelial-to-mesenchymal transition (EMT), enhancing cancer's invasive and metastatic potential[197].

Ciliary defects, whether primary (as in PCD) or secondary (as in asthma, COPD or CF) have significant health implications, particularly for respiratory health. Exploring ciliogenesis is crucial for understanding the vital role of cilia in health and disease, potentially leading to new therapeutic interventions for ciliopathies and their respiratory complications. Research on ciliated cells and their functions is essential for advancing our knowledge and improving the management of these complex respiratory conditions.

1.2.4 Manipulating ciliogenesis and FOXJ1 expression

As highlighted in section 1.2.3, ciliary dysfunction is a key characteristic of several chronic lung diseases, including asthma, COPD, CF. This dysfunction disrupts mucociliary clearance, a crucial respiratory defence mechanism that removes inhaled irritants, pathogens, and mucus. By delving into the complexities of ciliogenesis, we can better understand cilia formation and development, paving the way for novel therapeutic strategies aimed at restoring an optimal balance of functional ciliated cells.

The Notch pathway plays a crucial role in balancing ciliated and secretory cells, ensuring the integrity and functionality of the airway epithelium. This signalling cascade begins when JAGGED or DELTA ligands on one cell bind to the Notch receptor on a neighbouring cell, triggering a series of enzymatic events that release the Notch intracellular domain[198–200]. This Notch intracellular domain translocates to the nucleus, where it modulates gene expression, ultimately determining the fate of the cell. The γ-secretase enzyme is essential in this process, making γ-secretase inhibitors powerful tools for blocking Notch activity[201]. In the airway epithelium, activation of the Notch pathway promotes the differentiation of secretory cells, while cells that do not receive Notch signals become ciliated[198,199]. This dynamic interplay ensures a balanced population of these cell types, crucial for maintaining mucociliary clearance. Chronic lung diseases, such as COPD and asthma, often exhibit aberrant Notch signalling, particularly with dysregulated Notch3 levels, leading to mucus cell hyperplasia and further impairing mucociliary clearance and host defence[202–204].

Manipulating the Notch pathway to regulate ciliated cell populations is emerging as a promising strategy to address ciliated cell loss in affected airways. Vladar *et al.* demonstrated that inhibiting the Notch pathway with a γ-secretase inhibitor can restore ciliated cell counts in CF patient-derived epithelial cultures to levels seen in healthy individuals, enhancing epithelial barrier function[205]. This finding is supported by other studies showing that the γ-secretase inhibitor LY450139 promotes ciliated cell development in both differentiating and mature airway epithelial cell cultures, suggesting its effectiveness at various stages of epithelial development[206]. The influence of γ-secretase inhibition on ciliated cell count appears to be dose-dependent, allowing for controlled manipulation of cell numbers. Maintaining an optimal balance of ciliated and secretory cells is critical for preventing mucociliary clearance dysfunction and compromised host defence mechanisms. Interestingly, short-term administration of the γ-secretase inhibitor LY450139 in healthy adult mice increased ciliated cell numbers without detectable toxicity. However, the long-term effects and potential off-target effects of γ-secretase inhibitors need further exploration. Additionally, LY450139 has

been shown to increase ciliated cells and reduce excess mucus secretory cells in CF human airway epithelial cell cultures and in IL-13 remodelled healthy human airway epithelial cell cultures. These findings collectively underscore the potential of small molecule γ-secretase inhibitors in restoring the balance of ciliated cells in the airway epithelium. Nevertheless, the precise molecular mechanism underlying these effects are still unclear and warrant further investigation.

As discussed in section 1.2.2, FOXJ1, a key regulator of ciliogenesis, plays a crucial role in the formation and function of motile cilia through a complex transcriptional network. Studies employing murine models and transformed human cell lines have highlighted FOXJ1's essential role in the differentiation of ciliated cells in the airway epithelium[127,135,138,141,170,207–212]. This research has provided valuable insights into the fundamental mechanisms of ciliogenesis and mucociliary clearance[141,142]. However, significant differences exist between human and murine airways, particularly in the regulatory networks that control cell commitment and differentiation[213]. These differences highlight the importance of developing and using human models to study the differentiation of airway epithelial ciliated cells. The critical function of FOXJ1 in ciliogenesis and its association with various diseases has sparked interest in manipulating its expression, including strategies for both overexpression and downregulation. This approach is a promising avenue for further exploration into ciliogenesis, understanding the regulation of FOXJ1 and its downstream targets, and ultimately developing new therapeutic strategies for ciliopathies and related lung disorders.

You *et al.* investigated the role of FOXJ1 in the differentiation of ciliated airway epithelial cells by overexpressing FOXJ1 in polarised epithelial cell lines, rat alveolar epithelial cells and wild-type airway epithelial cells *in vitro*[141]. Interestingly, cilia development upon FOXJ1 overexpression using stable transfection techniques was observed exclusively in FOXJ1 null cells, which lacked FOXJ1 expression. This suggests that FOXJ1 may act as a master regulator in ciliogenesis within these cells. Further investigation revealed that FOXJ1 null cells contained precursor basal bodies for cilia, indicating a prior commitment to ciliogenesis. However, these basal bodies were disorganised and failed to dock with the apical membrane, preventing cilia formation. Delivery of FOXJ1 to these cells corrected basal body organisation and stimulated axoneme growth, demonstrating FOXJ1's capacity to fix these issues and promote cilia development. This finding emphasises FOXJ1's role in regulating the processes of basal body docking and axoneme formation, particularly in cells already on the pathway to ciliated cell differentiation. This study offered valuable insights into how FOXJ1 orchestrates ciliogenesis, but it was limited to rodent airway epithelial cells, highlighting the need to extend

this research to human models for a more comprehensive understanding of FOXJ1's role in human ciliogenesis.

Didon *et al.* investigated the regulatory mechanisms that control the differentiation of ciliated cells in the human airway epithelium[214]. By using a stable transfection method to introduce FOXJ1 into basal cells, they found that FOXJ1 overexpression triggered the activation of ciliated gene promoters, leading to a significant increase in the expression of genes associated with cilia. Additionally, the regulatory factor X (RFX)-family of TFs, known to be vital in ciliogenesis across various organisms, was also studied[215–219]. While introducing RFX3 alone did not stimulate ciliated cell gene expression, combining FOXJ1 and RFX3 gene transfers showed a synergistic effect. This combination led to a greater increase in ciliated gene promoter activity and the expression of ciliated cell genes than FOXJ1 alone. Immunoprecipitation studies confirmed an interaction between FOXJ1 and RFX3, suggesting that FOXJ1 is a crucial regulator of ciliated gene expression during the differentiation of basal/progenitor cells into ciliated cells. This study, utilising primary human airway basal cells, provides a more accurate model of the human airway epithelium compared to cell lines. Employing a comprehensive methodology, including gene transfection, promoter activity assays, mRNA expression analysis, and immunoprecipitation, the study thoroughly explored the roles of FOXJ1 and RFX3 in ciliated cell differentiation. However, the precise molecular mechanisms of how FOXJ1 and RFX3 work together to induce ciliated gene expression remain to be further investigated. This study provides evidence that FOXJ1 and RFX3 act together to enhance expression of ciliary genes during ciliated cell differentiation in the human airway epithelium.

Research into the role of FOXJ1 in preventing the inhibition of cilia growth caused by cigarette smoke was conducted using an *in vitro* model of the human airway epithelium[220]. Exposure to cigarette smoke extract (CSE) significantly reduced cilia length, mirroring the effects observed in the airway epithelium of smokers[221–224]. CSE also suppressed the expression of genes related to ciliated cells, including those involved in transcriptional regulation, basal body development, structural integrity, IFT, and cilia motility. This aligns with previous findings that cigarette smoke reduces the expression of cilia-related genes[221,225]. This led to the hypothesis that components of cigarette smoke inhibit cilia growth by interfering with various aspects of ciliogenesis at gene level. Overexpressing FOXJ1 through stable transfection effectively reversed the suppression of cilia-related genes caused by CSE exposure, suggesting that FOXJ1 overexpression might counteract the adverse effects of cigarette smoking on cilia length. Further research is needed to fully understand the clinical relevance of these findings

and their potential in developing therapeutic interventions to address the detrimental effects of cigarette smoking on airway cilia and respiratory health.

The role of FOXJ1 in ciliogenesis was further explored using knockdown approaches. Rapiteanu *et al.* established an efficient, scalable genome editing pipeline for an *in vitro* model of the human airway epithelium[226]. This method utilises transient, plasmid- and virus-free delivery of clustered regularly interspaced short palindromic repeats-CRISPR- associated protein 9 (CRISPR/Cas9), allowing for precise gene inactivation. This method was validated by successfully reducing FOXJ1 expression, which decreased the number of ciliated cells. This study provides the first evidence of FOXJ1's crucial role in ciliogenesis within this *in vitro* model.

Overall, the studies discussed above collectively suggest that manipulating FOXJ1 expression can affect cilia formation, numbers, and function. However, there remains a significant gap in research regarding the effects of FOXJ1 overexpression through transient overexpression tools. These tools offer several advantages over conventional stable transfection methods. Unlike stable transfection, which requires genomic integration, transient overexpression allows for controlled and transient overexpression of target genes. This minimises the risk of insertional mutagenesis, which can lead to unintended genetic modifications and potential off-target effects. Additionally, transient overexpression enables precise regulation of gene expression levels and duration, making it a vital tool for studying gene expression dynamics over time. In contrast, small molecules often exhibit off-target effects due to non-specific protein binding, which can lead to adverse side effects and limit their translational potential. Employing transient overexpression tools to manipulate FOXJ1 expression could provide new insights into FOXJ1 regulation, offering a fresh perspective that might enhance or differ from findings obtained through stable transfection methods. Investigating this possibility was a key objective of this thesis.

1.3 mRNA

1.3.1 General overview

Messenger ribonucleic acid (mRNA) is a single-stranded ribonucleic acid molecule that is transcribed from deoxyribonucleic acid (DNA). It plays a crucial role in protein synthesis, as it is translated by ribosomes to produce functional proteins that are vital for a variety of biological functions. Synthetic mRNA represents a promising tool for transient and dose-dependent expression of any protein of interest when effectively delivered to the cytoplasm of target cells (Figure 1.4). Synthetic mRNA functions exclusively within the cytoplasm, eliminating the risk

of insertional mutagenesis, a concern often associated with genetic manipulation. This cytoplasmic activity ensures that the encoded protein is expressed only transiently, providing a controlled therapeutic window, and minimising the potential for adverse effects.

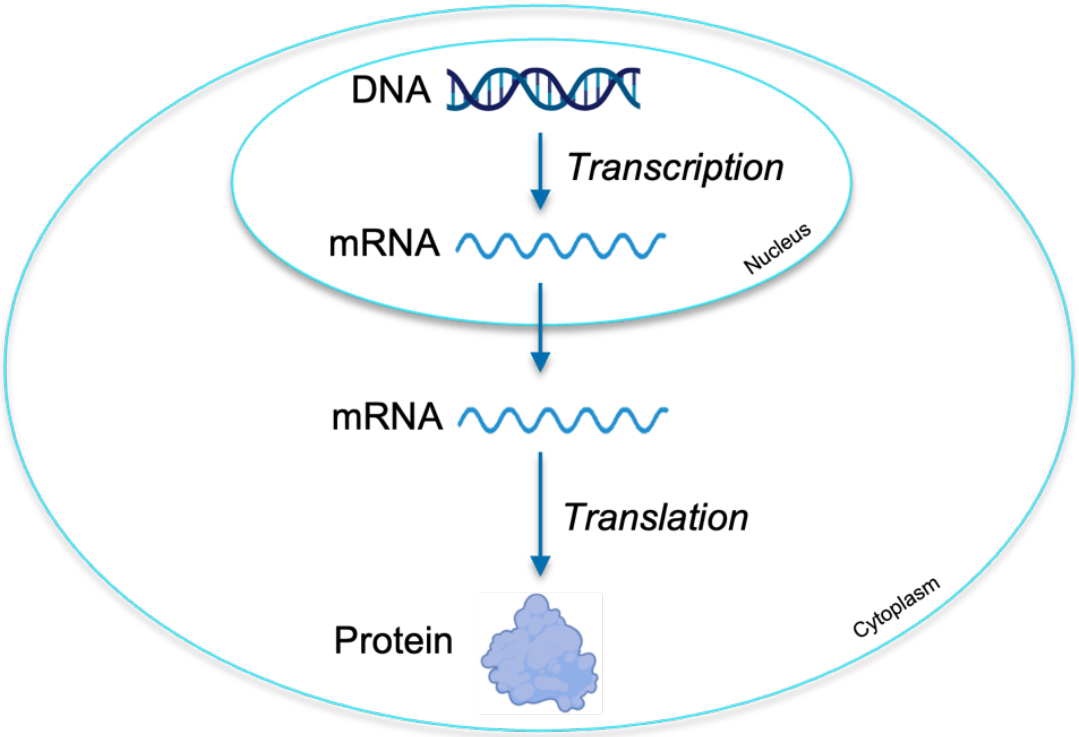


Figure 1.4 Exogenous mRNA as a tool for transient protein expression.

This diagram illustrates the process of genetic information transfer from DNA to protein via mRNA. The key feature of exogenous mRNA is its ability to function entirely in the cytoplasm. This feature is crucial as it bypasses the need for nuclear entry, thereby reducing safety concerns, including those related to insertional mutagenesis. Figure created with Biorender.com.

Since its initial demonstration of therapeutic potential *in vivo*[227], exogenous mRNA has become a powerful and versatile tool, offering great promise for diverse medical applications. Its remarkable versatility is evidenced in the development of vaccines against infectious diseases[228–244], including the rapid approval of mRNA-based Coronavirus disease 2019 (COVID-19) vaccines by major regulatory bodies such as the United States Food and Drug Administration (FDA) and the United Kingdom's Medicines and Healthcare products Regulatory Agency (MHRA)[245,246]. Beyond vaccines, mRNA has shown primise in cancer immunotherapy, particularly in exploring mRNA vaccines to elicit immune responses against tumour-specific antigens[247–269]. The therapeutic applications of mRNA extend to protein replacement therapies for various genetic disorders, including cardiac[270–273], lung[274–278], hematologic[279–281], metabolic[282–286], and neurogenic disorders[287,288]. Additionally, mRNA is pivotal in gene editing, where its transient nature makes it an ideal carrier for delivering gene-editing tools like zinc finger nucleases (ZFNs), transcription activator-like effector nucleases (TALENs) and CRISPR-Cas9[289–296]. In regenerative medicine, mRNA's ability to direct cellular reprogramming and differentiation shows promise for tissue repair and regeneration[297–300].

The mRNA technology platform, highlighted by its worldwide success during the COVID-19 pandemic, offers potential that extends beyond therapeutic applications. Its versatility makes it an effective tool for disease modelling, providing a platform to replicate and study various diseases in controlled laboratory settings[301]. This capability of mimicking disease processes at a molecular level is invaluable for understanding disease mechanisms and testing potential treatments. Additionally, mRNA technology can be used to manipulate biological pathways related to development and differentiation[302,303]. By controlling the expression of specific genes, it enables deeper insight into the complex processes of cell fate determination and differentiation, potentially modifying cellular behaviour. The dual utility of mRNA as both a therapeutic agent and a research tool opens new avenues for disease understanding and treatment.

1.3.2 *In vitro* transcribed (IVT) mRNA

IVT mRNA, also known as synthetic mRNA, is synthesised in laboratory settings to closely resemble the naturally occurring mRNA in cells[304]. This synthetic mRNA comprises several key components: a 5' cap, a 5' untranslated region (UTR), an open reading frame, a 3' UTR, and a 3' poly(A) tail, forming the fundamental structure of basic mRNA (Figure 1.5). The 5' cap is vital for mRNA stability and effective translation, protecting the mRNA from degradation and aiding in the initiation of protein synthesis by ribosomes. Originally, IVT mRNA used a natural eukaryotic mRNA cap structure, 7-methylguanosine (m^7G) 5'[305], but advancements have led to more efficient alternatives, such as the anti-reverse cap analogue (ARCA)[306–310].

The 3' poly(A) tail also contributes to the stability of mRNA and translation regulation[311]. The optimal poly(A) tail length ranges between 120 and 150 nucleotides[308,312]. The open reading frame encodes the desired protein, while UTRs at both ends regulate translation and stability of synthetic mRNA. These UTRs, often designed to mimic sequences from highly expressed genes like α- and β-globin genes, are included in IVT mRNA to improve its stability and translation efficiency[313–316]. These structural elements enable the synthetic mRNA to be efficiently translated into protein in cells. Moreover, these elements can be modified to improve mRNA stability and translation efficiency, highlighting the versatility and potential of IVT mRNA.

However, IVT mRNA faces a significant challenge due to its innate immunogenicity, which, while beneficial for vaccine development[317,318], is undesirable in other therapeutic contexts. The immune response to mRNA involves PRRs. In immune cells, endosome-bound TLRs - TLR3, TLR7 and TLR8 – recognise and respond to mRNA, triggering interferon secretion. In non-immune cells, cytosolic PRRs like RIG-I and MDA5 activate interferon production[319,320]. These receptors mediate immune stimulation and affect mRNA translation, leading to translation inhibition, mRNA decay, and antiviral actions. To mitigate this immunogenicity, a chemically modified nucleosides, such as pseudouridine (Ψ), N6-methyladenosine (m6A), 5-methylcytidine (m5C), and N1-methylguanosine (m1A)[321,322] are used. The Ψ modification was pivotal in the success of mRNA COVID-19 vaccines, leading to the Nobel Prize award to Katalin Karikó and Drew Weissman for their work in this area[323,324]. However, excessive modifications can disrupt the binding of other components and affect mRNA translation, necessitating careful balance between reducing immunogenicity and maintaining translational efficiency[325].

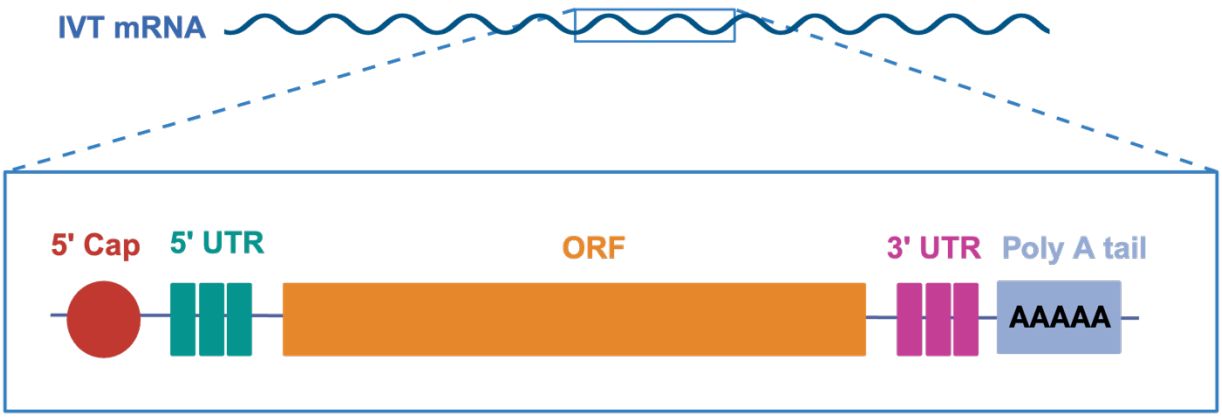


Figure 1.5 Structural elements of IVT mRNA.

This schematic presents the key structural components of *in vitro* transcribed (IVT) mRNA, crucial for its stability and functionality. It includes the 5' cap, which enhances mRNA stability and initiates translation, followed by the 5' untranslated region (UTR) that modulates translational efficiency. The open reading frame (ORF) represents the coding region encoding the gene of interest. This is flanked by the 3' UTR, which influences mRNA stability, and ends with the poly A tail, essential for stability and efficient translation. Figure created with BIorender.com.

1.3.3 mRNA encoded TFs as a platform for understanding and directing cell fate

TFs are specialised proteins that bind to specific DNA sequences, playing an essential role in regulating gene transcription[326–328]. Their interaction with DNA leads to either an enhancement of gene transcription by binding to an activation domain or a suppression of it by interacting with a repression domain. Crucial in cell fate determination, overexpressing TFs can significantly alter the differentiation pathways of pluripotent stem cells and other cell types[329]. For instance, certain TFs have been key in directing pluripotent stem cells to differentiate into muscle cells[330], neurons[331], and other cell types[332,333]. The impact of TF overexpression is even more pronounced when multiple TFs are used in combination[334–336]. A notable example is the use of the four Yamanaka factors (*Oct4*, *Sox2*, *Klf4*, and *c-Myc*), which reprogram fibroblasts into induced pluripotent stem cells[337–339]. This highlights the potential of TF overexpression in unravelling complex gene expression networks involved in cell differentiation. TFs are also gaining recognition as invaluable tools in tissue engineering and regenerative medicine, including in bone[340,341], cartilage[342,343], and cardiac repair[344,345]. However, the delivery of TFs as recombinant proteins or small molecules is challenging due to poor bioavailability, short half-life, and structural differences from endogenous proteins in terms of size and post-translational modifications. Additionally, TFs need to enter the cell nucleus to function effectively, which is difficult for proteins with high hydrophobicity and molecular weight, as they struggle to cross cell membranes and reach target cells[304,346].

The use of exogenous mRNA overcomes these challenges. By delivering mRNA to the cytoplasm of target cells, it enables transient translation by the cell's own ribosomes. This method avoids the risks of insertional mutagenesis associated with viral vectors and plasmids, while maintaining the functional integrity of the proteins. Proteins synthesised from exogenous mRNA undergo the same post-translational modifications and processing as endogenously expressed proteins, ensuring their natural functionality[304]. Moreover, mRNA encoded TFs offer a precise and targeted approach to gene expression regulation. By introducing specific mRNA sequences that encode TFs, it is possible to selectively manipulate the expression of targeted genes without altering others. Delivery of exogenous mRNA allows for transient in-cell production of proteins like TFs, which are otherwise challenging to deliver using conventional recombinant proteins.

1.3.3.1 mRNA encoded TFs: versatile tools for cellular reprogramming

Cellular reprogramming involves transforming differentiated adult cells into pluripotent or induced pluripotent stem cells by delivering specific TFs into cells. Initially, this was achieved using methods like lentiviruses or retroviral vectors, which despite their effectiveness[347–350], posed risks of insertional mutagenesis and potential tumorigenesis[351–354]. Safer alternatives, such as plasmid DNA or direct TF delivery, were subsequently explored[355–358], but these methods showed low efficiency[350,359,360]. As mentioned previously, a major challenge in direct TF delivery is the difficulty of penetrating the plasma membrane barrier. The use of mRNA encoded TFs has emerged as a promising, safer approach to cellular reprogramming.

The delivery of synthetic mRNA encoding TFs represents a novel approach in cellular reprogramming within developmental and cell-based regenerative biology. This concept was first demonstrated by Yakubov *et al.*, who successfully reprogrammed human foreskin fibroblasts into induced pluripotent stem cells using synthetic mRNA encoding TFs (*Oct4*, *Sox2*, *Lin28* and *Nanog*)[361]. Warren *et al.* further advanced this approach by reprogramming fibroblasts using synthetic mRNA encoding the Yamanaka factors (*Oct4*, *Sox2*, *Klf4*, and *cMyc*), incorporating modified nucleosides to avoid innate immune responses[360]. They also demonstrated the differentiation of induced pluripotent stem cells into myogenic cells using mRNA encoding *myoD*. Poleganov *et al*. adapted this method to transform blood-derived endothelial progenitor cells into induced pluripotent stem cells, using a combination of mRNA encoded reprogramming factors (*Oct4*, *Sox2*, *Klf4*, *c-Myc*, *Nanog* and *Lin28*) and mRNAs designed to circumvent immune responses (*E3*, *K3* and *B18R*)[362].

Numerous studies have shown the potential of mRNA encoded TFs in guiding the differentiation of induced pluripotent stem cells into specialised cell types, such as endothelial cells[363], myoblasts[364], cardiomyocytes[365], and neurons[366]. For instance, Wang *et al.* developed a method using modified mRNA to encode the TF *ETV2*[363]. This method successfully directed induced pluripotent stem cells into endothelial cells capable of forming vascular networks *in vivo*. Another study introduced a protocol for reprogramming induced pluripotent stem cells into neurons using synthetic mRNAs, generating dopaminergic neurons from both normal and Parkinson's disease induced pluripotent stem cells, through transfection with mRNAs encoding TFs *Atoh1* and *Ngn2*. These neurons showed biochemical and electrophysiological features characteristic of primary dopaminergic neurons. Overall, these studies highlight the promise of synthetic mRNA encoded TFs for efficient differentiation of induced pluripotent stem cells into various cell types, with significant implications for personalised disease modelling and the development of cell-replacement therapies. However, further research is needed to understand the long-term stability, functionality, and potential side effects of these cells in therapeutic contexts.

1.3.3.2 mRNA encoded TFs: versatile tools for transdifferentiation

Transdifferentiation, the process of directly converting one mature somatic cell type into another, is a significant advancement in cellular reprogramming as it bypasses the need for an intermediate pluripotent stage[367–369]. This method involves introducing mRNA encoding specific TFs into somatic cells, allowing them to modify their phenotype and produce the desired cell type[361,370]. The controlled expression of these TFs, induced through mRNA transfection, is crucial. This technique has enabled the successful transdifferentiation of various cell types into different lineages, including cardiomyocytes and insulin-secreting cells, using tailored combinations of TFs[365,371,372].

Lee *et al.* developed a novel method to directly transdifferentiate murine cardiac fibroblasts into functional cardiomyocytes[365]. The process involved repeated transfection over two weeks with mRNA encoding for TFs *Gata4*, *Mef2c*, and *Tbx5*, resulting in the conversion of fibroblasts into cardiomyocyte-like cells. These cells exhibited gene expression specific to cardiomyocytes, confirming successful transdifferentiation. This study underscores the potential of mRNA in direct cardiac transdifferentiation and its role in precisely controlling reprogramming factors. It lays the foundation for future advancements in developing *in vivo* mRNA tools for targeting infarcted heart tissues.

The advancement in mRNA-mediated transdifferentiation has also been demonstrated in converting pancreatic exocrine cells into insulin-secreting cells. A recent study demonstrated that pancreatic exocrine cells can be transdifferentiated into insulin-producing cells using synthetic mRNA encoding three key pancreatic TFs (*Neurogenin3*, *Pdx1*, and *MafA*)[371]. Following 10 days of transfection, the cells were successfully converted into insulin-producing cells. The synthetic mRNAs enhanced the expression of genes crucial for optimal pancreatic β-cell functionality. Although the reprogrammed cells' insulin response to glucose was not as strong as primary β-cells, this approach shows promise for cell-based diabetes treatments. However, further optimisation of synthetic mRNAs, culture conditions, and TF combinations is necessary for functionality equivalent to native β-cells.

Type 1 diabetes, an autoimmune disease where insulin-producing β-cells in the pancreas are destroyed, necessitates external insulin for blood glucose regulation. β-cell replacement therapy is a promising treatment for patients with type 1 diabetes, aiming to restore glucose homeostasis[373–375]. Cell therapy research is focusing on creating personalised β-cells derived from patients' own cells to avoid transplant rejection[376,377]. Corritore *et al.* developed a system for large-scale production of β-like cells from human pancreatic duct-derived cells using mRNA-based transdifferentiation[372]. By introducing mRNA encoding the pancreatic TF *MafA*, they drove these cells to transdifferentiate into β-cells. These cells not only displayed β-cell-specific markers but also secreted insulin in response to glucose. Remarkably, when transplanted into diabetic mice, these cells actively secreted insulin and significantly reduced hyperglycaemia within a week post-transplantation, highlighting the potential of this approach in diabetes treatment.

1.3.3.3 Emerging potential of mRNA encoded TFs in disease modulation

The potential of mRNA encoded TFs to modulate cell behaviour opens promising avenues for controlling various diseases, particularly those arising from dysfunctional or aberrant cellular processes. For instance, mRNA encoding *FOXP3*, a crucial TF for regulatory T cell function, has shown promise in controlling allergic asthma[278]. Delivery of *FOXP3* encoded mRNA effectively restored balance in pulmonary T helper cell responses and provided protection against allergen-induced tissue inflammation, airway hyperresponsiveness, and goblet cell metaplasia in a murine asthma model. Importantly, this protection was observed when the mRNA was administered both before and after allergen exposure, demonstrating its potential as both a preventive and therapeutic agent.

A more recent study explored the therapeutic potential of mRNA encoding the cartilage-anabolic TF *RUNX1* for cartilage tissue engineering[378]. *RUNX1* is essential in chondrogenesis, enhancing cartilage tissue anabolism and decreasing catabolism. Delivering mRNA encoding *RUNX1* successfully slowed the progression of osteoarthritis in a mouse model of knee osteoarthritis, with minimal toxicity and inflammatory responses. This study supports the use of mRNA encoding TFs in controlling degenerative conditions.

mRNA encoded TFs represent a promising tool in gene expression manipulation and cell fate modulation, offering several advantages over conventional methods. Their transient expression, minimal risk of genomic integration, and precise control over activity allow for the fine-tuning of cellular responses and pathways. An emerging area of research, and a central focus of this PhD project, is the application of mRNA encoded TFs to study airway epithelial cell differentiation *in vitro*. By manipulating the expression of specific pathways, such as ciliogenesis, and key genes, including *FOXJ1*, using mRNA encoded TFs, we could gain a deeper understanding of the mechanisms driving airway epithelial differentiation and related pathologies. This approach, a key investigation of this PhD project, could lead to new insights and therapeutic strategies for respiratory diseases and enhance our ability to model these conditions.

1.4 Recapitulating the airway epithelium *in vitro*

The airway epithelium, a dynamic and essential part of the respiratory system, acts as the first line of defence against inhaled pathogens and environmental insults. It is crucial for maintaining airway homeostasis, mucociliary clearance, and regulating immune responses in the respiratory tract. Dysfunction of airway epithelium can lead to various respiratory conditions, such as asthma, COPD, CF. Therefore, understanding the biology and disease processes of the airway epithelium is vital for enhancing our knowledge of respiratory diseases and for the development of effective treatments. *In vitro* models that recapitulate the airway epithelium have become invaluable in research. These models enable precise control over cellular and molecular aspects, allowing researchers to unravel the mechanisms behind the differentiation, functioning, and disease states of airway epithelium. Moreover, these models are instrumental in testing large libraries of compounds or genetic manipulations for their therapeutic potential, thus accelerating the discovery of novel treatments for airway diseases.

Several *in vitro* models have been developed to recapitulate the structure and functionality of the airway epithelium. Each model presents its own strengths and limitations, and the selection of a particular model depends on the specific research question being addressed.

1.4.1 Traditional primary cell culture

Submerged culture of basal human bronchial epithelial cells (HBECs) from healthy individuals and patients provides a simplified and widely used method for studying the human airway epithelium. In this process, isolated cells are cultured in specialised medium containing essential nutrients and growth factors, enabling the expansion and proliferation of HBECs. One of the key benefits of using primary HBECs is their physiological relevance: they closely resemble the cells in the human respiratory tract. However, when compared to immortalised airway cell lines that are simpler to use, primary HBECs maintain a better ability to differentiate and exhibit a wider range of physiological functions. Immortalised cell lines, altered to proliferate indefinitely, often lose their capacity to differentiate, which may result in a lack of important characteristics like mucociliary differentiation or barrier integrity[379,380]. This makes them less suitable for certain research applications. Primary HBECs, despite their advantages, face two primary challenges. First, their lifespan *in vitro* is limited, and they can undergo senescence after multiple passages, which limits the duration and scale of experiments that depend on them[381–385]. Second, there is often variability among cells from different donors, leading to inconsistent results in experiments[380]. Nevertheless, despite these challenges, primary HBECs remain an important tool for understanding the biology of the human respiratory epithelium.

1.4.2 Air-liquid interface (ALI) culture

ALI cultures represent a more sophisticated method for replicating the three-dimensional (3D) structure and cellular interactions of the native airway epithelium. This approach involves seeding HBECs onto a transwell insert with a porous membrane and initially growing them in a submerged state. In this phase, both the apical and basal chambers are supplied with medium. Once the cells form a confluent monolayer, the culture is transitioned to a specialised ALI differentiation medium, supplied only to the basal chamber[386]. This step exposes the cell layer and the apical chamber to air, crucial for inducing HBEC differentiation. Over time, influenced by both air exposure and the nutrient-rich medium, HBECs differentiate into a pseudostratified epithelium resembling the airway epithelium found *in vivo*[387]. This process results in a diverse cellular composition, including basal, ciliated, and secretory cells. ALI cultures are invaluable for studying bronchial epithelial differentiation and manipulating expression of genes to modulate this process *in vitro*[388]. They demonstrate the capacity to form a functional epithelial barrier, indicated by tight junction protein expression and the development of transepithelial electrical resistance[389]. The suitability of ALI cultures to recapitulate the *in vivo* airway environment is further supported by transcriptomic analyses showing gene expression linked to airway function[390]. Moreover, ALI cultures respond

physiologically to various insults, including toxins and pathogens, making them highly relevant for investigating airway physiology and diseases[391–393]. Notably, ALI cultures derived from primary cells of individuals with respiratory diseases, such as asthma, CF, and COPD, accurately recapitulate the *in vivo* disease characteristics[394,395]. This underscores their effectiveness as robust *in vitro* models for respiratory disease research. ALI cultures are also suitable for evaluating inhalation drug delivery and nebulised mRNA delivery formulations for the lungs[396,397]. However, establishing and maintaining ALI cultures is more complex than submerged cultures, requiring specialised equipment and materials. While they offer advanced physiological relevance, ALI cultures lack certain aspects of the *in vivo* environment, such as vascularisation and immune cell interaction. Overcoming these limitations could further enhance the translational potential of ALI cultures in respiratory research.

1.4.3 Organoids

Lung organoids are self-organising 3D structures that more accurately represent the complex architecture and cellular organisation of lung tissues. This technique involves embedding primary lung tissue or pluripotent stem cells into an extracellular matrix (ECM) scaffold. As the cells settle into this supportive environment, they proliferate and cluster together, forming spherical structures known as organoids[398]. In these organoids, goblet and ciliated cells align themselves toward the central lumen, whereas basal cells are oriented outward[399]. The self-renewal capability of organoids, attributed to their embedded basal cells, extends their lifespan, enabling prolonged research studies. This feature, combined with their capacity to recapitulate the cellular diversity of lung epithelium, makes organoids versatile tools for various applications. They are useful for investigating gene therapy approaches[400], studying the development of complex lung diseases like COVID-19[401], and aiding in the discovery of new drugs[401]. However, the creation and maintenance of lung organoid cultures are technically complex. Moreover, these organoids do not fully replicate the physiological conditions of the airways, primarily due to the absence of air exposure. This makes their practical application more challenging compared to traditional cell culture methods.

1.4.4 Lung-on-a-chip

The lung-on-a-chip is an advanced *in vitro* model that effectively replicates the complexities of the human lung within a compact chip. This platform reproduces respiratory mechanics by allowing cell layers to expand and contract, thereby mimicking the breathing process. It also mimics blood flow by circulating culture medium through microfluidic channels. Designed to replicate the intricate environment of the lung, this system enables researchers to examine the dynamic interactions of cells and their responses to various stimuli. Huh *et al.* created a

lung-on-a-chip system using polydimethylsiloxane (PDMS), a flexible material that facilitated the creation of two separate compartments divided by a membrane[402]. The upper compartment supported ALI culture of lung epithelial cells (focusing on alveolar epithelial cells rather than the diverse cell types in the airway epithelium), while the lower compartment accommodated endothelial cells with a continuous flow of culture medium. Including immune cells in the vascular compartment enabled bacterial phagocytosis and subsequent immune responses within the model. The flexibility of the PDMS membrane enabled physiological uptake of particles, making it a crucial tool for investigating particle toxicity. In the context of disease modelling, Nawroth *et al.* designed a lung-on-a-chip model to replicate key features of asthma[403]. By exposing lung cells to IL-13, a cytokine linked to chronic inflammation in asthma, the model induced goblet cell hyperplasia and reduced ciliary beat frequency, which are key indicators of the disease. This model, incorporating both epithelial cells and vascular endothelial cells, provides a powerful tool for exploring the pathogenesis of asthma and assessing potential treatments. Despite their promising capabilities, lung-on-a-chip models face limitations, primarily their high cost, which has restricted their reliable implementation to a small number of research groups.

1.5 Non-viral mRNA delivery systems

Delivery of mRNA into target cells presents challenges due to its large size, negative charge, and susceptibility to degradation by exonucleases and endonucleases. To address these issues, robust delivery systems are essential both *in vitro* and *in vivo*, to protect exogenous mRNA from degradation and improve its cellular uptake. Historically, viral vectors have been the preferred method for gene delivery because of their high transduction efficiency[404]. However, their use raises concerns related to immunogenicity, genomic integration risk, limited payload capacity, and production complexities. Consequently, there is growing interest in non-viral alternatives such as lipid-based, polymer-based, exosomes, and hybrid delivery systems[405]. These non-viral vectors offer several advantages over viral vectors, including reduced immunogenicity, suitability for repeated administration, and customisable properties for specific applications. Although generally less effective in gene delivery compared to viral vectors, non-viral vectors are considered safer and more versatile, making them appealing for certain applications. The choice between using viral and non-viral vectors should be based on the specific requirements of the gene delivery applications, evaluating the efficiency and safety concerns of each method.

1.5.1 Lipid-based vectors

Liposomes are spherical vesicles composed of one or more layers of phospholipid bilayers that envelop an aqueous core, ideal for protecting nucleic acids. Their formation is driven by the interaction of hydrophobic and hydrophilic forces in materials with polar head groups and non-polar tails[406]. Early versions of liposomal systems used cationic lipids such as DOTMA (1,2-di-*O*-octadecenyl-3-trimethylammonium-propane), which form complexes with anionic nucleic acids, including mRNA[406,407]. However, concerns about their toxicity and immunogenicity have been raised[408–410], especially considering the adverse effects such as liver damage[411] and significant inflammatory responses[412,413] following intravenous administration. These concerns highlight the importance of cautious application and management of liposomal systems.

Lipid nanoparticles (LNPs) are at the forefront of non-viral vectors for mRNA delivery. They protect mRNA from degradation, enhance cellular uptake, and facilitate endosomal escape. LNPs consist of cationic/ionizable lipids, phospholipids, cholesterol, and polyethylene glycol (PEG) lipids. Each component plays a vital role: cationic/ionizable lipids encapsulate mRNA, phospholipids and cholesterol aid in structure and membrane fusion[414–416], while PEG-lipids help in evading immune recognition and prolong the circulating half-life[415,417–420]. This combination forms a nanoparticle with an aqueous core, protecting the mRNA from degradation. Moreover, the flexibility in LNP design allows for specific modifications to target different tissues or cell types. For instance, attaching immune cell receptors, such as mannose receptor[421], DC-SIGN[422], DEC-205[423], and Langerin[424] to LNPs has been effective in enhancing the uptake of mRNA by dendritic cells. Additionally, LNPs modified with anti-Ly6c monoclonal antibodies have been successful in delivering mRNA that encodes *IL-10* to Ly6c+ leukocytes in a mouse model of inflammatory bowel disease[425]. In another study, LNPs were engineered for efficient delivery of therapeutic mRNA to the lungs via nebulisation[426]. This study discovered that increasing the PEG content in LNPs significantly enhanced their performance. This improvement was demonstrated by the protection of mice from a lethal influenza A virus challenge using nebulised mRNA that encoded a broadly neutralizing antibody targeting haemagglutinin. While this study thoroughly investigated LNP design parameters, such as composition and structure, further studies are needed to understand the long-term effects and potential toxicity of these optimised LNPs, especially when used in higher doses or for prolonged periods. However, LNPs tend to accumulate in the liver[427], a phenomenon linked to their similarity to very-low-density lipoprotein and their ability to adsorb apolipoprotein E in blood plasma, leading to liver accumulation and uptake by hepatocytes.

Addressing this challenge is crucial for maximising the use of mRNA LNP technology in a wide range of therapeutic applications.

Patisiran (Onpattro®), the first LNP-based (DLin-MC3-DMA/PEG2000-C-DMG/DSPC/cholesterol) RNA therapeutic approved by the FDA[428], was developed for treating polyneuropathy in patients with hereditary transthyretin-mediated amyloidosis. The development of LNP-mRNA formulations, including COVID-19 vaccines like mRNA-1273 by Moderna[246,429] and BNT162b2 by Pfizer/BioNTech,[245] has been extensive. These vaccines use LNPs to deliver nucleoside-modified mRNA encoding the spike protein of severe acute respiratory syndrome coronavirus 2 (SARS-CoV-2). Moderna's vaccine (mRNA-1273) consists of SM-102/DSPC/cholesterol/DMG-PEG2000[430,431], while Pfizer/BioNTech's vaccine (BNT162b2) is formulated with ALC-0315/DSPC/cholesterol/ALC-0159(PEG-lipid)[245,432]. Both LNPs incorporate a combination of ionizable lipids (ALC-0315 and SM-102), PEG lipids (ALC-0159 and PEG2000), cholesterol, and the phospholipid distearoyl-sn-glycero-3-phosphocholine (DSPC)[433], demonstrating the effectiveness and potential of LNP technology in clinical applications.

1.5.2 Polymers

Polymer-based nanoparticles are emerging as a highly promising class of non-viral vectors for mRNA delivery, offering advantages such as large packaging capacity, customisable physicochemical properties, and safety. Cationic polymers leverage their positive charge to bind efficiently with negatively charged mRNA molecules, creating structures known as polyplexes. This binding is essential for successful mRNA delivery.

One of the most widely studied cationic polymers for mRNA delivery is polyethyleneimine (PEI)[434,435]. A critical aspect of PEI's efficacy in enhancing mRNA delivery is its 'proton sponge' effect[436]. This effect is pivotal in releasing mRNA from endosomes following cellular internalisation of the polyplexes. When cells take up PEI/mRNA polyplexes through endocytosis, they initially trap them in endosomes. PEI's ability to buffer protons leads to chloride ions influx, maintaining osmotic balance but also increasing osmotic pressure. This pressure causes the endosomes to swell and eventually rupture, releasing the mRNA into the cytoplasm[437]. However, the use of PEI in therapeutics is often limited by its cytotoxicity, particularly with high molecular weight variants[438]. To address these issues, researchers have explored the use of lower molecular weight PEI. For instance, a 2kDa PEI conjugated with cyclodextrin has been developed for the intranasal delivery of mRNA that encodes for the human immunodeficiency virus (HIV) in mice[439]. This system effectively penetrated the epithelial barrier by transiently disrupting tight junctions, enhancing mRNA delivery to the nasal

cavity. It also achieved excellent intracellular mRNA delivery and prolonged retention in the nasal cavity. Consequently, the translation of this exogenous mRNA facilitated strong mucosal anti-HIV immune responses. This study highlights the potential of cationic polymers as effective carriers for intranasal mRNA vaccines against infectious diseases.

Chitosan, a polysaccharide naturally derived from the exoskeleton of shellfish, has been explored for mRNA delivery due to its biocompatibility, biodegradability, cationic nature and mucoadhesive properties, making it an attractive choice for mucosal administration. Mahiny *et al.* developed chitosan-coated nanoparticles for delivering endonucleases, encoded by chemically modified mRNA, as a novel strategy to treat surfactant protein-B (SP-B) deficiency[440]. The use of chitosan in this context was crucial for precise genome editing. Notably, this method significantly increased survival rates in SP-B deficient mice, highlighting the potential of chitosan as an effective agent for *in vivo* precision genome editing. Despite its benefits, chitosan's application faces certain challenges. One primary concern is the variability in its physical and chemical properties, which depends on its source and extraction method[441]. This variability can impact its effectiveness as a delivery vehicle. Additionally, chitosan becomes insoluble at physiological pH[442]. This solubility challenge requires either modifications to its chemical structure or the incorporation of solubility-enhancing agents, which may complicate its use and potentially affect its biocompatibility. These issues highlight the importance of careful formulation and testing when using chitosan in mRNA delivery applications.

Poly (β-amino esters) (PBAEs), a class of synthetic cationic polymers, have been recognised for their potential as non-viral vectors in mRNA delivery. Introduced by Chiellini *et al.* in 1983 as biodegradable cationic polymers[443], their use in DNA transfection was later pioneered by Langer's group in 2000[444]. PBAEs are synthesised through Michael addition polymerisation, which involves combining diacrylate and amine monomers. The presence of ester bonds in their backbone makes them susceptible to hydrolysis, rendering the polymers biodegradable and potentially reduces long-term toxicity concerns[444]. PBAEs effectively form nanoscale complexes, or polyplexes, with mRNA through electrostatic interactions between their positively charged amine groups and the negatively charged mRNA. These polyplexes enhance the cellular uptake of mRNA via endocytosis and may facilitate the release of mRNA from the endosomal compartment, possibly through a mechanism similar to the 'proton sponge effect' seen with PEI[445].

PBAEs stand out for their adaptability to chemical and structural modifications, which improves their interaction with mRNA, solubility, stability, cellular uptake, and transfection efficiency[446–448]. These aspects are elaborated in Chapters 3 and 5. Recently, Patel *et al.* highlighted the benefits of structural manipulation in PBAEs, such as branching to improve solubility and stability for nebulised mRNA delivery[449]. Branched PBAEs demonstrated stability and consistent size post-nebulisation, ensuring uniform distribution of mRNA in the mouse lung epithelium with minimal toxicity, unlike PEI. This platform was effective in delivering nebulised *Cas13a* mRNA, demonstrating high levels of translation and gene editing efficiency against SARS-CoV-2 and influenza infections in the respiratory tract of rodents[450]. Despite these advancements, the use of PBAEs for delivering mRNA to primary HBECs remains unexplored. While PBAEs have shown promising results in delivering mRNA to lung epithelium *in vivo*, their effectiveness in targeting primary HBECs has yet to be examined. Addressing this gap in knowledge was a key objective of this PhD thesis.

PBAEs present significant benefits for various applications, but they also have limitations. A major concern is their inherently cationic nature, marked by an excess positive charge, which may lead to cytotoxic effects. To address this, Fields *et al.* developed a modification strategy by combining PBAE with a solid polymer, poly (lactic-co-glycolic acid) (PLGA), and functionalising the surface of the nanoparticles with a cell-penetrating peptide[451]. This approach reduced the overall surface charge, thereby improving the safety profile of these nanoparticles, without compromising their ability to enter cells, a process partially facilitated by the positive charge of the cell-penetrating peptide. Moreover, PBAEs are noted for their potential immunomodulatory properties. Andorko *et al.* observed that PBAEs are immunologically inert in free solution but can activate antigen-presenting cells when they form nanoparticles through complexation with a polyanion[452]. The degree of immunological response generated by these PBAE particles depends on their polymer molecular weight. As the polymer degrades through hydrolysis, its stimulatory effect on the immune system decreases[453]. These findings highlight the importance of careful design and optimisation in the use of PBAEs for mRNA delivery, balancing their advantageous properties against potential risks. This balance is crucial for advancing their applications in a safe and effective manner.

1.5.3 Exosomes

Exosomes, nano-sized extracellular vesicles ranging from 30-150 nm in diameter, are secreted by various cell types and play a vital role in cellular communication by transporting bioactive molecules, such as proteins, lipids, and nucleic acids[454]. Their ability to transfer genetic material, coupled with their biocompatible nature, has made exosomes a promising non-viral delivery system for mRNA delivery.

A pioneering study by Skog *et al.* demonstrated that exosomes from glioblastoma cells, carrying the reporter gene Gaussian luciferase (GLuc), could effectively deliver mRNA to endothelial cells[455]. This resulted in a significant increase in GLuc activity in the treated cells, highlighting the potential of exosomes in mRNA delivery and protein synthesis. Another study by Bu *et al.* employed exosomes to deliver mRNA encoding the anti-inflammatory agent *IL-10*, targeting atherosclerosis, a chronic inflammatory disease characterised by arterial plaque buildup[456]. These mRNA-loaded exosomes effectively transfected macrophages in arterial plaques of apolipoprotein E deficient (ApoE -/-) mice, leading to IL-10 production and mitigation of atherosclerosis symptoms. Recent research has also explored the engineering of exosomes, such as modifying them to display neuron-targeting rabies virus glycoprotein (RVG) peptides. This was done to deliver nerve growth factor (NGF) mRNA to the ischemic cortex[457]. This strategy led to the production of NGF protein, reducing inflammation and enhancing cell survival, with the engineered exosomes demonstrating stability and prolonged effectiveness *in vivo*. Despite these promising developments, several challenges remain in the field of exosome-based mRNA delivery. These include standardizing exosome isolation, ensuring consistent quality and efficacy of exosome preparations, and scaling up production for clinical applications. Overcoming these challenges is essential for further advancement of exosome applications in mRNA delivery studies.

1.5.4 Hybrid delivery materials

Beyond the non-viral vectors previously discussed, hybrid non-viral vectors are emerging as a significant innovation in the field of mRNA delivery applications. These vectors combine features from various non-viral vectors, including lipids, polymers, and peptides, aiming to maximize stability and mRNA protection, enhance cell-specific targeting and transfection efficiency, and minimise cytotoxicity[458]. By integrating diverse properties, hybrid systems offer more versatile and effective solutions for mRNA delivery.

A key development in this area is the creation of lipid-polymer hybrid nanoparticles for mRNA delivery. These nanoparticles merge the protective and controlled-release properties of polymers with the cell membrane fusion abilities of lipids, resulting in improved stability and transfection efficiency compared to lipid-based nanoparticles alone. For example, Eltoukhy *et al.* designed a hybrid system combining a PBAE terpolymer with alkyl side chains and PEG-lipid[459], significantly enhancing transfection efficiency and ensuring more effective mRNA delivery to mouse lungs following systemic administration. These nanoparticles also demonstrated enhanced stability under physiological conditions. Another study showed that nanoparticles comprising PBAEs and PEG-lipid had better serum stability and *in vitro* potency, efficiently delivering mRNA to mouse lungs when injected intravenously[448]. Incorporating PEG-lipid into polymer structures appears to be crucial for optimising vector design for improved serum stability and effective mRNA delivery. Furthermore, a novel hybrid system that merged PBAE with liposomal components like 1,2-dioleoyl-*sn*-glycero-3-phosphoethanolamine (DOPE), cholesterol, and PEG-lipid was developed, showing superior stability in serum and mRNA transfection efficiency in both the lungs and spleen, outperforming conventional systems[446].

Another promising direction is peptide-polymer hybrid nanoparticles, which combine the biocompatibility and functionality of peptides with the stability of polymers. This synergy allows for the development of nanoparticles with tailored properties and functions, such as targeted cell delivery and efficient endosomal escape. For instance, a library of PBAEs combined with specific terminal oligopeptides (OM-PBAE) was designed for selective accumulation and mRNA transfection in the spleen[460]. These modifications also enabled targeted transfection of specific cell types, notably antigen-presenting cells[460–462]. This oligopeptide modification strategy effectively addresses the issue of non-specific liver accumulation common in many nanoplatforms[460]. Chapter 5 will provide a more detailed discussion on the modifications of PBAEs with peptides, exploring how these modifications can enhance transfection efficiency, and cell-targeting capabilities of these hybrid nanoparticles.

In summary, exploring various mRNA delivery systems, including lipid-based, polymer-based, exosomes, and hybrid delivery systems, highlights the diversity and complexity in the field of mRNA delivery. Each system offers unique advantages and limitations, emphasising the need for careful consideration in their application. The selection of a suitable non-viral vector for mRNA delivery must be specifically tailored to meet the requirements of the application and the target cell type, ensuring optimal efficacy and safety.

1.6 Hypothesis and aims

Previous research has demonstrated the potential of mRNA encoded TF tools in cellular reprogramming and modulation of cell fate. However, the use of this technology in the context of bronchial epithelial cell differentiation *in vitro* remains unexplored. This PhD project aimed to address this gap by investigating the influence of nanoparticle-mediated delivery of mRNA encoded FOXJ1 on the differentiation of HBECs at ALI.

Overall hypothesis

Nanoparticle-mediated delivery of mRNA encoding FOXJ1 can induce the expression of downstream cilia-related genes and thereby promote ciliogenesis in an ALI model of HBECs.

Overall aims

1. Establish a method for efficiently delivering mRNA to primary HBECs using PBAEs.
2. Investigate the impact of non-viral reporter mRNA delivery on the differentiation and integrity of primary HBECs in an ALI model.
3. Manipulate mucociliary differentiation of HBECs in an ALI model using nanoparticle-mediated mRNA encoded FOXJ1 delivery.

2 Materials & Methods

2.1 Primary HBECs

Primary HBECs used in this thesis were purchased from either Lonza (Basel, Switzerland) or Epithelix Sàrl (Geneva, Switzerland) (Table 2.1). Primary HBECs from Lonza were isolated from the airway epithelial lining above the tracheal bifurcation of the lungs, while primary HBECs from Epithelix Sàrl's were acquired from individuals undergoing surgical procedures.

Table 2.1 Donor information for primary human bronchial epithelial cells.

Donor ID	Sex	Age	Smoking history	Supplier
18TL052522	Female	66	No	Lonza
18TL290281	Male	75	No	Lonza
623950	Male	60	Yes	Lonza
20TL266566	Male	52	No	Lonza
02AB0839	Male	59	No	Epithelix
02AB0834	Male	71	No	Epithelix

2.2 Cell lines

16 human bronchial epithelial (16HBE) cell line (Sigma, SCC150) and A549 human alveolar adenocarcinoma epithelial cell line (Sigma, 86012804) were used in this thesis.

2.3 Cell culture

2.3.1 Cell maintenance, passaging and cryopreservation

All cells were maintained in appropriate media as shown in Table 2.2 and cultured under sterile conditions at 37°C in a humidified incubator with 5% CO_2. Cells from cryovials stored in liquid nitrogen were thawed in a 37°C water bath for 2 minutes. After thawing, the cell suspension was transferred to T75 cell culture flask, coated for at least 30 minutes with 30 µg/mL PureCol® bovine Type I Collagen Solution (Advanced BioMatrix, Carlsbad, USA), containing 12 mL of appropriate cell culture medium. The medium was replaced 24 hours after seeding. Cells were provided with fresh culture medium every 48-72 hours and passaged upon reaching 70-80% confluence. Cells were washed gently with 1X phosphate buffered saline (PBS) (Gibco, 14190250), then treated with TrypLE™ Express Enzyme 1X (6 mL/T75 flask) (Gibco, 12563029) and incubated at 37°C for 5-10 minutes to allow cell detachment. TrypLE activity was neutralised using 1X PBS (12 mL/T75 flask) and the cell suspension was centrifuged at 1500 rpm for 5 minutes. The supernatant was discarded, and the pelleted cells

were resuspended in 1 mL of appropriate cell culture medium (Table 2.2) and counted using Trypan Blue Solution (Gibco, 15250061) and a haemocytometer. For subculture, cells were seeded at 500,000 cells/T75 flask in 12 mL of appropriate medium or seeded at appropriate seeding density in plates, 8-well chamber slides or transwell inserts for downstream experiments. For cryopreservation of cells, the pellet was resuspended in freezing medium, consisting of the cell's regular culture medium supplemented with 10% foetal bovine serum (FBS) (Gibco, 11533387) and 10% Dimethyl sulfoxide (DMSO) (Sigma, D2650). Cell suspension was aliquoted into cryovials (500,000 cells in 1 mL) which were placed in isopropanol-filled Mr Frosty™ freezing container (Thermo Fisher Scientific, 5100-0001) for storage at -80^{o}C for 24 hours before permanent preservation in liquid nitrogen. Cell lines thawed from liquid nitrogen were passaged at least twice before use in experiments. Primary HBECs were not used beyond passage 5.

2.3.2 Air-liquid Interface culture of primary HBECs

For the establishment of ALI cultures, primary HBECs were seeded on collagen-coated (30 µg/mL) transwell inserts with polyethylene terephthalate membrane and 0.4 µm pore size (Greiner Bio-One, 662641) at a seeding density of 30,000 cells per transwell insert. Cells were initially cultured submerged in growth medium that was refreshed every 2-3 days (200 µl apical chamber, 500 µl basal chamber). Once cells reached confluency, the medium was removed from the apical chamber, exposing the cells directly to air, while the basal chamber remained in contact with the differentiation medium. Medium on the basal chamber was refreshed every 2-3 days for 4 weeks until cells were fully differentiated, as demonstrated by cilia beating and mucus production observed under a light microscope (Leica DMi1 microscope, camera MC170). The composition of growth and basal differentiation medium is provided in Table 2.2.

Table 2.2 Cell culture media for cell lines and primary HBECs (submerged & ALI).

Cell type		Media	Supplements	Supplier, Catalog number
A549		Dulbecco's Modified Eagle Medium (DMEM)	- FBS (10%) (Gibco, 11533387) - Penicillin/Streptomycin (P/S) (1%) (Gibco, 15140-122)	Gibco, 41966029
16HBE		Minimum Essential Medium (MEM)	- FBS (10%) (Gibco, 11533387) - L-Glutamine (1%) (Gibco, 25030081) - P/S (1%) (Gibco, 15140-122)	Gibco, 32360026
Submerged culture of primary HBECs		Airway Epithelium Growth Medium kit	- Bovine pituitary extract (0.004 mL/mL) - Epidermal growth factor (10 ng/mL) - Insulin (5 µg/mL) - Hydrocortisone (0.5 µg/mL) - Epinephrine (0.5 µg/mL) - Triiodo-L-thyronine (6.7 ng/mL) - Transferrin (10 µg/mL) - Retinoic acid (0.1 ng/mL) - P/S (1%) (Gibco, 15140-122)	Promocell, C-21160
ALI culture of primary HBECs	Seeding & submerged phase (growth medium)	1:1 mixture of Airway Epithelial Growth Medium and DMEM with GlutaMAX™	- P/S (1%) (Gibco, 15140-122) - HEPES (25 mM) (Gibco, H0887) - bovine serum albumin (BSA) (1.5 µg/ml) (Sigma, A9576) - all supplements provided with the Airway Epithelial Growth Medium kit except for Triiodo-L-thyronine	Promocell, C-21160 Gibco, 31966021
	Air-exposure phase (basal differentiation medium)	PneumaCult™ - ALI Medium	- 10X supplement (Stemcell, 5001) - maintenance supplement (100X) (Stemcell, 5001) - heparin (0.0004%) (Stemcell, 7980) - hydrocortisone (0.48 µg/mL) (Stemcell, 7925) - P/S (1%) (Gibco, 15140-122)	Stemcell, 5001

2.4 Histology processing of ALI transwell inserts

2.4.1 Agarose-embedding of ALI inserts

Primary HBECs cultured on transwell inserts were fixed in 4% paraformaldehyde (PFA) (Thermo Fisher Scientific, 29808) in PBS for 20 minutes at room temperature and washed three times in PBS. A solution of low melting point agarose (Thermo Fisher Scientific, 16520050) diluted in PBS to a concentration of 4% was prepared. The solution was heated in a microwave until the agarose completely dissolved, then allowed to cool to 37^{o}C. Membranes were excised from transwell inserts using a scalpel and embedded in 4% agarose solution in a 24-well plate (one membrane/well), ensuring each membrane was fully submerged in the agarose and remained flat. The plate was placed on ice until the agarose solidified. Post-solidification, the agarose-embedded membrane was excised using a scalpel and placed in a histology cassette. The cassettes were subjected to a graded dehydration process using ethanol concentrations of 30%, 50% and 70%, immersing them for 15 minutes in each solution. The samples were then transferred to Histology Core for subsequent histological processing.

2.4.2 Paraffin embedding, sectioning and histological stains

Paraffin embedding, sectioning (4 µm thickness) as well as haematoxylin and eosin (H&E) staining and periodic acid-Schiff (PAS) staining were performed by Lorraine Lawrence at the Inflammation, Repair and Development (IRD) Histology Core Facility, Imperial College London.

2.4.3 Imaging

H&E and PAS-stained ALI cross-sections were imaged using the Aperio VERSA 8 slide scanner microscope (Leica). Epithelial height was measured in H&E-stained sections, at ten distinct points across the epithelial layer per section, using the Aperio ImageScope Software (Leica, version 12.4.6.5003). The number of ciliated cells in H&E-stained sections and PAS-positive goblet cells in PAS-stained sections were quantified using the same software.

2.5 Transmission Electron Microscopy (TEM)

Primary HBECs cultured at ALI were fixed in 2.5% glutaraldehyde (Merck, G5882) in 1X PBS for 1 hour at room temperature. Fixed cultures were submitted to Dr Andrew Rogers, Electron Microscopy Unit, Royal Brompton Hospital. Samples were immersed in 0.05M sodium cacodylate (Agar Scientific, R1104) buffered at pH 7.4 and processed within two weeks. After a 1-hour post-fixation with 1% osmium tetroxide (TAAB, O001/1) in cacodylate buffer at room

temperature, samples were rinsed with purified water and then dehydrated through an ascending ethanol series: 70%, 90%, and 100%. Samples were transitioned to 100% Araldite CY212 (Agar Scientific, R1030) through an ethanol:Araldite gradient of 50:50, 25:75 mixtures and then 100% Araldite overnight. Samples were then embedded in moulds filled with 100% Araldite and polymerised at 60°C for 3 days in an oven. Araldite-embedded sample blocks were ultramicrotome sectioned at 1 µm thickness and sections were stained with toluidine blue (Agar Scientific, R1727) for the selection of regions of interest (ROI) by light microscopy. Sample blocks were trimmed to the ROIs, then ultrathin sectioned at 80 nm and sections mounted on 200 mesh thin bar copper grids for TEM. The ultrathin sections were contrast-stained with 1.5% uranyl acetate (Agar Scientific, R1260A) in methanol, followed by Reynolds lead citrate solution (lead nitrate, Agar Scientific, R1217; sodium citrate, BDH, 3012846). Sections were examined by transmission electron microscope at 120KV (1400+, JEOL UK Ltd) and micrographs acquired at suitable magnifications for morphological assessments (x10000 to x1000000) (AMT XR16 camera, Deben UK Ltd).

2.6 Functional assessment of primary HBECs in ALI culture

2.6.1 Transepithelial electrical resistance (TEER)

TEER of fully differentiated ALI cultures was measured using MILLICELL® ERS electrode probes (Millipore, MERSSTX01) and a MILLICELL® ERS-2 Voltohmmeter (Millipore, MERS00002) according to the supplier's guidelines. Before measuring TEER, the electrodes were sterilised using 70% ethanol and then rinsed with 1X sterile PBS. 100 µl of pre-warmed sterile 1X PBS was added to the apical chamber of each transwell insert. To avoid TEER fluctuations caused by the difference between the 37°C incubator temperature and room temperature, the temperature was equilibrated before taking TEER measurements. The electrodes were placed vertically in apical and basal chambers of the transwell insert. TEER of blank insert (without cells) was measured as a background control. TEER value (Ω * cm^2) was calculated using the following formula:

$$\boldsymbol{TEER} = [\boldsymbol{Resistance}\ (\boldsymbol{\Omega}) - \boldsymbol{Background\ resistance}\ (\boldsymbol{\Omega})] * \boldsymbol{Surface\ area\ of\ the\ insert's\ membrane}\ (\boldsymbol{cm^2})$$

2.6.2 Permeability assay

Permeability of fully differentiated ALI cultures was assessed using the fluorescein isothiocyanate (FITC)-Dextran permeability assay. Before starting the assay, the apical chamber was washed with 1X PBS (200 µl/transwell insert). FITC-Dextran 4kDa (Sigma, 46944) diluted in 1X sterile PBS at 1 mg/mL was added to the apical chamber of the transwell insert (200 µl/transwell insert). The basal chamber contained 500 µl PBS. Paracellular flux of FITC-Dextran from apical to basal chamber was assessed by taking 100 µl aliquots from the basal chamber after 30 minutes incubation at 37°C in a humidified 5% CO_2 incubator. Aliquots were transferred in a black-bottom 96-well plate and fluorescence was measured using the SpectraMax® i3 plate reader (Molecular Devices) with excitation and emission at 490 nm and 520 nm, respectively. To calculate FITC-Dextran leakage from the apical to the basal chamber relative to an empty transwell control, the following formula was used:

$$\boldsymbol{Leakage}\ (\%) = \frac{\boldsymbol{Fluorescence\ of\ sample}}{\boldsymbol{Fluorescence\ of\ control}} * \mathbf{100}$$

2.7 PBAE synthesis and characterisation

PBAEs were synthesised by Leigh-Anne Gavin as described by Patel *et al.* [463]. Monomers used for PBAE synthesis are listed in Table 2.3.

2.7.1 Linear PBAE synthesis

Linear DD90-118 1.2 and DD90-118 1.05 polymers were synthesised at a ratio of 1.2:1 and 1.05:1 acrylate (DD) to backbone amine (90) monomers, respectively. Monomers were stirred in 150 mg/mL anhydrous dimethylformamide (DMF) (Sigma, 227056) at 90°C for 48 hours. Mixtures were allowed to cool to 30°C before adding the end cap amine (118) at a molar equivalent to the excess acrylate and then stirring at 30°C for 24 hours. Polymers were purified by precipitating them into cold diethyl ether (Sigma, 296082) spiked with glacial acetic acid (Sigma, 338826). After vortexing to collect the polymer, the solvent was removed. The polymer precipitates were rinsed twice with fresh diethyl ether, and then dried under vacuum for 48 hours at room temperature. Polymers were aliquoted into single-use aliquots and stored at -80°C.

2.7.2 Branched PBAE synthesis

Branched DD90-118 polymer was synthesised at a ratio of 1:0.5:0.2 acrylate (DD) to backbone amine (90) to branching amine monomers. Monomers were stirred in 150 mg/mL DMF at 40°C for 4 hours and then at 90°C for further 48 hours. After cooling the mixtures to 30°C, the end cap amine (118) was added at one molar of the excess acrylate and stirred at 30°C for an additional 24 hours. Polymer was purified by precipitating in cold diethyl ether spiked with glacial acetic acid following by vortexing to aggregate the polymer. The remaining solvent was discarded, and the precipitated polymer underwent two rinses with fresh diethyl ether. The polymer was dried under vacuum for 48 hours at room temperature before being aliquoted into single-use aliquots and stored at -80°C.

2.7.3 Peptide-modified PBAE synthesis

2.7.3.1 DD90-Ala-Lys & DD90-Ala-Ala

Linear DD90-Ala-Lys and DD90-Ala-Ala polymers were synthesised at a ratio of 1.2:1 acrylate (DD) to backbone amine (90) monomers. Monomers were dissolved in anhydrous DMSO (Sigma, 227056) at a concentration of 200 mg/mL and stirred at 90°C for 48 hours. After cooling the mixtures to 30°C, either the Ala-Lys or Ala-Ala dipeptide was added, at a 0.44 molar equivalent to the excess acrylate, and the solution was subsequently stirred at 35°C for another 24 hours. Polymers were used without further precipitation from DMSO.

2.7.3.2 DD90-Ala-Gly & DD90-Gly-Sar

Linear DD90-Ala-Gly and DD90-Gly-Sar polymers were synthesised at a ratio of 1.2:1 acrylate (DD) to backbone amine (90) monomers. Monomers were stirred in 200 mg/mL DMF at 90°C for 48 hours. After cooling the mixtures to 30°C, either the Ala-Gln or Gly-Sar dipeptide was added at a molar equivalent corresponding to the excess acrylate. The solutions were then stirred at 30°C for a subsequent 6 hours. Polymers were precipitated in cold diethyl ether spiked with glacial acetic acid and then vortexed to aggregate the polymer. The excess solvent was discarded. Following this, polymers were washed twice in fresh diethyl ether and allowed to dry under vacuum for 24 hours at room temperature. Polymers were aliquoted into single-use aliquots and stored at -80°C.

Table 2.3 Monomers used for PBAE synthesis.

Monomers			Cas number	Supplier, Catalog number
	Symbol	Chemical name		
Polymer backbone	Diacrylate (DD)	Bisphenol A glycerolate	4687-94-9	Sigma, 411167
	Backbone amine (90)	4-(2-Aminoethyl) morpholine	2038-03-1	Sigma, A55004
	Branching amine	N-methyl 1,3-diaminopropane	6291-84-5	Sigma, 127027
End cap groups	End cap amine (118)	1,5 diamino 2 methylpentane	15520-10-2	Sigma, 329665
	Gly-Sar	Glycyl-sarcosine	29816-01-1	Sigma, G3127
	Ala-Lys	Alanyl-lysine hydrochloride	68973-27-3	Sigma, A2003
	Ala-Ala	L-alanyl-L-alanine	1948-31-8	Sigma, A9502
	Ala-Gly	Alanyl-glycine	687-69-4	Sigma, A0878

2.7.4 Proton Nuclear Magnetic Resonance (^{1}H NMR)

Polymers were dissolved in deuterated dimethyl sulfoxide (d6-DMSO) (Sigma, 716731) at 100 mg/mL. Polymer solutions were transferred to 178 mm NMR tubes (Norell, 507-HP-7) and spectra were acquired using the 500 MHz Avance III™ NMR Spectrometer (Bruker). Data were processed using the MestReNova software (MestRelab Research, version 14.3.3). NMR spectra acquisition and processing was performed by Leigh-Anne Gavin.

2.8 Non-viral mRNA transfection of cell lines, submerged and ALI cultured primary HBECs

Twenty-four hours prior to transfection, cells were seeded in PureCol® bovine collagen (30 µg/mL) coated 96-well plates/transwell inserts/8-well chamber slides using the appropriate cell culture medium detailed in Table 2.2. Specifically, cells were seeded at 12,000 cells/well of a 96-well plate in 100 µL volume per well, 30,000 cells/transwell insert in 200 µL volume per transwell insert, 50,000 cells/well of an 8-well chamber slide in 200 µL volume per well. Before cell transfection, appropriate fresh media was added to the cells (Table 2.2). mRNAs used in

this thesis are listed in Table 2.4. Firefly Luciferase (FLuc) mRNA transfections were performed in cells seeded in 96-well white bottom plates (Corning, 3917) and in transwell inserts. Cyanine 5-tagged mRNA encoding Green Fluorescent Protein (Cy5-GFP) and GFP mRNA transfections were performed in cells seeded in 8-well chamber slides (Thermo Fisher Scientific, 154534) and transwell inserts. FOXJ1 mRNA transfections were performed in cells seeded in 96-well clear bottom plates (Corning, 3596), transwell inserts and 8-well chamber slides.

For transfection experiments performed in peptide-supplemented media, Gly-Sar dipeptide was prepared at a concentration of 3 µg/mL in appropriate cell culture media, whereas Ala-Lys dipeptide was prepared at a concentration of 4 µg/mL in appropriate cell culture media.

Table 2.4 Commercial mRNAs used in transfection experiments.

mRNA	Stock concentration	Supplier, Catalog number	Structural components
FLuc (1929 nucleotides)	1 mg/mL	TriLink, L-7202	Cap1, polyadenylated, 5moU
FLuc	1 mg/mL	OzBiosciences, MRNA12	Cap1, polyadenylated, 5moU
FLuc	1 mg/mL	RiboPro, RB-015	Cap0, polyadenylated, no modification
FLuc	1 mg/mL	ApexBio, R1005	ARCA, polyadenylated, 5moU
Cy5-GFP	1 mg/mL	Trilink, 7701-100	Cap1, polyadenylated, 5moU
GFP (996 nucleotides)	1 mg/mL	TriLink, L-7201	Cap1, polyadenylated, 5moU
FOXJ1 (1709 nucleotides)	1 mg/mL	OzBiosciencces, custom synthesised	Cap1, polyadenylated, 5moU

mRNA was diluted in nuclease-free water (Invitrogen, 11538646) to the desired concentration (50/100/200 ng per well). For PBAE transfections, branched PBAE was used in transfection experiments described in Chapters 3 and 4, whereas linear PBAEs and peptide-modified PBAEs were used in Chapter 5. Unless specified, PBAE stock solutions, originally at 100 mg/mL in DMSO, were thawed at room temperature for 15 minutes and diluted to a concentration of 50 mg/mL in DMSO (Sigma, 276855). Next, PBAEs were diluted in appropriate buffer and concentration as shown in Table 2.5. PBAEs were further diluted at appropriate polymer to mRNA mass ratio as demonstrated in Table 2.5, and then complexed with diluted mRNA at 1:1 ratio. Formulations were mixed gently by pipetting up and down 5 times and incubated at room temperature for 10 minutes. For the 100 mM sodium acetate buffer (NaOAc) (Sigma, S7899) formulation, branched PBAE was diluted in 100 mM NaOAc, then complexed with mRNA (1:1) and polyplexes subsequently diluted in PBS at a 1:4 ratio, resulting in a final NaOAc concentration of 25 mM.

Table 2.5 PBAE formulations.

Chapter	PBAE	Buffer formulation – PBAE concentration	PBAE:mRNA mass ratio
3	Branched PBAE (DD90-118)	• PBS - 10 mg/mL (Gibco, 14190250) • NaCl - 10 mg/mL (Sigma, S8776) • 25 mM NaOAc - 10 mg/mL (Sigma, S7899) • 100 mM NaOAc/PBS - 10 mg/mL	20:1, 50:1
4	Branched PBAE (DD90-118)	100 mM NaOAc/PBS – 10 mg/mL	50:1
5	Linear PBAEs (DD90-118 1.2, DD90-118 1.05)	PBS – 1 mg/mL	50:1
5	Peptide-modified PBAEs (DD90-Gly-Sar, DD90-Ala-Lys, DD90-Ala-Ala, DD90-Ala-Gly)	PBS – 1 mg/mL	50:1

For transfection experiments using the commercial transfection reagent jetMESSENGER® (Polyplus, 101000005), the supplier's recommended protocol was followed. Briefly, mRNA was diluted in mRNA buffer provided with the kit to the desired concentration, and then jetMESSENGER reagent was added to the mixture and mixed gently by pipetting up and down. The formulations were incubated at room temperature for 15 minutes before transfection. jetMESSENGER formulations were prepared at a ratio of 0.5 : 50 : 1 [mRNA (µg) : mRNA buffer (µL) : jetMESSENGER (µL)] according to the suppliers protocol.

Lipofectamine 2000 (Invitrogen, 11668030) was prepared at 4 to 1 ratio of Lipofectamine 2000 to mRNA in OptiMEM Reduced Serum Media (Gibco, 319850700). Subsequently, diluted mRNA was combined equally with the diluted Lipofectamine 2000. After a gentle mix, the formulations were incubated at room temperature for 5 minutes before transfection.

The commercial transfection reagent jetPEI® (Polyplus, 101000053) was prepared according to the manufacturer's guidelines. Briefly, mRNA was diluted in an appropriate volume of 150 mM NaCl buffer provided with the kit. In another tube, jetPEI reagent was diluted in 150 mM NaCl. The diluted jetPEI was then added to the diluted mRNA and mixed gently by pipetting up and down. The formulations were incubated for 30 minutes at room temperature before transfection. jetPEI formulations were prepared at a ratio of 1 : 50 : 2 : 50 [mRNA (µg) : NaCl buffer (µL) : jetPEI reagent (µL) : NaCl buffer (µL)] according to the suppliers protocol.

For transfections using naked mRNA, mRNA was diluted at the desired concentration in sterile nuclease-free water and then added to the cells. Vector-only controls were prepared at the appropriate mass ratio as shown in Table 2.5 and then combined in a 1:1 ratio with sterile nuclease free water before adding to cells.

For transfections in 96-well plates, each transfection reagent was prepared at a concentration of 50/100/200 ng mRNA/15 µL. 15 µL of complexes was then added to each well, bringing the total medium volume to 150 µL. For transfections in 8-well chamber slides or transwell inserts, each transfection reagent was prepared at a concentration of 100/200 ng mRNA/30 µL. 30 µL of complexes was then added to each well, bringing the total medium volume to 200 µL.

Four hours after transfection, the existing cell culture media with complexes was discarded and replaced with fresh, pre-warmed media suitable for the specific cell type (Table 2.2). Cells were returned to a humidified incubator at 37°C with 5% CO_2 until further post-transfection assays.

2.9 Non-viral vector/mRNA particles characterisation

2.9.1 Dynamic Light Scattering (DLS)

Particles were prepared as described in methods for non-viral mRNA transfections (section 2.8). The size and zeta potential of the particles was determined by DLS using a Zetasizer NanoZSP (Malvern Instruments). For size measurements, particles were diluted 1 in 10 in deionised water (final volume 100 µL) and added to disposable sizing cuvettes (VWR, 612-5686) for analysis. For zeta potential measurements, particles were diluted 1 in 10 in deionised water (final volume 600 µL) and added to disposable zeta cuvettes (Malvern, DTS1070) for analysis.

2.9.2 mRNA encapsulation efficiency assay

mRNA encapsulation efficiency was determined using the Quant-iT™ RiboGreen™ RNA Kit (Invitrogen, R11490) following the manufacturer's protocol with slight modification. TE working solution was prepared by diluting the concentrated buffer provided with the kit 20-fold with nuclease-free water. Quant-iT™ RiboGreen™ RNA reagent was prepared by diluting the concentrated stock solution 200-fold with TE working solution. Unformulated mRNA solution at 2 µg/mL in TE working solution was further diluted to prepare the mRNA standard curve according to the supplier's instructions. Particles were prepared as described in section 2.8 to a final mRNA concentration of 2 µg/mL. Particles were diluted in TE to a final volume of 500 µL, followed by 1:1 addition of Quant-iT™ RiboGreen™ RNA reagent working solution. Thereafter, the mixture was centrifuged at 8000 x g for 5 minutes to pellet the particles and 100 µL of supernatant was transferred to a black bottom 96-well plate. Fluorescence of samples and mRNA standard curve was measured using the SpectraMax® i3 plate reader (Molecular Devices) at 480 nm excitation and 520 nm emission. The maximum fluorescence signal came from the free non-encapsulated mRNA positive control (0% encapsulation efficiency). Percentage encapsulation efficiency was calculated using the following formula:

$$\boldsymbol{mRNA\ encapsulation\ efficiency} = \mathbf{1} - \frac{(\boldsymbol{sample\ fluorescence - negative\ control\ fluorescence})}{\boldsymbol{positive\ control\ fluorescence}}$$

2.9.3 Gel electrophoresis

Particles were formulated to a final mRNA concentration of 200 ng in 200 µL volume following the method outlined in section 2.8. 20 µL of particles or naked mRNA was loaded into an E-gel™ Ex 2 % Agarose Gel (Invitrogen, G401002). The Riboruler™ High RNA ladder (ThermoFisher Scientific, SM1821) was also loaded as reference. The E-Gel™ Power Snap Electrophoresis System (Invitrogen, G8300) was run for 15 minutes. The gels were imaged using the iBright 1500 system (Invitrogen).

2.10 Biological assays

2.10.1 Luminescence assay & luciferase protein quantification

The BrightGlo™ Luciferase Assay System (Promega, E2620) was used to assay luminescence in FLuc mRNA transfected primary HBECs. The BrightGlo™ reagent was thawed at room temperature and mixed equally with 1X PBS. After preparing the BrightGlo™/PBS mix, 100 µL was added to each well of a 96-well plate for submerged cultured cells. The plate was covered and incubated at room temperature for 5 minutes to allow complete cell lysis and stabilisation of the luminescent signal. Luminescence was then measured using the SpectraMax® i3 plate reader (Molecular Devices), with an integration duration of 10000 milliseconds. For luciferase protein quantification, a calibration curve was generated using serially diluted QuantiLum® Recombinant Luciferase (Promega, E1701) in BrightGlo™ reagent. The luminescence readings of both the samples and the standard curves were taken simultaneously, and the luciferase protein quantities were interpolated from the standard curve of the QuantiLum® Recombinant Luciferase.

FLuc mRNA transfected cells cultured at ALI were detached from transwell inserts using TrypLE (section 2.3). The cell suspension was centrifuged at 1500 rpm for 5 minutes to pellet the cells. The pellet was resuspended in 150 µL reporter lysis buffer (Promega, E3971). The tubes with resuspended cells were frozen at -80^{o}C and then thawed once. After a brief 10-15 second vortex, the tubes were centrifuged at 1500 rpm for 3 minutes. Post-centrifugation, cells were lysed, releasing their intracellular proteins into the supernatant. 50 µL of supernatant was transferred to a white-bottom 96-well plate for the BrightGlo™ assay described above. 50 µL of BrightGlo™ reagent was added to each well and after 5 minutes of incubation luminescence was measured. 25 µL of supernatant was used to quantify total protein concentration in lysates (section 2.10.4).

2.10.2 Cytotoxicity assay

The Lactate Dehydrogenase (LDH) assay (Roche, 11644793001) was used to assess cellular cytotoxicity following the supplier's protocol. Briefly, culture supernatants were collected, then mixed with a reaction mixture, and incubated for 10 minutes at 37°C. Absorbance was measured at 490 nm wavelength using the SpectraMax® i3 plate reader (Molecular Devices). The following controls were included in each experiment; positive control: cells treated with 1% Triton-X-100 (Sigma, T8787) in the relevant cell culture medium for 4 hours to induce maximum LDH release, negative control: relevant cell culture medium alone (without cells), spontaneous LDH release control: untreated cells. The following modified formula was used to calculate % LDH release in the samples relative to the positive control (100% cell death-cytotoxicity):

$$\boldsymbol{LDH\ release\ } = \frac{(\boldsymbol{Sample\ absorbance - Negative\ control\ absorbance})}{(\boldsymbol{Positive\ control\ absorbance - Negative\ control\ absorbance})} * \boldsymbol{100}$$

2.10.3 Cell viability assay

Cell viability was assessed using the PrestoBlue cell viability reagent (Invitrogen, A13261) according to the supplier's protocol. A mixture of PrestoBlue reagent and appropriate pre-warmed cell culture media was prepared at a 9:1 ratio. This diluted reagent was then added into a 96-well plate containing the cells. The plate was incubated for 30 minutes at 37°C and 5% CO_2 in a humidified incubator. To minimise light interference, the plate was covered during the incubation period. After incubation, fluorescence measurements were obtained using the SpectraMax® i3 plate reader (Molecular Devices) at excitation and emission wavelengths of 560 nm and 590 nm, respectively. To account for background fluorescence, the measurements obtained from the negative control wells containing only media (no cells) and reagent were substracted from the fluorescence readings of each experimental well. The cell viability was calculated as a percentage relative to the viability of non-transfected cells (100% cell viability), using the following formula:

$$\boldsymbol{Cell\ viability} = \frac{(\boldsymbol{Sample\ fluorescence - Negative\ control\ fluorescence})}{(\boldsymbol{Non-transfected\ cell\ fluorescence - Negative\ control\ fluorescence})} * \boldsymbol{100}$$

2.10.4 Protein quantification

The Pierce™ BCA protein assay kit (Thermo Fisher Scientific, 23227) was used to determine protein concentration in cell lysates according to the supplier's protocol. The bicinchoninic acid (BCA) working reagent was prepared by mixing reagent A and B in a ratio of 50:1. Next, a protein standard curve was prepared by diluting the provided protein standard to produce a series of known concentrations. 25 µL of each standard and sample was added to each well of a 96-well plate. 200 µL of the prepared BCA working reagent was added to each standard and sample. All standards and samples were run in triplicates. Solutions were mixed thoroughly and incubated at 37^{o}C for 30 minutes, allowed to cool to room temperature and absorbance was measured at a wavelength of 562 nm using the SpectraMax® i3 plate reader (Molecular Devices). The protein concentrations of the samples were interpolated from the standard curve.

2.11 Gene expression analysis

2.11.1 Cell harvesting & RNA isolation

Cells were lysed in RLT Plus buffer with 1% 2-mercaptoethanol (100 µL/well of a 96-well plate for submerged cultured cells, 200 µL/transwell insert for ALI cultured cells). RNA was extracted using the RNeasy Micro Plus kit (Qiagen, 74034) according to the manufacturer's protocol. RNA concentration and purity were evaluated using the NanoDrop™ 1000 spectrophotometer (Thermo Fisher Scientific). RNA samples were stored at -80^{o}C.

2.11.2 cDNA synthesis

RNA (10 µL/reaction) was reverse transcribed into complementary DNA (cDNA) using the High-Capacity cDNA Reverse Transcription Kit (Thermo Fisher Scientific, 4374966) according to the supplier's protocol. Table 2.6 shows the components needed to prepare the reverse transcription master mix. The thermal cycler conditions are summarised in Table 2.7. cDNA samples were diluted in nuclease-free water (1:4 dilution) and stored at -20^{o}C.

Table 2.6 cDNA synthesis reactions.

Component	Volume/reaction (µL)
10X RT buffer	2
25X dNTP mix	0.8
10X RT random primers	2
Reverse transcriptase	1
Nuclease-free water	4.2
Total per reaction	**10**

Table 2.7 Thermal cycler conditions for cDNA synthesis.

	Step 1	Step 2	Step 3	Step 4
Temperature (°C)	25	37	85	4
Time	10 minutes	120 minutes	5 minutes	∞

2.11.3 Quantitative polymerase chain reaction (qPCR)

qPCR reactions were prepared using TaqMan™ FAM probes (Thermo Fisher Scientific) and Fast Advanced Master Mix (Thermo Fisher Scientific, 4444557) (Table 2.8). TaqMan™ assay IDs used throughout the thesis are listed on Table 2.9. All conditions were run in duplicates in a 384-well format using the ViiA™ 7 Real-Time PCR System (Thermo Fisher Scientific, Software version 1.2.3) following the supplier's recommended settings (Table 2.10). The QuantStudio™ Real-Time PCR software (Thermo Fisher Scientific, Software version 1.7.2) was used to determine cycle threshold (CT) values. Relative expression of each gene was calculated using the following formula. Actin beta (*ACTB*) was used as the housekeeping gene.

$$\boldsymbol{Relative\ Expression = 2^{-\Delta CT}}$$

$$\boldsymbol{Where\ \Delta CT = CT\ (gene\ of\ interest) - CT\ (housekeeping\ gene)}$$

Table 2.8 Reaction set-up for qPCR.

Component	Volume per well (µL)
Fast Advanced Master Mix	3.0
TaqMan™ FAM probe	0.3
Nuclease-free water	0.3
Diluted cDNA	2.4

Table 2.9 Human TaqMan™ gene expression assays.

Gene symbol	Gene name	TaqMan™ Assay ID
ACTB	Actin beta	Hs01060665_g1
SCGB1A1	Secretoglobin family 1A member 1	Hs00171092_m1
KRT5	Keratin 5	Hs00361185_m1
FOXJ1	Forkhead box protein J1	Hs00230964_m1
MUC5AC	Mucin 5AC	Hs01365616_m1
MUC5B	Mucin 5B	Hs00861595_m1
TJP1	Tight junction protein 1	Hs01551861_m1
CDH1	Cadherin 1	Hs01023895_m1
OCLN	Occludin	Hs05465837_g1
SLC15A2	Solute carrier family 15 member 2	Hs01113665_m1
CETN2	Centrin 2	Hs00942570_g1
DNAH11	Dynein axonemal heavy chain 11	Hs00361951_m1
DNALI1	Dynein axonemal light intermediate chain 1	Hs00185750_m1
DYNC2H1	Dynein cytoplasmic 2 heavy chain 1	Hs00300261_m1
RFX2	Regulatory factor X2	Hs00172177_m1
RFX3	Regulatory factor X3	Hs00231292_m1
RSPH9	Radial spoke head component 9	Hs01040988_m1
TUBA1A	Tubulin alpha 1a	Hs03045184_g1

Table 2.10 Thermal cycler conditions for qPCR.

			PCR (40 cycles)	
	Hold	**Hold**	**Denature**	**Anneal/extend**
Temperature	50°C	95°C	95°C	60°C
Time (minutes:seconds)	02:00	00:20	00:01	00:20

2.12 Characterisation of peptide transporter 2 in primary HBECs

2.12.1 Uptake of Ala-Lys-AMCA dipeptide

The fluorescence dipeptide Ala-Lys-AMCA (MedChemExpress, HY-111956B) was prepared at concentrations of 50 µM, 100 µM and 200 µM in PBS. Primary HBECs were exposed to 3 different concentrations of Ala-Lyc-AMCA dipeptide (100 µL/well). After 1 hour incubation at 37^{o}C, the uptake of dipeptide was terminated by washing the cells three times with ice-cold PBS. Fluorescence was measured using the SpectraMax® i3 plate reader (Molecular Devices) with excitation at 350 nm and emission at 455 nm.

2.12.2 Exposure to Cefadroxil

Cefadroxil (ApexBio, C3991-APE) was prepared at concentration of 1 mM in appropriate cell culture medium (Table 2.2). Primary HBECs were pre-incubated with Cefadroxil (100 µL/well) for 10-60 minutes at 37^{o}C prior to exposure to Ala-Lys-AMCA dipeptide as described in section 2.12.1 above. Alternatively, primary HBECs were pre-incubated with 1 mM Cefadroxil for 20 minutes at 37^{o}C prior to transfection with peptide-modified PBAEs or transfected with peptide-modified PBAEs in media containing 1 mM Cefadroxil. Transfection of primary HBECs with peptide-modified PBAEs is described in section 2.8.

2.13 Immunofluorescence

2.13.1 Fixation

Cells were fixed with 4% PFA in PBS (200 µL per well in 8-well chamber slides, 200 µL per transwell insert) for 20 minutes at room temperature and washed three times with 1X PBS. Fixed cells were stored in PBS at 4^{o}C until staining.

2.13.2 Immunofluorescence staining

2.13.2.1 Submerged cells on 8-well chamber slides

Fixed cells were permeabilised and blocked with 10% appropriate serum (normal goat serum: Abcam - ab7481, normal donkey serum: Abcam - ab7475) and 0.1% Triton X-100 (Sigma, 8787) in 1X PBS for 1 hour at room temperature. The serum of the species in which the secondary antibody was raised in was utilised. Permeabilisation/blocking step was followed by three five-minute washes in 1X PBS. Cells were incubated with primary antibodies diluted in 1% BSA (Sigma Aldrich, A7030) in PBS overnight at 4^{o}C. Cells were washed with 1X PBS and icubated with secondary antibodies diluted in 1% BSA in 1X PBS for 1 hour at room temperature and protected from light. Following secondary antibody staining, cells were

washed three times in 1X PBS and counterstained with DAPI (Invitrogen, D1306) diluted 1:2000 in 1X PBS for 10 minutes at room temperature in the dark. Lastly, the chamber was removed, and cells were mounted using ProLong™ Diamond Antifade Mountant (Invitrogen, P36961) and a coverslip. Slides were allowed to cure at room temperature for 24 hours before imaging or longer-term storage at 4^{o}C and protected from light. A list of antibodies used for immunofluorescence staining experiments in this thesis is shown in Table 2.11.

2.13.2.2 Primary HBECs cultured at ALI (wholemount)

Cells seeded on transwell inserts were permeabilised, blocked and stained as described in section 2.13.2.1 above. Following DAPI staining, the membrane was cut from each transwell insert using a scalpel and mounted on a glass slide using ProLong™ Diamond Antifade Mountant and a coverslip. Slides were cured overnight in the dark at room temperature before imaging or storage at 4^{o}C and protected from light.

2.13.2.3 Primary HBECs cultured at ALI (cross-sections)

Prior to permeabilisation and blocking, paraffin-embedded sections were passed through two changes of D-Limonene (Gentaclear, 433C) for 5 minutes each. Sections were rehydrated by sequentially immersing them in ethanol solutions of diminishing concentration: 100%, 90%, and 70%, each for a duration of 1 minute, and subsequently in PBS. For heat-induced antigen retrieval, slides were immersed in a 90^{o}C EDTA buffer solution (1mM EDTA, pH 8, Sigma, 3690) and were kept covered during the 30-minute incubation period. ALI cross-sections underwent permeabilisation, blocking, and staining as detailed in section 2.13.2.1 above. Sections were mounted using ProLong™ Diamond Antifade Mountant. Before imaging or storage at 4^{o}C, slides were given 24 hours to cure at room temperature protected from light.

2.13.3 Image acquisition and quantification

Fluorescence images were acquired using Leica SP5 inverted confocal microscope or Aperio VERSA 8 slide scanner. Images were processed using ImageJ software for cropping, brightness and contrast adjustments and addition of scale bars. In addition, the counting macro and automatic quantification setting of ImageJ software was used to count the number of positive cells for each marker of interest as well as the total number of cells (DAPI positive nuclei) in each image.

Table 2.11 Antibodies used for immunofluorescence staining experiments.

Marker	Host/Clone	Supplier, Catalog number	Fluorochrome	Dilution
Primary antibodies				
Acetylated alpha tubulin	Mouse/6-11B-1	Abcam, ab24610	unconjugated	1:100
Mucin 5AC (MUC5AC)	Rabbit/polyclonal	Abcam, ab78660	unconjugated	1:100
Cytokeratin 5 (KRT5)	Rabbit / EP1601Y	Abcam, ab52635	unconjugated	1:100
Zonula occludens 1 (ZO-1)	Mouse/ZO1-1A12	Thermo Fisher Scientific, 33-9100	unconjugated	1:100
Forkhead box protein J1 (FOXJ1)	Goat/polyclonal	R&D systems, AF3619	unconjugated	1:100
Uteroglobulin/ Secretoglobin family 1A member 1 (SCGB1A1)	Rat/394324	R&D systems, MAB4218	unconjugated	1:100
Peptide transporter 2 (PEPT2)	Rabbit/polyclonal	Novus Biologicals, NBP1-59626	unconjugated	1:250
Secondary antibodies				
Goat anti-rabbit IgG	Thermo Fisher Scientific, A21428		Alexa Fluor 555	1:500
Goat anti-rabbit IgG	Thermo Fisher Scientific, A11008		Alexa Fluor 488	1:500
Goat anti-mouse IgG	Thermo Fisher Scientific, A11001		Alexa Fluor 488	1:500
Goat anti-mouse IgG	Thermo Fisher Scientific, A21422		Alexa Fluor 555	1:500
Goat anti-rat IgG	Thermo Fisher Scientific, A11006		Alexa Fluor 488	1:500
Goat anti-rat IgG	Thermo Fisher Scientific, A21434		Alexa Fluor 555	1:500
Donkey anti-goat IgG	R&D systems, NL001		NorthernLights™ 557	1:200

2.14 Statistical Analysis

Data analyses and graph generation were performed using GraphPad Prism (software version 9.5.1). Data are primarily presented as mean ± standard deviation (SD), with detailed data representation provided in figure legends. Individual data points are shown where possible. Data distribution was evaluated using the D-Agostino-Pearson normality test. Parametric analyses, such as One-way ANOVA, were employed for data following a Gaussian distribution. Non-parametric analyses, such as Kruskal-Wallis test, were used for data that did not adhere to this distribution. The specific statistical test employed for each experiment is indicated in the corresponding figure legend, with P values ≤ 0.05 considered statistically significant. The number of technical and biological replicates used for each experiment is specified in the figure legend. Statistical analysis was not feasible for data with only three technical replicates.

3 Results I - Evaluating reporter mRNA delivery to primary HBECs using non-viral vectors and its impact on epithelial integrity and differentiation

3.1 Introduction

3.1.1 PBAEs for mRNA delivery to the lung

mRNA-mediated transgene overexpression is an emerging and powerful tool for understanding gene function and developing novel therapies for a variety of diseases[464]. However, one of the significant challenges in its application is the inherent instability of mRNA and its susceptibility to degradation by RNases[465]. These obstacles hinder effective delivery into cells. To address these challenges, advanced delivery methods are essential to protect mRNA from degradation by RNases, promote cellular uptake, and facilitate endosomal escape.

Among non-viral delivery methods, PBAEs have gained attention as effective vehicles for mRNA delivery due to their unique properties[466]. PBAEs are cationic polymers capable of condensing mRNA into nanoparticles, which facilitates cellular uptake and protects mRNA from degradation[467,468]. PBAEs are also biodegradable and can be synthesised easily using commercially available monomers[467]. Their application in pulmonary mRNA delivery has shown significant results. For instance, intravenous injection of PBAE-mRNA complexes has achieved mRNA delivery to mouse lungs[469–471]. PBAEs are also physically and chemically versatile, allowing modifications in their structure, molecular weight, and end-cap chemistry[472,473]. These modifications can influence key properties like solubility, stability, and transfection efficiency. For example, Patel *et al.* demonstrated that structural manipulation of PBAEs to create branched polymers enhanced their solubility, which is an important property for nebulised delivery of mRNA to lung epithelium in mice[463]. These branched PBAEs remained stable and achieved higher transfection efficiency with minimal toxicity following inhalation, compared to linear PBAEs and the commercial vector PEI. However, the use of branched PBAEs in mRNA delivery to primary HBECs has not been explored. This study aimed to address this gap by evaluating the potential of branched PBAEs as mRNA delivery vectors for HBECs.

3.1.2 Optimising formulations of non-viral vectors to improve *in vitro* performance

Gene delivery efficacy is highly dependent on both the intrinsic characteristics of the delivery vector and the careful optimisation of formulation parameters[474]. A crucial factor in this process is the mass ratio of PBAE to mRNA, which indicates the charge ratio between the positively charged polymer and the negatively charged mRNA. The ratio influences various aspects of gene delivery, including the binding strength between PBAE and mRNA, the stability and cellular uptake of the polyplexes formed, and their cytotoxicity[475–478]. A higher PBAE

concentration may lead to increased polymer-related cytotoxicity, while a low PBAE concentration may not be sufficient to form stable nanoparticles. Studies have shown that the optimal PBAE to nucleic acid mass ratio varies depending on both the cell type and the nucleic acid delivered. For example, Patel *et al.* found that a 50:1 PBAE to mRNA mass ratio was most effective for gene delivery to A549 alveolar epithelial cell line[463], whereas Fornaguera *et al.*, found a 25:1 ratio optimal for gene delivery to BEAS-2B and ARPE-19 cell lines[479]. Therefore, it is crucial to optimise the PBAE to mRNA mass ratio for each gene delivery application. This can be achieved by evaluating factors like mRNA encapsulation efficiency, transfection efficiency, and cytotoxicity of polyplexes prepared with different PBAE to mRNA mass ratios.

Buffer selection is another vital factor in formulating PBAE nanoparticles. The ionic strength and pH of the buffer can affect the nanoparticles' physicochemical properties, such as size, charge, stability, which can impact transfection efficiency[480]. For instance, Chivu *et al.* showed that nanoparticles formulated at pH 7.4 had higher zeta potential (surface charge) and cellular uptake than those formulated at pH 12[481]. Given PBAEs' susceptibility to degradation in aqueous solution, they are often formulated in a low-salt, acidic pH 5 sodium acetate (NaOAc) buffer to maintain the charge of the tertiary amines for complexation with mRNA[482]. While this buffer system is widely used, alternatives like magnesium and calcium acetate buffers have also shown promising transfection efficiencies[480]. However, the effectiveness of PBAEs in physiological pH 7.4 PBS or NaCl buffer remains unclear.

The physicochemical properties of polymeric nanoparticles, such as size and surface charge, are crucial for successful mRNA transfection[483–488]. The optimal size for endocytosis and cellular uptake is typically between 100-200 nm[489]. The surface charge influences both the stability of polyplexes and their interaction with negatively charged cellular membranes[490]. PBAE/mRNA polyplexes with a moderate positive charge facilitate electrostatic interactions with cell membranes, promoting cellular uptake. However, an excessively high positive charge can lead to cytotoxicity[491]. Therefore, carefully balancing the size and charge of these polyplexes is essential for maximizing transfection efficiency while minimizing cytotoxicity.

This project investigated the ability of branched PBAEs to deliver mRNA to primary HBECs and optimise their formulations (PBAE to mRNA mass ratio and buffer formulation) to achieve stable, positively charged nanoparticles below 200 nm in size for efficient delivery. Nanoparticles were formulated in different buffers (NaOAc, PBS, NaCl, and NaOAc/PBS) at 20:1 or 50:1 PBAE to mRNA mass ratios. Critical parameters such as mRNA condensation, polyplex size, surface charge, and stability were assessed to determine their collective impact on transfection efficiency.

3.1.3 ALI culture model

As previously mentioned in section 1.4.2, culturing primary HBECs at ALI leads to the formation of a polarised, pseudostratified columnar epithelium, composed of ciliated and secretory cells. ALI cultures address the limitations of traditional submerged monolayer models for culturing HBEC. Monolayer models fail to replicate key features of a differentiated airway epithelium, such as cellular composition, mucus production and secretion, and barrier function[492]. In contrast, ALI cultures effectively mimic these characteristics. Furthermore, differentiated ALI cultures closely resemble the *in vivo* airway epithelium at transcriptional level, making them a valuable *in vitro* tool for investigating the molecular mechanisms behind HBEC differentiation and function[493–495]. Additionally, they provide a platform for manipulating gene expression, allowing researchers to model diseases or test potential therapeutic applications.

3.1.4 Gene delivery to ALI cultures

Manipulating gene expression in primary HBECs provides a powerful tool for investigating gene functions, understanding disease pathogenesis, and identifying potential therapeutic targets. However, despite advancements in nucleic acid technologies, gene manipulation in polarised, pseudostratified differentiated ALI epithelial cultures faces challenges due to inefficient delivery of nucleic acid-based reagents (e.g. plasmids[496,497], double-stranded oligonucleotides[498–501], and single-stranded oligonucleotides[498,499]).

To overcome the challenges of delivering genes to polarised, pseudostratified, and differentiated primary airway epithelia, researchers have developed several effective methods. One such method, known as reverse transfection, involves adding the oligonucleotide reagents to primary epithelial cells at the seeding stage[501]. This method has successfully reduced gene expression, such as *CXCL8* and *CFTR*, for up to two weeks post-transfection, without compromising cell viability or epithelial integrity. Another approach, small interfering RNA (siRNA) passive transfection, relies on adding siRNAs to the basolateral side of ALI cultures during differentiation[502]. This method has been effective in decreasing the expression of target genes for up to 21 days without affecting differentiation or epithelial barrier resistance. Additionally, Rapiteanu *et al*. developed a transient, plasmid- and virus-free CRISPR/Cas9 delivery system for primary HBECs differentiated at ALI, which maintains high gene editing efficiency and protein depletion for up to 28 days without impacting barrier formation or differentiation[503]. These advances in gene delivery and manipulation techniques have opened new avenues for exploring the role of genes in biological processes and disease pathogenesis, modelling airway diseases using the ALI model system, and identifying novel gene targets for therapeutic interventions.

Despite the increasing number of human clinical trials using therapeutic mRNA[504], relatively little is known about the impact of delivering and translating synthetic mRNA in the lung epithelium. While many studies have explored the impact of loss-of-function gene approaches on epithelial integrity and differentiation, there is a lack of research exploring the effects of synthetic mRNA delivery on the integrity and differentiation of bronchial epithelium in the published literature.

The aim of this chapter was to optimise branched PBAE formulations (buffer formulation, PBAE to mRNA mass ratio) to establish mRNA delivery to primary HBECs and determine the ability of HBECs from healthy individuals to generate protein from synthetic mRNA. Furthermore, this chapter explored the impact of reporter mRNA delivery on the integrity and differentiation of primary HBECs cultured at ALI.

3.1.5 Hypothesis and aims

Hypothesis

See page 100.

Aims

1. Optimise branched PBAE formulation (buffer, PBAE to mRNA mass ratio) for efficient mRNA delivery to primary HBECs, and characterise their mRNA encapsulation efficiency, size, charge, transfection efficiency and cytotoxicity.
2. Develop an ALI model of differentiated bronchial epithelium using primary HBECs.
3. Compare mRNA transfection efficiency of submerged and ALI cultures of primary HBECs using branched PBAE.
4. Assess the impact of reporter mRNA transfection on primary HBEC integrity and differentiation in ALI cultures of primary HBECs.

3.2. Results

3.2.1 Synthesis of branched DD90-118 based PBAE

Branched PBAE polymers were synthesised by Leigh-Anne Gavin as previously described[463]. Briefly, PBAEs were synthesised via Michael addition of diacrylate (DD) with primary amine monomers (90) and end-capped with terminal amines (118). A trifunctional amine was introduced into the reaction to generate branched PBAE (branched DD90-118) (Figure 3.1A-B). ^{1}H NMR was performed by Leigh-Anne Gavin to confirm the polymer's chemical structure (section 2.7.4, data not shown).

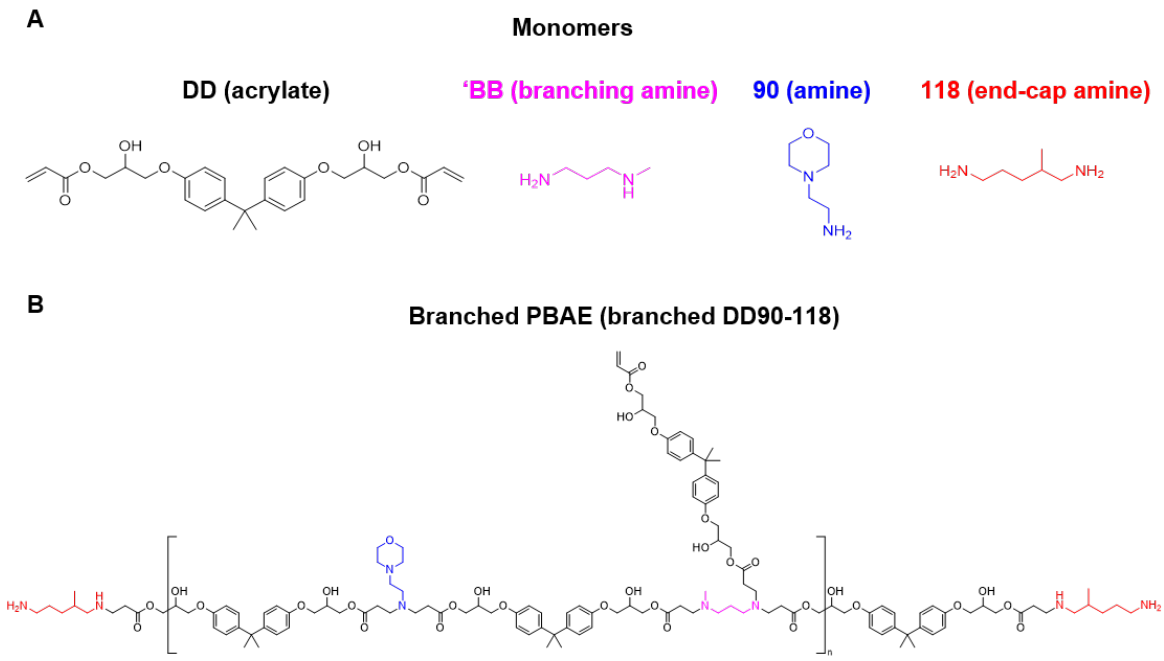


Figure 3.1 Synthesis schematic of branched poly (β-amino ester) (PBAE).
(A) Monomers used for branched PBAE (DD90-118) synthesis. (B) Chemical structure of branched PBAE. Synthesised by Leigh-Anne Gavin (Patel Group).

3.2.2 Branched PBAE mediates effective delivery of FLuc mRNA to 16HBE and A549 cell lines

To evaluate the ability of the newly synthesised branched PBAEs in delivering mRNA to airway epithelial cells, an initial assessment was conducted using the 16HBE cell line and reporter FLuc mRNA. Previous work by Patel et *al.* has shown that branched PBAEs are effective in facilitating the translation of IVT FLuc mRNA in the A549 cell line[505]. Consequently, alongside 16HBE cells, A549 cells were also transfected to serve as a comparator and positive control in this experiment. Luminescence and cytotoxicity were assessed 24 hours post-transfection.

Transfection efficiency as measured by luminescence is shown in Figure 3.2A and 3.2C. 16HBE and A549 cells were successfully transfected with FLuc mRNA complexed with branched PBAE (16HBE: $3.1x10^6$ RLU $\pm$ $6.9x10^4$, A549: $3.4x10^4$ RLU $\pm$ $8.6x10^3$). In both cell types, naked FLuc mRNA transfection was inefficient.

To evaluate the cytotoxicity of FLuc mRNA transfection in both 16HBE and A549 cells, an LDH release assay was performed on cell culture supernatants at 24 hours post-transfection (Figure 3.2B, 3.2D respectively). Both 16HBE and A549 cells showed a slight increase in LDH release following transfection with branched PBAE.

This data indicated that branched PBAE polymers effectively facilitated the translation of FLuc mRNA in both the A549 cell line, consistent with previous studies, and the 16HBE cell line. Data generated also showed that branched PBAE/FLuc mRNA transfection was well-tolerated in both cell lines. Given the project's aim to investigate mRNA delivery in bronchial epithelial cells, all subsequent optimisation experiments were focused exclusively in 16HBE cells.

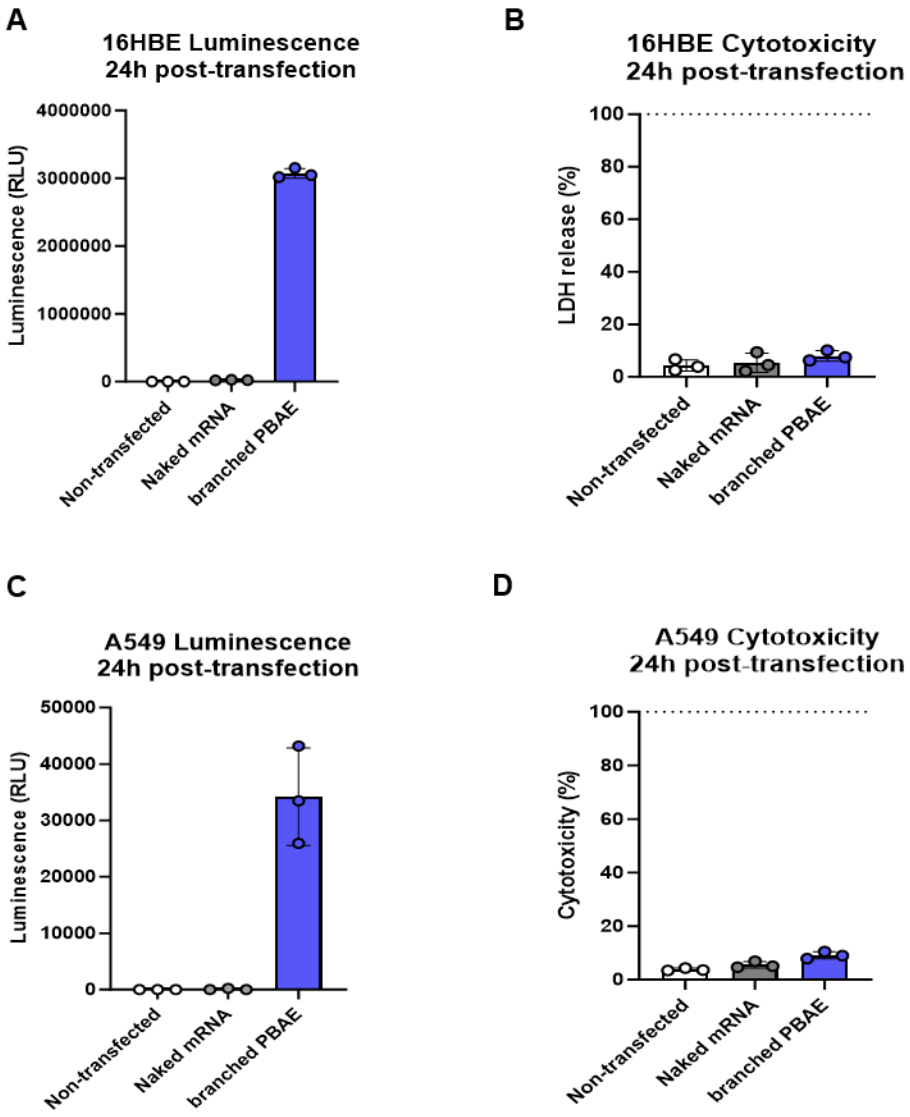


Figure 3.2 Transfection efficiency of branched poly (β-amino ester) (PBAE) on 16 human bronchial epithelial (16HBE) and A549 lung alveolar epithelial cell lines.

Firefly luciferase (FLuc) mRNA was complexed with branched PBAE or delivered naked to 16HBE and A549 cells. Luminescence was assessed 24 hours post-transfection in (A) 16HBE and (C) A549. Cytotoxicity measured by percentage lactate dehydrogenase (LDH) release in supernatants was assessed 24 hours post-transfection in (B) 16HBE and (D) A549. Dotted line indicates 100% LDH release of positive control cells treated with 1% Triton-X-100 and cytotoxicity was calculated relative to this control. Data represents mean ± SD. n = 3 technical replicates.

3.2.3 Determining the optimal DMSO concentration of dissolved PBAEs for transfection of 16HBE cells

To determine the optimal concentration of DMSO that ensures both high transfection efficiency and viability in 16HBE cells, branched PBAEs were prepared in concentrations of 25 mg/mL, 50 mg/mL, and 100 mg/mL DMSO. These solutions were then complexed with FLuc mRNA for transfection into 16HBE cells. While DMSO is essential for dissolving the polymer and thus enhancing transfection efficiency, its high concentrations can be toxic to cells[506]. Luminescence and cell viability were monitored over a 72-hour period following transfection. The commercial transfection reagent Lipofectamine 2000 was used as a positive control.

Transfection efficiency, as determined by luminescence, is shown in Figure 3.3A. Peak luminescence was observed at 24 hours post-transfection across all DMSO concentrations tested in cells transfected with PBAE. Naked FLuc mRNA transfection was ineffective. In contrast, cells transfected with Lipofectamine 2000, reached peak luminescence at 6 hours post-transfection.

This experiment also evaluated the effect of non-viral FLuc mRNA transfection on cell viability (Figure 3.3B). Lipofectamine 2000 transfection resulted in a reduction in cell viability from 24-72 hours post-transfection (>50%) compared to non-transfected cells. PBAE transfection led to a lesser decrease in cell viability (<50%) within the same timeframe (Figure 3.3B). Interestingly, transfection with PBAEs alone or naked mRNA maintained relatively stable viability levels, suggesting that the observed decline in cell viability might be due to the entry of mRNA/PBAE or mRNA/Lipofectamine 2000 polyplexes into the cells, or possibly due to the exogenous protein expression.

In summary, DMSO concentrations ranging from 25-100 mg/mL were found to be well-tolerated with comparable cell viability and transfection efficiency. Therefore, a concentration of 50 mg/mL DMSO was selected for subsequent experiments. This flexibility in DMSO concentration is valuable, as it can be adjusted to address potential solubility or toxicity challenges in future experiments.

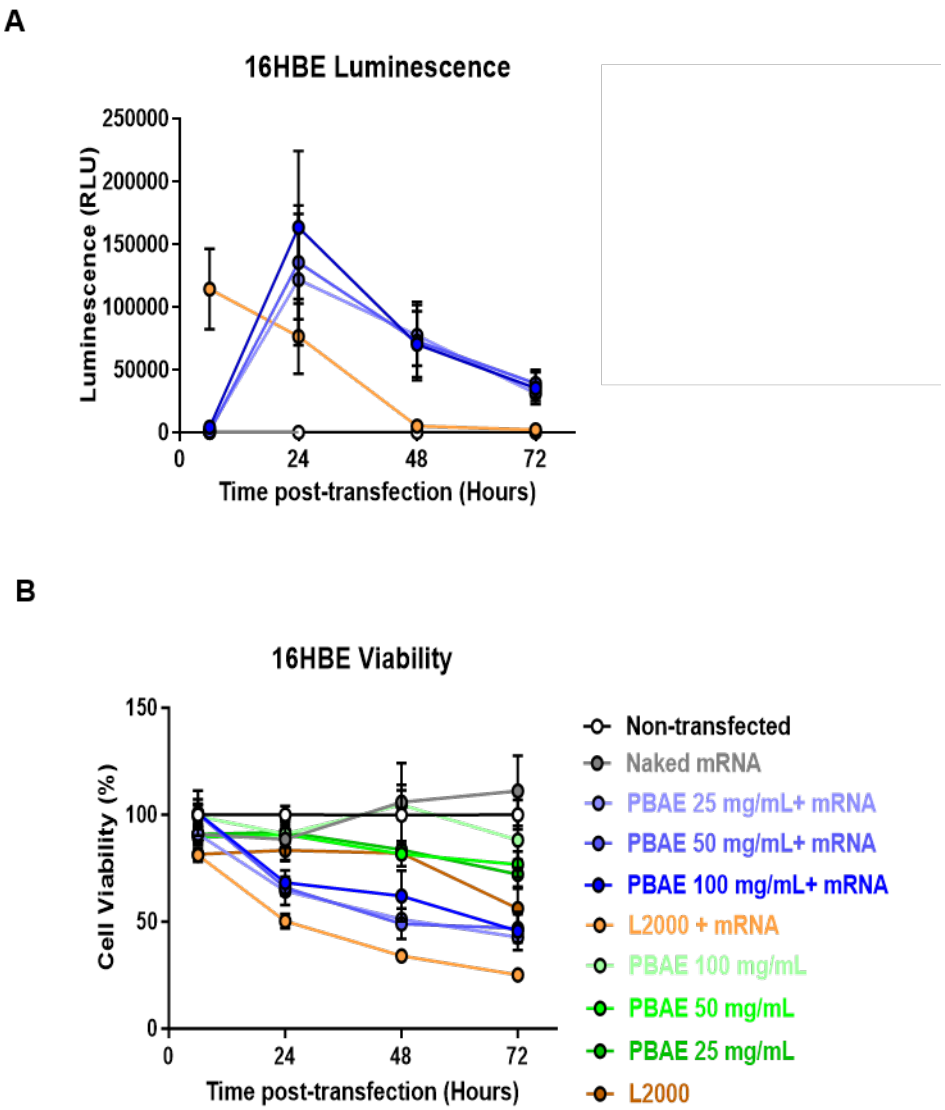


Figure 3.3 Optimal dimethyl sulfoxide (DMSO) concentration of dissolved branched poly (β-amino ester) (PBAE).

Firefly luciferase (FLuc) mRNA was complexed with branched PBAE formulated at three different DMSO concentrations (25, 50, 100 mg/mL), or commercial transfection reagent Lipofectamine 2000 (L2000), or delivered naked to 16 human bronchial epithelial (16HBE) cells. (A) Luminescence was assessed over 72 hours post-transfection. (B) Cell viability over 72 hours post-transfection was assessed using the Presto Blue cell viability assay. Data represents mean ± SD. n = 3 technical replicates.

3.2.4 Reporter mRNA transfection does not affect tight junction integrity in 16HBE confluent monolayers

16HBE cell line is a widely used model for studying epithelial barrier function due to its ability to form a polarised cell layer with tight junctions[507,508]. To determine whether reporter mRNA delivery affects the permeability of 16HBE confluent monolayers, a FITC-dextran permeability assay was performed comparing mRNA transfected cells to non-transfected controls. The paracellular flux of FITC-dextran from the apical to the basal chamber was similar across both groups 24 hours post-transfection, indicating that mRNA transfection does not adversely affect the permeability of the cell monolayers (Figure 3.4A).

Upon establishing tight junction formation in confluent 16HBE monolayers, immunofluorescence staining for the tight junction protein ZO-1 was performed, revealing no differences in the localisation of ZO-1 in mRNA transfected cells compared to non-transfected controls (Figure 3.4B). This indicates that mRNA transfection does not disrupt tight junctions in 16HBE monolayers.

Previous findings established that 16HBE cells can be effectively transfected with mRNA encoding FLuc using non-viral vectors, with no detrimental effects to the cells. While 16HBE cells are advantageous for optimising transfection conditions due to their ease of growth and extended lifespan, they lack physiological relevance as they do not fully differentiate into bronchial epithelium. Consequently, subsequent experiments shifted focus to transfecting primary HBECs with reporter mRNA and optimising branched PBAE formulations to establish mRNA delivery to these cells.

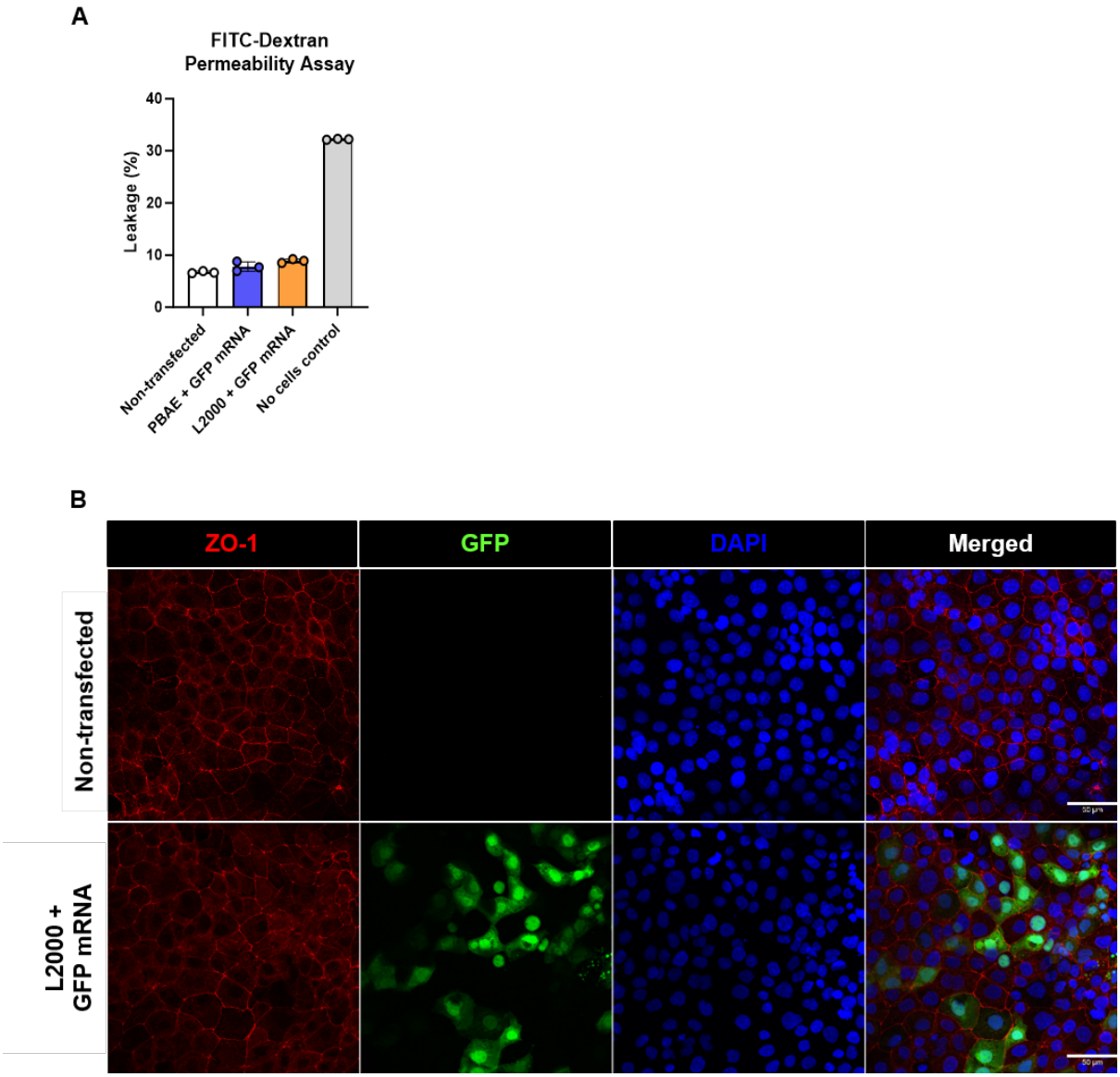


Figure 3.4 Impact of reporter mRNA transfection on permeability and tight junction integrity of 16 human bronchial epithelial (16HBE) confluent monolayers.

(A) Permeability was examined by 4 kDA Fluorescein isothiocyanate FITC-Dextran penetration through 16HBE confluent monolayers following mRNA transfection. Green fluorescent protein (GFP) mRNA was complexed with branched poly (β-amino ester) (PBAE) or Lipofectamine 2000 (L2000) and delivered to 16HBE cells. FITC-Dextran permeability assay was performed 24 hours post-transfection. No-cell control served as a positive control. Data represents mean ± SD. n = 3 technical replicates. (B) Immunofluorescence staining for tight junction protein, zonula occludens-1 (ZO-1), in non-transfected and mRNA transfected 16HBE cells. Scale bar: 50 μm.

3.2.5 Branched PBAE formulation affects mRNA condensation and encapsulation efficiency

The polymer to mRNA mass ratio, which reflects the charge ratio between negatively charged mRNA and positively charged polymer, influences mRNA encapsulation efficiency, stability, cellular uptake, and cytotoxicity of the resulting polyplex[475–478]. While PBAEs are traditionally prepared in acidic pH 5 NaOAc buffer to ensure amine charging and facilitate complexation with anionic mRNA, their susceptibility to degradation in aqueous solution raises concerns about their sensitivity to storage and nanoparticle preparation conditions[482]. To address this, I explored alternative buffer systems to the traditional NaOAc buffer for PBAE formulation. I aimed to optimise branched PBAE formulations (branched PBAE to mRNA mass ratio, buffer formulation) to achieve stable, positively charged nanoparticles below 200 nm to enable effective mRNA delivery to primary HBECs.

To confirm the ability of each formulation to complex FLuc mRNA, branched PBAE was formulated in different buffers (NaOAc, PBS, NaCl, NaOAc/PBS) at various mass ratios (1:1, 10:1, 20:1, 50:1). These formulations were then subjected to agarose gel electrophoresis. As shown in Figure 3.5, while naked FLuc mRNA migrated through the gel, most PBAE formulations effectively condensed mRNA, indicated by its reduced migration. mRNA condensation increased with the polymer-to-mRNA mass ratio, regardless of buffer used (Figure 3.5A+B).

Branched PBAE formulations at 20:1 and 50:1 mass ratio, which exhibited efficient mRNA condensation, were selected for further characterisation using the RiboGreen mRNA encapsulation efficiency assay. As shown in Figure 3.6, most branched PBAE formulations achieved mRNA encapsulation efficiencies greater than 90%. Notably, the NaCl and NaOAc/PBS formulations at 50:1 mass ratio showed higher mRNA encapsulation efficiencies compared to their 20:1 counterpart (NaCl 20:1: 38.6% $\pm$ 1.5, NaOAc/PBS 20:1: 52.1% $\pm$ 0.9). After evaluating the mRNA protection and encapsulation efficiency of various branched PBAE formulations, their ability to transfect primary HBECs was then assessed. The 20:1 and 50:1 formulations, chosen for their superior mRNA protection, were selected for further characterisation.

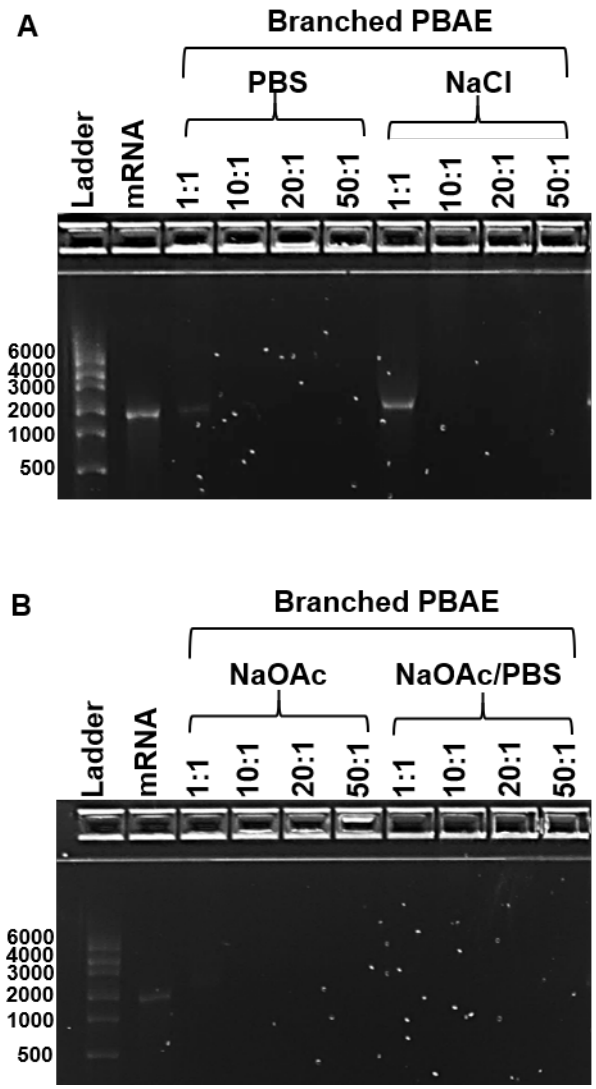


Figure 3.5 Agarose gel electrophoresis retardation assay.

(A) Branched poly (β-amino ester) (PBAE) formulated in PBS or NaCl buffers at different PBAE to mRNA mass ratios (1:1,10:1, 20:1, 50:1) was complexed with Firefly luciferase (FLuc) mRNA and run through gel electrophoresis. (B) Branched PBAE formulated in NaOAc or NaOAc/PBS buffers at different PBAE to mRNA mass ratios (1:1,10:1, 20:1, 50:1) was complexed with Firefly luciferase (FLuc) mRNA and run through gel electrophoresis.

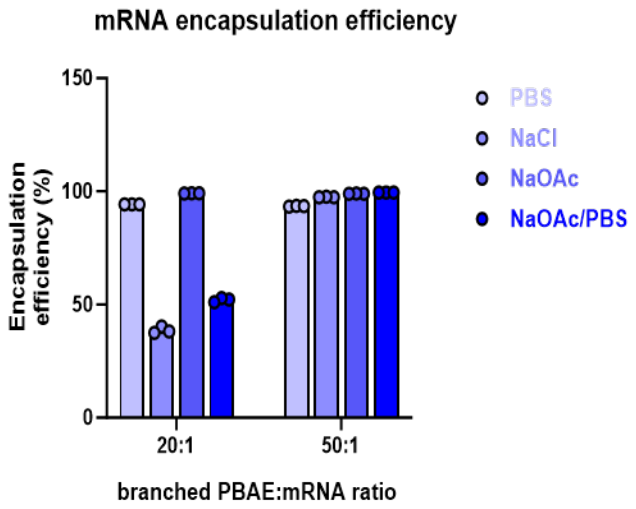


Figure 3.6 mRNA encapsulation efficiency of branched poly (β-amino ester) PBAE formulations.

Branched PBAE formulated in PBS, NaCl, NaOAc, NaOAc/PBS buffers at 20:1 or 50:1 PBAE to mRNA mass ratio was complexed with Firefly luciferase mRNA (FLuc). mRNA encapsulation efficiency was measured using the RiboGreen assay. Data represents mean ± SD. n = 3 technical replicates.

3.2.6 Branched PBAE polymer mediates effective delivery of FLuc mRNA to primary HBECs

In addition to evaluating mRNA condensation and encapsulation efficiency, the study also assessed the transfection efficiency and toxicity of branched PBAE formulations. Nanoparticles were formed by complexing branched PBAE complexed with FLuc mRNA at mass ratios of 20:1 or 50:1 using different buffers: NaOAc, NaCl, PBS, or NaOAc/PBS and were used to transfect submerged primary HBECs. Luminescence and cytotoxicity were assayed 24 hours post-transfection. Due to concerns about reduced cell viability following Lipofectamine 2000 transfection (section 3.2.3), JetMessenger, another commercial transfection reagent, was employed as a positive control for comparison.

As shown in Figure 3.7A, branched PBAE formulations were effective in transfecting primary HBECs with FLuc mRNA, with transfection efficiency varying based on the buffer and PBAE to mRNA mass ratio. PBAE formulated in PBS at 20:1 mass ratio and in NaOAc/PBS at 50:1 mass ratio achieved significantly higher luminescence compared to the other formulations tested ($P<0.0001$) (PBS 20:1: $4.1 \times 10^5 \pm 1.7 \times 10^5$, NaOAc/PBS 50:1: $5.1 \times 10^5 \pm 2.5 \times 10^5$). Naked mRNA failed to produce any detectable luminescence, corroborating the gel electrophoresis results from section 3.2.5, which showed efficient mRNA condensation by PBAE at these specific mass ratios.

The cytotoxicity of FLuc mRNA transfection in primary HBECs was evaluated using an LDH release assay on cell culture supernatants at 24 hours post-transfection (Figure 3.7B). A significant increase in LDH release was observed with NaCl formulations ($P<0.0001$) compared to non-transfected control cells. In contrast, other formulations did not elevate LDH release.

Having confirmed successful transfection of primary HBECs with these branched PBAE formulations, the next step was to characterise their physicochemical properties.

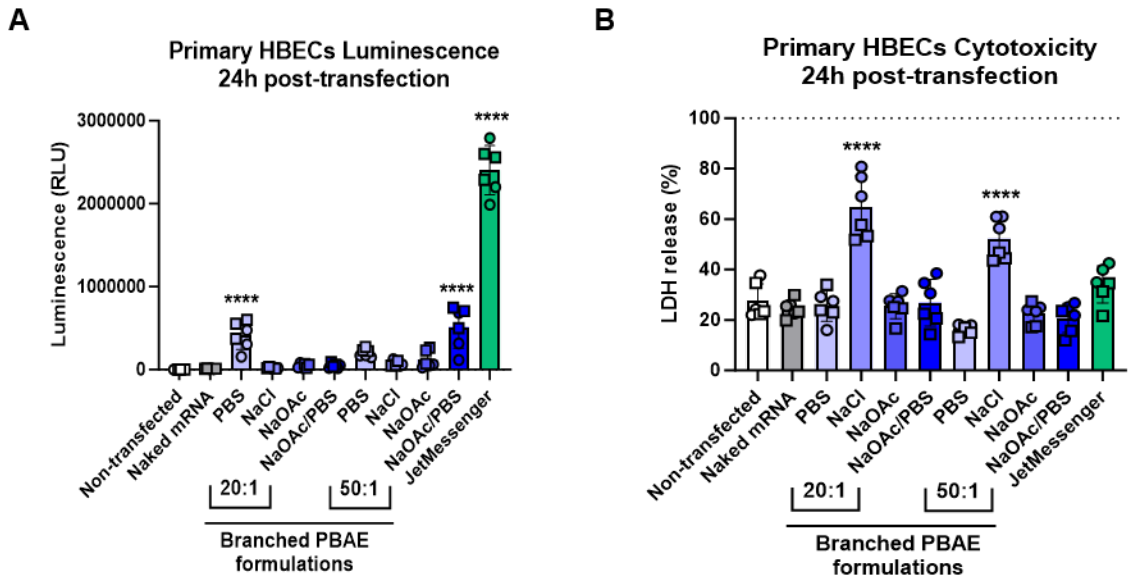


Figure 3.7 Transfection efficiency and cytotoxicity of branched poly (β-amino ester) (PBAE) formulations on submerged primary human bronchial epithelial cells (HBECs).
Branched PBAE formulated in PBS, NaCl, NaOAc, NaOAc/PBS buffers at 20:1 or 50:1 PBAE to mRNA mass ratio was complexed with Firefly luciferase (FLuc) mRNA (50 ng per well) and delivered to submerged primary HBECs. The commercial transfection reagent JetMessenger was used as a control. (A) Luminescence was assessed 24 hours post-transfection. (B) Cytotoxicity measured as percentage lactate dehydrogenase (LDH) release in supernatants was assessed 24 hours post-transfection. Dotted line indicates 100% LDH release of positive control cells treated with 1% Triton-X-100 and cytotoxicity was calculated relative to this control. Data represents mean ± SD. N = 2 primary cell donors, with 3 technical replicates each. Each symbol represents a different donor. Statistics: One-way ANOVA followed by Dunnett's multiple comparisons test. **** $P<0.0001$.

3.2.7 Branched PBAE formulation affects PBAE/mRNA polyplexes size and zeta potential

Following the assessment of transfection efficiency and cytotoxicity, the study delved deeper into the ability of branched PBAE to complex with and condense mRNA by analysing their size and surface charge. Branched PBAE, formulated in PBS, NaCl, NaOAc, or NaOAc/PBS, was complexed with FLuc mRNA at mass ratios of 20:1 or 50:1 PBAE to mRNA. DLS was utilised to determine the size of these polyplexes.

All branched PBAE formulations formed nano-sized polyplexes under 200 nm (Figure 3.8A-H). Figure 3.8I summarises the detectable sizes of branched PBAE/mRNA polyplexes. Specifically, polyplexes formulated in PBS and NaCl were larger compared to those in NaOAc at both tested PBAE to mRNA mass ratios (PBS 20:1 = 87.4 nm, PBS 50:1 = 137.8 nm, NaCl 20:1 = 169.5 nm, NaCl 50:1 = 147.4 nm, NaOAc 20:1 = 51.9 nm, NaOAc 50:1 = 77.1 nm). Polyplexes formulated in NaOAc/PBS were more compact than those in PBS, resulting in smaller particle sizes (NaOAc/PBS 20:1 = 72.8 nm, NaOAc/PBS 50:1 = 61.1 nm). PBS or NaCl formulated polyplexes were unstable, leading to larger particles, whereas those formulated in NaOAc or NaOAc/PBS were stable.

The surface charge, which is crucial for cellular uptake due to the need for cationic polymer-based polyplexes to maintain a positive charge for interaction with cell membranes, was also analysed using DLS. As shown in Figure 3.9, all formulations resulted in the formation of positively charged nanoparticles, with PBS and PBS/NaOAc formulations showing the highest zeta potential (PBS 20:1 = 38.1 $\pm$ 3.9 mV, PBS 50:1 = 42.6 $\pm$ 4.2 mV, NaOAc/PBS 20:1 = 35.5 $\pm$ 26.9 mV, NaOAc/PBS = 28.7 $\pm$ 6.1 mV).

Based on these findings, the NaOAc/PBS formulation at 50:1 PBAE to mRNA mass ratio was chosen for subsequent studies. This formulation demonstrated superior performance in terms of size, stability, charge, transfection efficiency and cytotoxicity.

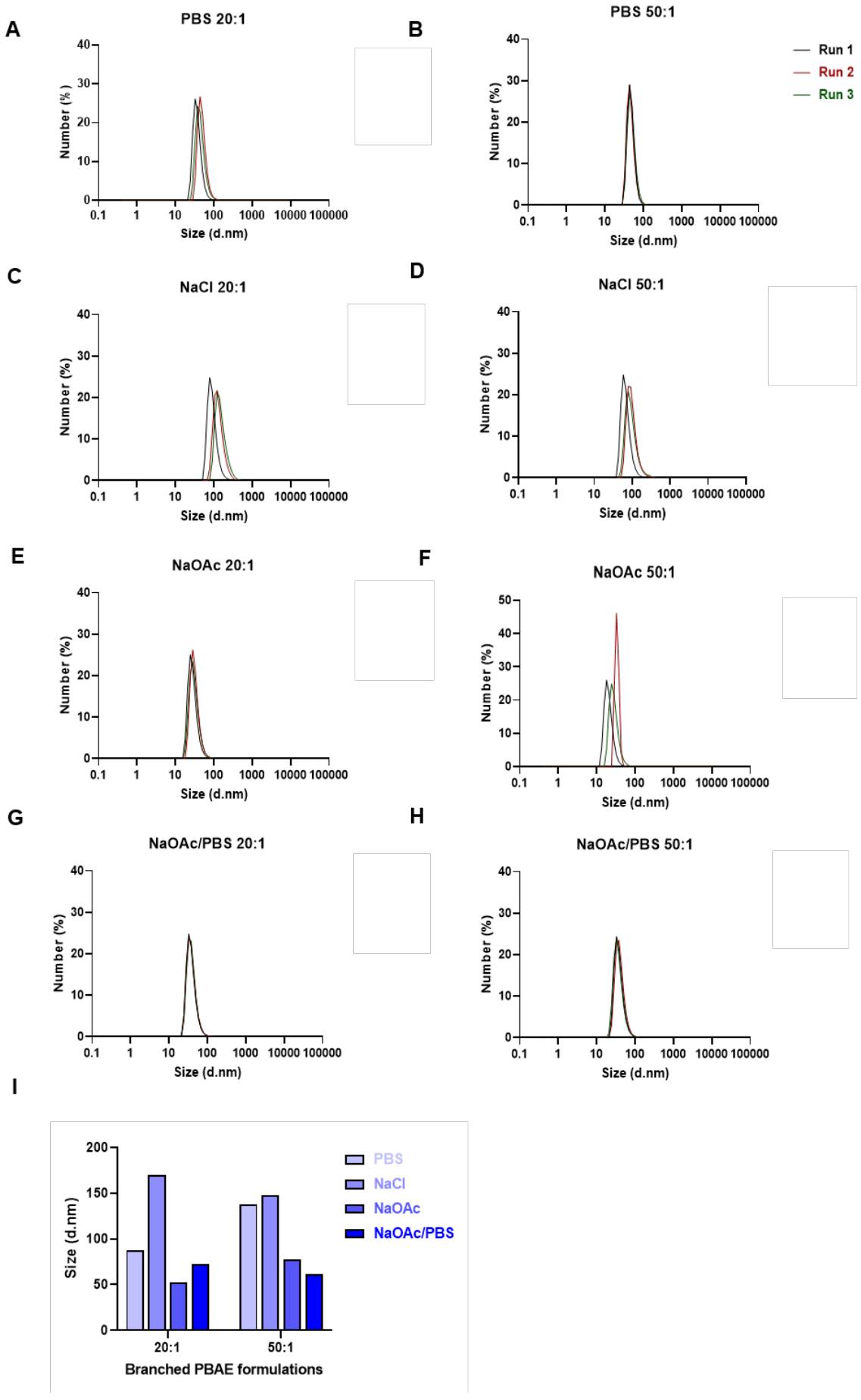

A
PBS 20:1
Number (%)
Size (d.nm)
B
PBS 50:1
Number (%)
Size (d.nm)
Run 1
Run 2
Run 3
C
NaCl 20:1
Number (%)
Size (d.nm)
D
NaCl 50:1
Number (%)
Size (d.nm)
E
NaOAc 20:1
Number (%)
Size (d.nm)
F
NaOAc 50:1
Number (%)
Size (d.nm)
G
NaOAc/PBS 20:1
Number (%)
Size (d.nm)
H
NaOAc/PBS 50:1
Number (%)
Size (d.nm)
I
Size (d.nm)
PBS
NaCl
NaOAc
NaOAc/PBS
20:1
50:1
Branched PBAE formulations

Figure 3.8 Size characterisation of branched poly (β-amino ester) (PBAE) formulations complexed with mRNA.

The size in nm of branched PBAE formulations complexed with Firefly luciferase (FLuc) mRNA was characterised using dynamic light scattering (DLS). Size distribution by number of (A) PBS formulation at 20:1 PBAE to mRNA mass ratio, (B) PBS formulation at 50:1 PBAE to mRNA mass ratio (C) NaCl formulation at 20:1 PBAE to mRNA mass ratio, (D) NaCl formulation at 50:1 PBAE to mRNA mass ratio, (E) NaOAc formulation at 20:1 PBAE to mRNA mass ratio, (F) NaOAc formulation at 50:1 PBAE to mRNA mass ratio, (G) NaOAc/PBS formulation at 20:1 PBAE to mRNA mass ratio, (H) NaOAc/PBS formulation at 50:1 PBAE to mRNA mass ratio, (I) Average size of branched PBAE formulations. Triplicate readings were obtained for each nanoparticle sample.

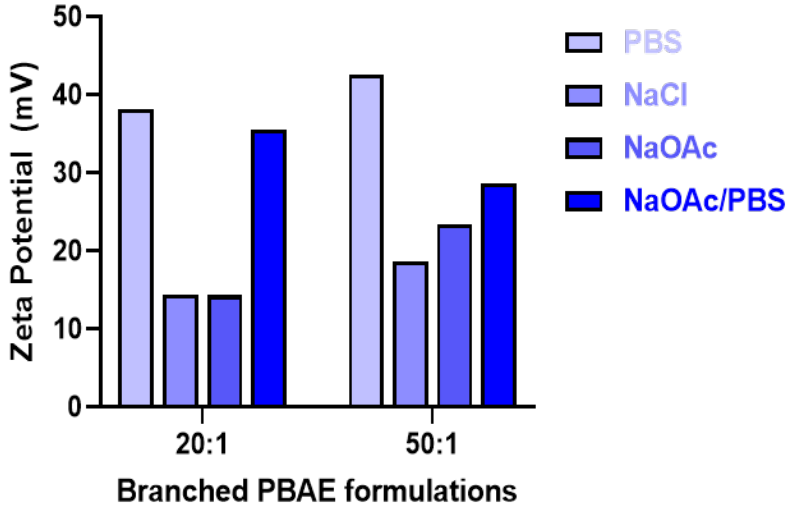


Figure 3.9 Zeta potential characterisation of branched poly (β-amino ester) (PBAE) formulations complexed with mRNA.

The zeta potential in mV of branched PBAE formulations complexed with Firefly luciferase (FLuc) mRNA was characterised using dynamic light scattering (DLS). Triplicate readings were obtained for each nanoparticle sample.

3.2.8 Assessing the consistency of optimised branched PBAE formulation across two different PBAE batches

After establishing the superior characteristics of the branched PBAE formulation prepared in NaOAc/PBS at 50:1 PBAE to mRNA mass ratio - including high mRNA encapsulation efficiency, optimal polyplex size, stability, charge, and enhanced transfection efficiency – its batch-to-batch consistency was evaluated. FLuc mRNA was complexed with branched PBAEs from two different batches, using the same NaOAc/PBS formulation at 50:1 PBAE to mRNA mass ratio. These complexes were then used to transfect submerged primary HBECs, with luminescence and cytotoxicity evaluated 24 hours post-transfection.

The results indicated consistency between the two PBAE batches. Luminescence readings across the batches were similar, indicating comparable levels of mRNA transfection in HBECs (Figure 3.10A). However, there was variation in luminescence among donors, reflecting differences in their transfection efficiency (Figure 3.10A). Furthermore, no significant increase in cytotoxicity was observed in HBECs transfected with the branched PBAE formulations (Figure 3.10B), suggesting that the cells tolerated the PBAE polyplexes.

Overall, the data presented in this section confirmed that the optimal branched PBAE formulation demonstrates reliable batch-to-batch consistency. This consistency, coupled with the formulation's high transfection efficiency and low cytotoxicity, highlights its potential as an effective vehicle for mRNA delivery to primary HBECs.

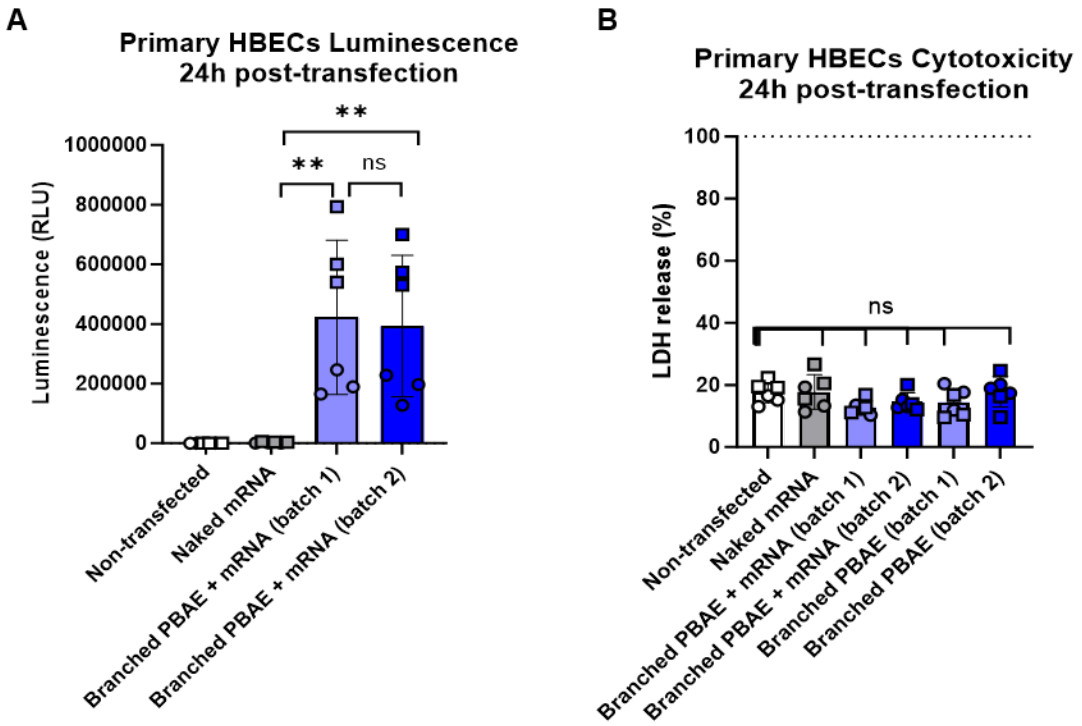


Figure 3.10 Batch-to batch consistency of the optimal branched PBAE formulation.

Two different batches of branched poly (b-amino esters) (PBAEs) formulated in NaOAc/PBS at 50:1 PBAE to mRNA mass ratio were complexed with Firefly luciferase (FLuc) mRNA (50 ng per well) and delivered to submerged primary human bronchial epithelial cells (HBECs). (A) Luminescence at 24 hours post-transfection. (B) Cytotoxicity measured as percentage lactate dehydrogenase (LDH) release in supernatants was measured 24 hours post-transfection. Dotted line indicates 100% LDH release of positive control cells treated with 1% Triton-X-100 and cytotoxicity was calculated relative to this control. Data represents mean ± SD. N = 2 primary cell donors, with 3 technical replicates each. Each symbol represents a different donor. Statistics: One-way ANOVA followed by Tukey's multiple comparisons test. ** P=0.0002, P=0.9911 ns: non-significant.

3.2.9 Primary HBECs retain their basal cell phenotype 24 hours after transfection with reporter mRNA

Basal cells are epithelial progenitor cells in the airways, capable of self-renewal after injury and differentiating into various types of epithelial cells such as club cells, ciliated cells, and goblet cells[509,510]. To assess the impact of reporter mRNA transfection on the basal phenotype of primary HBECs, immunofluorescence staining was performed for the basal progenitor HBEC marker KRT5[510] on both mRNA transfected and non-transfected control cells (Figure 3.11). The study confirmed that primary HBECs transfected with mRNA retained expression of KRT5 24 hours post-transfection (non-transfected cells: 96.4% ± 2.9, naked mRNA: 96.3% ± 1.4, PBAE/mRNA: 91.6% ± 2.5, JetMessenger/mRNA: 96.7% ± 1.5). Based on this finding, I further hypothesised that reporter mRNA transfection will not impact primary HBEC differentiation at ALI.

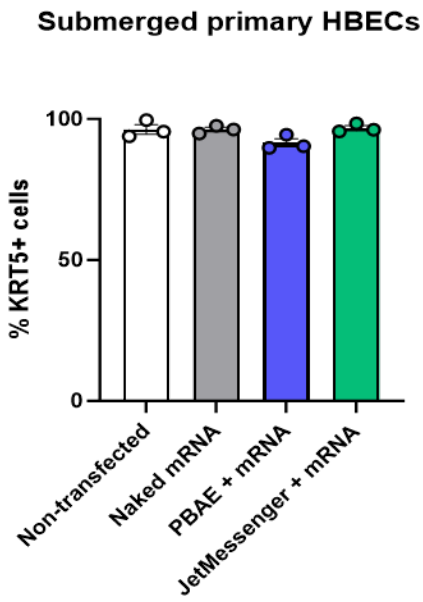


Figure 3.11 Expression of keratin 5 (KRT5) in submerged primary human bronchial epithelial cells (HBECs) following reporter mRNA transfection.

Reporter mRNA was complexed with branched poly (β-amino ester) PBAE, commercial transfection reagent JetMessenger or delivered naked to submerged primary HBECs. Cells were fixed 24 hours post-transfection and stained for KRT5. KRT5 positive cells were quantified in the total cell population and expressed as % KRT5 positive cells. Data represent mean ± SD. n = 3 technical replicates.

3.2.10 Differentiation of primary HBECs at ALI

ALI cultures of HBECs have emerged as a valuable tool for modelling the airway epithelium *in vitro*. These cultures aim to recapitulate the *in vivo* phenotypic and functional characteristics of the human airway epithelium. To achieve this, primary HBECs were cultured on transwell inserts and air-exposed once a confluent monolayer was formed (Figure 3.12A). After 28 days of air exposure, primary HBEC ALI cultures were fixed and processed for histological examination to analyse the structure of the differentiated epithelium. H&E and PAS staining of ALI cross-sections demonstrated the successful formation of a pseudostratified, fully differentiated bronchial epithelium (Figure 3.12B). However, obtaining good quality sections from agarose blocks was challenging due to the detachment of ALI cells from the transwell membranes. To address this, I included three replicates to increase the likelihood of success.

ALI cultures were further characterised by immunofluorescence staining to identify the presence of the three main cell types of the respiratory epithelium (basal cells, ciliated cells, goblet cells) in the differentiated HBEC ALI cultures. Confocal microscopy showed that these cultures contained basal cells (KRT5), cilia (acetylated alpha tubulin), and goblet cells (MUC5AC) (Figure 3.12C). Furthermore, the presence of ZO-1, a tight junction protein, in these cultures indicated the formation of epithelial barrier (Figure 3.12C).

TEM analysis confirmed that the fully differentiated HBEC ALI cultures had a pseudostratified mucociliary epithelium characterised by basal cells at the basal surface, ciliated cells at the apical surface, and secretory cells containing secretory granules (Figure 3.13). The analysis also showed tight junctional complexes between adjacent epithelial cells (Figure 3.13).

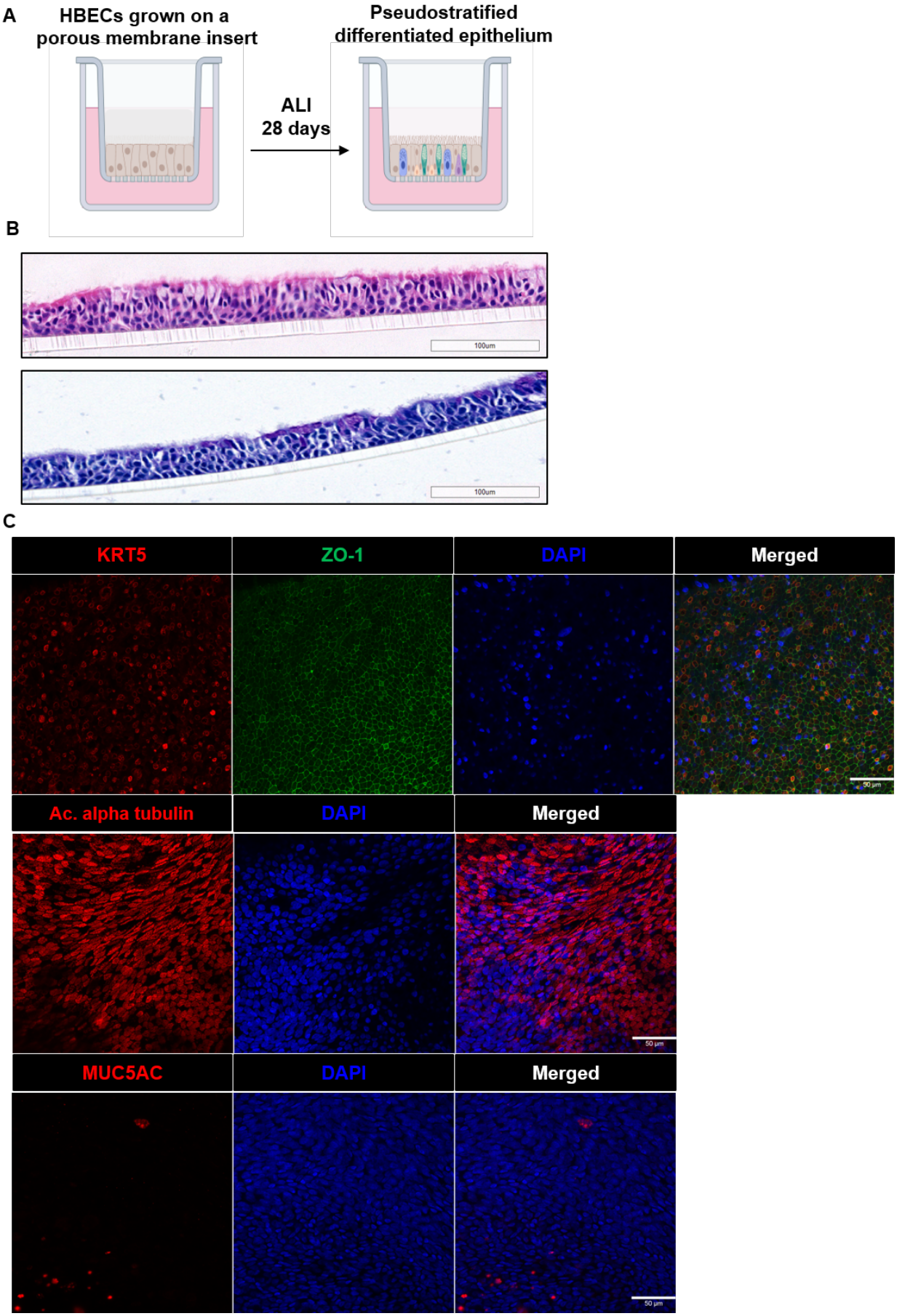

A
HBECs grown on a porous membrane insert
ALI
28 days
Pseudostratified differentiated epithelium
B
100um
100um
C
KRT5
ZO-1
DAPI
Merged
Ac. alpha tubulin
DAPI
Merged
MUC5AC
DAPI
Merged

Figure 3.12 Culture of primary human bronchial epithelial cells (HBECs) at air-liquid interface (ALI).

(A) Diagram of the experimental set up of ALI model. Primary HBECs are seeded on a porous membrane transwell insert. Initially the cells were grown submerged and once they formed a confluent monolayer, they were air exposed (basal side of cells is in contact with the culture medium through a porous membrane and the apical side is exposed to the air) and grown at ALI for 28 days. (B) Representative Hematoxylin and eosin (H&E) (top) and Periodic acid-Schiff (PAS) (bottom) stained ALI sections showing well differentiated and pseudostratified bronchial epithelia cell cultures. (C) Representative top-down immunofluorescence staining images of HBEC cultured at ALI for 28 days, showing expression of KRT5 (basal cells), ZO-1 (tight junctions), acetylated alpha tubulin (cilia), and MUC5AC (goblet cells). Scale bar: 50 mm.

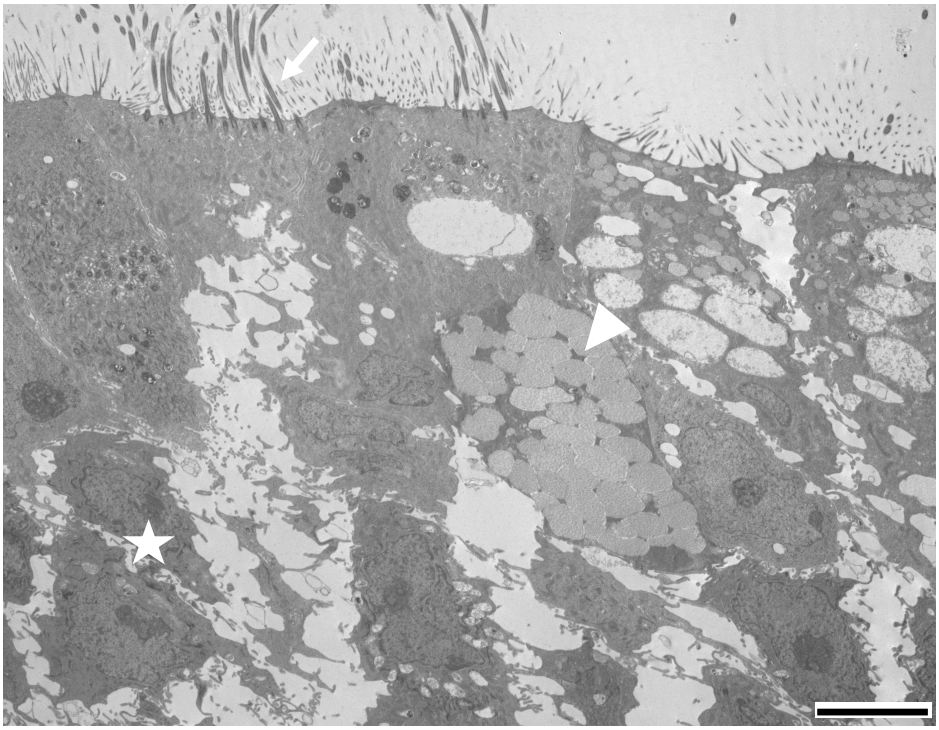


Figure 3.13 Ultrastructural analysis of primary human bronchial epithelial cell (HBEC) air liquid interface (ALI) cultures through transmission electron microscopy (TEM).

TEM image of primary HBECs cultured at ALI for 28 days. The image shows a differentiated epithelium with cilia (arrow) on the apical surface, secretory cells (arrowhead) with secretory granules, and basal cells (asterisk) on the basal surface. Scale bar: 6 µm.

3.2.11 Submerged primary HBECs demonstrate higher mRNA transfection efficiency than HBECs cultured at ALI for 7 days

Transfecting a fully differentiated epithelium is more complex than a single monolayer due to its barrier-like, differentiated characteristics, which restrict the penetration of transfection reagents. Despite these challenges, employing fully differentiated epithelial cells offers a more robust model for studying gene delivery barriers. I aimed to evaluate reporter mRNA transfection efficiency in submerged primary HBECs compared to those cultured at ALI. Submerged primary HBECs were transfected with Cy5-tagged GFP mRNA 24 hours after seeding on transwell inserts, while ALI-cultured HBECs were transfected with Cy5-tagged GFP mRNA 7 days post-ALI. For ALI cultures, mRNA was delivered either to apical or basolateral chamber. mRNA was complexed with the optimised branched PBAE or the commercial transfection reagent JetMessenger, as a positive control. Transfection efficiency was assessed by quantifying Cy5-positive cells (indicating mRNA uptake) and GFP-positive cells (indicating mRNA translation) at 24- and 48-hours post-transfection.

Figure 3.14A+D illustrates that both PBAE and JetMessenger mediated comparable mRNA uptake levels in submerged primary HBECs at both 24- and 48-hours post-transfection (Table 3.1). Specifically, PBAE/mRNA complexes led to 37% Cy5-positive cells at 24 hours post-transfection compared to 41% with JetMessengger/mRNA complexes. By 48 hours post-transfection, these percentages decreased to 32% and 29%, respectively. Despite similar uptake, PBAE transfection resulted in higher mRNA translation, with 11% GFP-positive cells at 24 hours and 19% at 48 hours post-transfection, as shown in Figure 3.14B+D (Table 3.1). However, HBECs cultured at ALI for 7 days and were transfected with either PBAE/mRNA or JetMessenger/mRNA complexes (applied apically or basolaterally) showed inefficient transfection, evidenced by a lack of Cy5-positive and GFP-positive cells (Figure 3.15).

Cell cytotoxicity was also evaluated using the LDH release assay. Both PBAE/mRNA and JetMessenger/mRNA transfections exhibited minimal cytotoxic effects, as indicated by the LDH levels measured at 24- and 48-hours post-transfection (Figure 3.14C and Figure 3.15C).

In summary, primary HBECs under submerged culture displayed enhanced mRNA transfection efficiency, marked by increased counts of Cy5- and GFP-positive cells, in comparison to HBECs cultured at ALI for 7 days. Furthermore, these cells tolerated PBAE and JetMessenger transfections with negligible cytotoxicity.

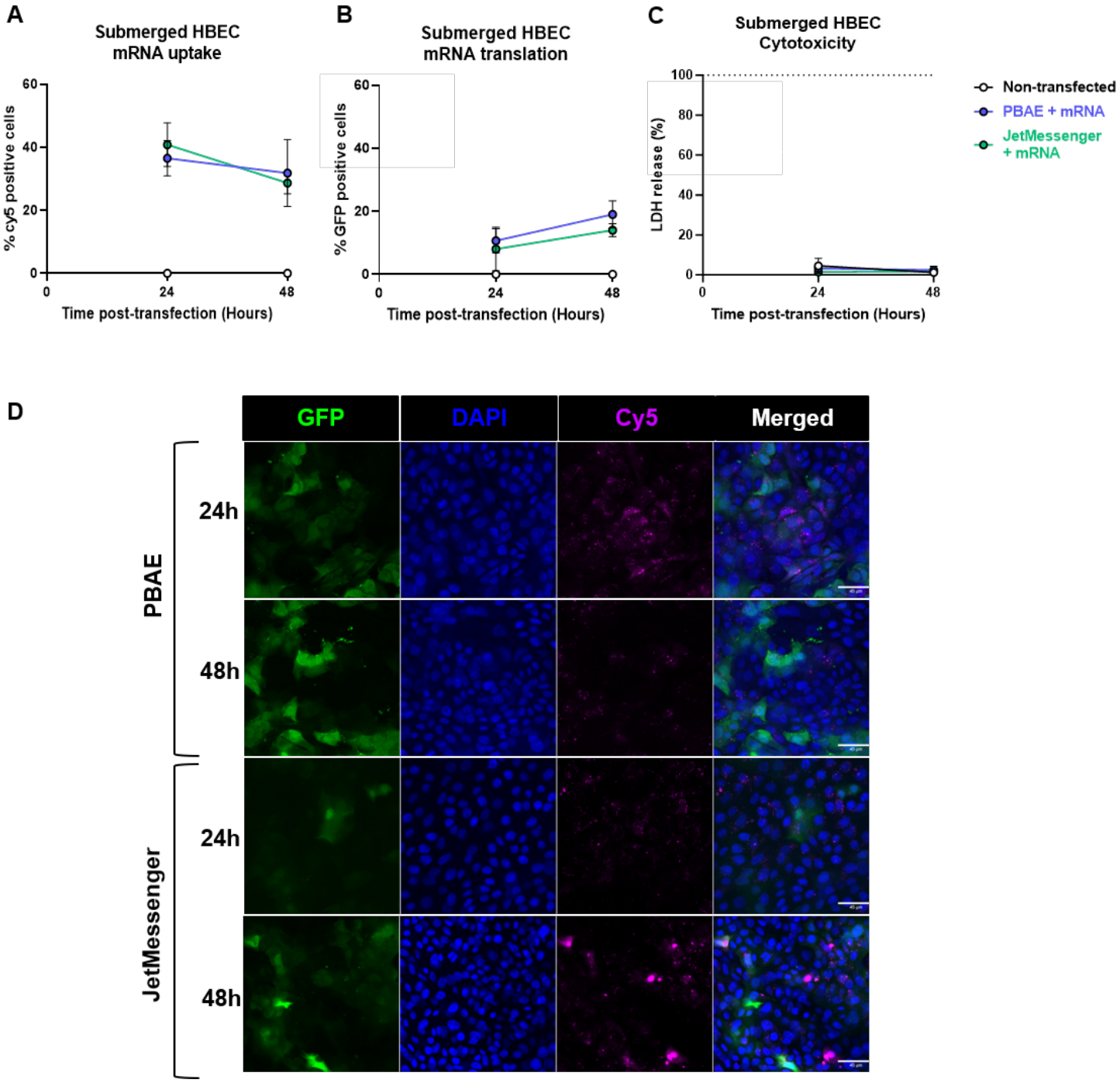


Figure 3.14 Cy5-tagged GFP mRNA transfection of submerged primary human bronchial epithelial cells (HBECs).

Cy5-tagged GFP mRNA was complexed with branched poly (b-amino ester) (PBAE) or commercial transfection reagent JetMessenger or delivered naked to submerged primary HBECs. (A) Percentage of Cy5-postive cells indicating successful mRNA uptake at 24- and 48-hours post-transfection. (B) Percentage of GFP-positive cells, reflecting mRNA translation at 24- and 48-hours post-transfection. (C) Cytotoxic assessment via lactate dehydrogenase (LDH) release assay at 24- and 48-hours post-transfection. Dotted line indicates 100% LDH release of positive control cells treated with 1% Triton-X-100 and cytotoxicity was calculated relative to this control. (D) Representative fluorescent microscopy images at 24 hours post-transfection, showing GFP expression, Cy5 signal, and DAPI-stained nuclei, corroborating the quantitative data presented in panels A and B. Data represents mean ± SD. N = 2 primary cell donors, with 3 technical replicates each. Statistics: 2way ANOVA followed by Tukey's multiple comparisons test. Statistical analysis results are summarised in Table 3.1.

Table 3.1 Summary of statistical analysis of mRNA uptake and mRNA translation in submerged primary HBECs following reporter mRNA transfection.

	Summary	Adjusted P value
mRNA uptake		
24h post-transfection: Non-transfected vs Branched PBAE	****	<0.0001
24h post-transfection: Non-transfected vs JetMessenger	****	<0.0001
24h post-transfection: Branched PBAE vs JetMessenger	ns	0.4677
48h post-transfection: Non-transfected vs Branched PBAE	****	<0.0001
48h post-transfection: Non-transfected vs JetMessenger	****	<0.0001
48h post-transfection: Branched PBAE vs JetMessenger	****	0.6921
mRNA translation		
24h post-transfection: Non-transfected vs Branched PBAE	****	<0.0001
24h post-transfection: Non-transfected vs JetMessenger	**	0.0026
24h post-transfection: Branched PBAE vs JetMessenger	ns	0.4459
48h post-transfection: Non-transfected vs Branched PBAE	****	<0.0001
48h post-transfection: Non-transfected vs JetMessenger	****	<0.0001
48h post-transfection: Branched PBAE vs JetMessenger	ns	0.0884

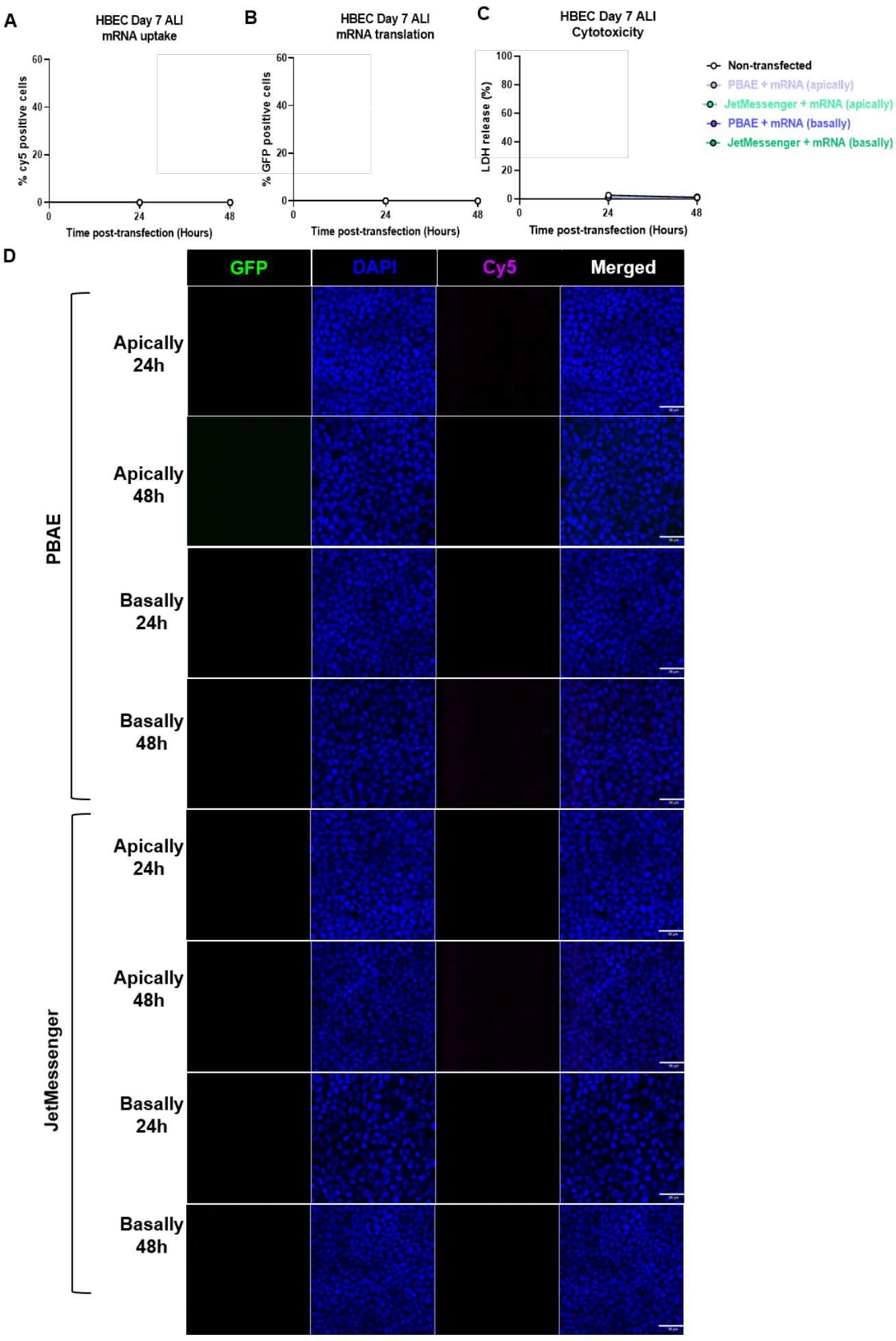

A
HBEC Day 7 ALI
mRNA uptake
% cy5 positive cells
Time post-transfection (Hours)
B
HBEC Day 7 ALI
mRNA translation
% GFP positive cells
Time post-transfection (Hours)
C
HBEC Day 7 ALI
Cytotoxicity
LDH release (%)
Time post-transfection (Hours)
Non-transfected
PBAE + mRNA (apically)
JetMessenger + mRNA (apically)
PBAE + mRNA (basally)
JetMessenger + mRNA (basally)
D
GFP
DAPI
Cy5
Merged
PBAE
Apically 24h
Apically 48h
Basally 24h
Basally 48h
JetMessenger
Apically 24h
Apically 48h
Basally 24h
Basally 48h

Figure 3.15 Cy5-tagged GFP mRNA transfection of primary human bronchial epithelial cells (HBECs) cultured at air liquid interface (ALI) for 7 days.

Cy5-tagged GFP mRNA was complexed with branched poly (b-amino ester) (PBAE) or commercial transfection reagent JetMessenger or delivered naked to primary HBECs 7 days post air exposure, to either apical chamber or basolateral chamber. (A) Percentage of Cy5-postive cells 24- and 48-hours post-transfection. (B) Percentage of GFP-positive cells at 24- and 48-hours post-transfection. (C) Cytotoxic assessment via lactate dehydrogenase (LDH) release assay at 24- and 48-hours post-transfection. (D) Representative fluorescent microscopy images at 24- and 48-hours post-transfection, showing a lack of GFP expression and Cy5 signal, and DAPI-stained nuclei. Data represents mean $\pm$ SD. N = 2 primary cell donors, with 3 technical replicates each.

3.2.12 Integrity of HBECs cultured at ALI remains intact after reporter mRNA transfection

To evaluate the impact of reporter mRNA transfection on the integrity of primary HBECs cultured at ALI, HBECs were transfected with reporter mRNA either complexed with branched PBAE in its optimised formulation (as detailed in section 3.2.6) or the commercial transfection reagent JetMessenger 24 hours post-seeding on transwell inserts. Following confluence, both mRNA transfected HBECs and non-transfected controls were air-exposed and cultured at ALI for 28 days.

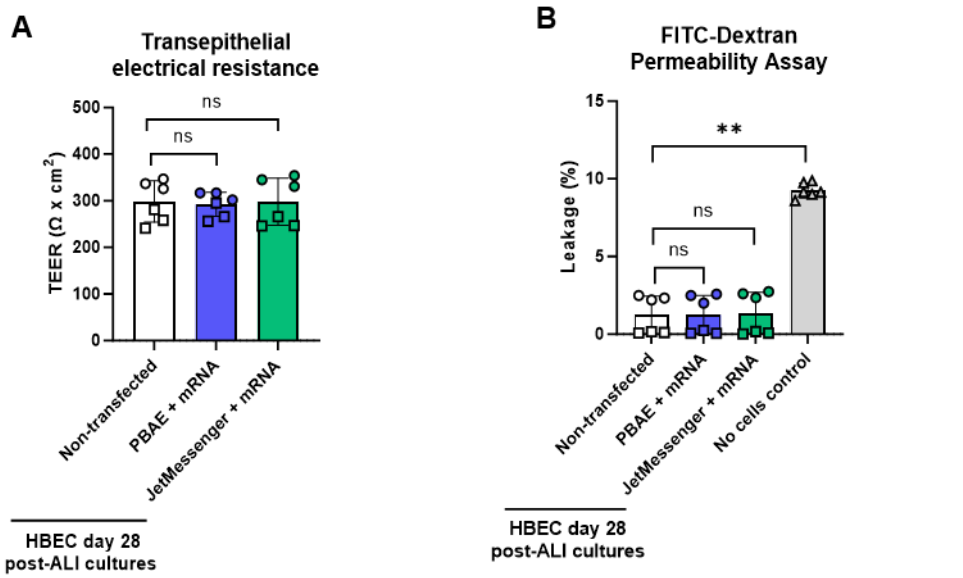
TEER was measured on day 28 post-ALI to evaluate the barrier integrity among three groups: non-transfected control HBECs, PBAE/mRNA transfected HBECs, and JetMessenger/mRNA transfected HBECs. Figure 3.16A demonstrates that all groups successfully developed TEER, indicating barrier formation. Notably, there were no significant differences in TEER values between non-transfected (298.3 Ωxcm^2 $\pm$ 44.4), PBAE/mRNA (292.2 Ωxcm^2 $\pm$ 25.8) or JetMessenger/mRNA (298.2 Ωxcm^2 $\pm$ 50.6) transfected groups.

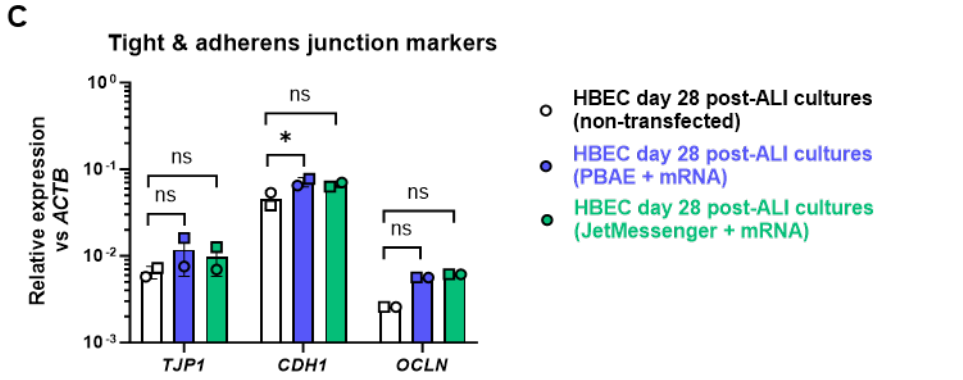
Additionally, the study measured the passive diffusion of FITC-Dextran across the differentiated HBEC cultures 28 days post-ALI. This assessment aimed to compare the permeability differences between non-transfected HBECs, HBECs transfected with PBAE/mRNA, and those transfected with JetMessenger/mRNA. The results indicated a comparable rate of apical to basal diffusion of FITC-Dextran across all groups (Figure 3.16B).

The integrity of the epithelial barrier was further corroborated through gene expression analysis. This involved assessing the expression of tight junction (*TJP1*, *OCLN*) and adherens junction (*CDH1*) markers via qPCR in non-transfected HBECs, HBECs transfected with PBAE/mRNA, and those transfected with JetMessenger/mRNA, all cultured at ALI for 28 days. The analysis revealed no variation in the gene expression of these junctional markers between mRNA transfected and non-transfected ALI cultures (Figure 3.16C).

Additionally, the study investigated the impact of reporter mRNA transfection on the morphology of tight junctions through immunofluorescence staining for the tight junction protein ZO-1. Both mRNA transfected and non-transfected HBEC day 28 post-ALI cultures showed positive ZO-1 staining, with no observed differences in ZO-1 cellular localisation among the groups (Figure 3.16D).

Collectively, these findings indicate that reporter mRNA transfection prior to air-exposure does not compromise the barrier integrity of HBECs cultured at ALI.


A
Transepithelial electrical resistance
TEER (Ω x cm²)
500
400
300
200
100
0
ns
ns
Non-transfected
PBAE + mRNA
JetMessenger + mRNA
HBEC day 28 post-ALI cultures
B
FITC-Dextran Permeability Assay
Leakage (%)
15
10
5
0
**
ns
ns
Non-transfected
PBAE + mRNA
JetMessenger + mRNA
No cells control
HBEC day 28 post-ALI cultures


C
Tight & adherens junction markers
Relative expression vs ACTB
10⁰
10⁻¹
10⁻²
10⁻³
ns
ns
ns
*
ns
ns
TJP1
CDH1
OCLN
HBEC day 28 post-ALI cultures (non-transfected)
HBEC day 28 post-ALI cultures (PBAE + mRNA)
HBEC day 28 post-ALI cultures (JetMessenger + mRNA)

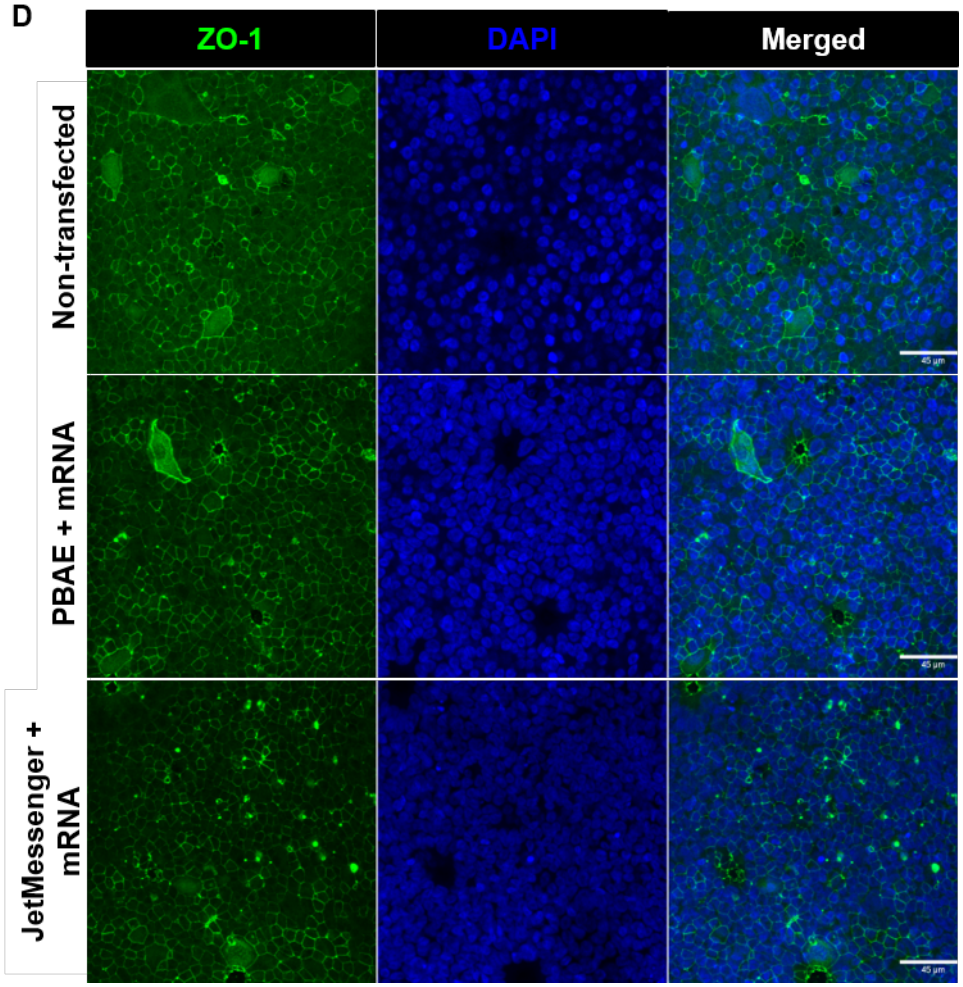

D
ZO-1
DAPI
Merged
Non-transfected
PBAE + mRNA
JetMessenger + mRNA

Figure 3.16 Assessment of epithelial barrier integrity and tight junction morphology in human bronchial epithelial cells (HBECs) cultured at air liquid interface (ALI) following reporter mRNA transfection.

Cy5-tagged GFP mRNA was complexed with branched poly (b-amino ester) (PBAE) or commercial transfection reagent JetMessenger and delivered to submerged primary HBECs. Once a confluent monolayer was formed, both mRNA transfected and non-transfected HBECs were grown at ALI for 28 days. (A) Transepithelial electrical resistance (TEER) measurements for non-transfected HBECs, PBAE/mRNA transfected HBECs, and JetMessenger/mRNA transfected HBECs, all cultured at ALI for 28 days. TEER is expressed as Ω x cm^2, which is the product of resistance in Ohms and the surface are of the membrane. N = 2 primary cell donors, with 3 technical replicates each. Each symbol represents a different donor. Statistics: Kruskal-Wallis test followed by Dunn's multiple comparisons test. P=0.9582 ns: non-significant. (B) Permeability of HBEC ALI cultures to 4kDa Fluorescein isothiocyanate FITC-Dextran. No-cell control served as a positive control. N = 2 primary cell donors, with 3 technical replicates each. Each symbol represents a different donor. Statistics: One-way ANOVA followed by Dunnett's multiple comparisons test. P>0.9999 ns: non-significant, ** P=0.0080. (C) qPCR analysis for tight junction markers (*TJP1*, *OCLN*) and adherens junction marker (*CDH1*) in the three groups of HBEC ALI cultures. Results are quantified relative to housekeeping gene *ACTB*. N = 2 primary cell donors. Each symbol represents a different donor. Statistics: 2way ANOVA followed by Dunnett's multiple comparisons test. P>0.9999 ns: non-significant, *P=0.0208. (D) Representative immunofluorescence staining for ZO-1 in non-transfected, PBAE/mRNA transfected, and JetMessenger/mRNA transfected HBEC day 28 post-ALI cultures.

3.2.13 Epithelial differentiation at ALI is successful following reporter mRNA transfection

To investigate the impact of reporter mRNA transfection on the differentiation of primary HBECs at ALI, primary HBECs were transfected with reporter mRNA using branched PBAE in its optimised formulation (as detailed in section 3.2.6) or the commercial transfection reagent JetMessenger. Transfection was performed 24 hours after seeding the cells on transwell inserts. Once a confluent monolayer was formed, both mRNA transfected and non-transfected control HBECs were air-exposed and cultured at ALI for 28 days.

The expression of genes indicative of epithelial cell subtypes was assessed through qPCR. This included a comparison of submerged (representing undifferentiated) HBECs to cells at day 28 post-ALI across three groups: non-transfected, PBAE/mRNA transfected, and JetMessenger/mRNA transfected HBECs. The expression levels of secretory cell markers (*MUC5AC*, *MUC5B*, *SCGB1A1*) and a ciliated cell marker (*FOXJ1*) were elevated in both non-transfected and mRNA transfected HBEC day 28 post-ALI cultures, suggesting successful differentiation at ALI culture (Figure 3.17A). Importantly, there was no difference in the expression of these markers between non-transfected and mRNA transfected groups.

The gene expression data were further validated through immunofluorescence staining. Both non-transfected and mRNA transfected HBECs at day 28 post-ALI demonstrated characteristics of a fully differentiated epithelium. This was evidenced by the presence of goblet cells (MUC5AC-positive) and cilia (acetylated alpha-tubulin-positive) (Figure 3.17B).

In summary, these findings indicate that transfecting HBECs with reporter mRNA prior to air-exposure does not impede their differentiation at ALI.

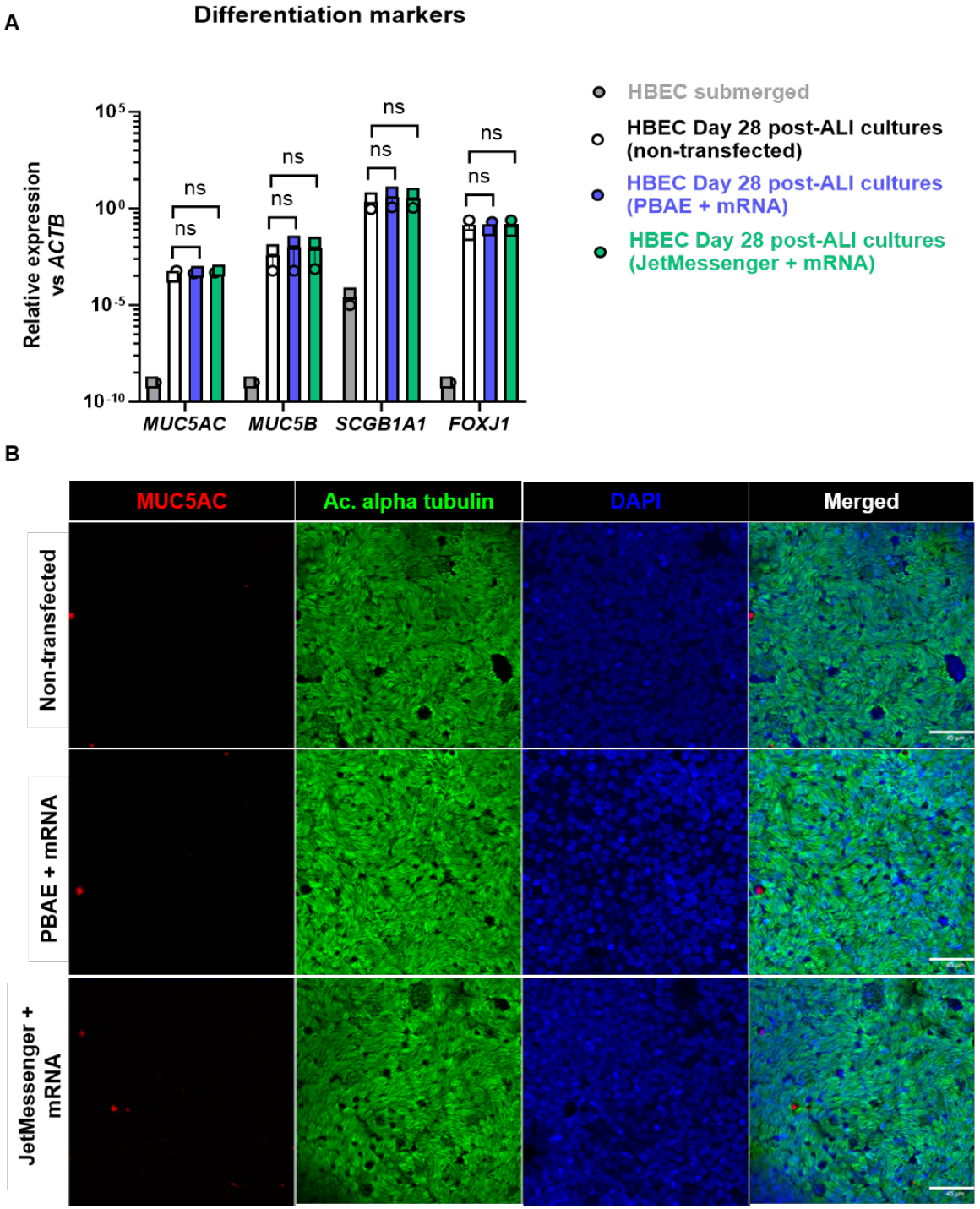


Figure 3.17 Assessment of epithelial differentiation in human bronchial epithelial cells (HBECs) cultured at air liquid interface (ALI) following reporter mRNA transfection.

Cy5-tagged GFP mRNA was complexed with branched poly (b-amino ester) (PBAE) or commercial transfection reagent JetMessenger and delivered to submerged primary HBECs. Once a confluent monolayer was formed, both mRNA transfected and non-transfected HBECs were grown at ALI for 28 days. (A) qPCR analysis for secretory cell markers (*MUC5AC*, *MUC5B, SCGB1A1*) and a ciliated cell marker (*FOXJ1*) in submerged HBECs and in the three groups of HBEC ALI cultures. Results are quantified relative to housekeeping gene *ACTB*. Data represents mean ± SD. N = 2 primary cell donors. Each symbol represents a different donor. Statistics: 2way ANOVA followed by Dunnett's multiple comparisons test. P=0.6155 ns: non-significant. (B) Representative immunofluorescence staining for MUC5AC and acetylated alpha tubulin in non-transfected, PBAE/mRNA transfected, and JetMessenger/mRNA transfected HBEC day 28 post-ALI cultures.

3.3 Discussion

In this chapter, I evaluated reporter mRNA delivery to primary HBECs using non-viral vectors and investigated its impact on the integrity and differentiation of HBECs cultured at ALI. I have demonstrated that 1) Primary HBECs can successfully translate exogenous reporter mRNA following non-viral transfection; 2) Branched PBAE prepared in NaOAc/PBS at 50:1 PBAE to mRNA mass ratio was identified as the top performing formulation in terms of size, charge, stability, and transfection efficiency; 3) Reporter mRNA transfection does not compromise the integrity or differentiation capacity of HBECs at ALI.

The potential of mRNA as a transient tool for transgene overexpression to study gene function is significant[464]. However, the negative charge of mRNA and its susceptibility to enzymatic degradation can impede its effective cellular uptake[465]. Non-viral vectors, such as polymers, offer a promising solution to these challenges by protecting mRNA from degradation while facilitating its delivery into target cells[511]. PBAEs have emerged as a promising class of non-viral vectors for mRNA delivery due to their biodegradability and ease of synthesis[466]. The cationic nature of PBAEs allows for complexation with negatively charged mRNA, forming polyplexes that can be internalised by cells[466–468]. In this study, branched PBAE formulations were optimised to establish effective delivery of mRNA into primary HBECs. The effect of buffer formulation and PBAE to mRNA mass ratio on mRNA protection, size, charge, and stability of resulting polyplexes, as well as transfection efficiency were investigated. Three different buffers were tested: NaOAc, PBS, and NaCl. NaOAc (pH 5) was selected due to its ability to stabilise polyplexes and facilitate endosomal escape[480,482,506]. PBS was chosen as a physiologically relevant buffer with a pH 7.4. NaCl is commonly used to formulate PEI, a commercial cationic polymer[512]. The combination of NaOAc and PBS (NaOAc/PBS) was evaluated for its potential synergistic effect on polyplex stability. Five different PBAE to mRNA mass ratios were explored: 1:1, 10:1, 20:1, and 50:1. The PBAE to mRNA mass ratio is a pivotal factor in achieving an optimal balance between effectively protecting mRNA and minimising cytotoxicity[475–480]. Lower ratios may fail to provide adequate protection for mRNA, potentially leading to its degradation. Conversely, excessively high ratios might result in cytotoxic effects or impede the release of mRNA within the cell.

Gel electrophoresis and the RiboGreen assay were used to evaluate the efficacy of various branched PBAE formulations in protecting mRNA. Gel electrophoresis offers a rapid and straightforward visual evaluation of complexation, as indicated by the retardation in mRNA migration. In contrast, the RiboGreen assay provides a more sensitive and quantitative assessment, measuring the extent of mRNA protection within the vector, termed as

encapsulation efficiency. The study found that increasing the PBAE to mRNA mass ratio across all buffer formulations resulted in enhanced protection of mRNA. This finding aligns with previous studies that identified improved protective effects at higher polymer to nucleic acid mass ratios[463,513]. This increased protection is attributed to the formation of more stable and compact polyplexes at higher polymer concentrations. Notably, the 20:1 and 50:1 PBAE to mRNA mass ratios exhibited superior mRNA protection capabilities. At the 50:1 ratio, all buffer formulations achieved high mRNA encapsulation efficiency, exceeding 90%. However, only the PBS and NaOAc buffer formulations at the 20:1 ratio maintained similar levels of high mRNA encapsulation efficiency. This study underscores the critical role of both gel electrophoresis and the RiboGreen assay in evaluating mRNA protection and encapsulation efficiency. These methods provide complementary insights into the protection and encapsulation efficiency of mRNA. Furthermore, the buffer formulation was observed to significantly influence mRNA encapsulation efficiency. The ionic composition of buffers can modulate the electrostatic interactions between the cationic polymer and the negatively charged mRNA, thereby influencing the encapsulation efficiency. Both gel electrophoresis and RiboGreen assays demonstrated the effectiveness of branched PBAE formulations in protecting mRNA. Based on their superior mRNA protection, the 20:1 and 50:1 formulations were chosen for further characterisation.

Upon confirming the efficient mRNA protection provided by the 20:1 and 50:1 PBAE to mRNA mass ratio formulations, their transfection efficiency in primary HBECs was evaluated using FLuc mRNA. The results revealed that branched PBAE formulations were effective in mediating the translation of FLuc mRNA into HBECs, with the PBS 20:1 and NaOAc/PBS 50:1 formulations exhibiting the highest luminescence readings. These findings demonstrate the potential of branched PBAE as an effective non-viral vector for mRNA delivery to primary HBECs, a cell type that is notoriously challenging to transfect[514]. The high transfection efficiency achieved by the PBS 20:1 and NaOAc/PBS 50:1 formulations is particularly encouraging, considering their demonstrated high mRNA encapsulation efficiency. Overall, the results suggest that branched PBAE holds promise as a non-viral vector for mRNA delivery to primary HBECs.

The size and charge of the polyplexes were characterised using DLS, as these properties are crucial for transfection efficiency. Smaller, uniformly sized particles generally exhibit better cellular uptake, while an optimal charge can enhance interaction with the cell membrane without causing significant cytotoxicity[483–488,490]. All formulations resulted in the formation of positively charged particles. However, the size and stability of the particles varied depending on the buffer formulation and mass ratio. Particles formulated in NaCl buffer at 20:1 or 50:1

PBAE to mRNA mass ratio were the largest in size and unstable. This aligns with their low transfection efficiency observed in HBECs and their significantly higher cytotoxicity. Interestingly, the particles formulated in PBS buffer at 20:1 mass ratio were larger and less stable than the particles formulated in NaOAc/PBS formulation at 50:1 mass ratio. Nevertheless, the PBS-formulated particles were still able to achieve comparable transfection efficiency to the NaOAc/PBS-formulated particles at 50:1 mass ratio. NaOAc formulations at 20:1 and 50:1 mass ratio resulted in similar-sized particles that were stable. This corroborates with Patel *et al.*, who reported that NaOAc formulations produced stable polyplexes of similar size[463]. Additionally, these formulations were comparable to the particles formulated in NaOAc/PBS at 20:1 and 50:1 mass ratio. Overall, the results suggest that the buffer formulation and PBAE to mRNA mass ratio have a significant impact on the size, stability, transfection efficiency, and cytotoxicity of branched PBAE/mRNA polyplexes. Future studies could explore the mechanisms underlying the superior transfection efficiency of the NaOAc/PBS at 50:1 mass ratio, such as cellular uptake, buffering capacity, and endosomal escape.

The formulation with NaOAc/PBS at 50:1 PBAE to mRNA mass ratio emerged as the optimal formulation for mRNA transfection in primary HBECs. This formulation exhibited a superior combination of particle size, charge, stability, mRNA encapsulation efficiency, transfection efficiency, and low cytotoxicity. Its superior performance over NaOAc alone is likely due to its synergistic buffering capacity and ionic strength offered by NaOAc/PBS mixture. PBAEs are recognised for their high buffering capacity in neutral to basic environments, which is crucial for enhancing transfection efficiency[515]. This buffering effect supports the proton sponge hypothesis, leading to an osmotic pressure gradient within endosomes, causing them to burst and release nucleic acids into the cell cytoplasm. Additionally, polyplex stability is influenced by the ionic strength of the surrounding environment[516]. In general, polyplexes are more stable in low ionic strength conditions. This stability is because low ionic strength weakens the interactions between polymer and nucleic acids and reduces electrostatic repulsion, which is essential in preventing aggregation[517]. On the other hand, higher salt concentrations can enhance these interactions and repulsions. Importantly, the 50:1 NaOAc/PBS formulation demonstrated consistent results across different batches, underscoring its reliability and consistency for mRNA transfection. This thorough exploration of branched PBAE-mediated mRNA transfection highlights the complex relationship between vector formulation and its biological effectiveness. The NaOAc/PBS formulation at 50:1 PBAE to mRNA with its effective mRNA protection, and improved transfection efficiency, emerges as a promising option for downstream transfection experiments.

Basal cells play a critical role in repairing and regenerating the lining of the airways following injury[518–520]. Their unique ability to self-renew and differentiate into various cell types is essential for maintaining the structural and functional integrity of the airway epithelium[521]. It is crucial to maintain the basal cell phenotype when employing gene manipulation techniques on these cells. mRNA transfection offers a promising approach to deliver genes of interest to basal cells and promote the expression of target proteins. This technique is valuable for exploring gene functions, studying disease mechanisms, and developing novel therapeutic strategies. However, it is essential to ensure that the transfection process itself does not alter the basal cell phenotype, as this could lead to adverse effects on the function of the bronchial epithelium.

This study focused on examining whether the basal cell phenotype remains unchanged following reporter mRNA transfection. To evaluate this, immunofluorescence was used to detect the expression of KRT5, a well-established marker for basal cells[522]. It was demonstrated that KRT5 expression was maintained in HBECs 24 hours-post transfection using both branched PBAE and the commercial transfection reagent JetMessenger. This outcome indicates that the basal phenotype of HBECs remained intact. Consequently, this finding supports the notion that non-viral mRNA transfection, under the conditions used in this thesis, is a safe method for mRNA delivery into basal HBECs. In addition, this suggests that any observed changes in cell behaviour or function in subsequent assays are likely due to the action of the encoded protein, rather than being non-specific effects of the transfection process itself. This methodology holds promise as a valuable tool for studying the function of genes involved in bronchial epithelial function and disease pathogenesis, modelling respiratory diseases *in vitro*, and developing novel therapeutic approaches. Exploring the long-term impact of mRNA transfection on HBEC ability to proliferate and differentiate will enhance our understanding of its broader implications for basal cell biology. The preservation of the basal cell phenotype in HBECs following reporter mRNA transfection led to the hypothesis that this approach would not impede the ability of primary HBECs to form a differentiated epithelium in ALI cultures.

HBEC ALI culture model was established to investigate the long-term impact of mRNA transfection on HBEC integrity and differentiation. ALI cultures recapitulate key features of the *in vivo* airway, including cellular composition, mucus production, and barrier function to enable investigation into the effects of mRNA transfection on HBEC integrity and differentiation over time[494,523,524]. HBEC ALI cultures were characterised using histology, immunofluorescence staining, and TEM. Histological analysis revealed that day 28 post-ALI cultures formed a well-differentiated epithelium, with a distinct basal cell layer, ciliated columnar cells, and secretory

cells. Immunofluorescence staining confirmed the presence of markers of epithelial differentiation, such as MUC5AC[525] (goblet cells), acetylated alpha tubulin[526] (cilia), and a marker of tight junctions[527] (ZO-1). TEM analysis of HBEC day 28 post-ALI cultures revealed a well-differentiated pseudostratified epithelium with ciliated cells, goblet cells, and basal cells. The TEM analysis also revealed the presence of tight junctions between adjacent cells, which are essential for barrier function.

Having established and characterised HBEC ALI cultures, I aimed to compare mRNA transfection efficiency between submerged HBECs and those cultured at ALI for 7 days. Due to the formation of robust barrier properties and cell-cell junctions within the ALI system, it was anticipated that primary HBECs cultured in submerged conditions would show higher transfection efficiency compared to those in ALI culture. To investigate this, both submerged HBECs and HBECs cultured at ALI for 7 days were transfected with reporter mRNA complexed with the optimised branched PBAE formulation and commercial transfection reagent JetMessenger. Submerged HBECs demonstrated effective uptake and translation of reporter mRNA. In contrast, HBECs cultured at ALI for 7 days showed no detectable mRNA transfection. This difference in transfection efficiency between the submerged and ALI HBECs is likely due to the development of robust barrier properties in the ALI culture system. In this system, cells undergo differentiation and polarisation, leading to the formation of tight junctions and a more complex, pseudostratified epithelium. This enhanced barrier function in ALI HBECs presents a significant challenge to mRNA transfection.

To evaluate whether reporter mRNA transfection would affect the integrity and differentiation of HBECs in the ALI culture system, HBECs were transfected prior to air exposure (submerged 24 hours post-seeding) and allowed to grow at ALI for 28 days. TEER, a quantitative method that evaluates the electrical resistance across a cell monolayer and provides an indication of barrier function and integrity of cellular tight junctions[528], was used in this study. TEER measurements showed no differences between the non-transfected and mRNA transfected cells, indicating that mRNA transfection does not impair the structural integrity of the epithelium. To further strengthen this conclusion, it would have been useful to include a positive control group where cells were treated with a reagent known to disrupt the epithelial barrier. Measuring TEER in this group would have established a baseline for a compromised barrier and provided a clearer comparison to the TEER values of the transfected and non-transfected cells. Non-transfected HBEC ALI cultures had lower TEER levels than those reported in previous studies[529,530], but these levels remained unaltered in mRNA transfected HBEC ALI cultures. TEER measurements can be influenced by various factors, including temperature, the composition of the culture medium, the passage number of cells, the

supporting material for the cell layer (transwell insert)[531]. Due to these potential variables, relying solely on the TEER assay may not provide a complete understanding of barrier permeability or the integrity of tight junctions. To further assess the impact of mRNA transfection on epithelial integrity, the FITC-Dextran permeability assay was used. This assay evaluates the movement of a fluorescently labelled dextran molecule across the epithelial monolayer and complements TEER measurements by offering a direct assessment of paracellular transport[532]. The absence of a difference in FITC-Dextran permeability between non-transfected and mRNA transfected HBEC ALI cultures confirms that epithelial permeability remained unaltered in mRNA transfected cells. Additionally, qPCR was used to quantify the expression of key barrier function markers, including *CDH1* (E-cadherin), *TJP1* (ZO-1), *OCLN* (occludin)[533]. The consistent/unaltered expression of these genes between non-transfected and mRNA transfected HBEC ALI cultures provided molecular evidence that mRNA transfection did not disrupt the transcriptional landscape governing epithelial barrier function. Immunofluorescence staining for ZO-1, a key tight junction protein that plays a critical role in maintaining epithelial barrier function[534], was used to visualise its localisation. Staining results further confirmed the preservation of tight junction architecture post-transfection, as demonstrated by comparable staining patterns in non-transfected and mRNA transfected HBEC ALI cultures. Collectively, the results from the TEER measurements, FITC-Dextran permeability assay, qPCR, and immunofluorescence staining demonstrated that mRNA transfection, under the conditions tested in this thesis, does not impair epithelial integrity or barrier function.

The impact of reporter mRNA transfection on the differentiation of HBECs cultured at ALI was examined. The transcriptional levels of key epithelial differentiation markers, including *MUC5AC*[535], *MUC5B*[535], *SCGB1A1*[536], and *FOXJ1*[537] were quantified using qPCR. Data revealed no difference in the expression of these markers between mRNA transfected and non-transfected control cultures at day 28 post-ALI. These findings indicated that mRNA transfection, under the conditions applied, did not adversely affect the differentiation trajectory of HBECs. To further validate these findings, immunofluorescence staining was used to visualise the protein expression of TUBA1A (for cilia)[526] and MUC5AC (for goblet cells)[525]. Consistent with the qPCR data, immunofluorescence staining demonstrated the presence of goblet cells and cilia in both mRNA transfected and non-transfected control HBEC cultures at day 28 post-ALI cultures. These findings further confirmed that the differentiation capacity of HBECs was unaltered by mRNA transfection.

It is important to acknowledge that these experiments were performed using two primary cell donors. The relatively small sample size limits the statistical power of the study, and this necessitates cautious interpretation of the findings. For future work, it will be essential to expand the donor pool to reinforce the validity of these results.

3.4 Conclusion

In conclusion, this chapter has demonstrated that primary HBECs in submerged culture can be efficiently transfected with reporter mRNA using non-viral vectors. Branched PBAE formulated with NaOAc/PBS at 50:1 PBAE to mRNA mass ratio exhibited superior mRNA encapsulation, physicochemical properties, transfection efficiency, and cytotoxicity profile, making it the preferred choice for subsequent transfection experiments. In addition, this study demonstrated that HBECs cultured at ALI for 7 days cannot be transfected with mRNA. Furthermore, I have provided evidence that transfection of primary HBECs with reporter mRNA prior to air exposure did not compromise the integrity or differentiation potential of HBECs cultured ALI. These findings provide a foundation for the subsequent investigation detailed in Chapter 4, where the impact of delivering a physiologically relevant mRNA, FOXJ1, on the integrity and differentiation of HBECs at ALI was explored.

4 Results II - Investigating the influence of mRNA encoded FOXJ1 delivery on differentiation of human bronchial epithelial cells

4.1 Introduction

4.1.1 Motile cilia in airway epithelium

Multiciliated cells are specialised airway epithelial cells with multiple cilia on their apical surface. These cells are important for maintaining airway homeostasis by trapping and expelling pathogens, mucus, and other debris through the rhythmic beating of their motile cilia, known as mucociliary clearance[533]. Each multiciliated cell has 200-300 cilia, which are 6-7 μm long and 0.2-0.3 μm in diameter[534,535]. Motile cilia are microtubule-based hair-like organelles with a central axoneme containing nine pairs of microtubules surrounding two single microtubules ('9+2' arrangement, Figure 1.2)[536]. The axoneme extends from a basal body containing microtubule triplets in a nine-fold symmetrical arrangement, similar to centrioles in the centrosome, and is anchored to the plasma membrane[537]. The structural arrangement and function of cilia are described in more detail in section 1.2.1 of Chapter 1.

Section 1.2.3 of Chapter 1 highlights that ciliary dysfunction is a feature in several airway diseases. This dysfunction can severely compromise mucociliary clearance, thereby increasing the risk of respiratory infections. Conditions such as CF and PCD are characterised by impaired mucociliary clearance, leading to frequent and recurrent lung infections[538–543]. *In vitro* ALI cultures of differentiated primary airway epithelial cells have proven effective in diagnosing PCD. These cultures accurately mimic the ciliary phenotype associated with PCD[544,545]. Furthermore, secondary, acquired non-genetic defects in ciliary function can arise due to factors such as cigarette smoke and inflammation in diseases such as asthma and COPD, further increasing lung infections risks[534,546–548]. Asthmatic airways, for instance, exhibit reduced cilia motility, disoriented beat direction, and structural damage to cilia[549–551]. In COPD, there are morphological changes in the airway epithelium, such as a transition from pseudostratified to squamous epithelium, a decrease in ciliated cells, and shorter cilia. ALI cultures derived from bronchial epithelial cells of COPD patients show similar ciliary changes, including fewer multiciliated cells and shorter cilia, reflecting the *in vivo* phenotype[552]. ALI cultures have become invaluable tools for investigating ciliogenesis, cilia-related diseases, and the biology of ciliated cells. They offer a more representative model than traditional submerged cultures, especially in their ability to replicate the ciliary phenotype of PCD and other cilia-related diseases.

4.1.2 Multiciliated cell differentiation

Mutliciliated cells in the airways originate from progenitor cells, which express the TFs *TP63* and *SOX2*. These TFs are essential for the development and regeneration of ciliated cells[553–555]. During post-natal growth and in adulthood, multiciliated cells can originate from either basal cells or secretory cells[556]. The process of ciliogenesis, which involves the formation of cilia, is complex and tightly regulated. It requires the activation of a transcriptional program and a network of proteins. For basal progenitor cells to differentiate into mutliciliated cells, the inhibition of Notch signalling is necessary[557,558].

The early steps of multiciliated cell differentiation involve a network of protein interactions, including GEMININ (encoded by *GMNN*), GEMC1 (geminin coiled-coil-domain-containing protein 1, encoded by *GMNC*), MCIDAS (multi-ciliate differentiation and DNA synthesis), E2F4/5, DEUP1. Protein expression analysis has shown high levels of GEMININ in progenitor cells. GEMININ plays a role in inhibiting the transcriptional activation of *MCIDAS* and *GEMC1*[559–561], delaying the onset of mutliciliogenesis until dividing cells exit the cell cycle559. *GEMC1*, in collaboration with *E2F4/5* and *DEUP1* TFs, aids in the transcriptional activation of *MCIDAS*[560]. *MCIDAS* then forms complexes with *E2F4/5* and *DEUP1*, triggering the activation of genes critical for centriole amplification (*cMYB*, *CCNO*) and cilia formation (*FOXJ1*, *RFX*), thereby promoting multiciliogenesis[559,562,563]. Moreover, *MCIDAS* acts upstream of *p73*, a crucial regulator of motile ciliogenesis in the airways. *p73* also controls the expression of genes involved in centriole amplification (*MYB*, *CCNO*) and cilia formation (*FOXJ1*, *RFX2/3*)[564,565].

Following the initial phases of multiciliated cell differentiation, the process can be categorised into four distinct stages, each characterised by specific TFs and protein localisations crucial for cilia formation. These stages are: 1) basal body biogenesis protein synthesis, 2) basal body biogenesis, 3) migration and docking of basal bodies on the apical membrane, and 4) generation of motile cilia from basal bodies. Alongside the previously mentioned *p73* TF, *c-MYB* is another TF instrumental in the first two stages of multiciliated cell differentiation[566,567]. It activates post-cell cycle exit, contributes to centriole amplification, and is downregulated following the docking of centrioles and the maturation of multiciliated cells. *CCNO*, another factor involved in the early stages of multiciliogenesis, also aids in centriole amplification[568].

FOXJ1 and *RFX* TFs are critical during the later stages (3 and 4) of multiciliated cell differentiation, particularly in apical docking and cilium maturation. *FOXJ1* is regulated by *p73*, *GEMC1*, and *MCIDAS*[532]. *RFX2/3* function as co-activators of *FOXJ1*[559,569–572], and form a transcriptional complex that enhances the expression of genes involved in multiciliated cell

differentiation570. *FOXJ1* can also induce the expression of *RFX2* and *RFX3* in the human airway epithelium, indicating their role in multiciliated cell differentiation[570].

Overall, a collaborative effort of multiple TFs regulates the complex transcriptional network responsible for multiciliated cell differentiation. This network encompasses basal body biogenesis, their migration, docking, and the generation of cilia. A deeper understanding of this differentiation process from basal cells, and the potential impact of gene manipulation on these programs, could provide insights into respiratory health and disease.

4.1.3 FOXJ1 is a master regulator of ciliogenesis

FOXJ1 is a TF that is pivotal in the differentiation of ciliated cells in the airway epithelium. The expression of FOXJ1 is linked with the development of motile cilia. This connection is clearly demonstrated in FOXJ1 knockout mice, which lack motile cilia in the airways, choroid plexus, and oviducts, and exhibit defects in left-right asymmetry[573,574]. TEM analysis of airway cells from FOXJ1 mutant mice has shown disrupted '9+2' microtubule arrangements and impaired docking of basal bodies to the apical cell membrane[573]. *In vitro* studies of airway cells from FOXJ1 mutant mouse embryos indicate that while basal bodies are formed normally, they are unable to dock at the apical membrane[575,576]. The role of FOXJ1 in regulating motile ciliogenesis is conserved across vertebrates, as evidenced by findings in Xenopus and zebrafish[577,578].

FOXJ1 has been shown to induce the formation of ectopic functional motile cilia in various tissues of zebrafish and Xenopus embryos[578,579]. While the ciliogenic potential of FOXJ1 in higher vertebrates is less clearly established, evidence suggests its conversation across species. For example, in murine lung development, FOXJ1 expression precedes the appearance of cilia in airway epithelial cells[580]. During respiratory virus-induced injury, a correlation has been observed between the loss of cilia and FOXJ1 expression; FOXJ1 re-expression is associated with the appearance of ultrastructural components necessary for ciliogenesis during airway repair[581,582]. Transgenic mice expressing FOXJ1 under the control of the surfactant protein C promoter exhibited the formation of ciliated cells in alveolar spaces[583]. Additionally, overexpression of FOXJ1 induced the formation of cilia in chick neural tube and NIH3T3 mouse embryonic fibroblastic cell line[584]. However, this effect was not replicated in MDCK canine kidney epithelial cells, BEAS2B non-ciliated human airway epithelial cells, or mouse tracheal epithelial cells[576]. This variability in outcomes may result from differences in expression strategies, FOXJ1's reliance on specific co-factors, limitations of *in vitro* culture systems, or it may reflect species-specific differences in the ability of FOXJ1 to induce ectopic cilia. These findings collectively underscore the pivotal role of FOXJ1 as a

regulator of motile cilia biogenesis. Investigating FOXJ1-mediated ciliogenesis could provide valuable insights into the processes of ciliogenesis and ciliopathies, which are conditions linked with abnormal ciliary differentiation and function.

FOXJ1, recognised as a master regulator of motile ciliogenesis, plays a crucial role in orchestrating the docking of basal bodies at the apical membrane and in inducing the assembly of axonemes. These actions are fundamental to the process of ciliogenesis in mutliciliated cells and to the expression of proteins that enable ciliary motility[585]. FOXJ1 achieves this by either directly or indirectly activating the transcription of a variety of genes. These genes are involved in various aspects of ciliary development, including centrosome and cilium assembly (*CETN2*), axonome assembly (*DNAH11*, *DNALI1*, *RSPH9, TUBA1A*), IFT processes (*IFT172*, *DYNC2H1*), and other TFs (*RFX2*, *RFX3*) among others[586].

4.1.4 Manipulation of FOXJ1 expression in primary HBECs *in vitro*

In vitro studies manipulating FOXJ1 expression have been instrumental in understanding its role in ciliogenesis. For instance, Rapiteanu *et al.* utilised a CRISPR/Cas9-based system to deplete FOXJ1, which significantly reduced the number of ciliated cells in human ALI cultures. This study provided the first evidence that FOXJ1 is essential for ciliation in ALI-differentiated primary HBECs *in vitro*[587]. Similarly, Zahid *et al.* found that using siRNA to knockdown FOXJ1 in tracheal epithelial cultures inhibited ciliation, further confirming its role as a central regulator of motile cilia[588]. Didon *et al.* also contributed to this area of research by showing that FOXJ1 expression, induced by plasmid-mediated gene transfer, can induce the expression of ciliated cell genes in primary human airway basal cells[589]. This discovery led to subsequent research investigating whether FOXJ1 overexpression via lentivirus in basal cells differentiated in ALI cultures could prevent cigarette smoke extract (CSE)-mediated inhibition of cilia growth[534]. FOXJ1 overexpression reversed the CSE-induced cilia growth inhibition and partially prevented the downregulation of IFT genes and a basal body development gene. This suggests that stimulating ciliogenesis through FOXJ1 overexpression could preserve normal cilia length even under the stress of cigarette smoke exposure. Therefore, gene-based manipulation of FOXJ1 expression offers valuable insights into its role in ciliogenesis and its potential as a therapeutic target for diseases associated with impared ciliary function.

Despite the interest in the role of FOXJ1 as a key regulator of ciliated cell differentiation, research efforts in primary HBECs have been limited to overexpression studies using DNA-based approaches. Unlike DNA, exogenous mRNA is delivered to the cytoplasm of target cells for transient translation using the cell's own ribosomal machinery without the same risk of insertional mutagenesis. A significant advantage of exogenous mRNA is that the translated

protein is functionally identical to the endogenous protein, as it undergoes the same post-translational modifications and processing[590]. The potential of using exogenous FOXJ1 mRNA to manipulate FOXJ1 expression in primary HBECs remains unexplored and represents a promising avenue for research.

4.1.5 Hypothesis and aims

This chapter characterises exogenous FOXJ1 mRNA translation in primary HBECs and the effect of exogenous translated FOXJ1 protein on inducing the transcriptional program of ciliated cell differentiation. Moreover, this chapter investigates the influence of exogenous FOXJ1 mRNA translation on primary HBEC differentiation cultured at ALI.

Hypothesis

Transient FOXJ1 protein expression induced by non-viral delivery of FOXJ1 mRNA to primary HBECs will accelerate ciliogenesis.

Aims

1. Establish non-viral transfection of FOXJ1 encoded mRNA in primary HBECs and characterise exogenous FOXJ1 mRNA translation.
2. Check functionality of synthetic FOXJ1 mRNA after non-viral delivery to primary HBECs.
3. Investigate the influence of synthetic FOXJ1 mRNA delivery on the differentiation of primary HBECs in ALI culture.
4. Assess the impact of synthetic FOXJ1 mRNA delivery on the organisation, morphology, and integrity of primary HBECs cultured at ALI.

4.2 Results

4.2.1 Selection of supplier for ordering synthetic FOXJ1 mRNA

To identify the optimal source of synthetic FOXJ1 mRNA, the performance of reporter FLuc mRNAs from four different commercial suppliers (Trilink, Stratech/ApexBio, RiboPro, OzBiosciences) was evaluated on submerged 16HBE cells. FLuc mRNAs were complexed with branched PBAE (optimised formulation from Chapter 3), the selected commercial transfection reagent JetMessenger or delivered without a transfection reagent termed 'naked mRNA'. To assess the cytotoxicity of FLuc mRNA transfection in 16HBE cells, an LDH release assay was performed on cell culture supernatants 24 hours post-transfection. All FLuc mRNAs were well tolerated (Figure 4.1D-F), successfully translated, and achieved luminescence above the naked mRNA control 24 hours post-transfection (Figure 4.1A-C). However, the performance of FLuc mRNAs varied, and this could be attributed to differences in IVT mRNA structural elements, such as type of cap, poly A tail length, and base modification (Table 2.4). The OzBiosciences' FLuc mRNA achieved the highest luminescence with both delivery vectors. Therefore, synthetic FOXJ1 mRNA was purchased from OzBiosciences commercial supplier.

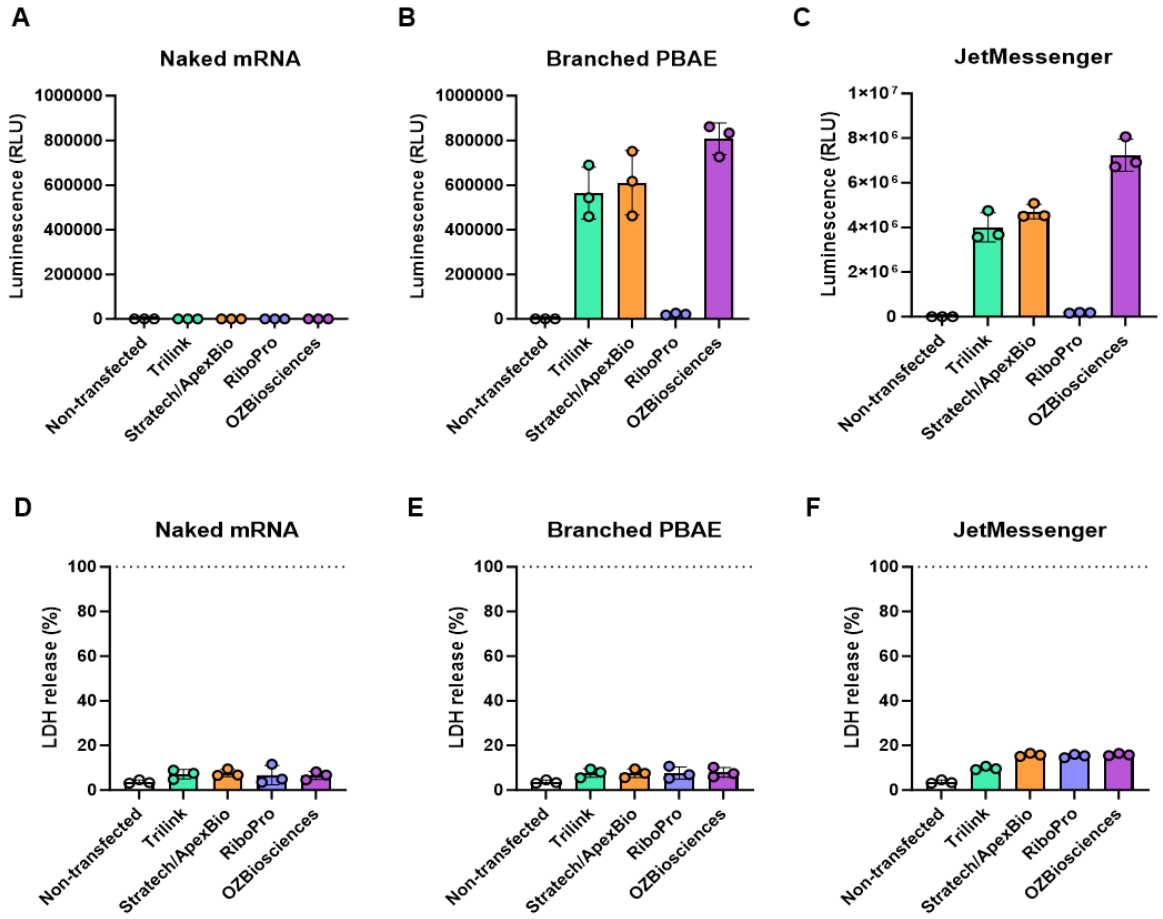


Figure 4.1 Performance of reporter FLuc mRNA from four different commercial suppliers following non-viral transfection in 16HBE cells.

Submerged 16 human bronchial epithelial (16HBE) cells were transfected with reporter Firefly Luciferase (FLuc) mRNA (50 ng) from four different commercial suppliers. (A-C) Luminescence (relative light units) at 24 hours post-transfection with FLuc mRNA delivered (A) naked, complexed with (B) branched poly β-amino ester (PBAE) or (C) commercial transfection reagent JetMessenger. (D-F) Lactate dehydrogenase (LDH) release (%) from 16HBE cells at 24 hours post-transfection with FLuc mRNA delivered (D) naked, formulated with (E) branched PBAE or (F) commercial transfection reagent JetMessenger. Dotted line indicate 100% LDH release of positive control cells treated with 1% Triton-X-100 and LDH release of samples was calculated relative to this control. Data represents mean ± SD. n = 3 technical replicates.

4.2.2 Functionality of synthetic FOXJ1 mRNA on 16HBE cells

Prior to initiating primary HBEC transfection experiments with FOXJ1 mRNA, I used 16HBE cells to test the functionality of synthetic FOXJ1 mRNA. FOXJ1 mRNA was complexed with branched PBAE (optimised formulation from Chapter 3), selected commercial transfection reagent JetMessenger or delivered naked to submerged 16HBE cells to determine whether 16HBE cells can be transfected with FOXJ1 mRNA. Control transfections with vectors (PBAE/JetMessenger) formulated with reporter mRNA (GFP) were also performed to determine if reporter mRNA transfection can induce FOXJ1 expression. Cells were fixed and immunofluorescence stained with FOXJ1 over 48 hours post-transfection, and transfection efficiency (% FOXJ1 positive cells) was quantified.

FOXJ1 expression was detected in cells transfected with FOXJ1 mRNA complexed with non-viral vectors (PBAE or JetMessenger) (Figure 4.2A). No expression of FOXJ1 was observed in non-transfected cells, naked FOXJ1 mRNA transfected cells or GFP mRNA transfected cells (Figure 4.2A). FOXJ1 protein, as a TF, is expressed in the nuclei of cells591,592. This assay confirmed the correct localisation of FOXJ1 protein after transfection. Quantification of transfection efficiency, shown in Figure 4.2B, demonstrated that FOXJ1 expression levels peak 12 hours post-transfection with PBAE transfected cells reaching 20.6% ± 0.8 FOXJ1 positive cells while JetMessenger transfected cells reaching 48.9% ± 0.9 FOXJ1 positive cells (Figure 4.2B). Cytotoxicity as measured by LDH release was assessed over 48 hours post-transfection. 16HBE cells tolerated FOXJ1 mRNA transfection as demonstrated by no elevation in LDH release compared to non-transfected control cells (Figure 4.2C).

The functionality of synthetic FOXJ1 mRNA was evaluated by assessing the expression of FOXJ1-downstream genes involved in ciliogenesis following successful FOXJ1 mRNA translation using qPCR. Upregulation of FOXJ1 downstream genes (*RFX2*, *DNAH11*) was observed in conditions that received FOXJ1 mRNA transfection compared to non-transfected and naked FOXJ1 mRNA transfected cells (Figure 4.3).

Together this data confirmed that 16HBE cells can be successfully transfected with mRNA encoded FOXJ1 complexed with non-viral vectors and supported future FOXJ1 mRNA transfection experiments in primary HBECs.

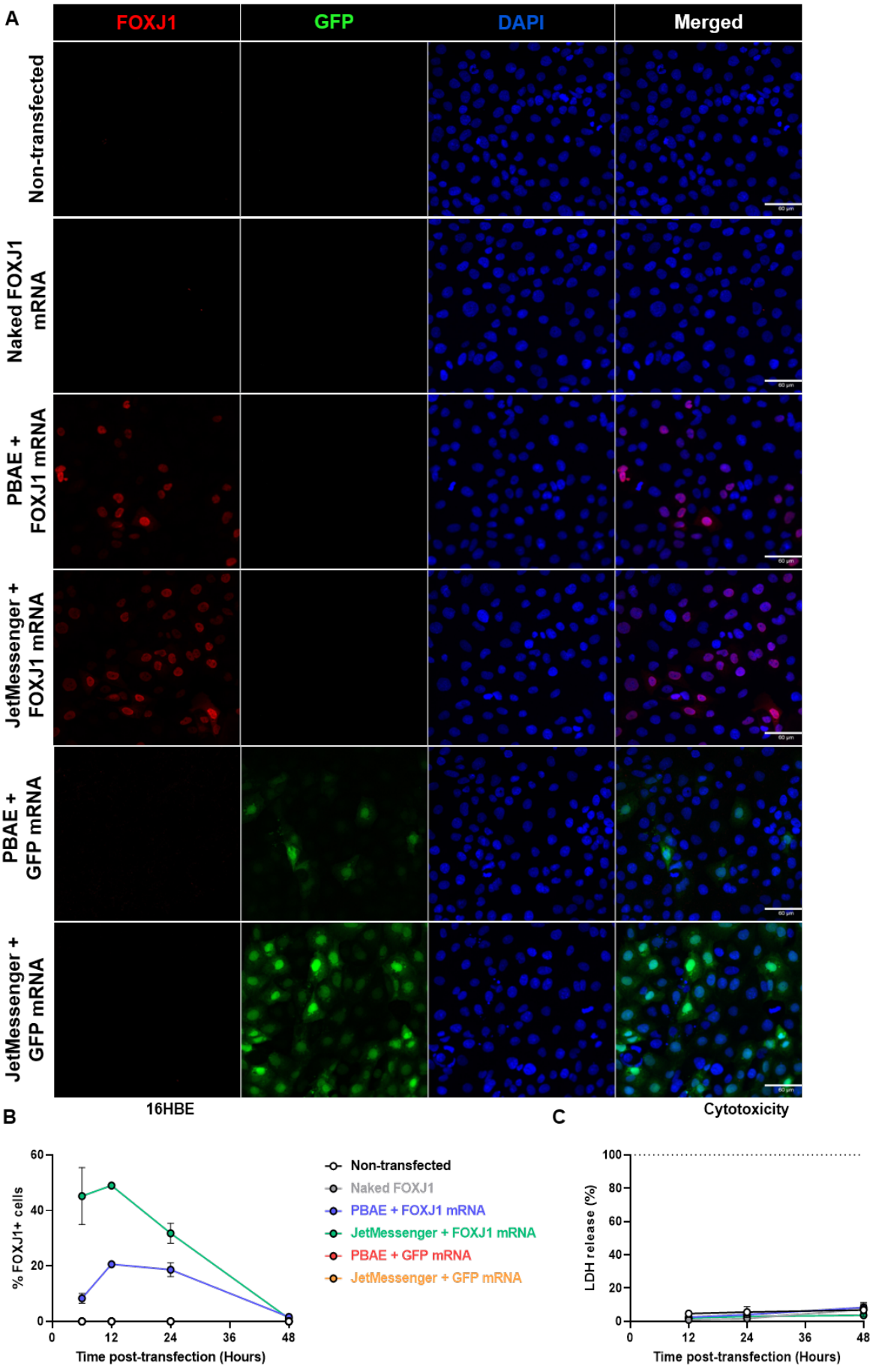

A
FOXJ1
GFP
DAPI
Merged
Non-transfected
Naked FOXJ1 mRNA
PBAE + FOXJ1 mRNA
JetMessenger + FOXJ1 mRNA
PBAE + GFP mRNA
JetMessenger + GFP mRNA
16HBE
B
% FOXJ1+ cells
Time post-transfection (Hours)
Non-transfected
Naked FOXJ1
PBAE + FOXJ1 mRNA
JetMessenger + FOXJ1 mRNA
PBAE + GFP mRNA
JetMessenger + GFP mRNA
C
Cytotoxicity
LDH release (%)
Time post-transfection (Hours)

Figure 4.2 Transfection efficiency of synthetic FOXJ1 mRNA in 16HBE cells.

(A) Representative images of 16 human bronchial epithelial (16HBE) cells at 12 hours post-transfection with synthetic FOXJ1 mRNA or control green fluorescent protein (GFP) mRNA (100 ng/well) delivered naked or complexed with poly β-amino ester (PBAE) or commercial transfection reagent JetMessenger. Cells were fixed with 4% paraformaldehyde (PFA), stained with anti-FOXJ1 antibody and cell nuclei were counter stained with DAPI. (B) FOXJ1 transfection efficiency measured by determining the percentage of FOXJ1 positive cells (% FOXJ1+ cells) in 16HBE cells over 48 hours post-transfection. (C) Lactate dehydrogenase release (LDH) release (%) in 16HBE cells over 48 hours post-transfection. Dotted line indicates 100% LDH release of positive control cells treated with 1% Triton-X-100 and LDH release of samples was calculated relative to this control. Data represents mean ± SD. n = 3 technical replicates.

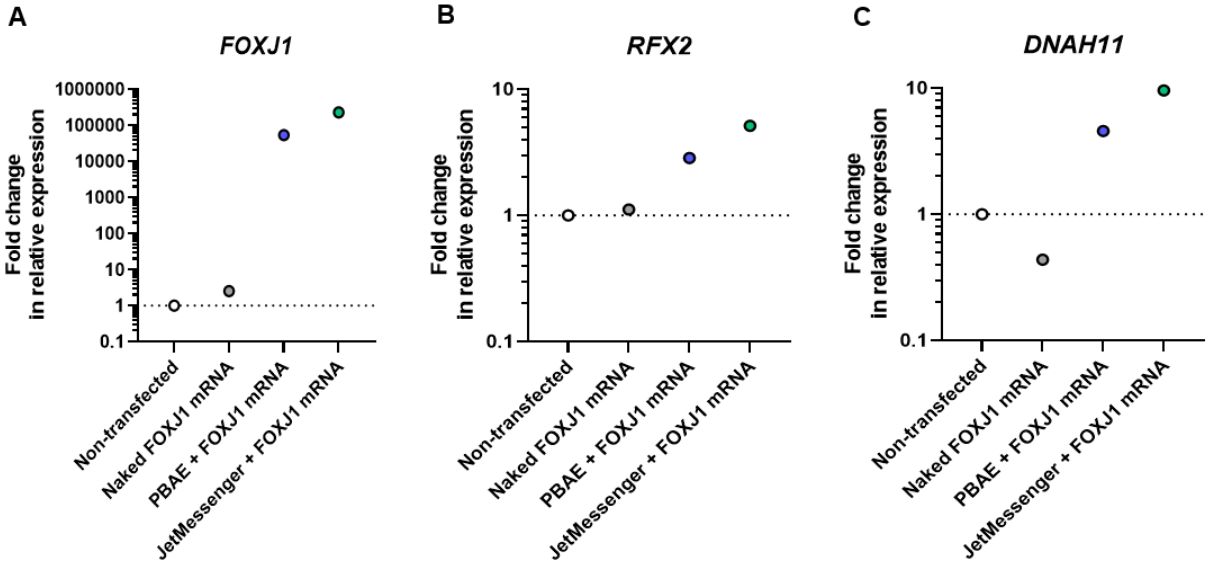


Figure 4.3 Expression of FOXJ1 and two downstream genes following FOXJ1 mRNA transfection in 16HBE cells.

16 human bronchial epithelial (16HBE) cells were transfected with FOXJ1 mRNA (100 ng/well) delivered naked or complexed with poly β-amino ester (PBAE) or commercial transfection reagent JetMessenger. Cells were harvested 12 hours post-transfection and qPCR was used to quantify A) *FOXJ1*, (B) *RFX2*, (C) *DNAH11* fold change from non-transfected control. n = 3 technical replicates, each dot represents a pooled technical triplicate.

4.2.3 Submerged primary HBECs can be transfected with mRNA-encoded FOXJ1

The confirmation that 16HBE cells can be transfected with FOXJ1 mRNA in section 4.2.2 of this chapter supported the application of exogenous FOXJ1-encoded mRNA in primary HBECs. 16HBE cells are immortalised cells that do not fully recapitulate the characteristics of normal differentiated bronchial epithelium[593]. Therefore, a switch to primary HBECs, which are more physiological relevant, was essential to investigate the influence of FOXJ1 mRNA transfection on bronchial epithelial differentiation. To establish non-viral transfection and characterise FOXJ1 mRNA expression profile in primary HBECs, increasing doses of FOXJ1 encoded mRNA (50/100/200 ng per well) were formulated with branched PBAE (optimised formulation Chapter 3) or JetMessenger non-viral vectors.

Expression of FOXJ1 mRNA was assessed in cell lysates via qPCR and a dose-dependent relationship between the amount of transfected mRNA (50/100/200 ng) and the detected mRNA levels of FOXJ1 was demonstrated across all time-points after transfection (6-48 hours) (Figure 4.4A-D). Control transfections with naked FOXJ1 mRNA and non-viral vectors (PBAE/JetMessenger) formulated with reporter mRNA (GFP), and vector-only conditions were also performed to determine whether vectors or reporter transfection can induce FOXJ1 mRNA expression. No induction of FOXJ1 expression in these control conditions was observed (Figure 4.5).

Similar to the 16HBE FOXJ1 mRNA transfection efficiency described in section 4.2.2 above, primary HBEC FOXJ1 transfection efficiency was evaluated over 48 hours post-transfection. Immunofluorescence staining for FOXJ1 confirmed a robust FOXJ1 expression in FOXJ1 mRNA transfected cells only (Figure 4.6A). FOXJ1 was localised in the nuclei of cells as anticipated[591,592]. No FOXJ1 expression was observed in control transfection conditions (naked FOXJ1 mRNA, non-viral vectors formulated with GFP mRNA, non-viral vectors only) (Figures 4.6A and 4.7). PBAE transfection with 50 ng of FOXJ1 mRNA resulted in peak FOXJ1 transfection efficiency (14.8% $\pm$ 4.9) at 12 hours post-transfection, while JetMessenger transfection with 50 ng of FOXJ1 mRNA resulted in peak FOXJ1 transfection efficiency between 6- and 12-hours post-transfection (6 hours: 7.1% $\pm$ 3.6, 12h: 7.9% $\pm$ 5.2) (Figure 4.6B). PBAE or JetMessenger transfection with 100 ng of FOXJ1 mRNA resulted in peak of FOXJ1 transfection efficiency at 12 hours post-transfection, with PBAE transfection yielding 50.9% $\pm$ 19.2 FOXJ1 positive cells, whereas JetMessenger transfection yielded 30.6% $\pm$ 4.5 FOXJ1 positive cells (Figure 4.6C). PBAE transfection with 200 ng of FOXJ1 mRNA resulted in peak FOXJ1 transfection efficiency (5.9% $\pm$ 1.3) at 24 hours post-transfection, while JetMessenger transfection with 200 ng of FOXJ1 mRNA resulted in peak FOXJ1 transfection

efficiency (13.4% ± 6.9) at 12 hours post-transfection (Figure 4.6D). PBAE transfection with 100 ng of FOXJ1 mRNA exhibited a more prolonged duration of FOXJ1 expression compared to JetMessenger transfection with the same dose of FOXJ1 mRNA (PBAE transfection 24 hours: 37.9% ± 19.9, PBAE transfection 48 hours: 5.4% ± 4.7, JetMessenger transfection 24 hours: 6.7% ± 2.3, JetMessenger transfection 48 hours: 1% ± 0.1) (Figure 4.6C, Table 4.1).

In addition, naked and PBAE transfections with 50 ng, 100 ng and 200 ng of FOXJ1 mRNA as well as JetMessenger transfection with 50 ng of FOXJ1 mRNA did not result in significant elevation of LDH release at 6-48 hours post-transfection compared to non-transfected primary HBECs (Figure 4.8A-C). However, naked transfection with 200 ng of FOXJ1 mRNA and JetMessenger transfections with 100 ng and 200 ng of FOXJ1 mRNA significantly elevated LDH release compared to non-transfected primary HBECs (100 ng: non-transfected vs JetMessenger+FOXJ1 mRNA *P=0.0354, 200 ng: non-transfected vs naked FOXJ1 mRNA ***P=0.0003, non-transfected vs JetMessenger+FOXJ1 mRNA ****P<0.0001) (Figure 4.8B-C, Table 4.2).

These data demonstrated successful transfection of primary HBECs with FOXJ1 mRNA at an optimal dose of 100 ng. This dose was chosen based on its high transfection efficiency and low cytotoxicity. When the dose of FOXJ1 mRNA was increased from 100 ng to 200 ng, no further benefits were observed. The higher dose led to lower transfection efficiency and increased cytotoxicity. Therefore, the 100 ng dose was selected for subsequent investigations.

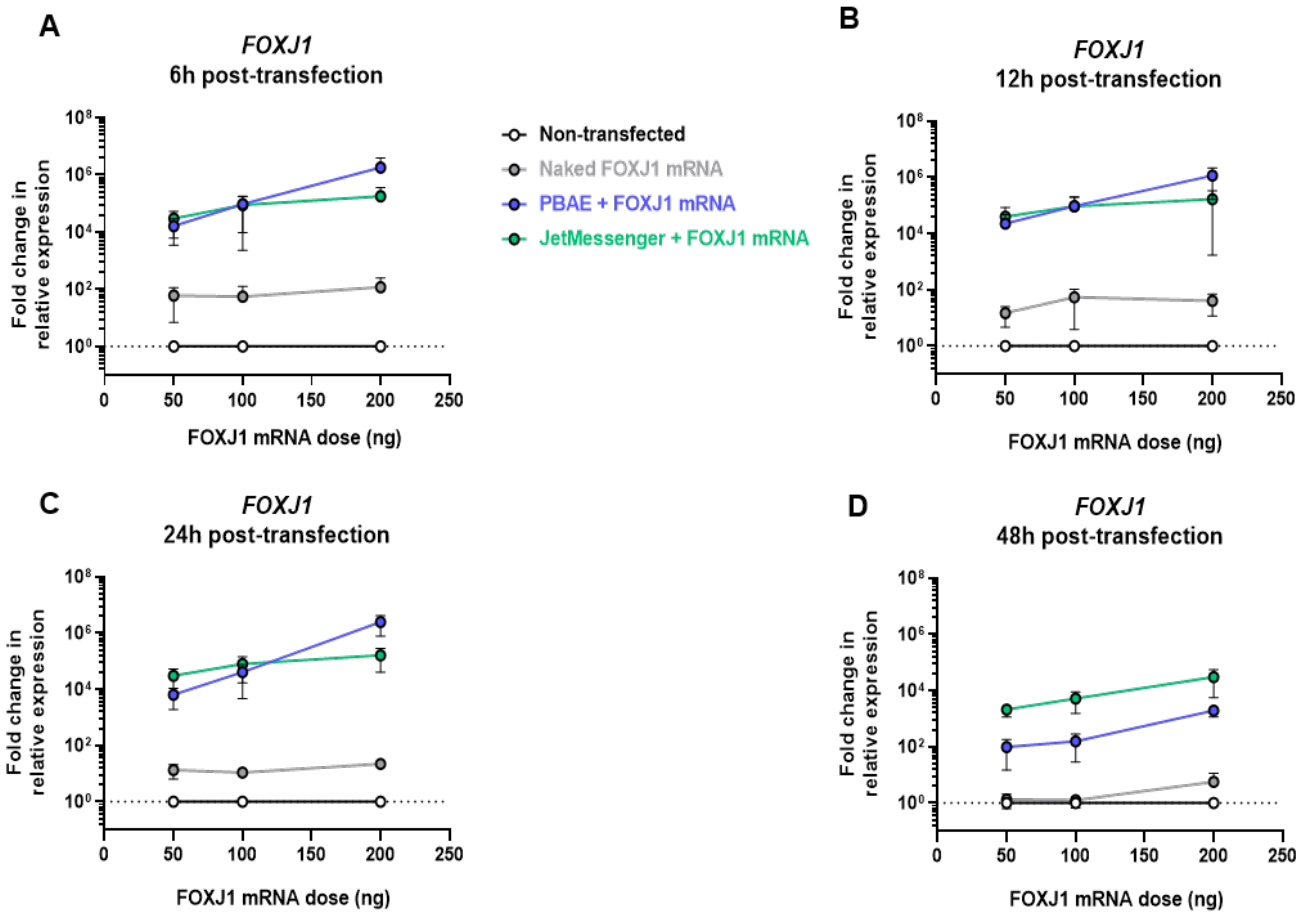


Figure 4.4 Expression of FOXJ1 following FOXJ1 mRNA transfection in submerged primary HBECs.

Submerged primary human bronchial epithelial cells (HBECs) were transfected with increasing doses of FOXJ1 mRNA (50/100/200 ng) delivered naked or complexed with branched poly β-amino ester (PBAE) or commercial transfection reagent JetMessenger. Cells were harvested between 6-48 hours post-transfection and qPCR was used to quantify *FOXJ1* fold change from non-transfected controls at (A) 6 hours post-transfection, (B) 12 hours post-transfection, (C) 24 hours post-transfection, (D) 48 hours post-transfection. Data represents mean ± SD. N = 3 primary cell donors with 3 technical replicates each.

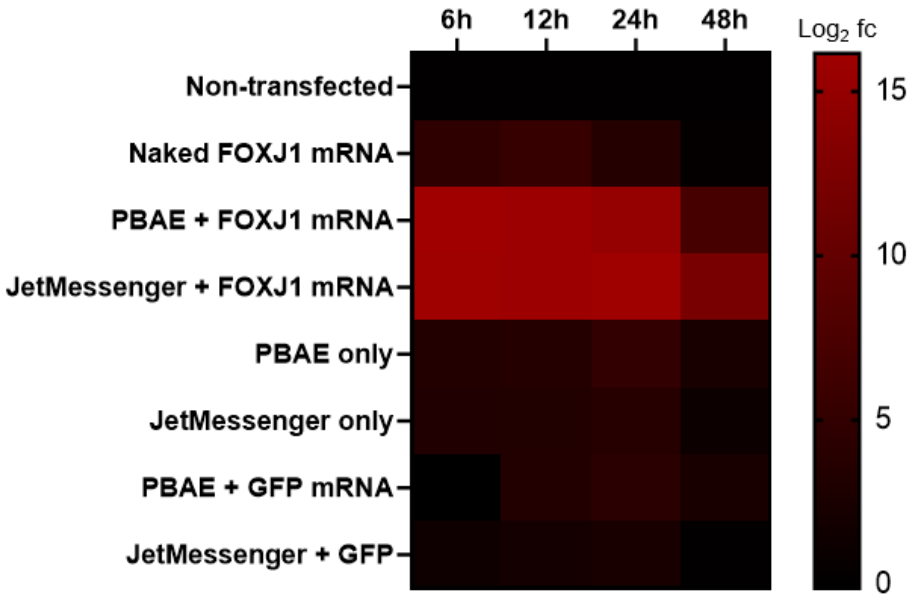


Figure 4.5 Expression of FOXJ1 following FOXJ1 mRNA and reporter mRNA transfection in submerged primary HBECs.

Submerged primary human bronchial epithelial cells (HBECs) were transfected with 100 ng FOXJ1 mRNA delivered naked or complexed with branched poly β-amino ester (PBAE) or commercial transfection reagent JetMessenger. Cells were also transfected with reporter green fluorescent protein (GFP) mRNA complexed with branched PBAE or JetMessenger or vector only-controls. Cells were harvested between 6-48 hours post-transfection and qPCR was used to quantify *FOXJ1* mRNA expression. Data represents $\log_2$ fold change from non-transfected control. N = 3 primary cell donors with 3 technical replicates each.

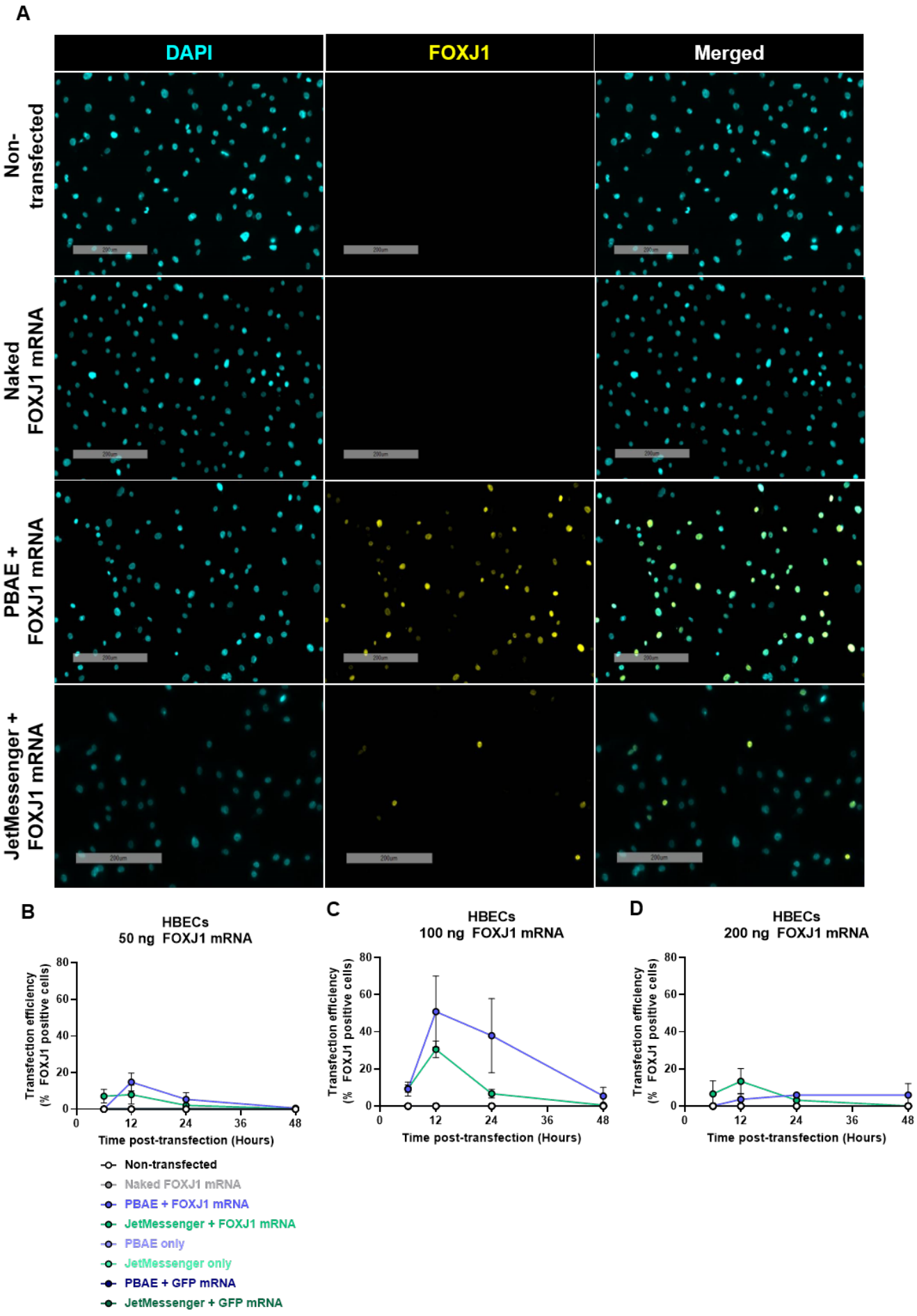

A
DAPI
FOXJ1
Merged
Non-transfected
Naked FOXJ1 mRNA
PBAE + FOXJ1 mRNA
JetMessenger + FOXJ1 mRNA
B
HBECs
50 ng FOXJ1 mRNA
C
HBECs
100 ng FOXJ1 mRNA
D
HBECs
200 ng FOXJ1 mRNA
Transfection efficiency (% FOXJ1 positive cells)
Time post-transfection (Hours)
Non-transfected
Naked FOXJ1 mRNA
PBAE + FOXJ1 mRNA
JetMessenger + FOXJ1 mRNA
PBAE only
JetMessenger only
PBAE + GFP mRNA
JetMessenger + GFP mRNA

Figure 4.6 Transfection efficiency of synthetic FOXJ1 mRNA in submerged primary HBECs.

Submerged primary human bronchial epithelial cells (HBECs) were transfected with increasing doses of FOXJ1 mRNA (50/100/200 ng) delivered naked or complexed with branched poly β-amino ester (PBAE) or commercial transfection reagent JetMessenger. (A) Representative images of non-transfected control cells and FOXJ1 mRNA transfected cells stained with anti-FOXJ1 antibody and cell nuclei counter stained with DAPI at 12 hours post-transfection. FOXJ1 transfection efficiency was measured at 6, 12, 24, and 48 hours post-transfection and expressed as percentage of FOXJ1 positive cells with (B) 50 ng mRNA dose, (C) 100 ng mRNA dose, (D) 200 ng mRNA dose. Data represents mean ± SD. N = 3 primary cell donors with 3 technical replicates each. Statistics: 2way ANOVA followed by Dunnett's multiple comparisons test. Statistical analysis results are summarised in Table 4.1.

Table 4.1 Summary of statistical analysis of FOXJ1 transfection efficiency in submerged primary HBECs.

	Summary	Adjusted P value
50 ng FOXJ1 mRNA		
6h post-transfection: Non-transfected vs JetMessenger + FOXJ1 mRNA	****	<0.0001
12h post-transfection: Non-transfected vs PBAE + FOXJ1 mRNA	****	<0.0001
12h post-transfsection: Non-transfected vs JetMessenger + FOXJ1 mRNA	****	<0.0001
24h post-transfection: Non-transfected vs PBAE + FOXJ1 mRNA	****	<0.0001
100 ng FOXJ1 mRNA		
6h post-transfection: Non-transfected vs PBAE + FOXJ1 mRNA	*	0.0135
6h post-transfection: Non-transfected vs JetMessenger + FOXJ1 mRNA	**	0.0099
12h post-transfection: Non-transfected vs PBAE + FOXJ1 mRNA	****	<0.0001
12h post-transfection: Non-transfected vs JetMessenger + FOXJ1 mRNA	****	<0.0001
24h post-transfection: Non-transfected vs PBAE + FOXJ1 mRNA	****	<0.0001
200 ng FOXJ1 mRNA		
6h post-transfection: Non-transfected vs JetMessenger + FOXJ1 mRNA	****	<0.0001
12h post-transfection: Non-transfected vs PBAE + FOXJ1 mRNA	*	0.0226
12h post-transfection: Non-transfected vs JetMessenger + FOXJ1 mRNA	****	<0.0001
24h post-transfection: Non-transfected vs PBAE + FOXJ1 mRNA	****	<0.0001
48h post-transfection: Non-transfected vs PBAE + FOXJ1 mRNA	****	<0.0001

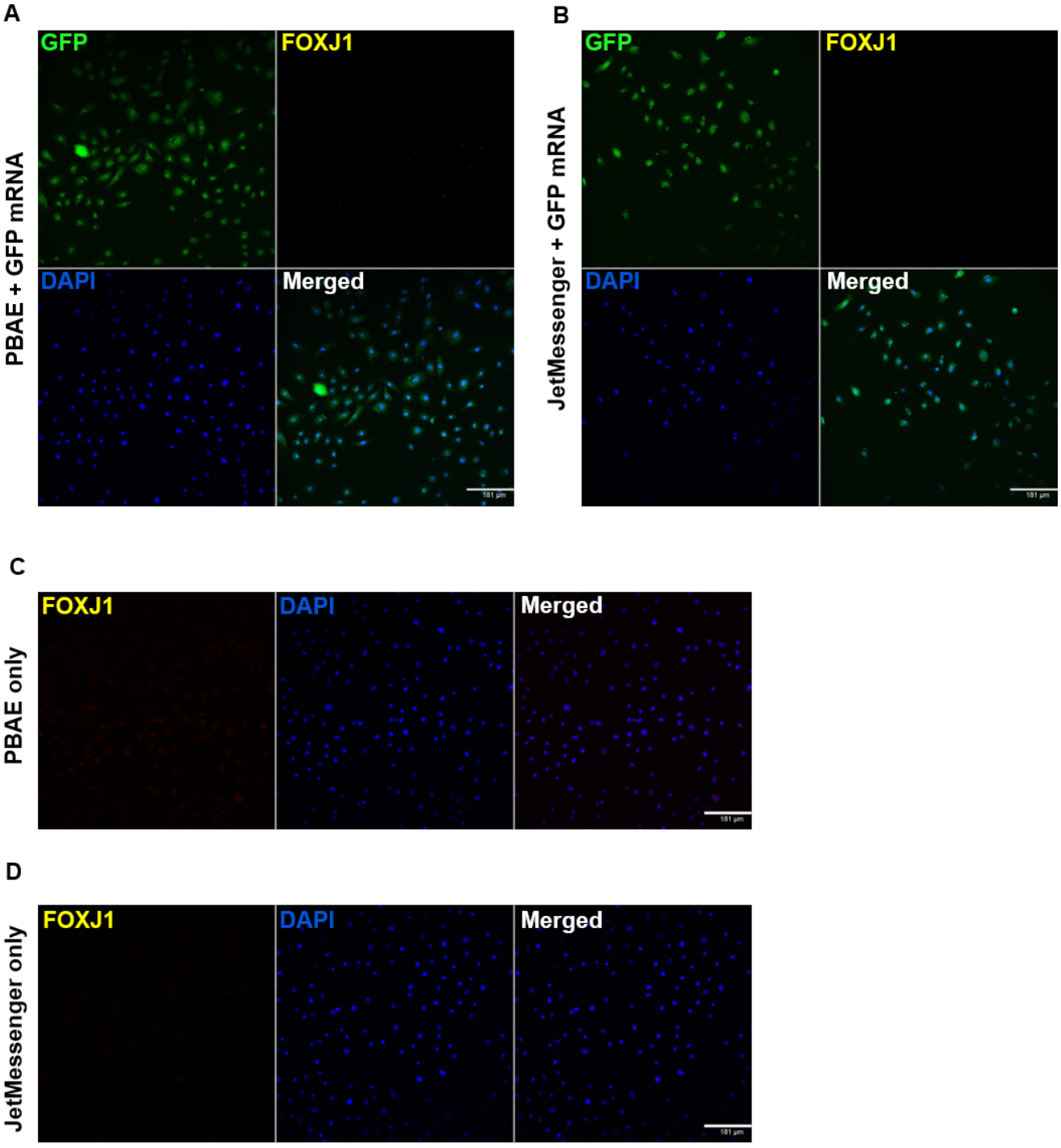


Figure 4.7 FOXJ1 expression following control mRNA transfections in submerged primary HBECs.

Submerged primary human bronchial epithelial cells (HBECs) were transfected with reporter green fluorescent protein (GFP) mRNA complexed with (A) branched poly β-amino ester (PBAE) or (B) commercial transfection reagent JetMessenger or vector-only controls; (C) PBAE, (D) JetMessenger. Representative images of transfected cells stained with anti-FOXJ1 antibody and cell nuclei counter stained with DAPI at 12 hours post-transfection.

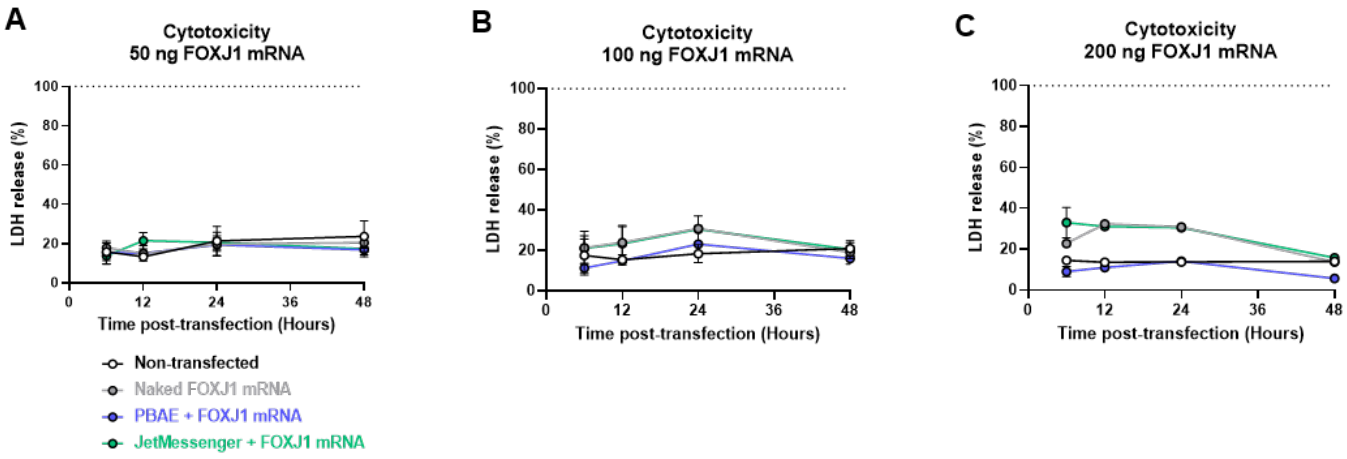


Figure 4.8 Cytotoxicity of FOXJ1 mRNA transfected submerged primary HBECs.

Submerged primary human bronchial epithelial cells (HBECs) were transfected with increasing doses of FOXJ1 mRNA (50/100/200 ng) delivered naked or complexed with branched poly β-amino ester (PBAE) or commercial transfection reagent JetMessenger. Cytotoxicity at 6, 12, 24, and 48 hours post-transfection with (A) 50 ng FOXJ1 mRNA, (B) 100 ng FOXJ1 mRNA, (C) 200 ng FOXJ1 mRNA was quantified by lactate dehydrogenase (LDH) release (%) relative to LDH release from positive control cells treated with 1% Triton-X-100. Data represents mean ± SD. N = 3 primary cell donors with 3 technical replicates each. Statistics: 2way ANOVA followed by Dunnett's multiple comparisons test. Statistical analysis results are summarised in Table 4.2.

Table 4.2 Summary of statistical analysis of cytotoxicity in submerged primary HBECs following FOXJ1 mRNA transfection.

	Summary	Adjusted P value
50 ng FOXJ1 mRNA		
12h post-transfection: Non-transfected vs JetMessenger + FOXJ1 mRNA	*	0.0471
100 ng FOXJ1 mRNA		
24h post-transfection: Non-transfected vs JetMessenger + FOXJ1 mRNA	*	0.0273
200 ng FOXJ1 mRNA		
6h post-transfection: Non-transfected vs JetMessenger + FOXJ1 mRNA	***	0.0002
12h post-transfection: Non-transfected vs JetMessenger + FOXJ1 mRNA	***	0.0003
24h post-transfection: Non-transfected vs JetMessenger + FOXJ1 mRNA	***	0.0005

4.2.4 FOXJ1 mRNA transfection induces ciliogenesis transcriptional program in submerged primary HBECs

In section 4.2.3 I demonstrated that primary HBECs can translate exogenous FOXJ1 mRNA complexed with non-viral vectors for up to 48 hours, with the highest transfection efficiency observed with the 100 ng FOXJ1 mRNA dose per well. Next, I aimed to investigate whether FOXJ1 mRNA transfection of basal submerged primary HBECs with 100 ng dose, under conditions that normally prevent mucociliary differentiation, was sufficient to induce differentiation towards the ciliated cell lineage. The expression of FOXJ1 downstream genes associated with ciliated cell differentiation was assessed via qPCR. FOXJ1 supplementation in basal submerged primary HBECs induced the expression of a panel of cilia-associated genes including *CETN2*, *DNAH11*, *DNALI1*, *RFX3*, *RFX2*, *TUBA1A*, *RSPH9*, *DYNC2H1*, *IFT172* (Figure 4.9). A notable increase in the expression of FOXJ1-downstream genes was observed at 24 hours-post FOXJ1 mRNA transfection with *DNALI* (**P=0.0038, *P=0.0365), RSPH9 (****P<0.0001) and *DYNC2H1* (*P=0.0111) showing significant upregulation compared to non-transfected HBECs. To control for the effects of FOXJ1 mRNA transfection, naked FOXJ1 mRNA, vector-formulated reporter mRNA encoding GFP, and vector-only conditions were used as negative controls. Control transfections with naked FOXJ1 mRNA, vector-formulated reporter mRNA, and vector-only conditions did not induce expression of FOXJ1 downstream genes (Figure 4.9).

Together these data suggests that FOXJ1 protein following successful FOXJ1 mRNA transfection in submerged primary HBECs can induce the expression of several FOXJ1-downstream genes involved in different stages of ciliogenesis. The submerged FOXJ1 mRNA transfection experiments formed the basis of further investigation of FOXJ1 mRNA supplementation in ALI-cultured HBECs, presented in sections 4.2.6 – 4.2.11.

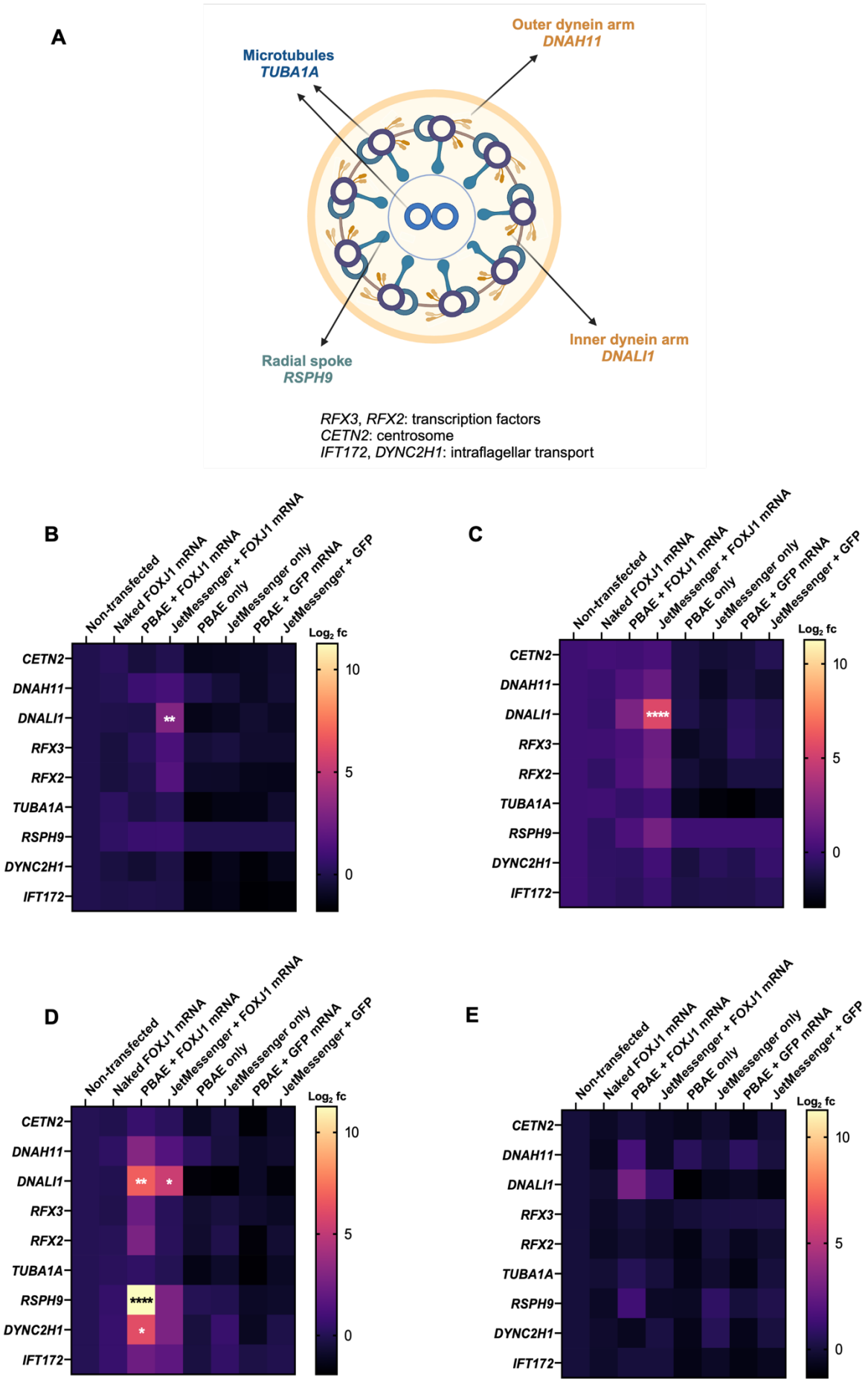

A
Outer dynein arm
DNAH11
Microtubules
TUBA1A
Inner dynein arm
DNALI1
Radial spoke
RSPH9
RFX3, RFX2: transcription factors
CETN2: centrosome
IFT172, DYNC2H1: intraflagellar transport
B
C
D
E
Non-transfected
Naked FOXJ1 mRNA
PBAE + FOXJ1 mRNA
JetMessenger + FOXJ1 mRNA
PBAE only
JetMessenger only
PBAE + GFP mRNA
JetMessenger + GFP
Log2 fc
10
5
0
CETN2
DNAH11
DNALI1
RFX3
RFX2
TUBA1A
RSPH9
DYNC2H1
IFT172
**
****
*

Figure 4.9 FOXJ1-mediated expression of ciliogenesis genes in submerged primary HBECs following non-viral FOXJ1 mRNA transfection.

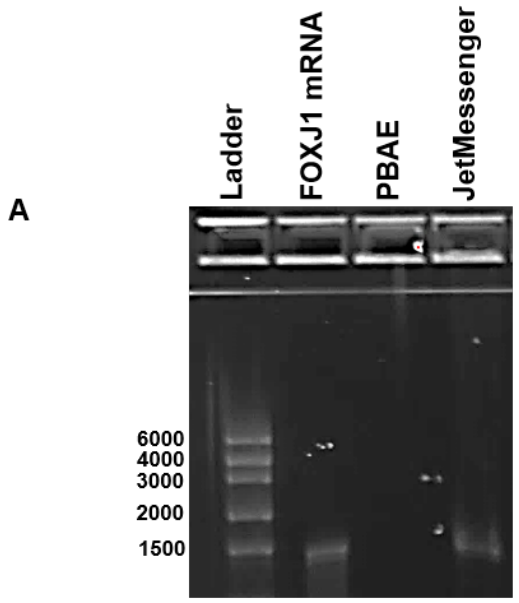
(A) Subset of genes directly regulated by FOXJ1. Figure created with Biorender.com. Submerged primary human bronchial epithelial cells (HBECs) were transfected with 100 ng FOXJ1 mRNA delivered naked or complexed with branched poly β-amino ester (PBAE) or commercial transfection reagent JetMessenger. Cells were also transfected with reporter green fluorescent protein (GFP) mRNA complexed with branched PBAE or JetMessenger or vector only-controls. Cells were harvested between 6-48 hours post-transfection and quantitative PCR (qPCR) was used to quantify expression of ciliated cell associated genes at (B) 6 hours post-transfection, (C) 12 hours post-transfection, (D) 24 hours post-transfection, and (E) 48 hours post-transfection. Data represents log2 fold change from non-transfected control. N = 3 primary cell donors with 3 technical replicates each. Statistics: 2way ANOVA followed by Dunnett's multiple comparisons test. *P=0.0111, **P=0.0011, ****P< 0.0001.

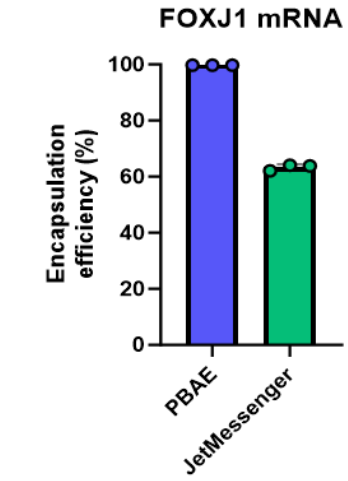
4.2.5 Characterisation of FOXJ1 mRNA/non-viral vector formulations

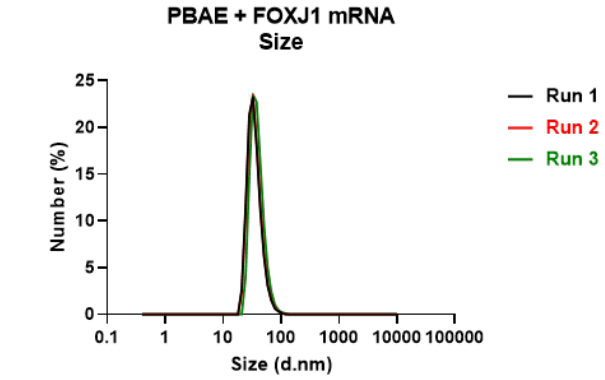
In section 4.2.3, I established that primary HBECs can translate exogenous FOXJ1 mRNA complexed with non-viral vectors for up to 48 hours post-transfection, with peak expression at 12 hours post-transfection. After observing that PBAE transfection resulted in a higher and more sustained FOXJ1 expression compared to JetMessenger transfection, I sought to characterise further FOXJ1 mRNA/PBAE and FOXJ1 mRNA/JetMessenger formulations.

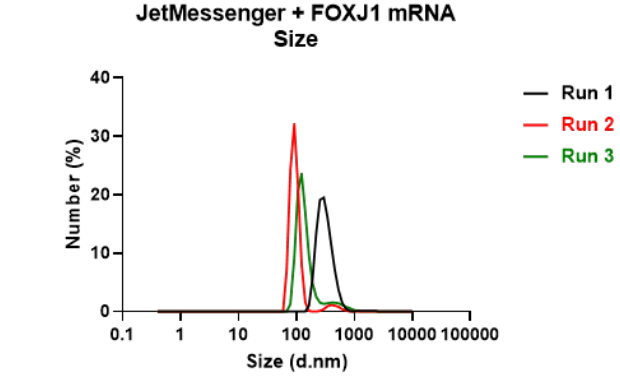
First, the complexation of FOXJ1 mRNA to PBAE or JetMessenger was evaluated by gel electrophoresis. The gel retardation assay demonstrated that PBAE was able to completely protect FOXJ1 mRNA as evidenced by the lack of mRNA migration through the gel (Figure 4.10A). JetMessenger was not able to efficiently protect FOXJ1 mRNA as evidenced by mRNA migration through the gel (Figure 4.10A). Next, FOXJ1 mRNA encapsulation efficiency was quantified using the Ribogreen assay. PBAE encapsulated the FOXJ1 mRNA efficiently, yielding almost 100% encapsulation efficiency, while only ~60% of FOXJ1 mRNA was encapsulated by JetMessenger (Figure 4.10B). DLS was then used to characterise the size, stability, and zeta potential of PBAE/FOXJ1 mRNA and JetMessenger/FOXJ1 mRNA nanoparticles. The DLS results showed that PBAE formed stable nanoparticles around 60 nm in size and positively charged when complexed with FOXJ1 mRNA (Figure 4.10C, E, F). However, JetMessenger condensed FOXJ1 mRNA into larger nanoparticles (400 nm) which were less stable and negatively charged (Figure 4.10D-F).

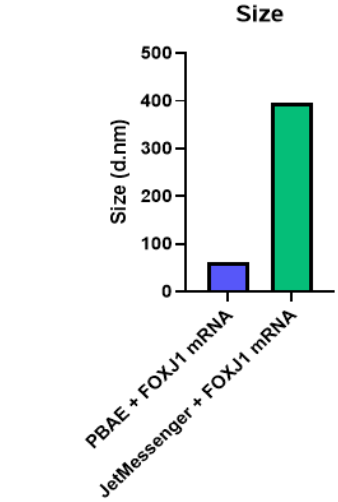
The observed differences in encapsulation efficiency, size, stability, and zeta potential of FOXJ1 mRNA polyplexes between PBAE and JetMessenger could be linked to the lower FOXJ1 transfection efficiency with JetMessenger. Therefore, it was decided to proceed with the PBAE/FOXJ1 mRNA formulation to assess the impact of FOXJ1 supplementation on the differentiation of HBECs cultured at ALI.


A
Ladder
FOXJ1 mRNA
PBAE
JetMessenger
6000
4000
3000
2000
1500


B
FOXJ1 mRNA
Encapsulation efficiency (%)
100
80
60
40
20
0
PBAE
JetMessenger


C
PBAE + FOXJ1 mRNA
Size
Number (%)
25
20
15
10
5
0
0.1
1
10
100
1000
10000
100000
Size (d.nm)
Run 1
Run 2
Run 3


D
JetMessenger + FOXJ1 mRNA
Size
Number (%)
40
30
20
10
0
0.1
1
10
100
1000
10000
100000
Size (d.nm)
Run 1
Run 2
Run 3


E
Size
Size (d.nm)
500
400
300
200
100
0
PBAE + FOXJ1 mRNA
JetMessenger + FOXJ1 mRNA

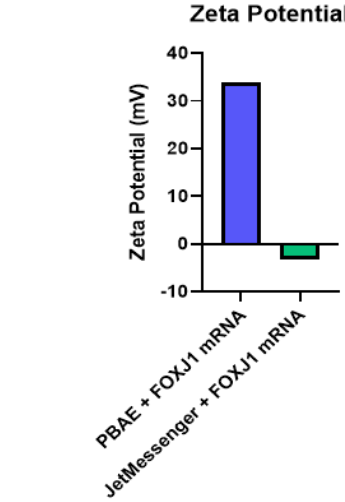

F
Zeta Potential
Zeta Potential (mV)
40
30
20
10
0
-10
PBAE + FOXJ1 mRNA
JetMessenger + FOXJ1 mRNA

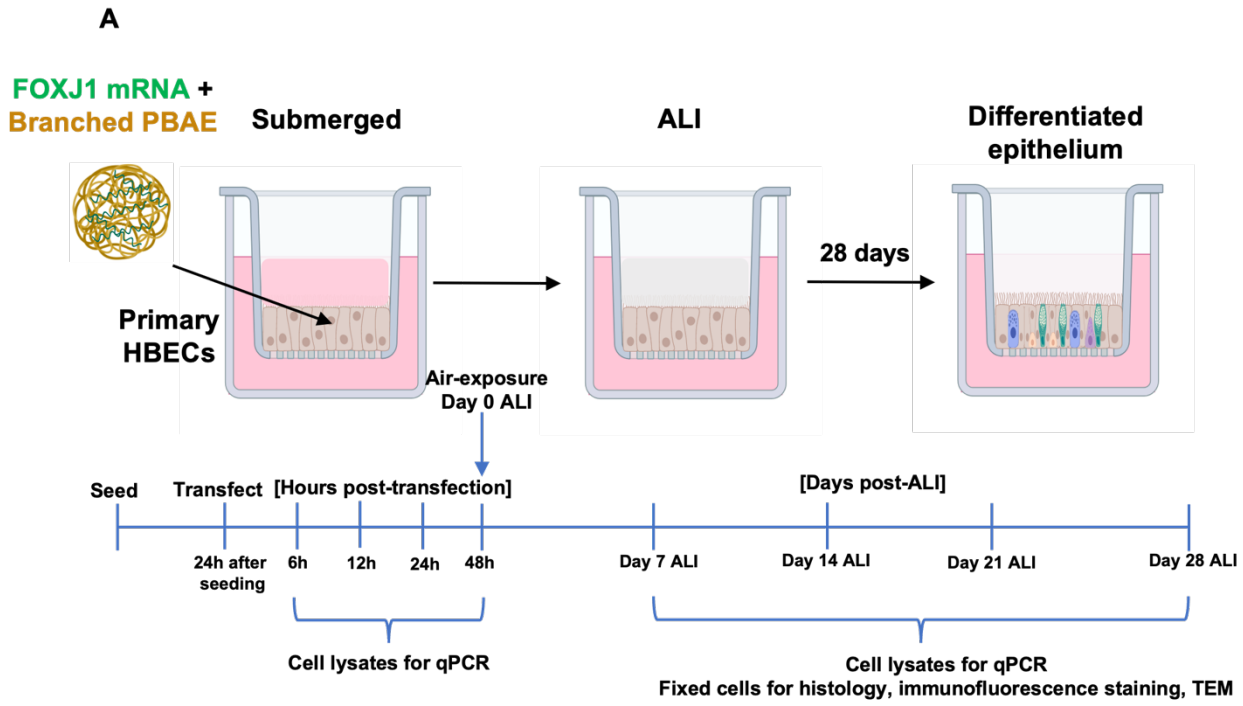
Figure 4.10 Characterisation of FOXJ1 mRNA/non-viral vector formulations.

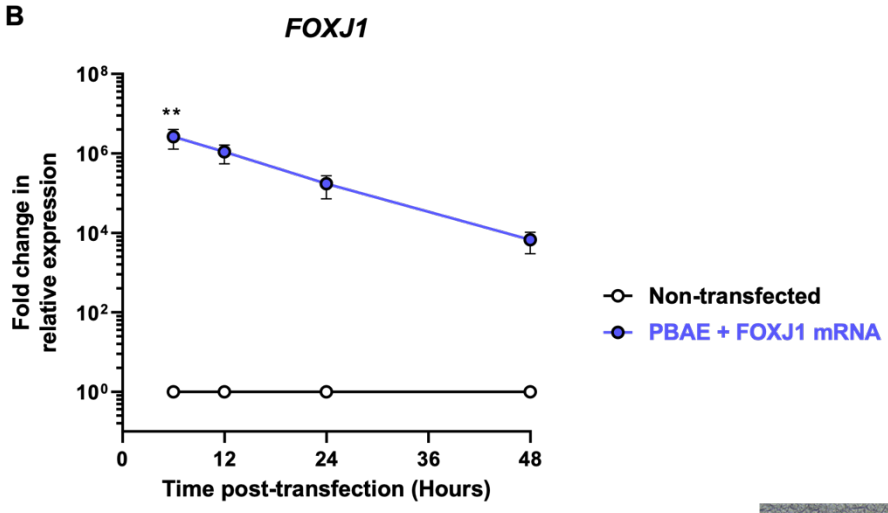
(A) Gel retardation assay of poly β-amino ester (PBAE)/FOXJ1 mRNA and commercial transfection reagent JetMessenger/FOXJ1 mRNA nanoparticles run through a 2% agarose gel. 200 ng of mRNA was loaded in each well. (B) Encapsulation efficiency of FOXJ1 mRNA complexed with PBAE or JetMessenger using the RiboGreen assay. Measurements were performed in triplicates for each condition and data are shown as mean ± SD. (C) Size analysis of PBAE particles formulated with FOXJ1 mRNA using dynamic light scattering (DLS). (D) Size analysis of JetMessenger transfection reagent formulated with FOXJ1 mRNA using DLS. (E) Summary size analysis in nanometres (nm) of PBAE/FOXJ1 mRNA and JetMessenger/FOXJ1 mRNA particles. (F) Zeta Potential measurements of PBAE/FOXJ1 mRNA and JetMessenger/FOXJ1 mRNA particles. Size and zeta potential measurements taken in triplicate.

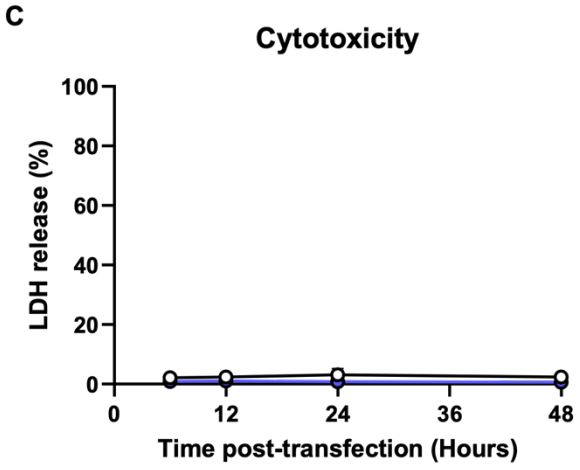
4.2.6 Primary HBECs transfected with FOXJ1 encoded mRNA formed a confluent monolayer and were maintained at ALI culture for 28 days

The confirmation that exogenous FOXJ1 encoded mRNA can induce the expression of cilia associated FOXJ1 downstream genes in submerged primary HBECs (section 4.2.4) supported the investigation of FOXJ1 mRNA delivery to primary HBEC ALI cultures. I sought to investigate the influence of FOXJ1 supplementation on the differentiation of primary HBECs cultured at ALI compared to non-transfected control primary HBECs. Primary HBECs were transfected with FOXJ1 encoded mRNA formulated with PBAE (100 ng per well, optimised condition determined in sections 4.2.3, 4.2.4, 4.2.5 above) 24 hours post-seeding on transwell inserts. Experimental design of FOXJ1 mRNA transfection in HBECs is shown in Figure 4.11A. Expression of FOXJ1 mRNA in cells transfected with FOXJ1 mRNA complexed with PBAE was confirmed via qPCR at 6, 12, 24, and 48 hours post-transfection (Figure 4.11B).

Cytotoxicity measured by LDH release was assessed after transfection comparing FOXJ1 mRNA transfected and non-transfected primary HBECs. Figure 4.11C indicates that LDH release was low in both non-transfected (below 6%) and FOXJ1 mRNA transfected groups and was not significantly different. In addition, Figure 4.11D shows that both conditions formed a confluent monolayer 48 hours post-transfection. After reaching confluence (Day 0 ALI), the apical medium was removed and FOXJ1 mRNA transfected and non-transfected HBECs were maintained in ALI culture for 28 days.


A
FOXJ1 mRNA +
Branched PBAE
Submerged
ALI
Differentiated
epithelium
28 days
Primary
HBECs
Air-exposure
Day 0 ALI
Seed
Transfect
[Hours post-transfection]
[Days post-ALI]
24h after
seeding
6h
12h
24h
48h
Day 7 ALI
Day 14 ALI
Day 21 ALI
Day 28 ALI
Cell lysates for qPCR
Cell lysates for qPCR
Fixed cells for histology, immunofluorescence staining, TEM


B
FOXJ1
Fold change in
relative expression
**
Time post-transfection (Hours)
Non-transfected
PBAE + FOXJ1 mRNA


C
Cytotoxicity
LDH release (%)
Time post-transfection (Hours)

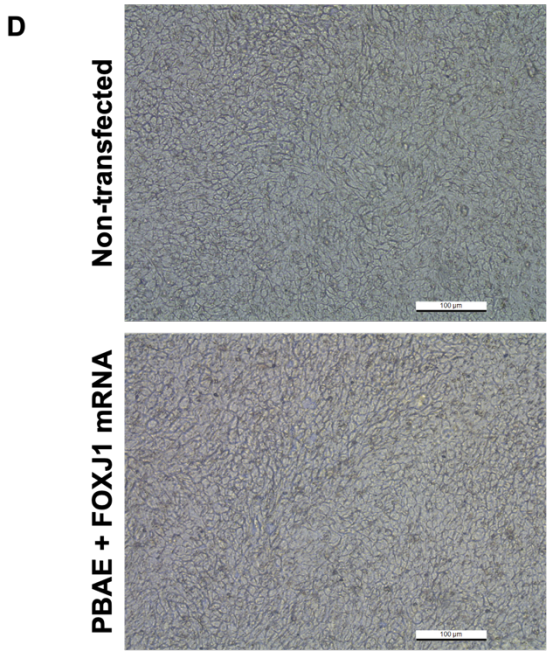

D
Non-transfected
PBAE + FOXJ1 mRNA

Figure 4.11 Primary HBECs transfected with FOXJ1 mRNA formed a confluent monolayer and cultured at ALI.

(A) Schematic showing experimental design of FOXJ1 mRNA transfection. Primary human bronchial epithelial cells (HBECs) were seeded on transwell inserts and 24 hours after seeding were transfected with FOXJ1 mRNA (100 ng per transwell) complexed with branched poly β-amino ester (PBAE). Cells were harvested at 6, 12, 24, 48 hours post-transfection to assess expression of FOXJ1 downstream genes using qPCR. Once FOXJ1 mRNA transfected cells and non-transfected control cells formed a confluent monolayer they were air-exposed and cultured at ALI for 28 days. Cells were harvested for qPCR, fixed for histology, immunofluorescence staining, and transmission electron microscopy at day 7, 14, 21, and 28 post-ALI. (B) Expression of FOXJ1 at 6, 12, 24, 48 hours following FOXJ1 mRNA transfection plotted as fold change from non-transfected cells. Data represents mean ± SD. N = 3 primary cell donors. Statistics: 2way ANOVA followed by Dunnett's multiple comparisons test. **P= 0.0024. (C) Cytotoxicity at 6, 12, 24, 48 hours post-FOXJ1 mRNA transfection was quantified by lactate dehydrogenase (LDH) release (%) relative to LDH release from positive control cells treated with 1% Triton-X-100. Data represents mean ± SD. N = 3 primary cell donors. Statistics: 2way ANOVA followed by Dunnett's multiple comparisons test. (D) Representative images of non-transfected primary HBECs and FOXJ1 mRNA transfected cells once they formed a confluent monolayer before air exposure.

4.2.7 FOXJ1 supplementation mediates induction of FOXJ1-downstream genes involved in ciliogenesis before air-exposure

After confirmation of successful transfection of primary HBECs seeded on transwell inserts with FOXJ1 encoded mRNA (Figure 4.11B), the expression of FOXJ1-downstream genes was assessed via qPCR at 6, 12, 24, and 48 hours post-transfection. Cilia-associated genes (*RFX3, RFX2, CETN2, DNAH11, DNALI1, RSPH9, DYNC2H1, IFT172, TUBA1A*) were upregulated following FOXJ1 mRNA transfection (Figure 4.12). However, donor-dependent variability in the expression of FOXJ1-downstream genes in cultures derived from 3 independent donors was observed. Gene expression changes were more pronounced in donors 1 and 3 than in donor 2. Together these data indicate that FOXJ1 supplementation induces expression of FOXJ1 downstream genes in primary HBECs prior to air exposure at ALI culture compared to non-transfected cells.

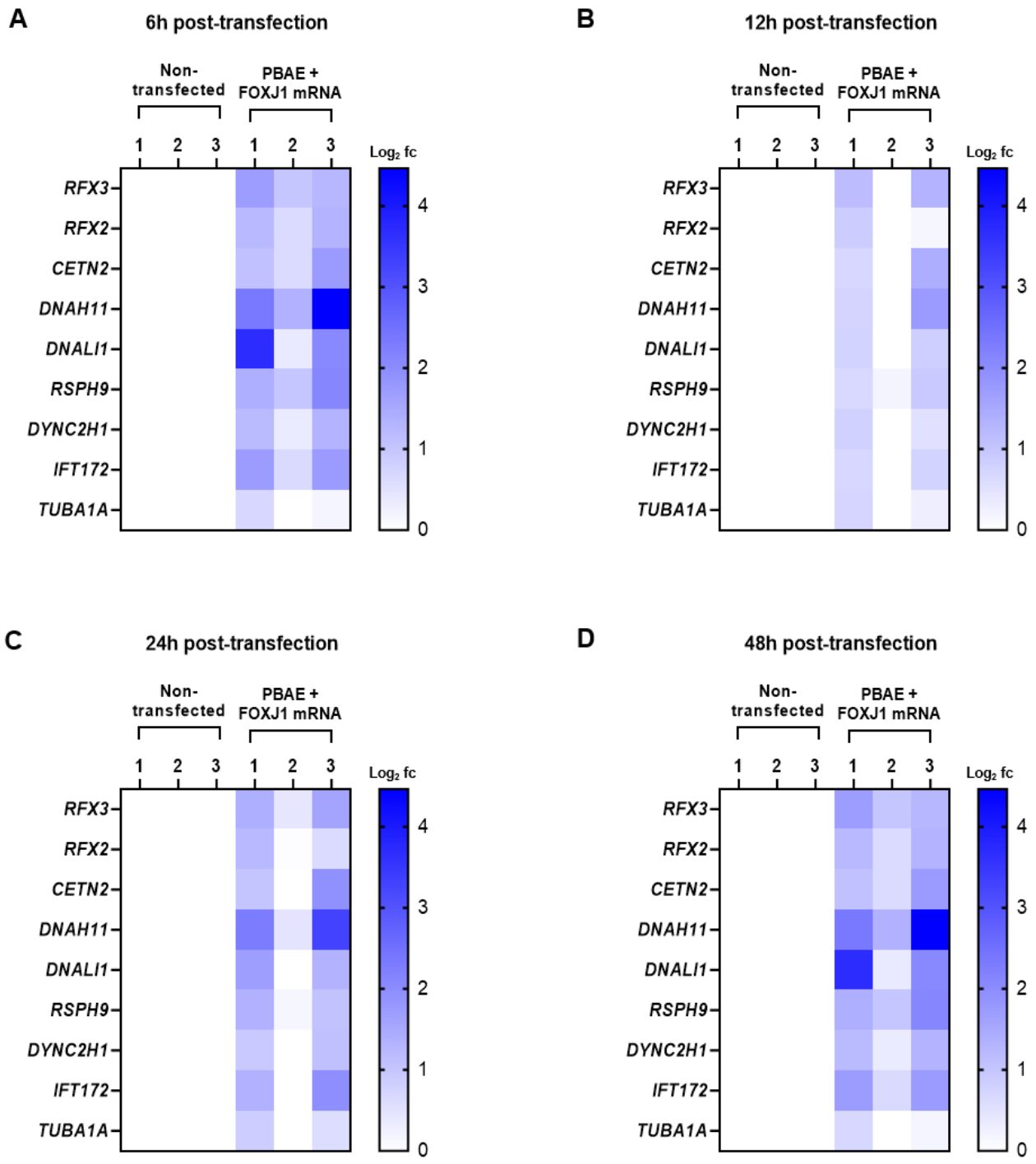


Figure 4.12 Induction of FOXJ1 downstream genes following FOXJ1 mRNA transfection in primary HBECs before air-exposure.

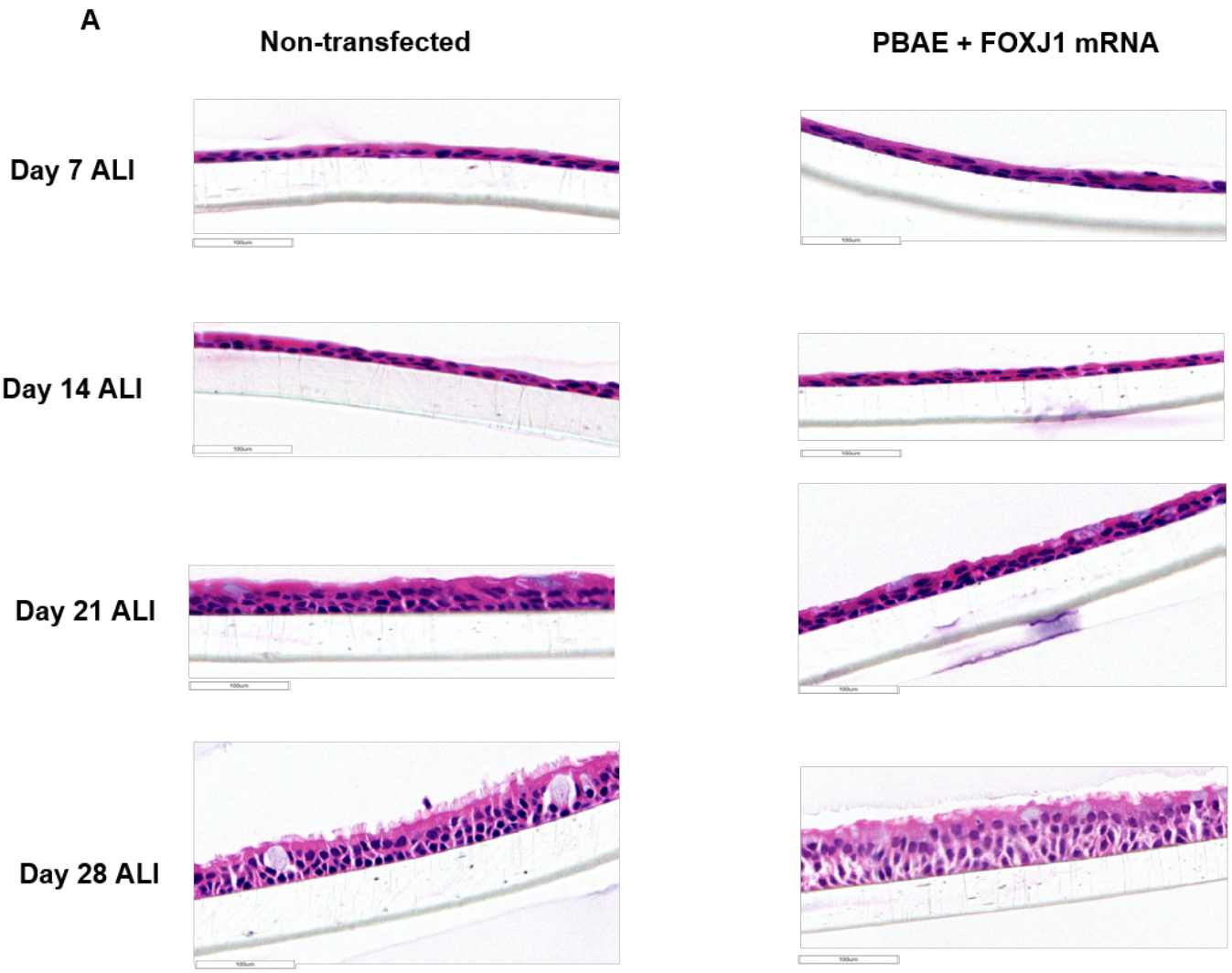
Primary human bronchial epithelial cells (HBECs) were transfected with FOXJ1 mRNA (100 ng per transwell insert) complexed with branched poly β-amino ester (PBAE). Cells were harvested following FOXJ1 mRNA transfection to assess expression of FOXJ1 downstream genes using qPCR. Expression of FOXJ1 downstream genes was quantified at (A) 6 hours post-transfection, (B) 12 hours post-transfection, (C) 24 hours post-transfection, and (D) 48 hours post-transfection. Data represents log2 fold change from non-transfected control. N = 3 primary cell donors.

4.2.8 Impact of FOXJ1 supplementation on epithelial morphology

Primary HBECs transfected with FOXJ1 encoded mRNA and non-transfected primary HBECs were maintained at ALI for 28 days. To explore the impact of FOXJ1 supplementation on the epithelial morphology, morphological evaluations of the epithelial structure were conducted at 7-day intervals from day 7 to day 28 post-ALI, using histological sections stained with H&E. Representative H&E-stained sections are shown in Figure 4.13A. Initially, at day 7 post-ALI, both FOXJ1 mRNA transfected and non-transfected primary HBECs displayed a squamous morphology. By day 14 post-ALI, cells in both groups had differentiated into a double-layered structure with more cuboidal morphology. Progressing to day 21, the cultures in both conditions nearly tripled in depth, developing into an increasingly columnar and pseudostratified. By day 28, both FOXJ1 mRNA transfected and non-transfected HBECs exhibited a pseudostratified morphology with mucociliary differentiation. Measurements of epithelial thickness demonstrated a gradual increase in both groups, with the maximum thickness reaching 17. 9 $\pm$ 1.2 µm in non-transfected HBECs and 19.8 $\pm$ 9.8 µm between day 7 and 28 post-ALI (Figure 4.13B). Notably, there were no differences in thickness between the two groups. These data suggests that FOXJ1 supplementation does not influence the overall morphology or thickness of the epithelial layers.

The study further investigated the differentiation changes in HBEC ALI cultures, both in non-transfected and transfected with FOXJ1 mRNA, using TEM at 7-day intervals. At day 7 post-ALI, epithelial cells in both groups showed a uniform cuboidal morphology without any signs of differentiation or cilia formation, although some secretory granules were present (Figure 4.14A). By day 14 post-ALI, the initial stages of ciliogenesis were evident, with the emergence of short cilia (Figure 4.14B). This process was more pronounced by day 21 post-ALI, where ciliation was well-established (Figure 4.15A), reaching its peak development and coverage by day 28 post-ALI (Figure 4.15B). In addition, secretory cells were observed either individually or in clusters among the ciliated cells. Cross-sectional views of the cell layer at day 28 post-ALI displayed a pseudostratified morphology (Figure 4.15B). ALI cultures from both non-transfected and FOXJ1 mRNA transfected HBECs remained well-preserved and organised throughout the four-week period, showing no evidence of degradation or de-differentiation. No differences were noted in the overall epithelial morphology between non-transfected and FOXJ1 mRNA transfected HBECs. However, an exception was observed in the case of donor 3, who uniquely exhibited early signs of ciliogenesis, such as the formation of basal bodies at day 7 post-ALI (Figure 4.16). This phenomenon was not seen in the non-transfected counterpart or in any of the other two donors transfected with FOXJ1 mRNA.

A


Non-transfected
PBAE + FOXJ1 mRNA
Day 7 ALI
Day 14 ALI
Day 21 ALI
Day 28 ALI

B

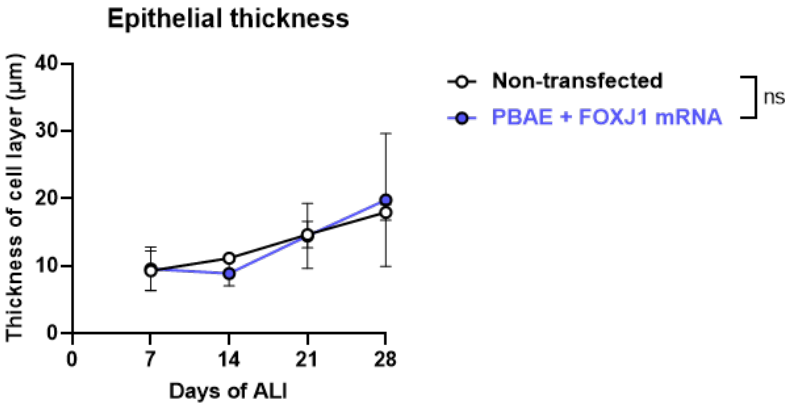

Epithelial thickness
Thickness of cell layer (µm)
40
30
20
10
0
0
7
14
21
28
Days of ALI
Non-transfected
PBAE + FOXJ1 mRNA
ns

Figure 4.13 Overall morphology and thickness of epithelial layers remain unaffected following FOXJ1 mRNA transfection in primary HBECs cultured at ALI.

Primary human bronchial epithelial cells (HBECs) were transfected with FOXJ1 mRNA (100 ng per transwell insert) complexed with branched poly β-amino ester (PBAE) before air exposure. Once they formed a confluent monolayer, cells were air-exposed and cultured at air-liquid interface (ALI) for 28 days. Non-transfected control cells and FOXJ1 mRNA transfected cells were fixed at day 7, 14, 21, and 28 post-ALI for histology characterisation. (A) Representative images of Hematoxylin and eosin (H&E) staining of sections from non-transfected and FOXJ1 mRNA transfected HBECs at Day 7, 14, 21, 28 post-ALI. (B) Thickness of epithelial cell layer as measured in H&E-stained cross-sections from Day 7, 14, 21, 28 post-ALI. Data represents mean $\pm$ SD. N = 3 primary cell donors. Statistics: 2way ANOVA followed by Dunnett's multiple comparisons test. Not-significant (ns) P>0.9999

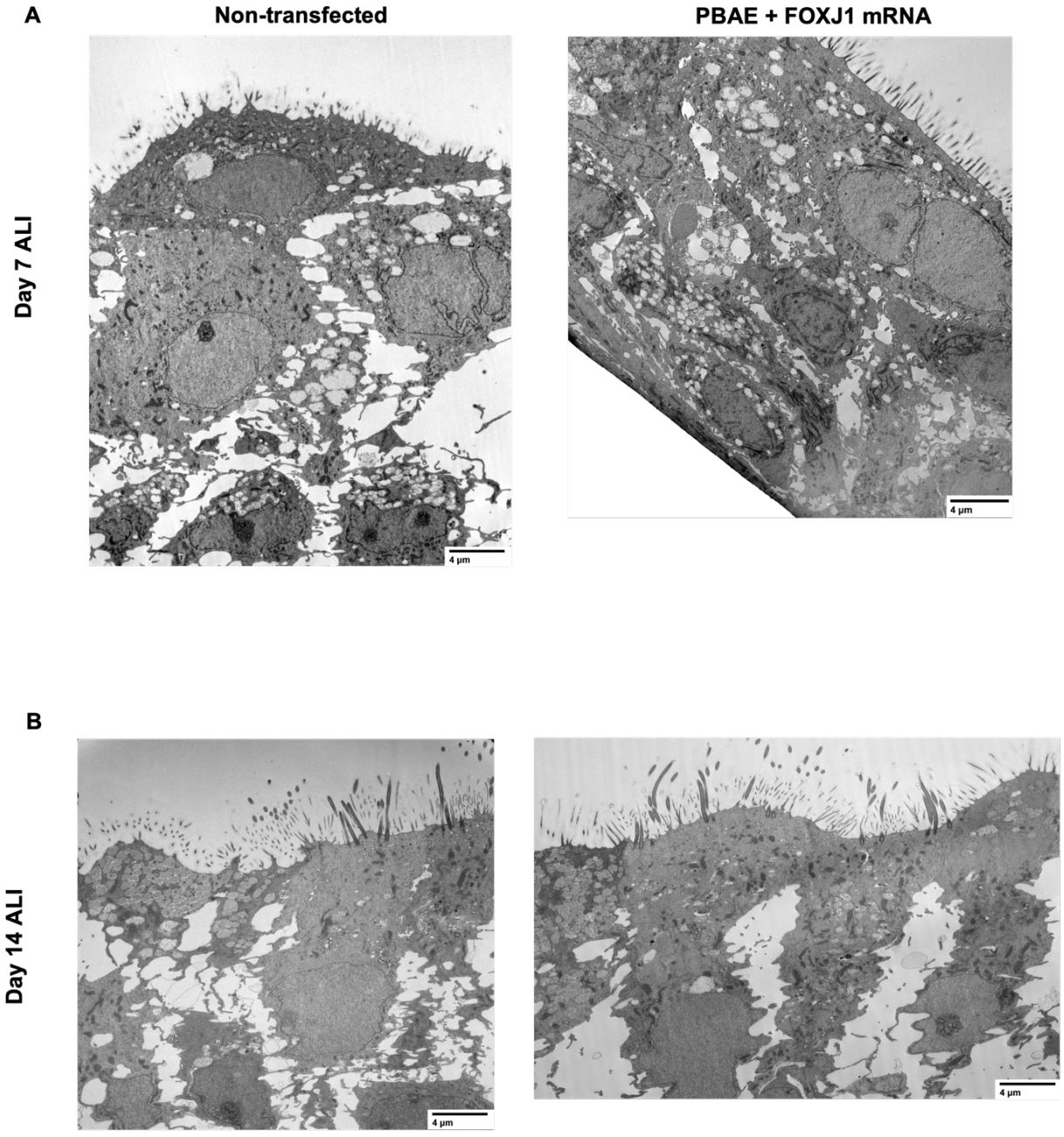


Figure 4.14 Transmission electron microscopic (TEM) assessment of ultrastructural changes in non-transfected and FOXJ1 mRNA transfected human bronchial epithelial cell air-liquid interface cultures over time.

Primary human bronchial epithelial cells (HBECs) were transfected with FOXJ1 mRNA complexed with branched poly β-amino ester (PBAE) before air exposure. Once they formed a confluent monolayer, cells were air-exposed and cultured at air-liquid interface (ALI) for 28 days. Non-transfected control and FOXJ1 mRNA transfected HBEC ALI cultures were fixed at seven-day intervals and processed for TEM. Representative micrographs show (A) day 7 post-ALI cultures and (B) day 14 post-ALI cultures.

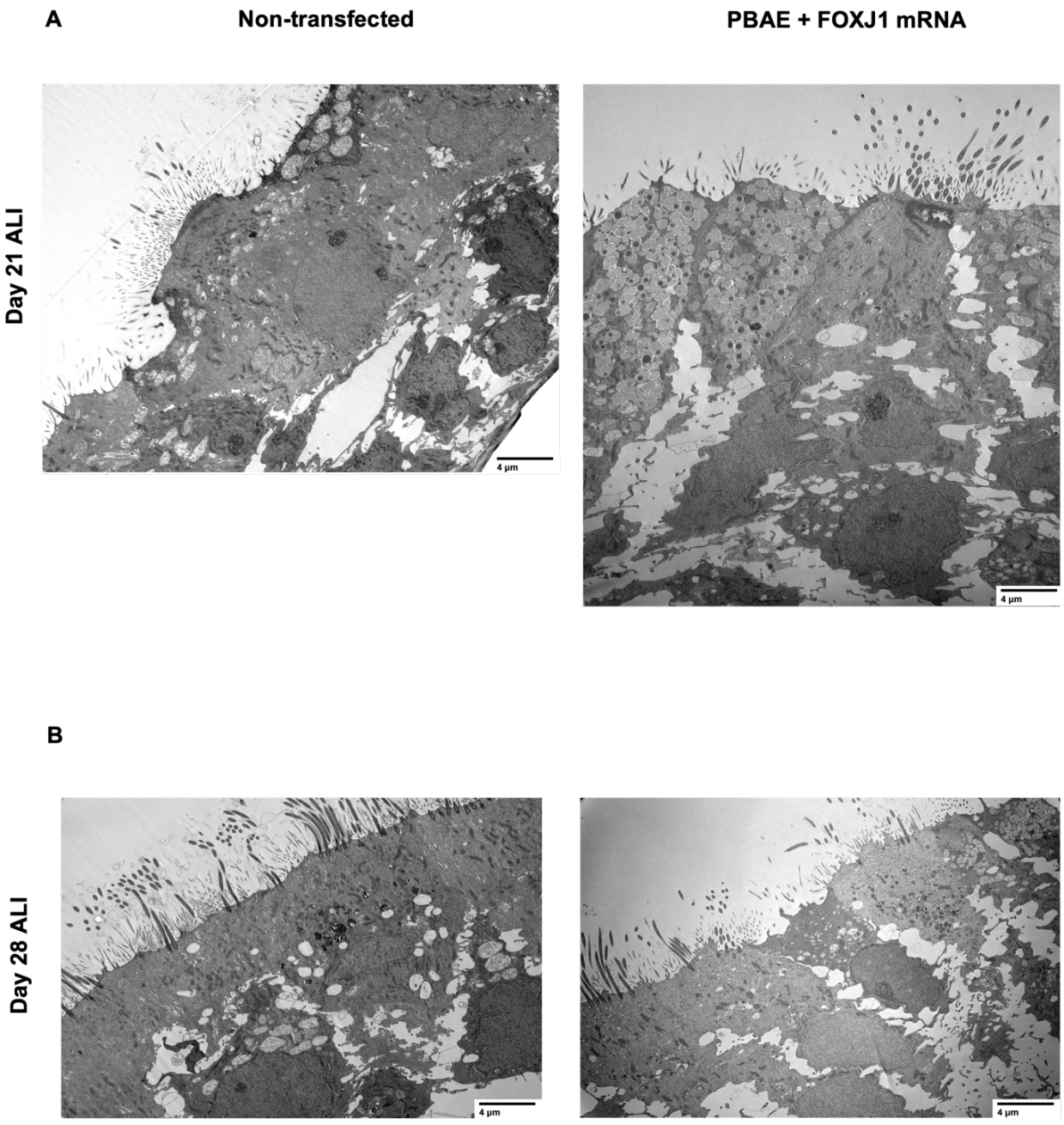


Figure 4.15 Transmission electron microscopic (TEM) assessment of ultrastructural changes in non-transfected and FOXJ1 mRNA transfected human bronchial epithelial cell air-liquid interface cultures over time.

Primary human bronchial epithelial cells (HBECs) were transfected with FOXJ1 mRNA complexed with branched poly β-amino ester (PBAE) before air exposure. Once they formed a confluent monolayer, cells were air-exposed and cultured at air-liquid interface (ALI) for 28 days. Non-transfected control and FOXJ1 mRNA transfected HBEC ALI cultures were fixed at seven-day intervals and processed for TEM. Representative micrographs show (A) day 21 post-ALI cultures and (B) day 28 post-ALI cultures.

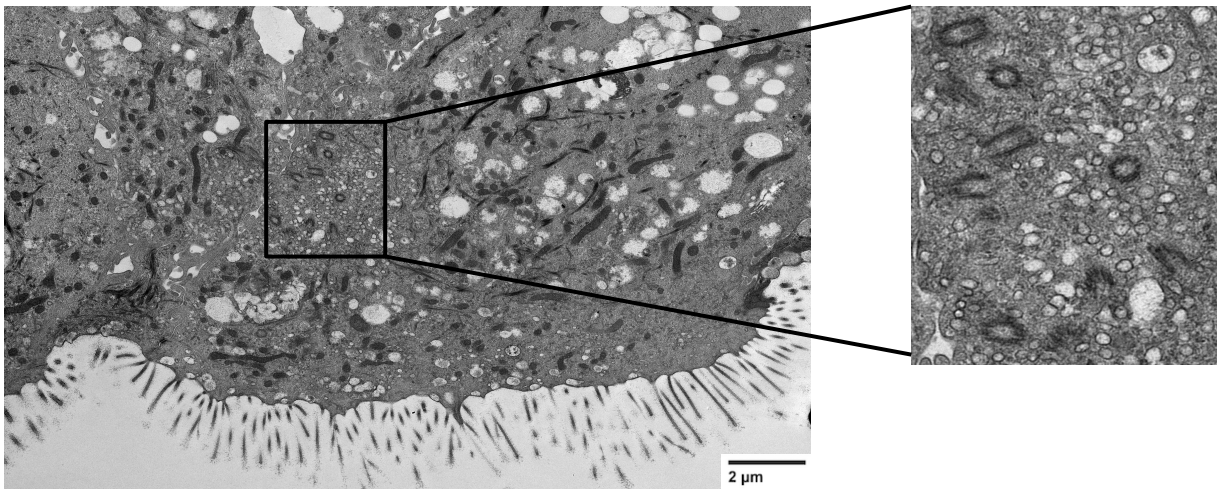


Figure 4.16 Transmission electron microscopic (TEM) assessment of ultrastructural changes in FOXJ1 mRNA transfected human bronchial epithelial cell air-liquid interface culture at day 7 post-ALI.

Primary human bronchial epithelial cells (HBECs) (donor 3) were transfected with FOXJ1 mRNA complexed with branched poly β-amino ester (PBAE) before air exposure. Once they formed a confluent monolayer, cells were air-exposed and cultured at air-liquid interface (ALI) for 28 days. FOXJ1 mRNA transfected HBEC ALI cultures were fixed at seven-day intervals and processed for TEM. Representative micrographs show FOXJ1 mRNA transfected HBEC ALI culture at day 7 post-ALI from donor 3.

4.2.9 Impact of FOXJ1 supplementation on epithelial integrity

To investigate the influence of FOXJ1 supplementation on epithelial integrity, the expression of cell adhesion markers including *CDH1* (E-cadherin for adherens junctions), *TJP1* (ZO-1 for tight junctions) and *OCLN* (Ocludin for tight junctions) was assessed using qPCR. The study found that the levels of *CDH1*, *TJP1* and *OCLN* were comparable in both FOXJ1 mRNA transfected and non-transfected cultures at 6, 12, 24, and 48 hours post-transfection and days 7, 14, 21, and 28 post-ALI (Figure 4.17A-C). In addition to gene expression analysis, the study utilised TEM to visually confirm the presence of tight junctions. TEM identified tight junctions and desmosomes in both FOXJ1 mRNA transfected and non-transfected ALI cultures (Figure 4.17D). This visual evidence further confirmed the presence of junctional complexes and the maintenance of barrier integrity in HBEC ALI cultures. Collectively, these findings suggest that epithelial integrity remains unaltered following transfection with FOXJ1 mRNA.

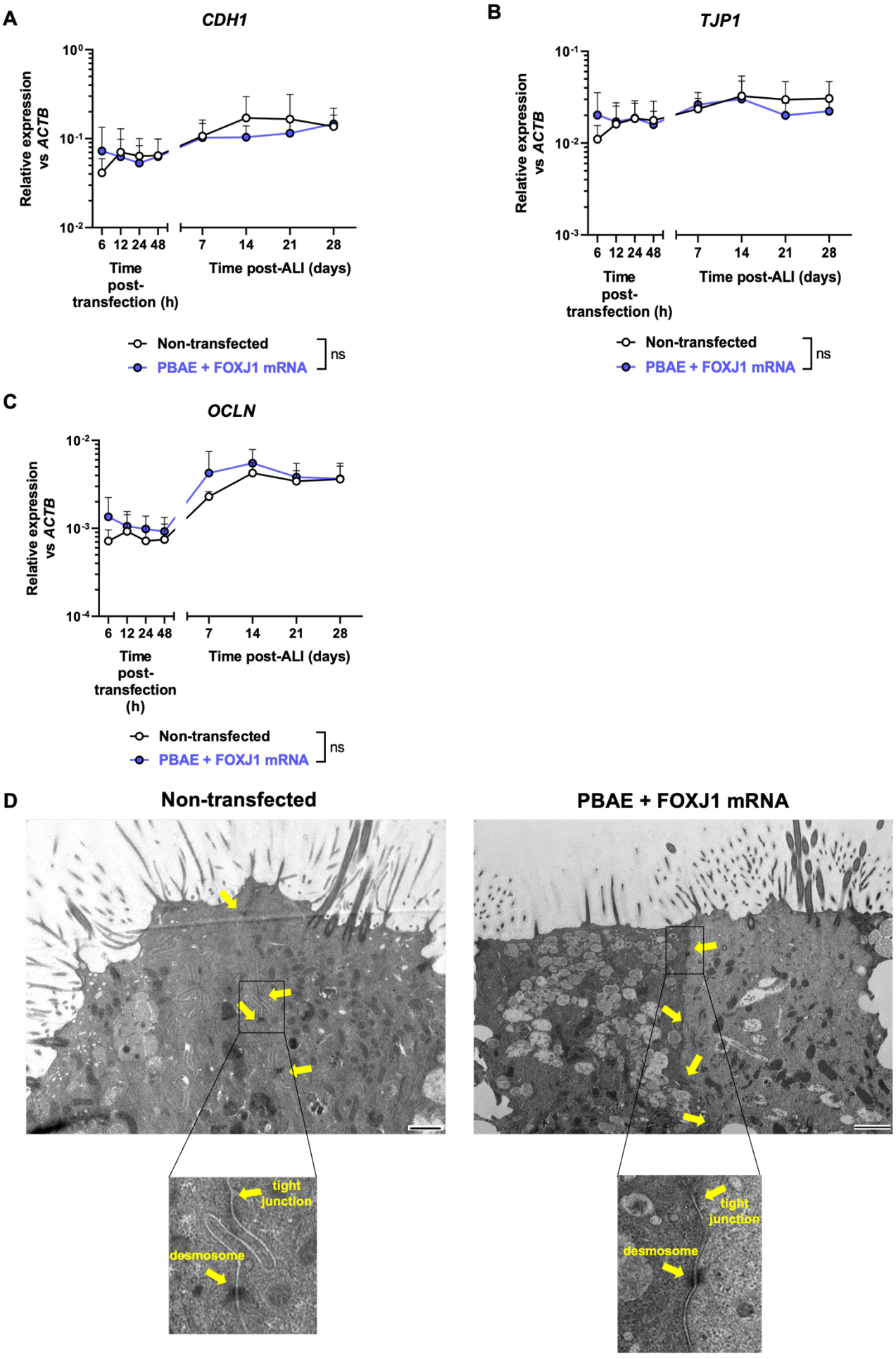

A
CDH1
Relative expression vs ACTB
10^0
10^-1
10^-2
6 12 24 48
7 14 21 28
Time post-transfection (h)
Time post-ALI (days)
Non-transfected
PBAE + FOXJ1 mRNA
ns
B
TJP1
Relative expression vs ACTB
10^-1
10^-2
10^-3
6 12 24 48
7 14 21 28
Time post-transfection (h)
Time post-ALI (days)
Non-transfected
PBAE + FOXJ1 mRNA
ns
C
OCLN
Relative expression vs ACTB
10^-2
10^-3
10^-4
6 12 24 48
7 14 21 28
Time post-transfection (h)
Time post-ALI (days)
Non-transfected
PBAE + FOXJ1 mRNA
ns
D
Non-transfected
PBAE + FOXJ1 mRNA
tight junction
desmosome
tight junction
desmosome

Figure 4.17 Epithelial integrity is unaffected following FOXJ1 mRNA transfection in primary HBECs cultured at ALI.

Primary human bronchial epithelial cells (HBECs) were transfected with FOXJ1 mRNA (100 ng per transwell insert) complexed with branched poly β-amino ester (PBAE) before air exposure. Non-transfected control cells and FOXJ1 mRNA transfected cells were harvested at 6, 12, 24, and 48 hours post-transfection to assess expression of epithelial integrity genes using qPCR. Once they formed a confluent monolayer, cells were air-exposed and cultured at air-liquid interface (ALI) for 28 days. Non-transfected control cells and FOXJ1 mRNA transfected cells were harvested at Day 7, 14, 21, and 28 post-ALI to assess expression of epithelial integrity genes using qPCR. Expression of (A) *CDH1*, (B) *TJP1*, and (C) *OCLN* genes was quantified relative to housekeeping gene *ACTB*. Data represents mean ± SD. N = 3 primary cell donors. Statistics: 2way ANOVA followed by Dunnett's multiple comparisons test. Not-significant (ns) P>0.9999. (D) Junctional complexes (yellow arrows) of non-transfected and FOXJ1 mRNA transfected HBEC ALI cultures was assessed using transmission electron microscopy (TEM). Scale bar: 6 µm.

4.2.10 Impact of FOXJ1 supplementation on epithelial differentiation

To investigate the impact of FOXJ1 supplementation on epithelial differentiation, the expression of key genes in differentiated HBEC ALI cultures was assessed using qPCR (*KRT5* for basal cells594, *MUC5AC* and *MUC5B* for goblet cells595,596, *SCGB1A1* for club cells[597], *FOXJ1* for ciliated cells[598]). The findings revealed that, except for *KRT5*, all genes showed increased expression during ALI differentiation (Figure 4.18). This enhancement was most notable between day 0 post-ALI (48 hours post-transfection) and day 14 post-ALI, after which gene expression generally stabilised. *KRT5*, a basal cell marker, exhibited a minor decrease in FOXJ1 mRNA transfected HBECs compared to non-transfected HBECs at 6, 12, 24, and 48 hours post-transfection and day 14, 21 and 28 post- ALI (Figure 4.18A). In contrast, genes associated with club and goblet cell differentiation were upregulated following air exposure in both groups. *SCGB1A1*, expressed by club cells597, which are progenitors to both goblet and ciliated cells, showed a significant upregulation between day 0 post-ALI and day 14 post-ALI (Figure 4.18B). However, the increase in *SCGB1A1* expression in FOXJ1 mRNA transfected HBECs compared to non-transfected HBECs was minor and statistically insignificant (Figure 4.18B). *MUC5AC* and *MUC5B,* encoding mucus components in goblet cells, followed a similar expression pattern. Their upregulation commenced between day 0 and day 7 post-ALI, peaking at day 14 post-ALI (Figure 4.18C+D). FOXJ1 supplementation did not trigger early expression of these genes (6-48 hours post-transfection), and at later stages (day 14, 21, and 28 post-ALI), their expression was lower in FOXJ1 mRNA transfected HBECs compared to controls (Figure 4.18C+D). As expected, FOXJ1 expression increased in FOXJ1 mRNA transfected cells between 6- and 48-hours post-transfection (Figure 4.18E). Expression of FOXJ1 in non-transfected cells commenced at day 7 post-ALI, reached a plateau by day 14 post-ALI, and remained lower than in FOXJ1 mRNA transfected HBECs throughout the study

(Figure 4.18E). These observations suggest that FOXJ1 supplementation does not impact the expression of epithelial cell differentiation markers during ALI differentiation.

The differentiation of FOXJ1 mRNA transfected and non-transfected ALI cultures was further explored at day 28 post-ALI using histological analysis to quantify the proportion of ciliated cells, PAS positive cells and non-ciliated PAS negative cells. Representative images of PAS-stained cross-sections of HBECs grown at ALI for 28 days are shown in Figure 4.19A. FOXJ1 mRNA transfected and non-transfected HBEC ALI cultures displayed similar pseudostratified morphology and mucociliary differentiation. Through manual cell counting, the proportions of different cell types were determined. The percentage of ciliated cells in non-transfected (79.3% $\pm$ 1.2) and FOXJ1 mRNA transfected cultures (79.3% $\pm$ 3.1) were nearly identical, with no statistically significant difference ($P>0.99$). Similarly, the proportions of PAS-positive cells (9% $\pm$ 2.7 in non-transfected vs 16% $\pm$ 6.3 in transfected, $P=0.0886$) and non-ciliated, PAS-negative cells (11.7 % $\pm$ 2.5 in non-transfected vs 4.7 % $\pm$ 3.2 in transfected, $P=0.0886$) were comparable between the two groups (Figure 4.19B).

To further confirm these findings, end-point immunofluorescence analyses were performed on Day 28 post-ALI. This analysis aimed to verify the presence of differentiation markers in both groups: MUC5AC for goblet cells, acetylated alpha tubulin for cilia, KRT5 for basal cells, and SCGB1A1 for club cells (Figure 4.19C). Together, these data reinforce the conclusion that FOXJ1 mRNA supplementation does not alter the proportion of ciliated cells, PAS-positive cells, and non-ciliated, PAS-negative cells in differentiated ALI cultures.

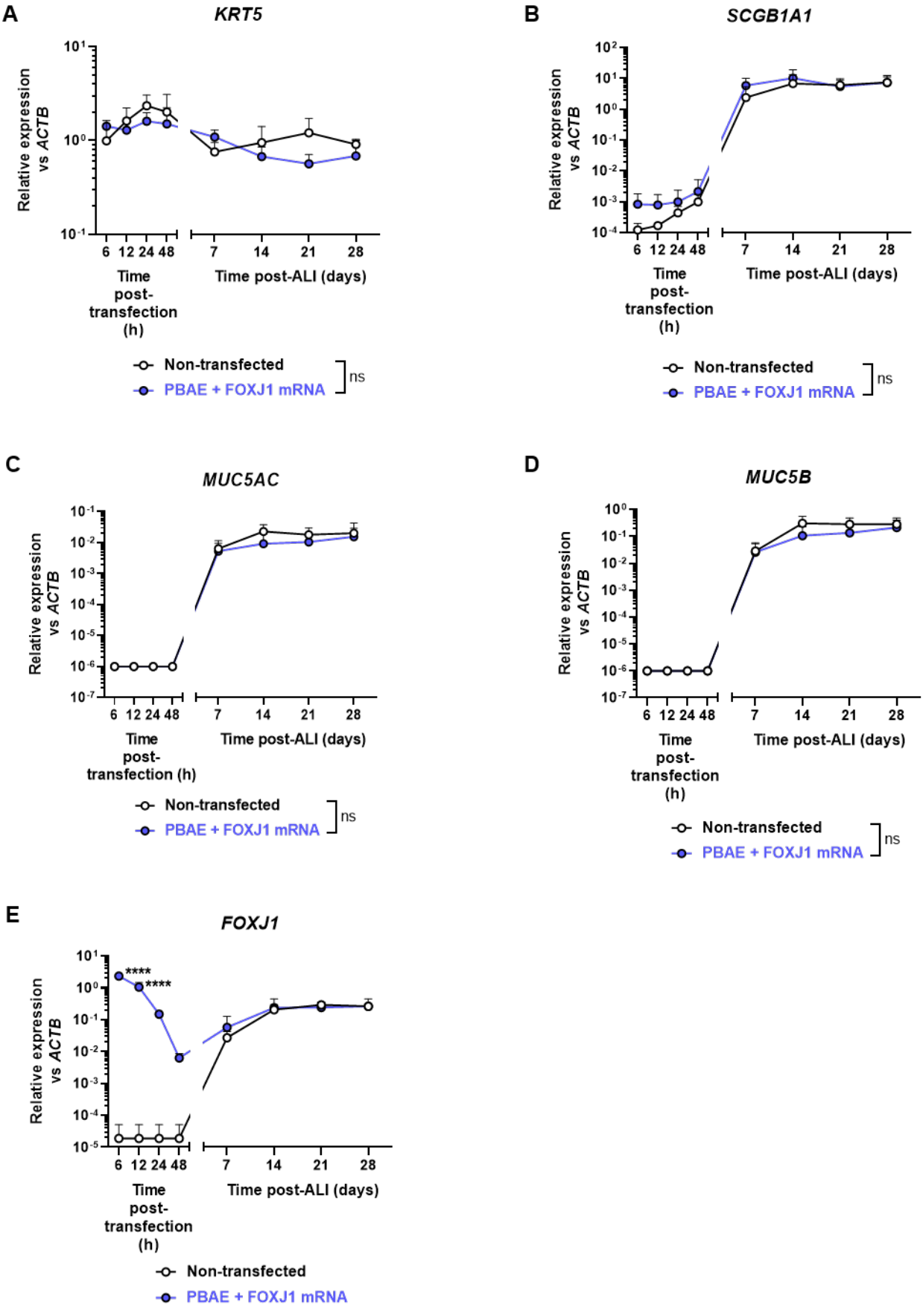
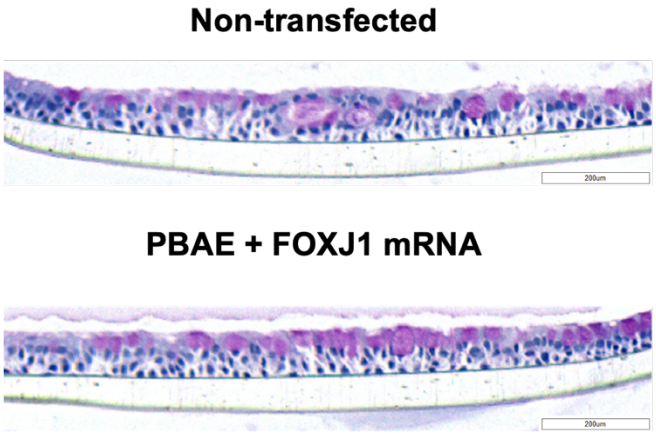

A
KRT5
Relative expression vs ACTB
Time post-transfection (h)
Time post-ALI (days)
Non-transfected
PBAE + FOXJ1 mRNA
ns
B
SCGB1A1
C
MUC5AC
D
MUC5B
E
FOXJ1
****

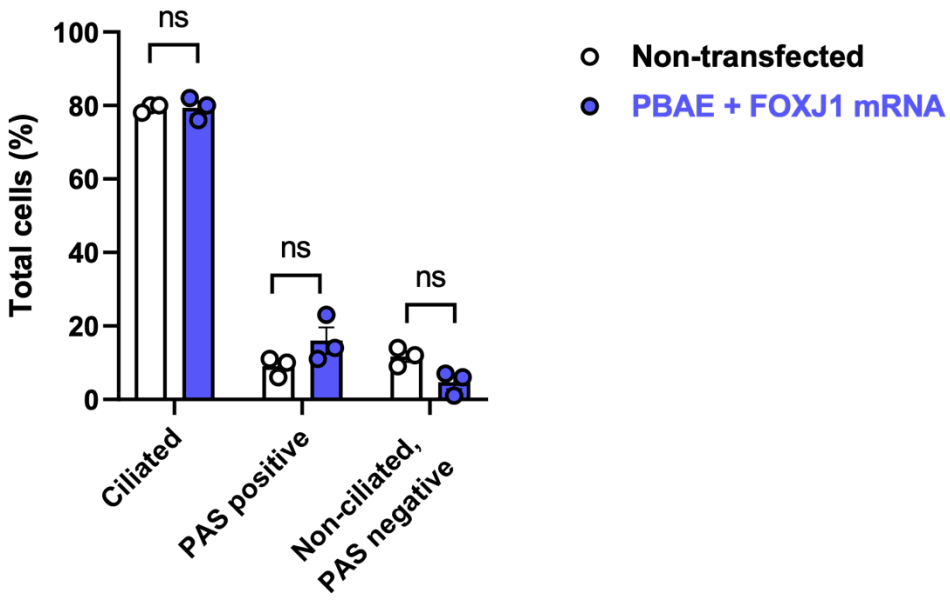
Figure 4.18 Expression of epithelial differentiation markers is unaffected following FOXJ1 mRNA transfection in primary HBECs cultured at ALI.

Primary human bronchial epithelial cells (HBECs) were transfected with FOXJ1 mRNA (100 ng per transwell insert) complexed with branched poly β-amino ester (PBAE) before air exposure. Non-transfected control cells and FOXJ1 mRNA transfected cells were harvested at 6, 12, 24, and 48 hours post-transfection to assess expression of epithelial differentiation genes using qPCR. Once they formed a confluent monolayer, cells were air-exposed and cultured at air-liquid interface (ALI) for 28 days. Non-transfected control cells and FOXJ1 mRNA transfected cells were harvested at Day 7, 14, 21, and 28 post-ALI to assess expression of epithelial differentiation genes using qPCR. Expression of (A) *KRT5*, (B) *SCGB1A1*, (C) *MUC5AC*, (D) *MUC5B* and (E) *FOXJ1* genes was quantified relative to housekeeping gene *ACTB*. Data represents mean ± SD. N = 3 primary cell donors. Statistics: 2way ANOVA followed by Dunnett's multiple comparisons test. Non-significant (ns)P>0.9999, ****P< 0.0001.

A


Non-transfected
PBAE + FOXJ1 mRNA

B


Total cells (%)
100
80
60
40
20
0
ns
ns
ns
Ciliated
PAS positive
Non-ciliated, PAS negative
Non-transfected
PBAE + FOXJ1 mRNA

C

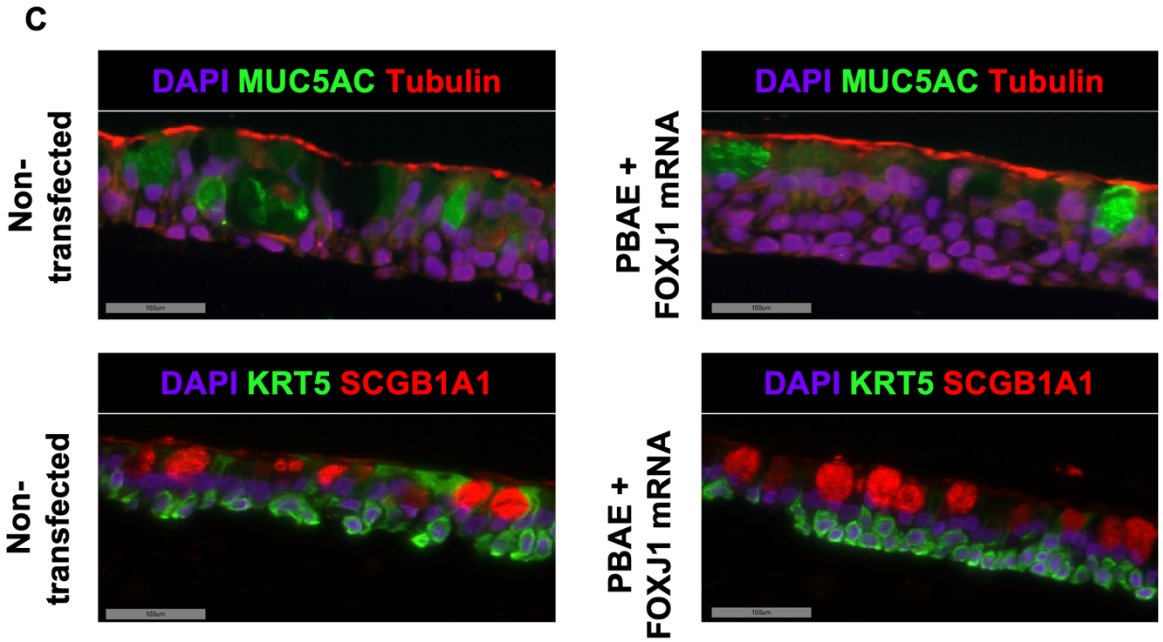

Non-transfected
PBAE + FOXJ1 mRNA
DAPI MUC5AC Tubulin
DAPI KRT5 SCGB1A1

Figure 4.19 Epithelial differentiation is not influenced following FOXJ1 mRNA transfection in primary HBECs cultured at ALI.

Primary human bronchial epithelial cells (HBECs) were transfected with FOXJ1 mRNA (100 ng per transwell insert) complexed with branched poly β-amino ester (PBAE) before air exposure. Once they formed a confluent monolayer, cells were air-exposed and cultured at air-liquid interface (ALI) for 28 days. Non-transfected control cells and FOXJ1 mRNA transfected cells were fixed at Day 28 post-ALI for histology and immunofluorescence characterisation. (A) Representative images of periodic acid-Schiff (PAS) staining of sections from non-transfected and FOXJ1 mRNA transfected HBECs at 28 post-ALI. (B) Proportions of ciliated, PAS positive and non-ciliated PAS negative cells were manually counted from PAS-stained sections of Day 28 post-ALI cultures and expressed as percentage of total cells. Data represents mean ± SD. N = 3 primary cell donors. Statistics: 2way ANOVA followed by Dunnett's multiple comparisons test. Non-significant (ns) P>0.9999. (C) Representative images of immunofluorescence staining for goblet cells (MUC5AC), cilia (acetylated alpha tubulin), basal cells (KRT5), and club cells (SCGB1A1).

4.2.11 Impact of FOXJ1 supplementation on transcriptional network of ciliated cell differentiation and cilia ultrastructure

To investigate the impact of FOXJ1 supplementation on ciliogenesis, the expression of FOXJ1-downstream genes associated with cilia formation was assessed using qPCR. Three of the analysed genes encode key structural components of cilia: radial spoke (*RSPH9*), and inner and outer dynein arms (*DNALI1* and *DNAH11*, respectively) (Figure 4.20A-C). These genes exhibited early upregulation between 6-48 hours post transfection in FOXJ1 mRNA transfected HBECs compared to non-transfected HBECs. Their maximum expression was observed at 14 days post-ALI, after which it plateaued. *CETN2*, a gene encoding a structural component of the centrosome, showed early induction in FOXJ1 mRNA transfected HBECs before air exposure, within 6-48 hours post-transfection (Figure 4.20D). In non-transfected cells, *CETN2* expression first increased on day 7 post- ALI, reaching a plateau between days 21 and 28 post-ALI. The expression profile of *CETN2* in FOXJ1 mRNA transfected cells was comparable to non-transfected HBECs from day 7 to 28 post-ALI (Figure 4.20D). Furthermore, *RFX2* and *RFX3,* which encode TFs regulating cilia gene expression, showed an increased in expression from 6-48 hours post-transfection in FOXJ1 mRNA transfected HBECs, remaining elevated throughout the culture period (Figure 4.20E+F). In contrast, upregulation of *RFX2* and *RFX3* in non-transfected HBECs was first noted on day 7 post-ALI, peaking on day 21 post-ALI (Figure 4.20E+F). Genes involved in IFT, specifically *DYNC2H1* and *IFT172*, were also analysed. These genes were upregulated in FOXJ1 mRNA transfected cells between 6-48 hours post-transfection (Figure 4.20G+H). In non-transfected cells, increased expression was detected starting day 7 post-ALI, reaching maximum values at day 21 post-ALI. The expression patterns of *DYNC2H1* and *IFT172* in FOXJ1 mRNA transfected cells were similar to those in non-transfected HBECs (Figure 4.20G+H). The expression of *TUBA1A*, which encodes microtubule constituents of the tubulin superfamily, showed

negligible increase in FOXJ1 mRNA transfected cells during the initial 6-48 hours post-transfection (Figure 4.20I). A notable increase in *TUBA1A* expression in both FOXJ1 mRNA transfected and non-transfected HBECs commenced from day 7 post-ALI, with maximum mRNA levels reached at day 21 post-ALI (Figure 4.20I).

The ultrastructure of cilia in day 28 post-ALI non-transfected and FOXJ1 mRNA transfected HBEC cultures was compared using TEM (Figure 4.21). The ultrastructure of the cilia in non-transfected and FOXJ1 mRNA transfected HBEC cultures was very similar. The configurations of the cilia basal bodies (Figure 4.21) and the 9+2 axonemes, characterised by their distinct arrangement of microtubules, radial spokes, and dynein arms arrangements (Figure 4.21) were highly consistent across both groups. No signs of cilia malformation in differentiated HBEC cultures were observed. Together, these data suggest that FOXJ1 supplementation induces the expression of cilia-associated genes before air exposure, but it does not appear to affect their expression during ALI differentiation. In addition, FOXJ1 supplementation does not alter the ultrastructure of cilia.

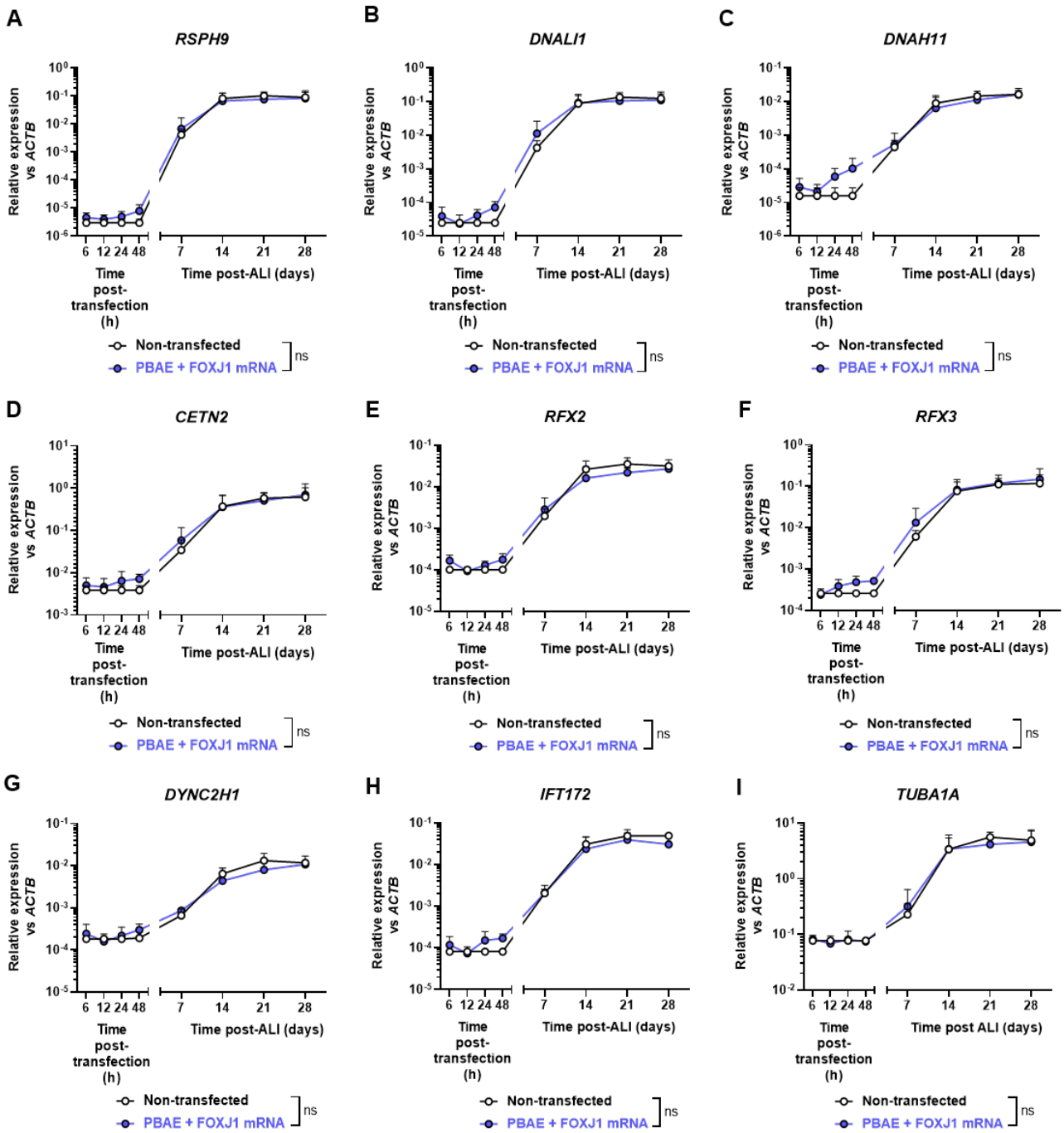

A
RSPH9
B
DNALI1
C
DNAH11
D
CETN2
E
RFX2
F
RFX3
G
DYNC2H1
H
IFT172
I
TUBA1A
Relative expression vs ACTB
Time post-transfection (h)
Time post-ALI (days)
Non-transfected
PBAE + FOXJ1 mRNA
ns

Figure 4.20 Impact of FOXJ1 supplementation on ciliogenesis transcriptional network following FOXJ1 mRNA transfection in primary HBECs cultured at ALI.

Primary human bronchial epithelial cells (HBECs) were transfected with FOXJ1 mRNA (100 ng per transwell insert) complexed with branched poly β-amino ester (PBAE) before air exposure. Non-transfected control cells and FOXJ1 mRNA transfected cells were harvested at 6, 12, 24, and 48 hours post-transfection to assess expression of ciliogenesis genes using qPCR. Once they formed a confluent monolayer, cells were air-exposed and cultured at air-liquid interface (ALI) for 28 days. Non-transfected control cells and FOXJ1 mRNA transfected cells were harvested at Day 7, 14, 21, and 28 post-ALI to assess expression of ciliogenesis genes using qPCR. Expression of (A) *RSPH9*, (B) *DNALI1*, (C) *DNAH11*, (D) *CETN2,* (E) *RFX2,* (F) RFX3, (G) *DYNC2H1*, (H) *IFT172*, and (I) *TUBA1A* genes was quantified relative to housekeeping gene *ACTB*. Data represents mean ± SD. N = 3 primary cell donors. Statistics: 2way ANOVA followed by Dunnett's multiple comparisons test. Non-significant (ns) P>0.9999.

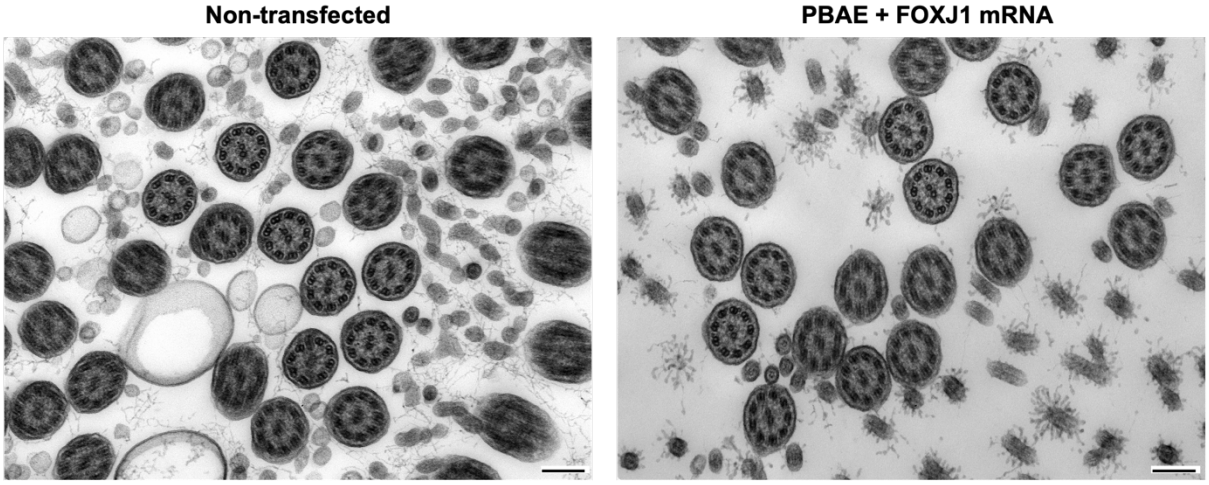


Figure 4.21 Transmission electron microscopic (TEM) assessment of cilia ultrastructure in non-transfected and FOXJ1 mRNA transfected human bronchial epithelial cell air-liquid interface cultures.

Primary human bronchial epithelial cells (HBECs) were transfected with FOXJ1 mRNA complexed with branched poly β-amino ester (PBAE) before air exposure. Once they formed a confluent monolayer, cells were air-exposed and cultured at air-liquid interface (ALI) for 28 days. Non-transfected control and FOXJ1 mRNA transfected HBEC ALI cultures were fixed at seven-day intervals and processed for TEM. Representative micrographs show transverse sections of cilia showing '9+2' axoneme arrangement in day 28 post-ALI cultures. Scale bar: 200 nm.

4.3 Discussion

In this chapter, I investigated the influence of mRNA encoded FOXJ1 delivery on the differentiation of primary HBECs. I have demonstrated that 1) Primary HBECs can successfully translate exogenous FOXJ1 mRNA following non-viral transfection; 2) Translated exogenous FOXJ1 mRNA induces the expression of FOXJ1 downstream genes involved in ciliogenesis; 3) FOXJ1 supplementation maintains the morphology, integrity, and mucociliary differentiation of primary HBECs in ALI culture; 4) FOXJ1 mRNA transfected primary HBECs cultured at ALI for 28 days have normal cilia ultrastructure.

In the study presented in this chapter, submerged primary HBECs were transfected with FOXJ1 encoded mRNA complexed with non-viral vectors (branched PBAE and commercial transfection reagent JetMessenger). Synthetic FOXJ1 mRNA was custom synthesised by OzBiosciences with a Cap 1 structure and poly-A tail incorporated as per request. Furthermore, the nucleoside uridine was replaced with pseudouridine. Collectively, these modifications contribute to diminishing inflammation, which is caused by the activation of innate immune system following mRNA delivery. Moreover, these modifications enhance both the stability and translation efficiency of IVT mRNA molecules[599–601].

Initially, qPCR was performed to confirm FOXJ1 mRNA transfection of primary HBECs before proceeding to downstream assays. Immunofluorescence staining for FOXJ1, followed by fluorescent microscopy, was used to assess transfection efficiency. Unlike Western Blot or enzyme-linked immunosorbent (ELISA), which measure the total protein in a population of cells, immunofluorescence staining allows for the direct visualisation of transfected cells and the subcellular localisation of the translated protein. This is important for intracellular targets like FOXJ1, as it can be used to confirm that mRNA is being translated into protein and it is being trafficked to the correct location within the cell. However, immunofluorescence staining is prone to artifacts, such as non-specific antibody binding. To overcome this challenge, additional controls were used, including non-transfected cells, naked FOXJ1 mRNA, reporter mRNA formulated with non-viral vectors, and non-viral vectors only. These controls ensured that the detection of FOXJ1 was specific only to cells transfected with FOXJ1 mRNA complexed with non-viral vectors. Flow cytometry, a quantitative method that measures the expression of proteins, is an alternative method for quantifying transfection efficiency[602–604]. However, it was less suitable for assessing transfection efficiency in primary HBECs following FOXJ1 mRNA transfection due to the requirement for a relatively large number of cells to be analysed. Therefore, immunofluorescence staining was chosen as the preferred method for assessing FOXJ1 transfection efficiency in this study. To the best of my knowledge, this is the

first demonstration that primary HBECs can be transfected with exogenous FOXJ1 mRNA without detrimental elevation in cytotoxicity, and the translated FOXJ1 protein is localised in the nuclei as expected[591,592].

The observed increase in FOXJ1 transfection efficiency in primary HBECs transfected with PBAE compared to the commercial transfection reagent JetMessenger may be due to differences in the physicochemical properties of the vectors, such as size and charge. The optimised branched PBAE formulation, established in Chapter 3 of this thesis, encapsulated FOXJ1 mRNA more efficiently and facilitated the formation of smaller, more stable, and more positively charged particles. As reported in the literature, smaller, positively charged particles generally facilitate higher transfection efficiency than larger, negatively charged particles due to enhanced cellular uptake and endosomal escape[605–607].

The mRNA's transient and dose-dependent properties provide precise control over protein production. This aspect is particularly valuable in applications where exact regulation of protein expression is essential[608]. Interestingly, in this study, the relationship between FOXJ1 mRNA dose escalation (50/100/200 ng) and FOXJ1 transfection efficiency was non-linear. Transfection efficiency did not increase proportionally with increasing mRNA dose, and the maximum efficiency was achieved with 100 ng of FOXJ1 mRNA. This is likely due to either the cytotoxic effects associated with the highest dose of FOXJ1 mRNA (200 ng), or the extended time needed for mRNA to be released from the endosome and translated. While increasing the mRNA dose can enhance transfection efficiency, it can also lead to increased cytotoxicity, counteracting the desired effect and resulting in a plateau or even a decline in transfection efficiency. Therefore, it is crucial to carefully consider the dose of mRNA when optimising transfection efficiency while minimising cytotoxicity. Previous studies have shown that the dose of mRNA-encoded TFs can have a significant impact on TF-driven differentiation[609–612]. For instance, Ledo *et al.* found that reducing *SOX9* mRNA dose by four times decreased SOX9 expression (cartilage) but had only a slight effect on the expression of a chondrogenic marker named aggrecan[612]. Similarly, reducing the dose of mRNA encoded myogenic determination protein 1 (*MYOD*) by half resulted in a 1000-fold drop in MYOD expression, whereas the maximum expression of myogenic differentiation marker Myogenin (*MYOG*) remained consistent[612]. These findings suggest that excessive upregulation of TFs may hinder cell phenotype maturation, likely due to negative feedback on their target gene expression. Therefore, maintaining elevated TF levels is not always beneficial for differentiation. Overall, these studies highlight the importance of considering mRNA encoded TF dose as a key design parameter in the context of TF mRNA differentiation, especially since

increasing mRNA dose may negatively affect transfection efficiency and block cell differentiation.

Exogenous FOXJ1 mRNA was translated over 48 hours, with peak expression at 12 hours post-transfection. However, the percentage of FOXJ1 positive cells declined by 48 hours post-transfection. These results demonstrate the transient nature of mRNA mediated FOXJ1 overexpression and suggest that repeated mRNA transfections may be needed to maintain higher levels of protein expression. Consistent with the findings presented in this thesis, other studies have also shown that mRNA-encoded TFs are rapidly expressed following non-viral transfection. For example, Qabrati *et al.* showed that 60-70% of mouse embryonic fibroblasts expressed MYOD within 5 hours of transfection with mRNA encoded *MYOD*, but expression declined to about 20% after 24 hours[611]. Similarly, Ma *et al.* confirmed protein expression of four mRNA-encoded TFs in hepatocytes 12 hours post-transfection[610]. In another study investigating the role of FOXJ1 in human airway epithelial ciliated cell differentiation, FOXJ1 expression was induced in primary human airway basal cells using a FOXJ1-expression plasmid[589]. The authors reported that 1000 ng of DNA were needed to achieve 55-65% transfection efficiency. In contrast, the data presented in this thesis demonstrated that only 100 ng of mRNA formulated with PBAE is needed to achieve a similar 50% transfection efficiency 12 hours post-transfection.

While FOXJ1 overexpression has been studied in murine models and transformed human cell lines, showing that FOXJ1 is a key regulator of airway epithelial ciliated cell differentiation, the effect of exogenous mRNA encoded FOXJ1 on primary HBECs remains unexplored. This chapter investigated the effect of mRNA encoded FOXJ1 on submerged primary HBECs, focusing on its ability to induce cilia-associated gene expression. Given the complexity of the FOXJ1 cilia-associated gene signalling network, it was impractical to evaluate the expression of all genes directly or indirectly regulated by FOXJ1 using qPCR. Therefore, a subset of genes representing different categories was selected. Three categories of ciliated cell-related genes were examined, including 1) cilia-related TFs: *RFX3*, *RFX2*; 2) genes encoding ciliary structural components and microtubule-based movement proteins: *CETN2*, *DNAH11*, *DNALI1*, *RSPH9*, *TUBA1A*; and 3) cilia IFT genes: *DYNC2H1*, *IFT172*. Transfection of primary HBECs with 100 ng FOXJ1 mRNA formulated with PBAE or commercial transfection reagent JetMessenger upregulated FOXJ1 downstream cilia-associated genes, especially 24 hours post-transfection. PBAE transfection resulted in a more potent induction of FOXJ1 downstream genes, likely due to its higher transfection efficiency compared to commercial transfection reagent JetMessenger. Importantly, naked FOXJ1 mRNA, non-viral vector-only controls, and reporter mRNA formulated with non-viral vectors did not induce FOXJ1 or

downstream genes. This finding strongly suggests that the observed gene expression changes are specifically attributable to FOXJ1 expression. While this data offers insights into the temporal dynamics of gene regulation following mRNA encoded FOXJ1 transfection, changes beyond 48 hours may be missed, necessitating an extended observation period to capture the full spectrum of gene expression dynamics. These findings are consistent with those of Didon *et al.*, who showed that plasmid-mediated FOXJ1 transfer in basal cells induced cilia-associated genes, including *CETN2*, *DNAH11*, dynein axonemal intermediate chain 1 (*DNAI1*), *DNALI1*, EF-hand domain C-terminal containing 1 (*EFHC1*), sperm associated antigen 6 (*SPAG6*), Tektin 1 (*TEKT1*), *TEKT2*, and *TUBA1A*[209]. The work presented in this chapter represents the first demonstration that FOXJ1 mRNA transfection induces the expression of FOXJ1 downstream genes involved in ciliogenesis in submerged primary HBECs.

While submerged transfection data has shown that FOXJ1 mRNA transfection can induce the expression of a subset of FOXJ1 downstream cilia-associated genes, it does not provide a complete understanding of its long-term impact on bronchial epithelial differentiation or whether it is sufficient to induce ciliogenesis. It has been demonstrated that ciliated cell differentiation is prevented in submerged airway epithelial cell cultures, suggesting that an ALI is essential for this process[613,614]. Gerovac *et al.* investigated the molecular mechanisms underlying the inhibition of ciliated cell differentiation in submerged cultures and showed that submersion creates a hypoxic environment that enhances Notch signalling and represses the expression of genes essential for ciliated cell differentiation[615]. ALI cultures are a valuable tool for studying the differentiation of airway epithelial cells, as they more closely resemble the *in vivo* environment than submerged cultures[383,616]. FOXJ1 mRNA transfected HBECs were cultured at ALI to study the long-term impact of FOXJ1 mRNA transfection on HBEC differentiation. To comprehensively assess the impact of FOXJ1 mRNA transfection on HBEC differentiation, a detailed 28-day analysis of temporal differentiation at 7-day intervals post-ALI was conducted. While it was possible to study the differentiation of ALI cultures for longer, it was decided to limit observations to 28 days post-ALI to ensure the health, integrity, and ciliation of the samples. Prytherch *et al.* showed that normal HBEC ALI cultures remained fully differentiated and stable for up to day 33 post-ALI. HBECs cultured beyond 33 days post-ALI developed squamous and vacuolated epithelium[617].

FOXJ1 mRNA transfection was non-toxic to primary HBECs, as evidenced by the formation of a confluent monolayer post-transfection. This implies that the cells maintained their proliferative and adhesive capabilities in the presence of exogenous FOXJ1 mRNA. In addition, FOXJ1 mRNA transfection induced expression of downstream genes in primary HBECs before air exposure. Traditionally, the establishment of an ALI is required for the induction of ciiliogenesis genes to initiate differentiation of HBECs towards a ciliated cell fate[618]. This is because the ALI configuration, with the basal surface of cells in contact with medium and the apical surface exposed to air, mimics conditions in the human airway and drives differentiation towards a mucociliary phenotype[617]. In addition to the ALI environment, factors present in the media, such as retinoic acid and growth factors, also play a role in triggering HBEC differentiation. However, FOXJ1 mRNA transfection bypassed the requirement for ALI-mediated induction of ciliogenesis and activated the associated downstream cascade. This observation highlights FOXJ1 as a central regulator of ciliogenesis, showing that FOXJ1 mRNA transfection can prime HBECs for subsequent differentiation into ciliated cells, even without air exposure.

Preserving HBEC morphology post-gene overexpression is essential, as the bronchial epithelium is the primary defence against inhaled pathogens and particles[619]. Morphological disruptions could compromise barrier function and disrupt the balanced interplay between ciliated, secretory, and basal cells. The effect of FOXJ1 supplementation on the morphology of HBECs cultured at ALI was assessed through histological analysis. H&E staining of HBEC ALI culture sections demonstrated that cultures derived from both non-transfected and FOXJ1 mRNA transfected HBECs develop a polarised pseudostratified epithelium with ciliated cells facing the apical side. It was observed that FOXJ1 mRNA transfection did not alter the morphology of HBECs cultured at ALI for 28 days compared to non-transfected controls. The mean epithelial thickness of FOXJ1 mRNA transfected HBEC cultures and non-transfected HBEC cultures after 28 days culture at ALI was similar to that of normal human bronchial epithelium *in vivo* (28 μm)[620]. It is important to note that while cilia were captured (6 μm long), tissue processing can introduce shrinkage, potentially leading to underestimation of the true epithelial thickness.

TEM was used to study the differentiation of HBECs cultured at ALI over time. TEM is a powerful tool that provides high-resolution images of cellular structures, allowing for the direct observation of morphological changes associated with differentiation that are not easily detectable with other methods, such as histology analysis. TEM results showed that both FOXJ1 mRNA transfected and non-transfected HBECs cultured at ALI were able to form a stable, well-differentiated, mucociliary bronchial epithelium. Extensive morphological

characterisation of non-transfected HBEC ALI cultures through histology and TEM was essential to determine the baseline morphology over the course of ALI differentiation (day 7, 14, 21, and 28 post-ALI) and better understand the morphological modifications that may have occurred in HBEC ALI cultures transfected with FOXJ mRNA. The results of this study demonstrated that FOXJ1 mRNA transfection does not alter the overall morphology of HBEC ALI cultures. Interestingly, TEM analysis revealed early signs of ciliation, such as basal body formation, in FOXJ1 mRNA transfected HBECs from donor 3 as early as day 7 post-ALI. This was earlier than the typical onset of ciliation in HBEC ALI cultures, which is typically observed between day 14 and 21 post-ALI[617]. This observation suggests that FOXJ1 mRNA transfection may accelerate HBEC differentiation into ciliated cells, a finding supported by the pre-airlift gene expression data from the same donor, which showed higher changes in FOXJ1 downstream genes involved in ciliogenesis. However, it is important to acknowledge that this study was limited by a small sample size, and future studies with a larger number of donors are needed to validate the TEM results and confirm whether FOXJ1 mRNA transfection can accelerate HBEC differentiation into ciliated cells.

Junctional complexes, compromising tight junctions, adherens junctions, and desmosomes, play a significant role in maintaining the overall integrity and barrier function of bronchial epithelium[621–624]. Tight junctions physically hold epithelial cells together and regulate the paracellular movement of ions, water, and macromolecules across epithelia, restricting the entry of potential pathogens and maintaining a stable environment in the airways[621,625,626]. Adherens junctions and desmosomes play crucial roles in promoting cell-to-cell attachment and preserving the structural integrity of the respiratory epithelium[621,627–629]. In the context of respiratory diseases, disruptions to these junctional complexes have been associated with increased susceptibility to infections, altered epithelial repair mechanisms, and exacerbation of inflammatory responses[625]. Thus, maintaining bronchial epithelial integrity post gene manipulation studies is crucial. To evaluate the effect of FOXJ1 mRNA transfection on bronchial epithelial integrity, gene expression analysis was employed to assess the expression of tight (*TJP1*, *OCLN*) and adherens junction (*CDH1*) markers 6, 12, 24, and 48 hours post-FOXJ1 mRNA transfection (short-term impact) and day 7, 14, 21, 28 post-ALI (long-term impact). The findings of this study showed no significant difference between FOXJ1 mRNA transfected cells and non-transfected cells in terms of the expression of tight and adherens junction markers. To further investigate this, TEM was used which allowed direct observation of the formation and organisation of junctional complexes. TEM revealed the formation of tight junctions and desmosomes in both FOXJ1 mRNA transfected HBEC ALI cultures and non-transfected HBEC ALI cultures. Overall, the data from this study showed that epithelial integrity is unaffected following FOXJ1 mRNA transfection. The unaltered gene expression of junctional

markers coupled with the TEM observations suggest that FOXJ1 mRNA transfection does not alter the expression of these markers or compromise the ultrastructural integrity of the bronchial epithelium.

Proper differentiation of bronchial epithelium is essential for the respiratory system to function properly[630]. It ensures the respiratory epithelium can perform its important barrier function, mucociliary clearance, and host defence mechanisms. This study aimed to assess the expression of key differentiation genes (*KRT5* for basal cells, *SCGB1A1* for club cells, *MUC5AC* and *MUC5B* for goblet cells, *FOXJ1* for ciliated cells) in HBECs following FOXJ1 mRNA transfection and over the course of ALI differentiation in both non-transfected and FOXJ1 mRNA transfected HBECs. The findings of this study showed that FOXJ1 supplementation did not induce the expression of *MUC5AC* and *MUC5B* within 6-48 hours post-FOXJ1 mRNA transfection. Over the first 7 days of ALI differentiation, the expression of genes involved in epithelial differentiation gradually increased, reaching a peak between days 14 and 21 post-ALI. This increase was accompanied by a decrease in the expression of the stemness marker *KRT5*. There were no significant differences in the expression of any of the genes between non-transfected and FOXJ1 mRNA transfected cells. Bukowy-Bleryllo *et al.* previously reported that the expression of differentiation genes *SCGB1A1* and *MUC5AC* in human nasal epithelial cell ALI cultures was most strongly upregulated between days 3 and 6 post-ALI, followed by a decrease[631]. These differences may be due to differences in experimental setup, or innate differences between epithelial cells from distinct anatomical compartments. As expected, *FOXJ1* expression was induced in FOXJ1 mRNA transfected HBECs. However, it declined by 48 hours post-transfection and then increased again, reaching a peak at day 14 post-ALI. Interestingly, *FOXJ1* expression in FOXJ1 mRNA transfected cells up to 24 hours post-transfection was higher than FOXJ1 expression induced by air-exposure in non-transfected cells during ALI differentiation.

PAS staining is a common method used to identify mucus-producing cells in histological sections[632]. Previous studies showed that PAS-positive mucus-producing cells start to appear in human airway ALI cultures around 6 days post-ALI and their numbers increase up to day 21 post-ALI[633]. The number of PAS-positive cells was correlated with increased expression of *MUC5AC* and *MUC5B* during the same period[633]. In contrast, Prytherch *et al.* observed that HBEC ALI sections showed PAS positive goblet cells from day 12-15 post-ALI[617]. In this study, PAS staining demonstrated the presence of secretory cells and intracellular mucins at day 28 post-ALI in both non-transfected and FOXJ1 mRNA transfected HBEC ALI cultures. The increased expression of *MUC5AC* and *MUC5B* during HBEC ALI differentiation, as measured

by qPCR, correlated with the appearance of secretory granules and goblet cells, as observed by TEM, in both FOXJ1mRNA transfected and non-transfected HBECs.

Bronchial epithelial differentiation was also assessed at protein level, in addition to the insight provided into its regulation at transcriptional level. Immunofluorescence microscopy confirmed the presence of basal cells (KRT5), club cells (SCGB1A1), goblet cells (MUC5AC) and cilia (acetylated alpha tubulin) in both non-transfected and FOXJ1 mRNA transfected HBEC ALI cultures. Quantitative analysis revealed that the proportions of differentiated cell types remained consistent, regardless of whether the HBECs were non-transfected or FOXJ1 mRNA transfected. Specifically, ciliated cells comprised approximately 80% of the population at day 28 post-ALI cultures, PAS positive goblet cells approximately 10%, and non-ciliated PAS negative cells made up the remaining 10%. This uniformity in differentiation proportions post-transfection suggests that FOXJ1 mRNA transfection does not compromise the intrinsic differentiation capability of HBECs. It is important to note that these proportions are only a snapshot of the cellular composition at a specific time-point. Assessing the cellular composition at earlier time points could provide insights into the progression of differentiation and dynamics of cellular interactions, highlighting any transient variations in cell proportions and capturing potential shifts in cell fate during ALI differentiation mediated by FOXJ1 mRNA transfection. The observed proportions of differentiated cell types are consistent with the published literature, which shows that ciliated cells are the predominant cell type in differentiated HBEC ALI cultures[634]. For instance, Leung *et al.* showed that primary HBECs cultured at ALI differentiate into a pseudostratified mucociliary phenotype, with relative proportions of apical cell types in ALI cultures grown in Pneumacult media similar to those observed *in vivo* (approximately 70% ciliated cells, 28% goblet cells, 2% non-ciliated PAS negative cells)[634,635]. Other studies have reported varying proportions of cell types in HBEC ALI cultures, likely due to differences in methodologies, cell sources, or experimental conditions[616,636]. Overall, the findings of this study suggest that FOXJ1 mRNA transfection does not compromise the intrinsic differentiation capability of primary HBECs cultured at ALI.

Ciliogenesis is a complex and tightly regulated process that involves the coordinated expression of a network of genes to generate the structural and regulatory components of cilia[637,638]. The expression of subset FOXJ1 downstream genes involved in ciliogenesis was assessed at day 7, 14, 21, and 28 post-ALI in both non-transfected and FOXJ1 mRNA transfected HBEC ALI cultures. The transcriptional regulators of ciliogenesis, *RFX2* and *RFX3*, were maximally expressed at day 21 post-ALI, while IFT genes, *DYNC2H1* and *IFT172*, were upregulated from day 7 post-ALI, peaking between days 21 and 28 post-ALI. Accordingly, genes encoding ciliary structural components and microtubule-based movement proteins

were also upregulated, reaching a peak between days 21 and 28 post-ALI. The data of this study showed that the temporal expression profile of FOXJ1 downstream genes was similar between non-transfected and FOXJ1 mRNA transfected HBECs. This suggests that FOXJ1 mRNA transfection did not accelerate the expression of FOXJ1 downstream genes during HBEC ALI differentiation. The profile of ciliogenesis genes observed in this study were generally consistent with the results reported in other studies, where airway epithelial cells were differentiated under similar conditions (Pneumacult ALI medium)[639–641]. Differentiation media composition has been shown to have a strong impact on the level of gene expression changes during ciliogenesis, with Pneumacult ALI medium promoting ciliogenesis and gene expression changes to a greater extent than other commercially available media[519,640,642,643]. Variability in the expression of genes between donors has been previously reported in the literature, with studies showing donor-to-donor variability in the expression of ciliogenesis genes during ALI differentiation[383,639,640]. For example, Bukowy-Blerytto *et al.* showed that inter-donor differences in the expression of ciliogenesis genes are likely due to external factors, such as the epigenetic memory of primary airway epithelial cells from different donors[640]. This may lead to donor-specific differences in cell-type composition in ALI cultures, which may in turn contribute to inter-donor variability in gene expression.

TEM revealed ciliated cells with cilia anchored into the ciliated cell via basal bodies[644] in both non-transfected and FOXJ1 mRNA transfected HBEC ALI cultures by day 14 post-ALI. Early gene expression changes at day 0 to 7 post-ALI likely relate to active cell differentiation, with ciliation itself occurring rapidly between days 7 to 14 post-ALI when cilia-related genes become expressed. Ultrastructural analysis of ciliated cells by TEM demonstrated that cilia of differentiated FOXJ1 mRNA transfected HBECs were morphologically comparable to non-transfected HBECs, in terms of both basal body structure and 9+2 axoneme arrangement. Overall, this study demonstrated that FOXJ1 mRNA transfection of HBECs induces the expression of FOXJ1 downstream cilia-associated genes before air exposure but does not accelerate the expression of these genes during ALI differentiation. FOXJ1 supplementation does not impair the ciliogenesis potential of HBECs, and their cilia ultrastructure is similar to that of non-transfected cells.

4.4 Conclusion

In conclusion, this study demonstrated that efficacy of PBAE in delivering exogenous FOXJ1 mRNA to primary HBECs, resulting in the induction of a subset FOXJ1 downstream genes involved in ciliogenesis. FOXJ1 mRNA transfected cells formed a confluent monolayer and were successfully cultured at ALI for 28 days, without any impairment in the integrity of the epithelium or the ability of HBECs to differentiate into a pseudostratified epithelium with club, ciliated, and goblet cells. Furthermore, the cilia ultrastructure of FOXJ1 mRNA transfected HBECs was comparable to non-transfected controls. Overall, these findings demonstrate the potential of FOXJ1 encoded mRNA as a powerful tool for studying ciliated cell differentiation of HBECs at ALI and advancing our understanding of ciliogenesis.

5 Results III – Investigating PBAE design for improved mRNA delivery to bronchial epithelium

5.1 Introduction

5.1.1 Barriers in gene delivery to ALI-cultured HBECs

Primary HBECs cultured under ALI conditions undergo differentiation, forming a pseudostratified columnar epithelium with tight junctions, cilia, and mucin production[645,646]. Gene delivery in these well-differentiated ALI-cultured HBECs remains a significant challenge[647]. As demonstrated in Chapter 3 of this thesis, HBECs grown at ALI cannot be transfected with mRNA. This reduced transfection efficiency is likely attributed to a combination of factors, including the robust barrier function, mucus production, cilia-mediated clearance mechanisms, and complex interactions between differentiation and proliferation[648,649].

Despite these barriers, studies have shown that viral vectors can successfully transduce fully differentiated human ALI cultures[650–652]. However, virus-based gene transfer faces several limitations, including complex manufacturing process, inherent safety concerns, potential for insertional mutagenesis, limited cargo capacity, and difficulties in transducing non-dividing cells[653]. Non-viral vectors, such as PBAEs, emerge as a promising alternative, addressing some of these issues with their reduced immunogenicity, improved scalability, high gene capacity, and versatile chemical design. This chapter explored PBAE modifications to improve mRNA transfection efficiency in HBEC ALI cultures.

5.1.2 Modifying PBAEs

As discussed previously in Chapters 1 and 3, PBAEs have emerged as a promising class of non-viral vectors due to their unique combination of properties, including: 1) straightforward synthesis using commercially available monomers, 2) biodegradability through hydrolytic cleavage of their ester bonds, 3) capacity for electrostatic interactions with negatively charged nucleic acids, such as mRNA, leading to the formation of polyplexes, 4) minimal cytotoxicity, 5) structural diversity and 6) potential for varied chemical modification, making them highly versatile for different applications[654–662]. PBAEs are synthesised via the Michael addition polymerisation reaction and are composed of diacrylate monomers, primary amine monomers and an end-modified group.

5.1.2.1 Molecular weight/chain length modification

The chain length or molecular weight of cationic polymers plays a crucial role in their gene delivery efficiency. Studies have shown that PBAEs with higher molecular weights generally exhibit enhanced transfection efficiency[663–666]. This enhanced transfection efficiency is attributed to the ability of higher molecular weight PBAEs to form more stable polyplexes with

nucleic acids, thereby protecting nucleic acids from degradation and facilitating their cellular uptake. The desired molecular weight of PBAEs can be controlled by adjusting the monomer stoichiometry during synthesis. Eltoukhy *et al.* demonstrated that PBAEs with intermediate length were most effective in delivering DNA into HeLa cells, due to their optimal nanoparticle size and DNA complexation efficiency[667]. Cordeiro *et al.* further explored the impact of varying the molecular weight of PBAE segments within copolymers composed of poly[2-(dimethylamino) ethyl methacrylate] and poly(β-amino ester) (PDMAEMA-b-PBAE-b-PDMAEMA) on biological activity[668]. Their comprehensive evaluation, encompassing physicochemical characterisation (agarose gel electrophoresis, DLS, zeta potential) and biological assessments (luciferase, GFP expression in HeLa and COS-7 cell lines and cytotoxicity) indicated that copolymers with larger molecular weight PBAEs show enhanced activity in HeLa and COS-7 cell lines. These findings underscore the importance of tailoring the molecular weight/chain length of PBAEs through modulation of monomer selection, reaction conditions, and polymerization parameters to optimise gene delivery efficiency[669–673].

5.1.2.2 End group modification

Recent studies have shed light on the critical role of terminal functional groups in polymer chains, particularly for PBAEs, in determining their gene delivery efficiency[656,661,674–681]. These end-groups impart distinct chemical properties that modulate the physicochemical characteristics of the resulting nanoparticles, consequently influencing their cellular uptake and gene delivery efficiency.

PBAEs can be tailored for cell-type-specific interactions by incorporating ligands that specifically bind to designated cell membrane receptors[682–684]. This can be achieved by utilising peptides as end-cap groups in PBAE design. Peptides, short chains of amino acids, possess a wide range of biological functions and can be designed to bind selectively to certain cell types, enabling targeted gene delivery[685,686]. For instance, Fornaguera *et al.* demonstrated the potential of PBAEs end-modified with specific oligopeptides, CH3 (NH_2-Cys-His-His-His-COOH) and CK3 (NH_2-Cys-Lys-Lys-Lys-COOH) to target antigen-presenting cells in the spleen following intravenous administration *in vivo*. These modified PBAEs effectively directed mRNA transfection to these target cells while reducing their accumulation in the liver, making them promising candidates for immunotherapy strategies[687]. Recently, Núñez-Toldrà *et al*. demonstrated the ability of oligopeptide end-modified PBAEs to simultaneously deliver anti-OCT3/4 siRNA, anti-NANOG siRNA, and RUNX2 plasmid to dental pulp stem cells, effectively inducing their osteogenic differentiation, and expressing osteogenic markers[688].

The impact of oligopeptides as terminal groups on the gene transfection capabilities of PBAEs was investigated[689]. It was found that PBAEs end-capped with arginine or lysine oligopeptides exhibited superior transfection efficiency compared to those with histidine or diamine oligopeptides. Interestingly, the efficacy of these modifications varied across distinct cell types. Arginine-modified PBAEs successfully transfected human immortalised keratinocytes and normal human dermal fibroblasts, while histidine-terminated PBAEs transfected A549 alveolar epithelial cell line. Notably, a synergistic combination of PBAE polymers modified with both arginine and histidine resulted in significant transfection of HeLa cells[683]. These findings highlight the potential of tailoring specific oligopeptides as terminal groups to enhance transfection efficiency of PBAEs, enabling a customizable approach to gene delivery tailored to the target cell type.

Oligopeptide end-modification of PBAEs holds promise for enhancing their specificity and efficiency as gene delivery vectors. Strategic peptide selection enables tailoring of PBAEs for specific applications or targeting distinct cell types. While significant progress has been made, the potential of peptide-modified PBAEs for mRNA delivery to HBECs remains unexplored. This unexplored area presents an exciting opportunity for future research and development of novel, functionalised vectors with enhanced gene delivery capabilities. This PhD project investigated the potential of peptide-modified PBAEs for mRNA delivery to HBECs.

5.1.3 Harnessing peptide transporter for targeted polyplex internalisation and mRNA transfection

Solute carrier family 15 (SLC15) transporters are proteins that play a crucial role in cellular nutrient uptake and drug absorption, utilising the proton motive force for their function[690]. Within this diverse family of transporters, organic anion/cation transporters and oligopeptide transporters are essential for the transport of a wide range of molecules, including xenobiotics, and therapeutic agents[690–692]. Among these, PEPT2 is a high-affinity, low-capacity transporter, predominantly expressed in the kidney, brain, and lung[693–696]. PEPT2 facilitates the uptake of di- and tripeptides along with a diverse array of peptidomimetics drugs[695,697–700]. The presence of PEPT2 in the lung holds particular significance for combating respiratory infections and developing novel pulmonary drug delivery stategies[701,702]. Studies have shown that PEPT2 significantly influences drug deposition and distribution within the respiratory tract, suggesting its potential for targeted inhaled drug delivery of peptide-based therapeutics[703–707]. While PEPT2 has been extensively investigated for its role in small molecule drug transport, its potential to facilitate nanoparticle internalisation remains unexplored.

5.1.4 Hypothesis and aims

Patel *et al.* developed stable and scalable PBAEs[468]. These materials facilitate gene transfection in lung epithelium *in vivo* through either systemic or inhaled delivery routes[442,444,445]. A yet-to-be-explored advantage of these materials is their capacity to modify end-group functionality without altering the core structure. This property presents a novel opportunity to investigate how the introduction of biological ligands, such as peptides, may influence mRNA delivery to primary HBECs. While the core provides stability for nucleic acid condensation, the end groups play a crucial role in cellular uptake.

In this chapter, I investigated the impact of PBAE modifications on the transfection efficiency of primary HBECs. The use of peptides as targeting ligands to enhance mRNA transfection of primary HBECs cultured at ALI was explored. Transfection efficiency, cytotoxicity and physicochemical properties of peptide-modified PBAEs were characterised.

Hypothesis

Modifying PBAE end-groups with peptides will improve mRNA transfection of ALI-cultured primary HBECs compared to the simple amine monomers that have traditionally been used to end-cap PBAEs.

Aims

1. Explore the impact of PBAE chain length modification on mRNA transfection in primary HBECs.
2. Determine the expression and functional activity of PEPT2 in submerged and ALI-cultured primary HBECs.
3. Characterise the physicochemical properties and transfection efficiency of novel peptide-modified PBAEs in primary HBECs.
4. Investigate whether peptide-modified PBAEs interact and function through PEPT2-mediated cellular uptake.
5. Assess the ability of peptide-modified PBAEs to enhance mRNA transfection of primary HBECs cultured at ALI.

5.2 Results

5.2.1 Synthesis of linear PBAEs

This project explored the application of linear PBAEs to evaluate potential enhancements in mRNA transfection efficiency in HBEC ALI cultures. The choice of linear PBAEs was driven by their simpler synthesis and characterisation processes using methods such as ^{1}H NMR. PBAEs were synthesised through Michael addition of amines (DD) to diacrylate groups (90) and end-capped with terminal amines (118) (DD90-118) (Figure 5.1)444,708,709. The polymer's chain length was manipulated by altering the amine to diacrylate monomer ratio as shown previously[656,671,677]. To investigate the impact of polymer chain length on the transfection of primary HBECs, linear PBAEs with two distinct chain lengths were synthesised employing ratios of 1.2:1 (DD90-118 1.2) and 1.05:1 (DD90-118 1.05) diacrylate:amine[671]. The chemical structure of the polymers was confirmed by 'H NMR (data not shown). The chain lengths were estimated to be approximately 10 and 23 repeat units for DD90-118 1.2 and DD90-118 1.05, respectively. The polymer synthesis, NMR characterisation, and chain length estimation were performed by Leigh-Anne Gavin.

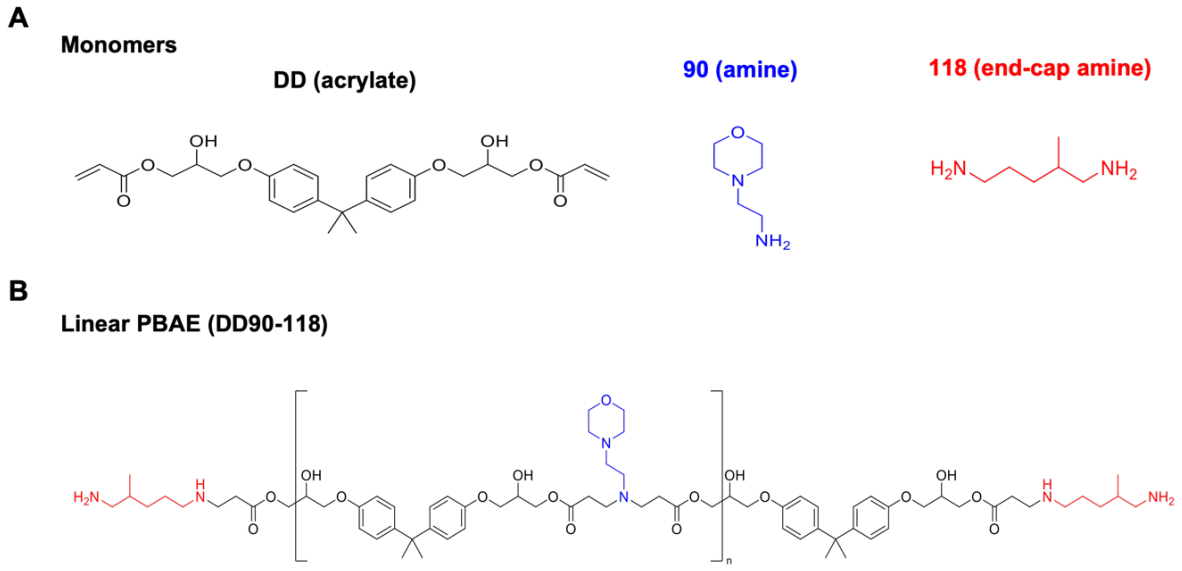


Figure 5.1 Synthesis schematic of linear poly (β-amino ester) (PBAE).
(A) Monomers used for linear PBAE synthesis (DD90-118). It was synthesised via Michael addition of diacrylate (DD) with primary amine monomers (90) and end-capped with terminal amines (118). The polymer chain length was controlled by varying the amine/diacrylate monomer ratios. Linear PBAEs were synthesised by reacting together diacrylate (DD) and amine (90) monomers at 1.05:1.0 and 1.2:1.0 diacrylate:amine molar ratios (DD90-118 1.05, DD90-118 1.2). (B) Chemical structure of linear PBAE. Synthesised by Leigh-Anne Gavin (Patel group).

5.2.2 Evaluation of transfection efficiency and cytotoxicity of linear PBAEs in submerged primary HBECs

To determine whether linear PBAEs DD90-118 1.05 and DD90-118 1.2 were capable of functional reporter mRNA delivery to primary HBECs their transfection efficiency was assessed *in vitro*. mRNA encoding for FLuc was complexed with either DD90-118 1.05 polymer, DD90-118 1.2 polymer, or delivered naked to submerged primary HBECs. Commercial transfection reagent JetMessenger was also included as a positive control. Transfection efficiency was assessed by measuring luminescence 24 hours post-transfection.

Results indicated that both linear polymers were effective in facilitating the translation of FLuc mRNA, with DD90-118 1.2 polymer achieving higher luminescence ($4.3x10^5$ RLU $\pm$ $1.3x10^5$) than DD90-118 1.05 polymer ($2.5x10^5$ RLU $\pm$ 6.9 $x10^5$) (Figure 5.2A). To confirm these findings and assess particle uptake, the polymers were complexed with Cy5-tagged GFP mRNA. Cy5 expression was observed in submerged primary HBECs, indicating that the particles were successfully taken up by cells and the mRNA was translated (GFP) (Figure 5.2C).

To quantify the cytotoxic effects associated with the transfection process, LDH release was measured 24 hours post-transfection. The data showed an increase in LDH levels for cells transfected with DD90-118 1.2/mRNA, DD90-118 1.05/mRNA, and JetMessenger/mRNA, compared to non-transfected control HBECs (Figure 5.2B).

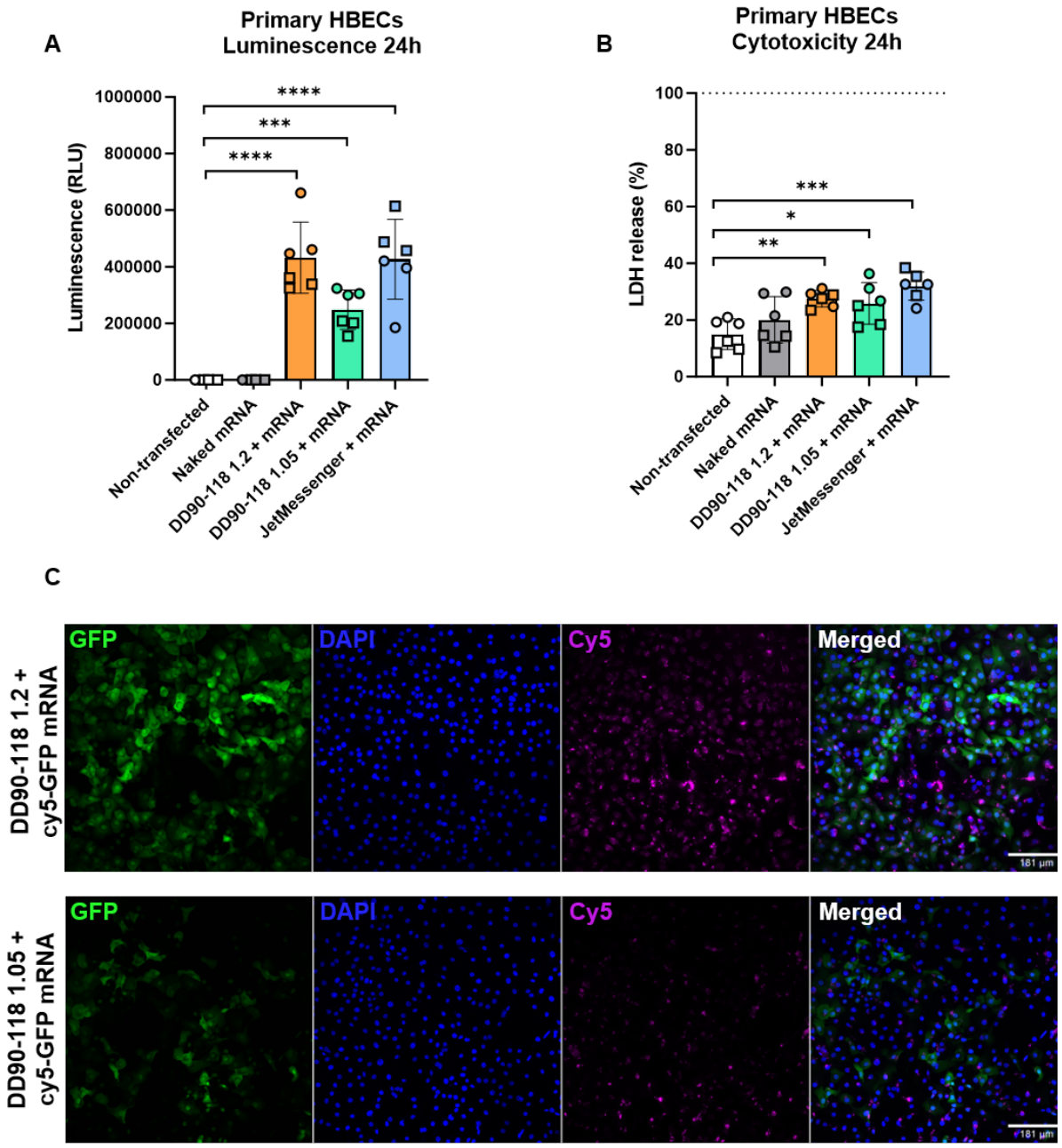


Figure 5.2 Transfection efficiency and cytotoxicity of linear poly (β-amino esters) (PBAEs), DD90-118 1.2 and DD90-118 1.05, in primary human bronchial epithelial cells (HBECs).

Firefly luciferase (FLuc) mRNA was complexed with either DD90-118 1.2 polymer, DD90-118 1.05 polymer, commercial transfection reagent JetMessenger or delivered naked to submerged primary HBECs (A) Transfection efficiency was assessed by measuring luminescence at 24 hours post-transfection. Data represents mean ± SD. N = 2 primary cell donors with 3 technical replicates each. Each symbol represents a different donor. Statistics: One-way ANOVA followed by Dunnett's multiple comparisons test. ***P=0.0002, *****P<0.0001. (B) Cytotoxicity was assessed by measuring lactate dehydrogenase (LDH) release 24 hours post-transfection. Dotted line indicates 100% LDH release of positive control cells treated with 1% Triton-X-100 and cytotoxicity was calculated relative to this control. Data represents mean ± SD. N = 2 primary cell donors, with 3 technical replicates each. Each symbol represents a different donor. Statistics: One-way ANOVA followed by Dunnett's multiple comparisons test. * P=0.0159, **P=0.0051, ***P=0.0002. (C) Particle uptake (Cy5) and mRNA translation (GFP) were assessed by transfecting HBECs with Cy5-tagged GFP mRNA complexed with either DD90-118 1.2 polymer or DD90-118 1.05 polymer. Cy5 and GFP expression was visualised by confocal microscopy 24 hours post-transfection.

5.2.3 Size characterisation of linear PBAE/mRNA polyplexes

To investigate the effect of polymer chain length on the physicochemical properties of the polymer/mRNA complexes, linear PBAEs DD90-118 1.05 and DD90-118 1.2 were complexed with FLuc mRNA, and the size of the complexes formed was measured using DLS. The same mRNA concentrations and polymer/mRNA complexing methods as in the transfection experiment described in section 5.2.2 were used. This ensured that the nanoparticle physicochemical properties measured in this experiment reflected the particle properties in the transfection experiment.

The results showed that the polymers condensed mRNA into nanometre-sized particles, with DD90-118 1.05/mRNA polyplexes having an average size of 539.4 nm and DD90-118 1.2/mRNA polyplexes having an average size of 344.9 nm (Figure 5.3A-C). Despite their large size, these complexes were able to deliver mRNA (Figure 5.2). However, the difference in transfection efficiency between DD90-118 1.2 polymer and DD90-118 1.05 polymer observed in the previous section is likely due to the difference in polyplex size, as smaller particle sizes are important for achieving maximal transfection efficiency710. Based on the transfection and size characterisation data, the linear DD90-118 1.2 polymer was selected as a base polymer for further modification with peptides.

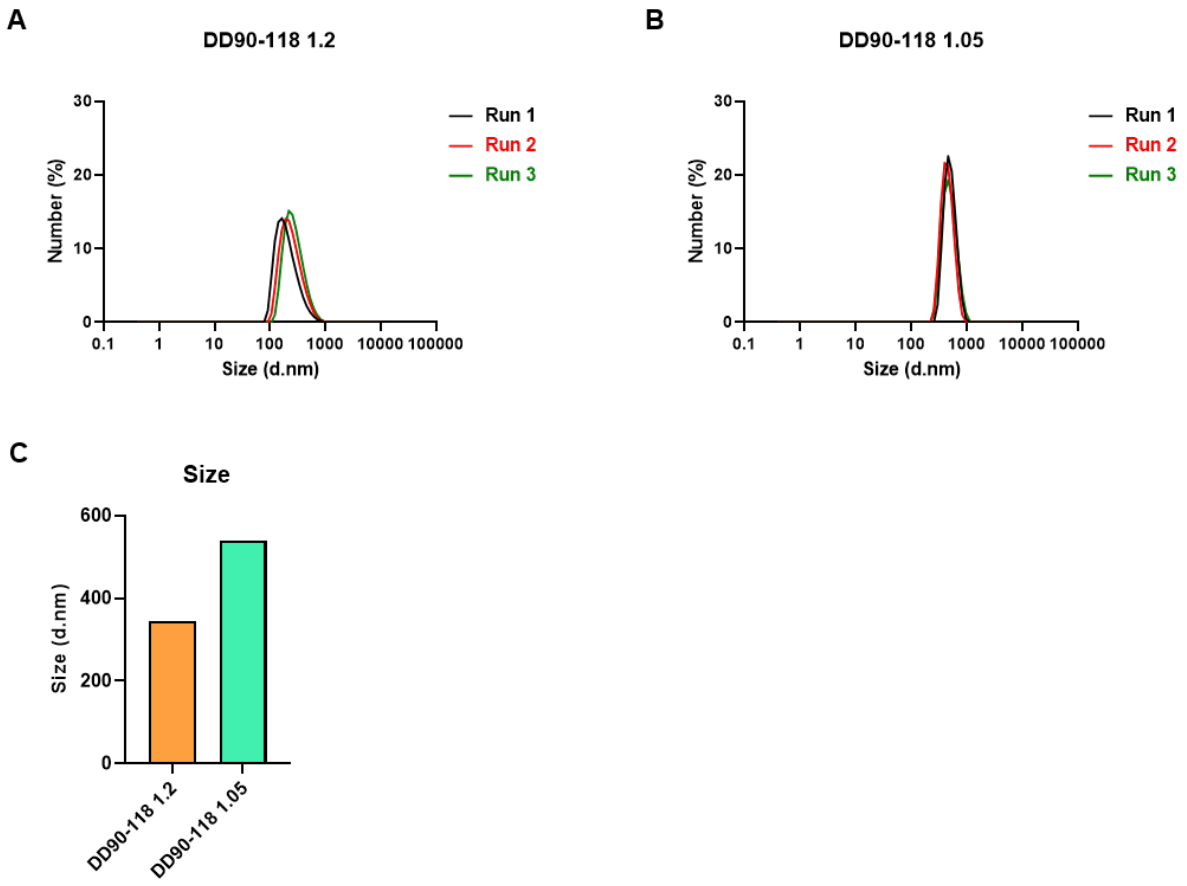


Figure 5.3 Size of linear poly (β-amino esters) (PBAE)/mRNA polyplexes formed by complexing linear PBAEs DD90-118 1.2 and DD90-118 1.5 with Firefly Luciferase (FLuc) mRNA.

(A) Size distribution by number of DD90-118 1.2/mRNA polyplexes. (B) Size distribution by number of DD90-118 1.05/mRNA polyplexes. (C) Average size of DD90-118 1.2/mRNA and DD90-118 1.05/mRNA polyplexes. Triplicate readings were obtained for each nanoparticle sample.

5.2.4 Expression of PEPT2 in submerged and ALI-cultured primary HBECs

To confirm that PEPT2 is expressed in bronchial epithelial cells, submerged primary HBECs were stained with PEPT2 and KRT5, a basal cell epithelial marker[513]. Primary HBECs stained positive for KRT5 (Figure 5.4B). Positive staining of PEPT2 was also observed in submerged primary HBECs, indicating that the cells express PEPT2 (Figure 5.4B). In addition, expression of *SLC15A2*, which encodes PEPT2, was validated in submerged and ALI-cultured primary HBECs through qPCR (Figure 5.4A). Interestingly, expression of *SLC15A2* was upregulated in Day 7, Day 14, and Day 28 ALI-cultured primary HBECs compared to submerged primary HBECs. These findings supported the modification of PBAEs with peptides to explore whether peptide-modified PBAEs can improve mRNA transfection efficiency in HBEC ALI cultures.

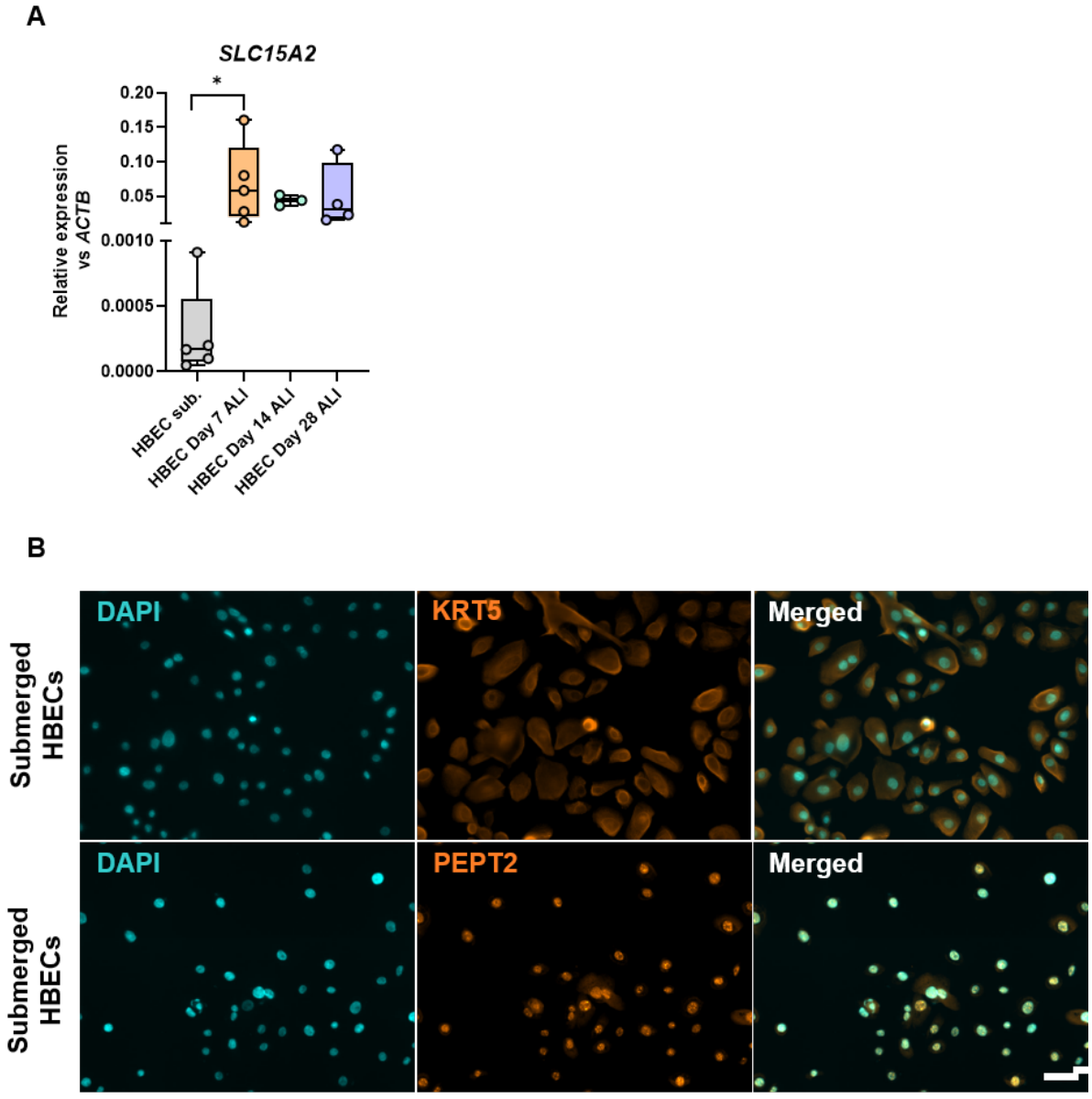


Figure 5.4 Expression of peptide transporter (PEPT2) in primary human bronchial epithelial cells (HBECs).

(A) Relative expression of *SLC15A2*, which encodes PEPT2, in submerged and air liquid interface (ALI)-cultured primary HBECs, as measured by qPCR. Data are shown as box-and-whisker plots with the whiskers ranging from minimum to maximum, the box indicating the interquartile range, and the line denoting the median. N = 3-5 primary cell donors. Statistics: Kruskal-Wallis test followed by Dunn's multiple comparisons test. *P=0.0238. (B) Immunofluorescence staining of submerged primary HBECs for PEPT2 and KRT5, a basal cell epithelial marker. Nuclei were stained with DAPI. Scale bar: 50 μm.

5.2.5 Functional activity of peptide transporter (PEPT2) in submerged and ALI-cultured primary HBECs

To assess the functional activity of PEPT2, the uptake of Ala-Lys-AMCA, a fluorescent dipeptide, under increasing concentrations ranging from 0 to 200 μM in submerged HBECs and ALI-cultured HBECs at days 7 and 14 post-ALI was investigated. Several studies have used the Ala-Lys-AMCA dipeptide to visualise and characterise dipeptide transport by peptide transporters in different cells and tissues[711–714]. As shown in Figure 5.5, Ala-Lys-AMCA was taken up by both submerged and ALI-cultured HBECs in a concentration-dependent manner, confirming the functionality of PEPT2 transporter in both culture conditions. The uptake of Ala-Lys-AMCA was more pronounced in ALI-cultured HBECs than in submerged HBECs, suggesting that PEPT2 activity may be increased in ALI-cultured HBECs. Overall, these data confirmed the presence and functional activity of PEPT2 transporter in submerged and ALI-cultured primary HBECs.

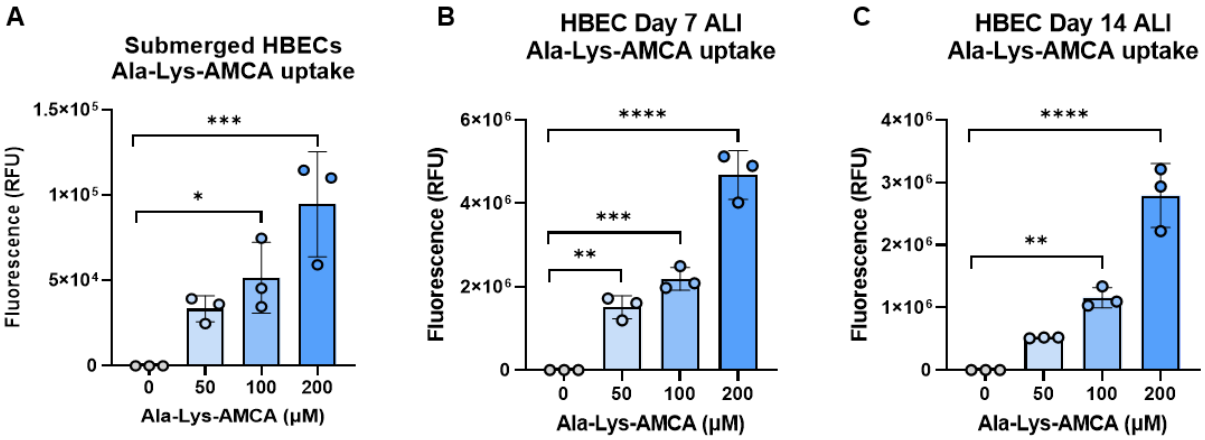


Figure 5.5 Concentration-dependent uptake of Ala-Lys-AMCA dipeptide by submerged and air liquid interface (ALI)-cultured primary human bronchial epithelial cells (HBECs).

(A) Submerged, (B) Day 7 HBEC ALI cultures, and (C) Day 14 HBEC ALI cultures were incubated with Ala-Lys-AMCA at different concentrations (0 to 200 μM) for 1 hour at 37°C. The uptake of Ala-Lys-AMCA was measured using a fluorescence plate reader. The data are presented as mean ± SD. N = 3 primary cell donors. Statistics: One-way ANOVA followed by Dunnett's multiple comparisons test. *P=0.0255, **P=0.002, ***P=0.0007, ****P< 0.0001.

5.2.6 Synthesis of peptide-modified PBAEs

Having confirmed that primary HBECs express PEPT2 at both gene and protein levels, peptide-modified linear polymers were synthesised. Dipeptides (Gly-Sar, Ala-Lys, Ala-Ala, Ala-Gly) were used to end-cap linear PBAEs (Figure 5.6). These di-peptides were chosen based on their structural diversity, solubility in DMSO, and ability to act as substrates for PEPT2[694,715–720]. PBAE synthesis was performed by Leigh-Anne Gavin.

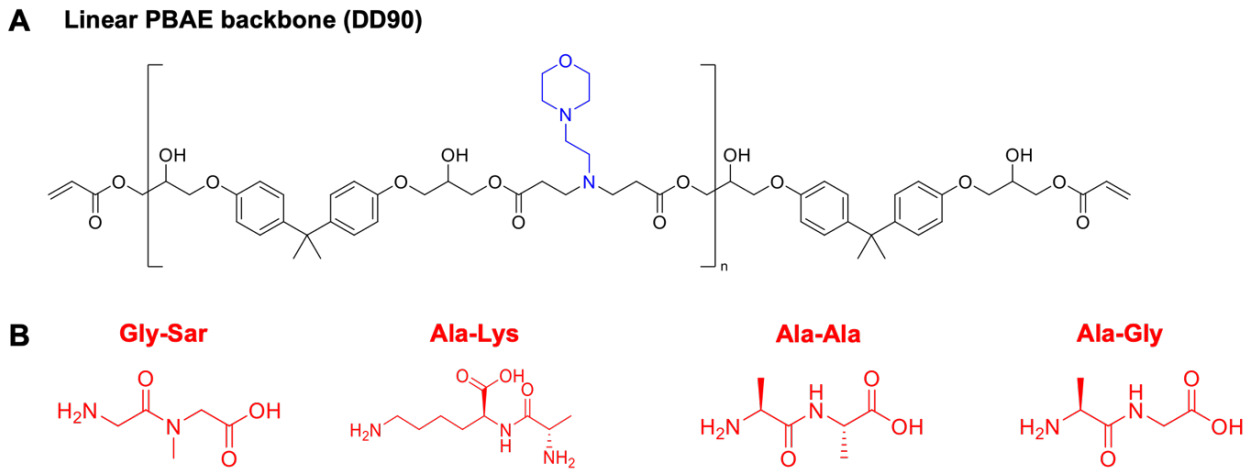


Figure 5.6 Modification of linear poly (β-amino esters) (PBAEs) with dipeptides.
(A) Linear PBAE backbone composed of diacrylate (DD) and amine groups (90). (B) Dipeptides used to end-cap linear PBAEs: glycyl-sarcosine (Gly-Sar), alanyl-lysine (Ala-Lys), alanyl-alanine (Ala-Ala), alanyl-glycine (Ala-Gly). Synthesised by Leigh-Anne Gavin (Patel group).

5.2.7 Screening of peptide-modified polymers on 16HBE cells

Initial screening of peptide-modified polymers was performed on 16HBE cells to assess their potential for delivering reporter mRNA to cells. Although 16HBE cannot fully recapitulate the barriers to mRNA delivery faced in primary HBEC ALI cultures, 16HBE cells divide rapidly and can be used to exclude ineffective polymers. mRNA encoding for FLuc was complexed with peptide-modified PBAEs (DD90-Gly-Sar, DD90-Ala-Lys, DD90-Ala-Ala, DD90-Ala-Gly), PBAE without end-cap group (DD90), jetPEI or delivered naked to 16HBE cells. jetPEI is a well-characterised commercial transfection reagent for which the chemical structure is fully elucidated. In contrast, the composition of the proprietary JetMessenger is not publicly available. Therefore, jetPEI was chosen as a positive control for the transfection experiments

in this chapter. Transfection efficiency measured by luminescence was assessed 24 hours post-transfection.

Data shown in Figure 5.7A demonstrate that peptide-modified polymers containing either Ala-Lys (DD90-Ala-Lys) or Gly-Sar (DD90-Gly-Sar) achieved higher transfection efficiency compared to other peptide-modified PBAEs tested (DD90-Ala-Ala and DD90-Ala-Gly). DD90-Gly-Sar and DD90-Ala-Lys polymers showed $1.9 \times 10^4 \pm 605$ RLU and $7.0 \times 10^4 \pm 1.0 \times 10^4$ RLU, respectively. In contrast, other peptide-modified PBAEs, DD90-Ala-Ala and DD90-Ala-Gly, were less effective in transfecting 16HBE cells, showing $7.2 \times 10^3 \pm 551$ RLU and $8.1 \times 10^3 \pm 520$ RLU, respectively. Transfection with PBAE without end-cap group (DD90) was not effective in delivering FLuc mRNA to 16HBE cells, suggesting that the end-cap group is important for efficient transfection.

To evaluate the effect of dipeptide modification on the biocompatibility of these polymers, cytotoxicity was assessed using the LDH release assay 24 hours post-transfection. LDH was not significantly increased 24 hours after transfection, indicating that the peptide-modified PBAEs are not cytotoxic to 16HBE cells (Figure 5.7B).

Overall, the results of this initial screening suggested that peptide-modified PBAEs, particularly DD90-Gly-Sar and DD90-Ala-Lys polymers, are promising candidates for mRNA delivery and were selected for further characterisation.

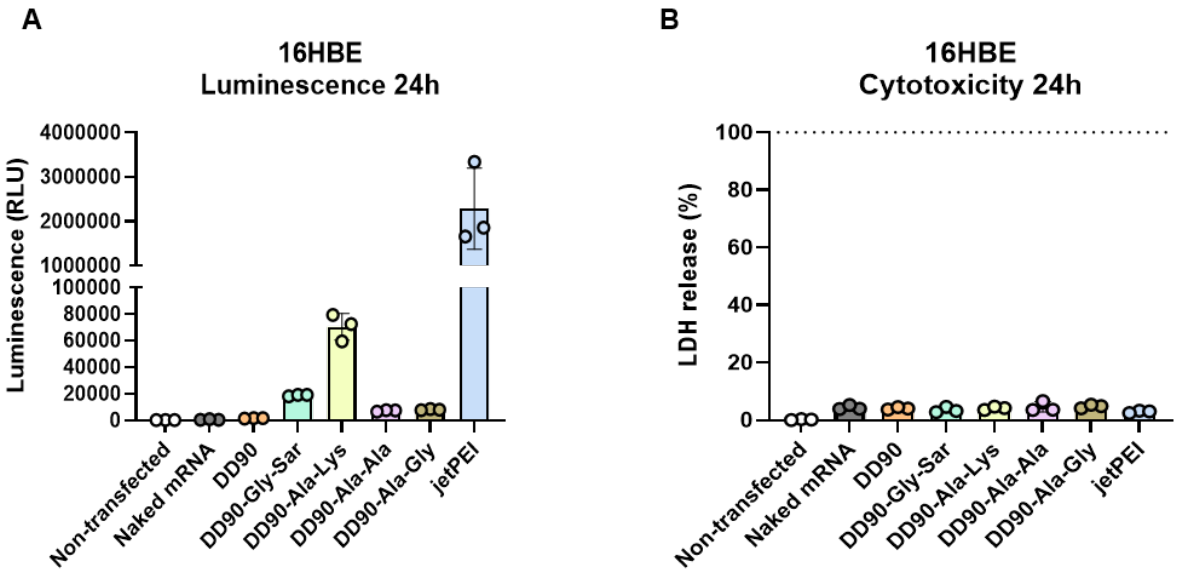


Figure 5.7 Transfection efficiency and cytotoxicity of peptide-modified peptide-modified poly (β-amino esters) (PBAEs) in 16 human bronchial epithelial (16HBE) cells.

(A) Transfection efficiency of peptide-modified PBAEs (DD90-Gly-Sar, DD90-Ala-Lys, DD90-Ala-Ala, DD90-Ala-Gly), PBAE without end-cap (DD90) and commercial transfection reagent jetPEI complexed with Firefly luciferase (FLuc) mRNA in 16HBE cells. Luminescence was measured 24 hours post-transfection. (B) Cytotoxicity of peptide-modified PBAEs in 16HBE cells, assessed by lactate dehydrogenase (LDH) release assay 24 hours post-transfection. Dotted line indicates 100% LDH release of positive control cells treated with 1% Triton-X-100 and cytotoxicity was calculated relative to this control. Data are presented as mean ± SD. n = 3 technical replicates.

5.2.8 Characterisation of DD90-Gly-Sar and DD90-Ala-Lys polymers

The two top-performing peptide-modified PBAEs (DD90-Gly-Sar, DD90-Ala-Lys) identified from screening on 16HBE cells were taken forward alongside control PBAEs (DD90-118, DD90, jetPEI) for further characterisation.

5.2.8.1 mRNA binding and encapsulation efficiency

To assess the mRNA binding capability of the peptide-modified PBAEs, agarose gel electrophoresis was performed. FLuc mRNA/PBAE complexes were prepared using DD90 (PBAE without end-cap group), peptide-modified PBAEs (DD90-Gly-Sar, DD90-Ala-Lys), DD90-118 (PBAE end-capped with traditional amine group), and jetPEI commercial transfection reagent. The migration of these complexes was compared to naked mRNA. As shown in Figure 5.8A, naked mRNA migrated through the gel evidenced by the formation of one distinct band. Complexation of mRNA with peptide-modified PBAEs and DD90-118 retarded its movement through the gel, indicating successful mRNA complexation. In contrast, when mRNA was complexed with DD90, a significant amount of free, non-complexed mRNA was observed, suggesting inefficient mRNA complexation with this polymer. This observation implies the inability of DD90 polymer to form stable complexes with mRNA, which could be a factor in its lack of transfection efficiency. Surprisingly, jetPEI polymer did not display effective mRNA binding as indicated by migration of mRNA through the gel.

To quantitatively assess PBAE/mRNA interactions, the Ribogreen assay was performed to quantify mRNA encapsulation efficiency by vectors. As shown in Figure 5.8B, peptide-modified PBAEs (DD90-Gly-Sar, DD90-Ala-Lys) and DD90-118 displayed high mRNA encapsulation efficiencies of almost 100%, whereas DD90 polymer demonstrated low mRNA encapsulation efficiency around 60%. These data correlate with the gel electrophoresis assay data mentioned previously. However, the mRNA encapsulation efficiency data of jetPEI were

not in agreement with the gel electrophoresis data, since jetPEI showed almost 100% mRNA encapsulation efficiency but not efficient mRNA protection on the gel retardation assay.

Overall, the results of mRNA binding and encapsulation efficiency assays suggest that peptide-modified PBAEs (DD90-Gly-Sar, DD90-Ala-Lys) are capable of efficiently binding and encapsulating mRNA.

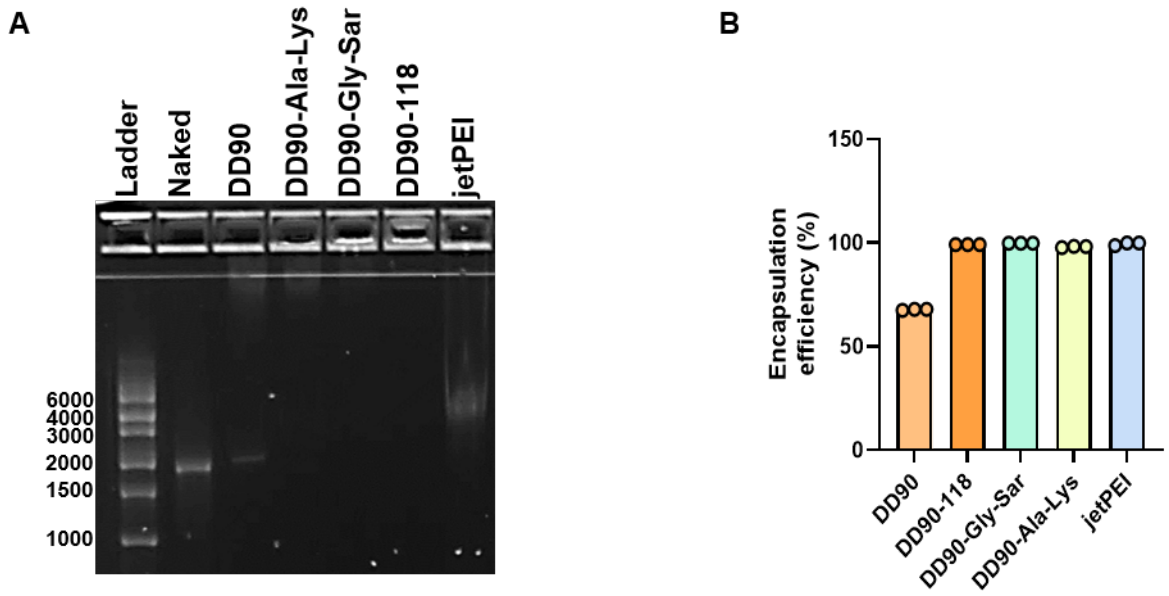


Figure 5.8 mRNA binding and encapsulation efficiency of peptide-modified poly (β-amino esters) (PBAEs).

(A) Agarose gel electrophoresis of Firefly luciferase (FLuc)/polymer complexes. FLuc mRNA was complexed with DD90 (PBAE without end-cap group), peptide-modified PBAEs (DD90-Gly-Sar, DD90-Ala-Lys), DD90-118 (PBAE end-capped with traditional amine group) or jetPEI commercial transfection reagent. The migration of these complexes was compared to naked mRNA. (B) mRNA encapsulation efficiency of PBAEs quantified by the Ribogreen assay. Data are presented as mean ± SD. n = 3 technical replicates.

5.2.8.2 Size and zeta potential measurements

The size and zeta potential of PBAE/mRNA complexes are important factors that can influence transfection efficiency. To evaluate these parameters, DLS was utilised. FLuc mRNA was complexed with peptide-modified PBAEs (DD90-Gly-Sar, DD90-Ala-Lys) using the same mRNA concentration and polymer/mRNA complexation methods as those employed in the transfection experiments. This ensured that the physicochemical properties of nanoparticles being assessed accurately represented those in the transfection experiments.

DLS measurements revealed that peptide-modified PBAEs formed large and unstable complexes with FLuc mRNA. Complexes prepared with DD90-Ala-Lys polymer and FLuc mRNA had a size of 635.3 nm and a zeta potential of -0.03 mV (Figure 5.9A,C,D). Particles obtained from DD90-Gly-Sar polymer and FLuc mRNA were smaller, with a size of 533.7 nm and a zeta potential of 0.08 mV (Figure 5.9B-D). Despite their large size and neutral zeta potential, peptide-modified PBAEs were able to deliver mRNA into cells, as shown in Figure 5.7.

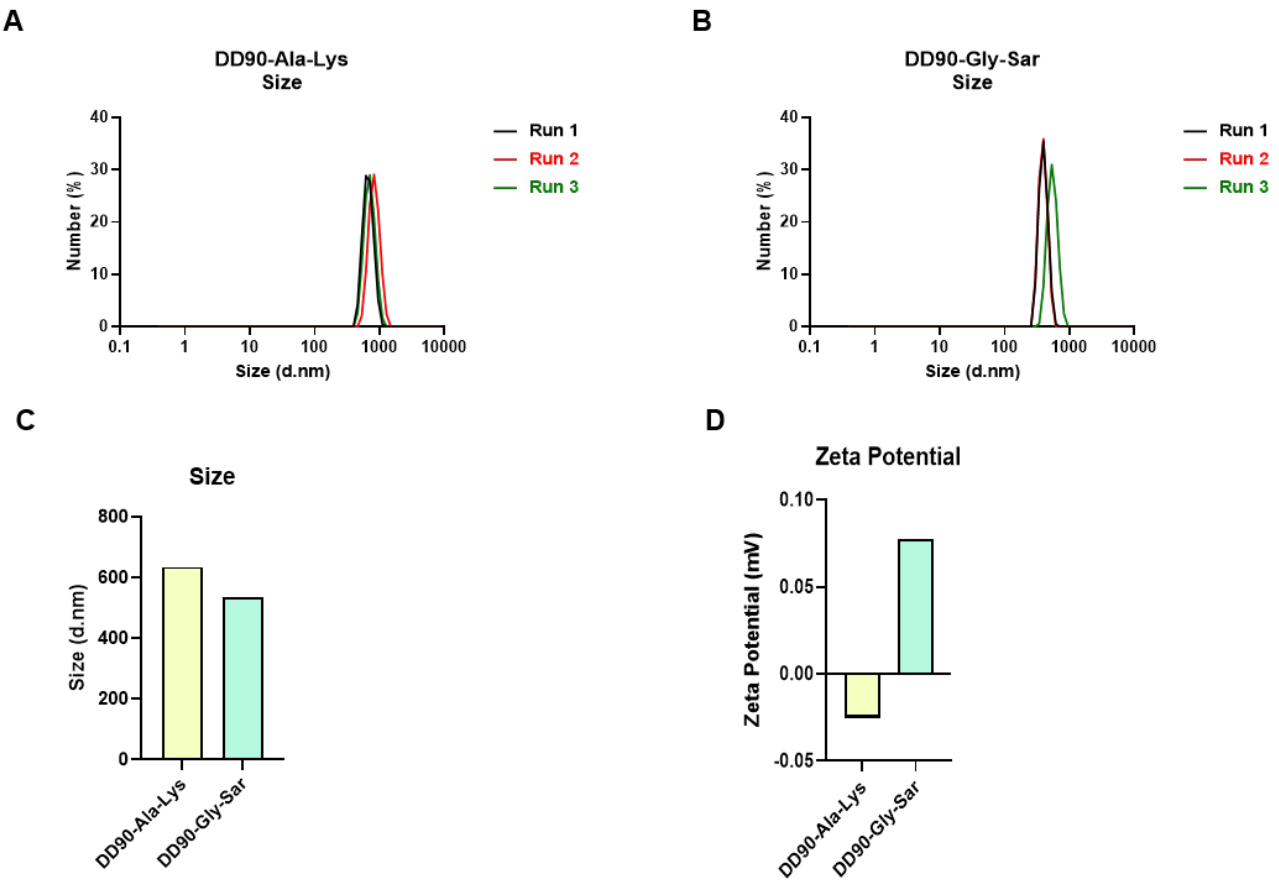


Figure 5.9 Size and zeta potential of peptide-modified PBAE/mRNA polyplexes.

Dynamic light scattering (DLS) was used to measure the size and zeta potential of peptide-modified PBAE/mRNA complexes. (A) Size distribution by number of DD90-Ala-Lys/mRNA polyplexes. (B) Size distribution by number of DD90-Gly-Sar/mRNA polyplexes. (C) Average size of DD90-Ala-Lys/mRNA and DD90-Gly-Sar/mRNA polyplexes. (D) Average zeta potential of DD90-Ala-Lys/mRNA and DD90-Gly-Sar/mRNA polyplexes. Triplicate readings were obtained for each nanoparticle sample.

5.2.9 Transfection efficiency and cytotoxicity of peptide-modified polymers on submerged primary HBECs

The two top-performing peptide-modified PBAEs, DD90-Gly-Sar and DD90-Ala-Lys were evaluated for their ability to deliver FLuc mRNA to submerged primary HBECs. Additionally, PBAE end-capped with traditional amine group (DD90-118) and PBAE lacking an end-cap group (DD90) were tested along with the commercial transfection reagent jetPEI. Transfection efficiency was assessed by luminescence 24 hours post-transfection.

As shown in Figure 5.10A-C, DD90-Gly-Sar achieved the highest transfection efficiency, among all HBECs donors tested, compared to DD90-Ala-Lys, DD90-118 and the commercial transfection reagent jetPEI. These findings highlight the influence of terminal end-groups on the transfection efficiency of polymers. Transfections with PBAE without end-cap group (DD90) or naked mRNA were inefficient.

To assess the cytotoxicity of peptide-modified PBAEs on primary HBECs, an LDH release assay was performed on cell culture supernatants 24 hours post-transfection (Figure 5.10D). No significant elevation in LDH release was observed in most conditions compared to non-transfected cells. However, a significant increase in LDH release was observed following transfection with DD90-Ala-Lys polymer.

Overall, these data demonstrated that primary HBECs can be transfected with FLuc mRNA complexed with peptide-modified PBAEs, specifically DD90-Gly-Sar and DD90-Ala-Lys. Among these, DD90-Gly-Sar was identified as the most effective option, demonstrating superior transfection efficiency compared to DD90-Ala-Lys polymer.

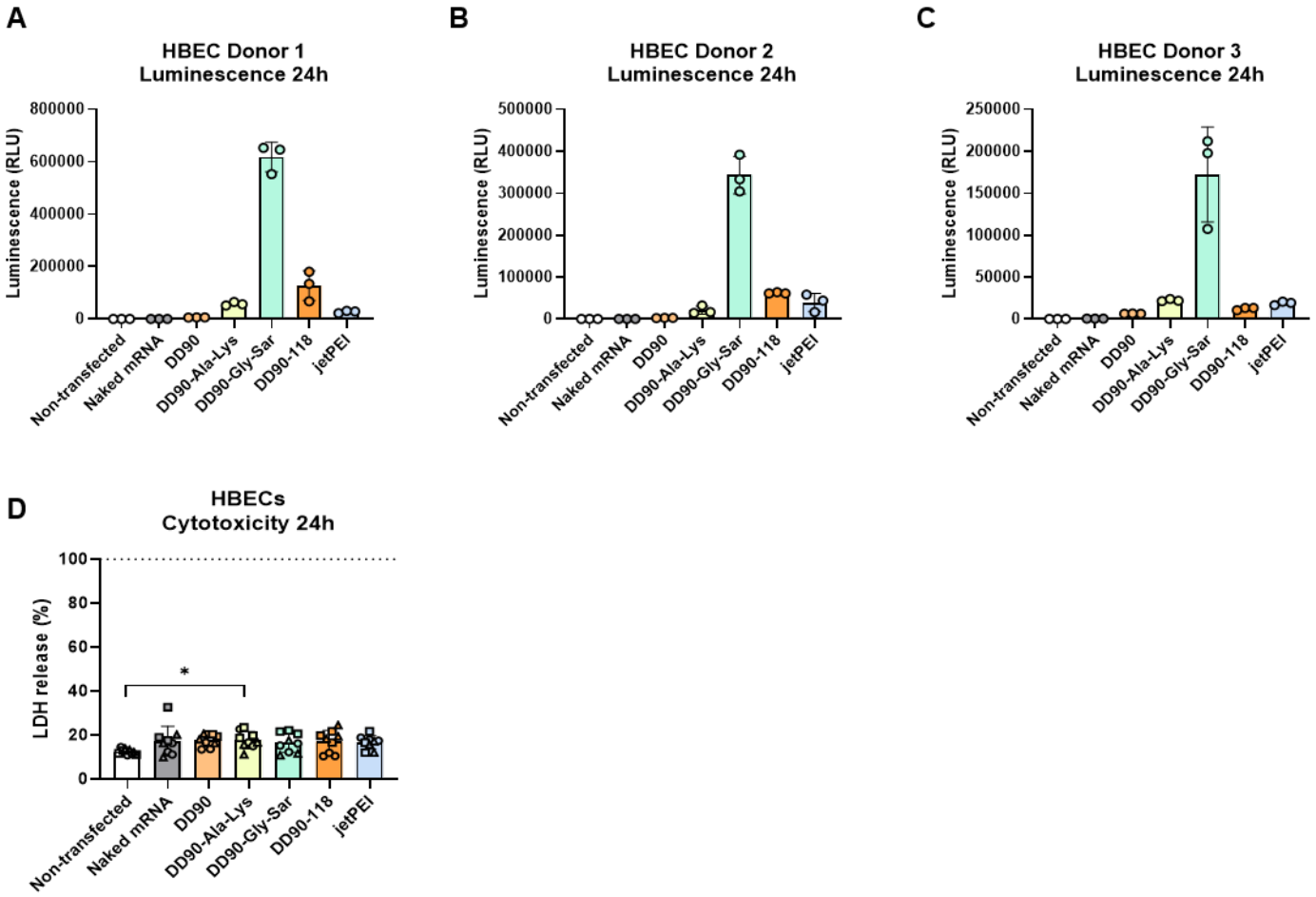


Figure 5.10 Transfection efficiency and cytotoxicity of peptide-modified poly (β-amino esters) (PBAEs) in submerged primary human bronchial epithelial cells (HBECs).

(A-C) Transfection efficiency of peptide-modified PBAEs (DD90-Gly-Sar, DD90-Ala-Lys), PBAE without end-cap (DD90) and commercial transfection reagent jetPEI complexed with Firefly luciferase (FLuc) mRNA in three different donors of primary HBECs. Luminescence was measured 24 hours post-transfection. Data are presented as mean ± SD. N = 1 primary cell donor per graph with 3 technical replicates each. (B) Cytotoxicity of peptide-modified PBAEs in HBECs, assessed by lactate dehydrogenase (LDH) release assay 24 hours post-transfection. Dotted line indicates 100% LDH release of positive control cells treated with 1% Triton-X-100 and cytotoxicity was calculated relative to this control. Data are presented as mean ± SD. N = 3 primary cell donors with 3 technical replicates each. Statistics: One-way ANOVA followed by Dunnett's multiple comparisons test. *P=0.0460.

5.2.10 Chemically conjugated dipeptides on PBAEs facilitate functional delivery of reporter mRNA to submerged primary HBECs

It was demonstrated that submerged primary HBECs can be transfected with peptide-modified PBAEs (section 5.2.9). Building on this, it was then explored whether adding dipeptides to the culture media could enhance transfection efficiency. To investigate this, two approaches were compared: firstly, transfection using FLuc mRNA complexed with chemically conjugated dipeptide-modified PBAEs (DD90-Gly-Sar, DD90-Ala-Lys), and secondly, transfection using non-end-capped PBAEs (DD90) in media that was supplemented with the same dipeptides (DD90 + Gly-Sar, DD90 + Ala-Lys). Luminescence was measured 24 hours post-transfection.

As shown in Figure 5.11 only peptide-modified PBAEs with chemically conjugated dipeptides (DD90-Gly-Sar, DD90-Ala-Lys) facilitated transfection of submerged primary HBECs. DD90-Gly-Sar polymer achieved higher transfection efficiency than DD90-Ala-Lys polymer. Transfection using DD90 in media supplemented with dipeptides was inefficient. These results suggested that chemical conjugation of dipeptides to PBAEs is necessary for functional delivery of mRNA to cells, rather than simply adding dipeptides to the formulation.

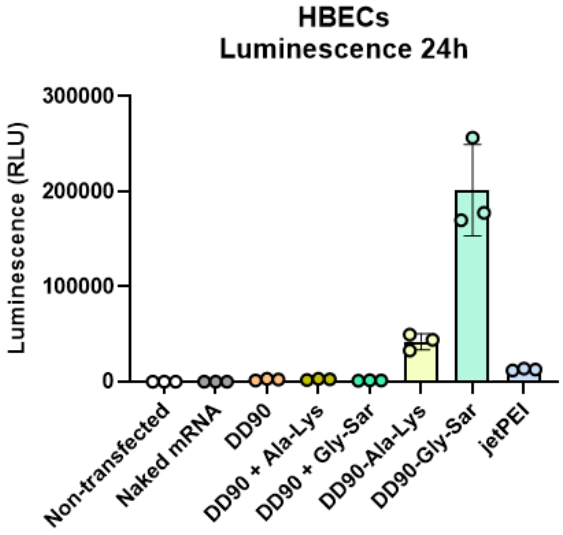


Figure 5.11 Chemically conjugated dipeptides on poly (β-amino esters) (PBAEs) facilitate delivery of mRNA to primary human bronchial epithelial cells (HBECs).

Transfection efficiency of Firefly luciferase (FLuc) mRNA was assessed 24 hours post-transfection using non-end-capped PBAEs in peptide-supplemented media (DD90 + Gly-Sar, DD90 + Ala-Lys) and peptide-modified PBAEs (DD90-Gly-Sar, DD90-Ala-Lys). Data are presented as mean ± SD. N = 1 primary cell donor with 3 technical replicates.

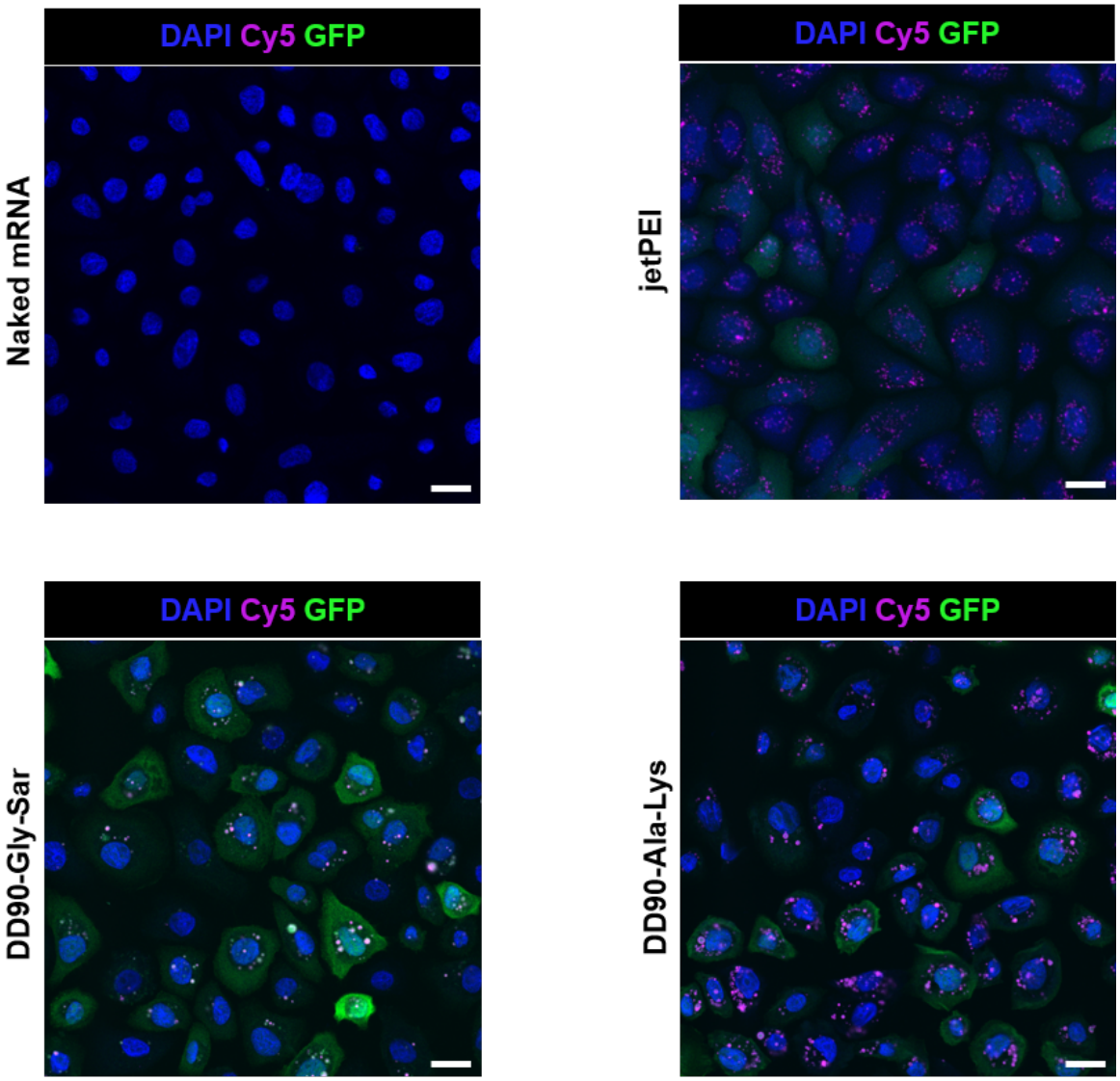
5.2.11 Investigation of peptide-modified PBAE-mediated reporter mRNA uptake and translation in submerged primary HBECs

The efficacy of peptide-modified PBAEs in mediating cellular uptake and subsequent translation of reporter mRNA in submerged primary HBECs was examined. Cy5-tagged GFP mRNA was used to evaluate the transfection efficiency of two peptide-modified PBAEs: DD90-Gly-Sar, DD90-Ala-Lys. As a control, the commercial transfection reagent jetPEI was included, along with a naked mRNA where mRNA was introduced without any vector. Cells were fixed 24 hours post-transfection and imaged using an SP5 Leica confocal microscope.

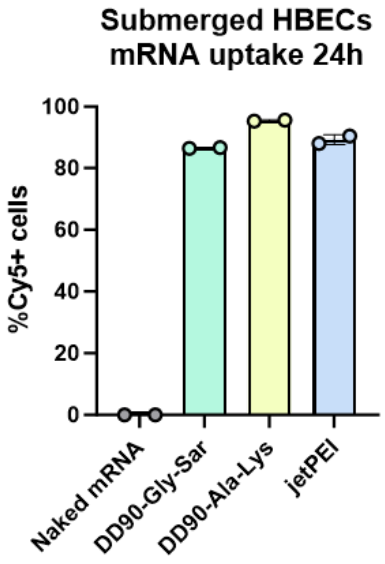
The results demonstrated successful Cy5 expression, indicating mRNA uptake in cells transfected with both peptide-modified PBAEs (Figure 5.12A). Moreover, these cells displayed GFP expression, a sign of mRNA being translated into protein. Quantitative analysis showed that the DD90-Gly-Sar polymer achieved mRNA uptake efficiency of 86.6% $\pm$ 0.2, which was comparable to that of jetPEI (89.3% $\pm$ 1.7) and DD90-Ala-Lys (95.5% $\pm$ 0.3) (Figure 5.12B). In contrast, cells transfected with naked mRNA showed no transfection signs, underscoring the necessity of non-viral vectors for effective mRNA uptake. Examination of GFP expression levels showed differences in translation efficiency between the two peptide-modified PBAEs. Transfection with DD90-Gly-Sar resulted in 61.2% $\pm$ 4.6 GFP-positive cells, markedly higher than DD90-Ala-Lys (44.9% $\pm$ 1.1 GFP-positive cells). This rate was significantly higher than the 16.2% $\pm$ 8.3 GFP-positive cells resulting from jetPEI-mediated transfection (Figure 5.12C).

Overall, the findings from this study identified DD90-Gly-Sar as the most effective peptide-modified PBAE for transfecting submerged primary HBECs. Consequently, this polymer was chosen for further testing.

A


DAPI Cy5 GFP
Naked mRNA
DAPI Cy5 GFP
jetPEI
DAPI Cy5 GFP
DD90-Gly-Sar
DAPI Cy5 GFP
DD90-Ala-Lys

B


Submerged HBECs
mRNA uptake 24h
%Cy5+ cells
100
80
60
40
20
0
Naked mRNA
DD90-Gly-Sar
DD90-Ala-Lys
jetPEI

C

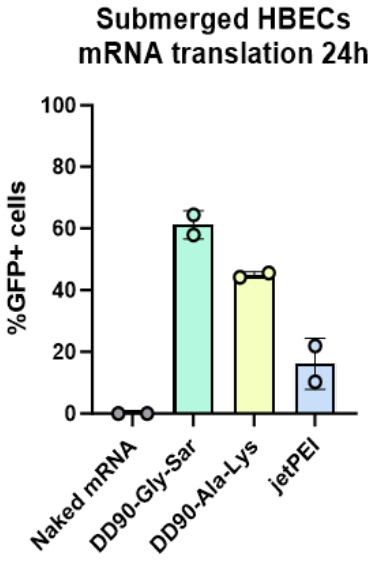

Submerged HBECs
mRNA translation 24h
%GFP+ cells
100
80
60
40
20
0
Naked mRNA
DD90-Gly-Sar
DD90-Ala-Lys
jetPEI

Figure 5.12 Reporter mRNA uptake and translation in submerged primary human bronchial epithelial cells (HBECs) using peptide-modified poly (β-amino esters) (PBAEs).
(A) Representative confocal microscopy images of submerged primary HBECs transfected with peptide-modified PBAEs (DD90-Gly-Sar, DD90-Ala-Lys), jetPEI, or naked mRNA. Cells were fixed 24 hours post-transfection and stained with nuclear stain DAPI. (B) Quantitative analysis of Cy5 expression, expressed as % Cy5-positive cells. (C) Quantitative analysis of GFP expression, expressed as % GFP-positive cells. Data are presented as mean ± SD. N = 1 primary cell donor with 2 technical replicates. Scale bar: 50 μm.

5.2.12 Investigating the effect of PEPT2 transporter blockage on peptide-modified PBAEs uptake

5.2.12.1 Effect of cefadroxil pre-incubation on Ala-Lys-AMCA uptake

Cefadroxil is a cephalosporin antibiotic which serves as a PEPT2 substrate721,722 and has been shown to inhibit dipeptide transport in murine bronchial and type II pneumocyte models through competitive binding[702,705,717,720]. It was hypothesised that if peptide-modified PBAEs were interacting with PEPT2 transporter, particle uptake would be reduced in cells pre-treated with cefadroxil. Primary HBECs were pre-incubated with 1 mM cefadroxil for 10-60 minutes at 37^{o}C, following protocols adapted from published literature[702,711]. Subsequently, cells were exposed to a fluorescent dipeptide Ala-Lys-AMCA, a known PEPT2 substrate723,724, at a concentration of 25 μM for 1 hour at the same temperature. This dipeptide served as a positive control for transporter activity, with fluorescence readings serving as a direct indicator of its cellular uptake.

Figure 5.13 demonstrates a reduction in the internalisation of Ala-Lys-AMCA following Cefadroxil pre-incubation. This is evident from the decrease in fluorescence intensity compared to the control group without Cefadroxil. This reduction exhibited a clear time-dependence pattern, suggesting a temporal aspect to the inhibitory mechanism of Cefadroxil on PEPT2. Nevertheless, it is important to note that while Cefadroxil pre-treatment resulted in decreased Ala-Lys-AMCA uptake, it did not completely abolish the activity of PEPT2, as evidenced by the measurable fluorescence. This partial inhibition highlights the potential for residual transporter activity even in the presence of a competitive substrate.

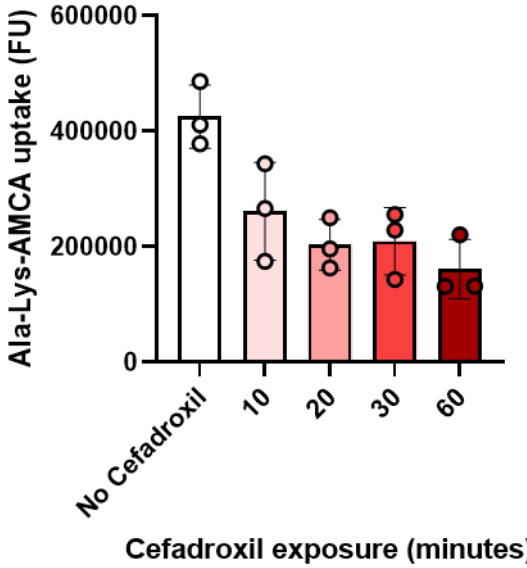


Figure 5.13 Inhibition of Ala-Lys-AMCA uptake by Cefadroxil in submerged primary human bronchial epithelial cells (HBECs).

Cells were pre-incubated with 1 mM Cefadroxil for durations ranging from 10 to 60 minutes at 37°C, followed by exposure to 25 µM Ala-Lys-AMCA for 1 hour. Fluorescence intensity, indicative of Ala-Lys-AMCA uptake, was measured post-incubation. Control samples without Cefadroxil are shown for comparison. Data are presented as mean ± SD. N = 1 primary cell donor with 3 technical replicates.

5.2.12.2 Impact of cefadroxil pre-incubation on peptide-modified PBAE transfection efficiency in primary HBECs

To investigate whether peptide-modified PBAEs utilise the PEPT2 transporter for cellular entry, primary HBECs were pre-incubated with Cefadroxil for 60 minutes. This incubation aimed to saturate the PEPT2 transporters and potentially inhibit the uptake of the peptide-modified PBAEs. Subsequently, HBECs were transfected with FLuc mRNA, complexed with two peptide-modified PBAEs (DD90-Gly-Sar, DD90-Ala-Lys), alongside several controls. These controls included PBAE end-capped with an amine group (DD90-118), PBAE without an end-cap group (DD90), the commercial transfection reagent jetPEI, and naked mRNA. Luminescence was measured 24 hours post-transfection.

Luminescence data revealed that Cefadroxil pre-incubation did not alter the transfection efficiency of the peptide-modified PBAEs (Figure 5.14A). To assess the cytotoxicity of this approach, an LDH release assay was performed 24 hours post-transfection. As shown in Figure 5.14B, primary HBECs tolerated the Cefadroxil pre-incubation, with no significant cytotoxic response observed.

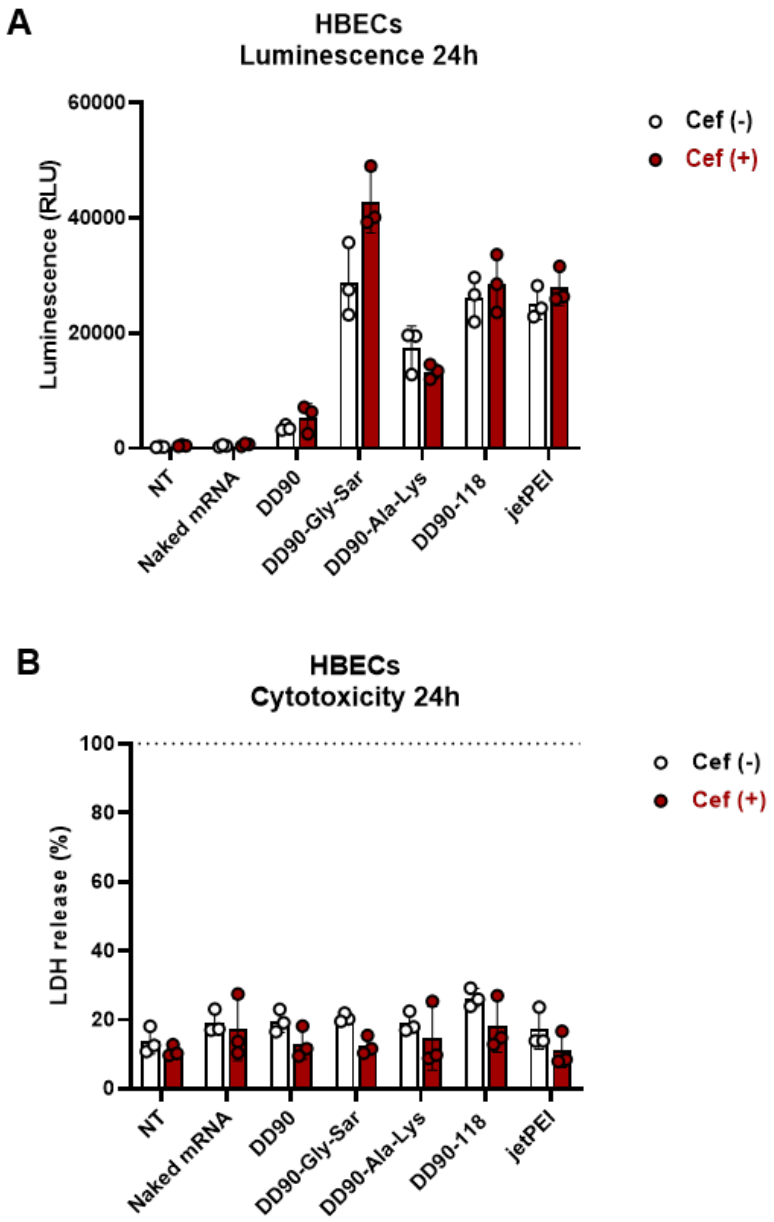


Figure 5.14 Assessing the impact of Cefadroxil pre-incubation on transfection efficiency and cytotoxicity of peptide-modified poly (β-amino esters) (PBAEs) in submerged primary human bronchial epithelial cells (HBECs).

(A) Transfection efficiency following Cefadroxil pre-incubation. Luminescence readings taken 24 hours after transfection with Firefly luciferase (FLuc) mRNA complexed with peptide-modified PBAEs (DD90-Gly-Sar, DD90-Ala-Lys), and controls (DD90-118, DD90, jetPEI, and naked mRNA). (B) Cytotoxic evaluation via lactate dehydrogenase release (LDH) assay 24 hours post-transfection. Dotted line indicates 100% LDH release of positive control cells treated with 1% Triton-X-100 and cytotoxicity was calculated relative to this control. Data are presented as mean ± SD. N = 1 primary cell donor with 3 technical replicates. (Cef: cefadroxil, NT: non-transfected).

5.2.12.3 Transfection efficiency of peptide-modified PBAEs in cefadroxil-containing media

Initial experiments showed that pre-incubating primary HBECs with cefadroxil did not impact the transfection efficiency of peptide-modified PBAEs. Consequently, a different approach was pursued, examining the effects of cefadroxil when present during the transfection process. Transfection was carried out in either standard culture media or media supplemented with 1 mM cefadroxil. Transfection efficiency was quantified by measuring luminescence 24 hours post-transfection.

Figure 5.15A shows a significant decrease in luminescence when cefadroxil was included in the media at the same time as transfection. Interestingly, this inhibitory effect of cefadroxil was also evident in control vectors, suggesting that its impact is not vector-specific. Further analysis demonstrated an elevated release of LDH in all conditions containing cefadroxil, compared to those without it (Figure 5.15B). This increase in LDH release suggests that the observed reduction in luminescence is likely due to increased cytotoxicity from cefadroxil exposure. These results indicate that the reduced transfection efficiency in the presence of cefadroxil might be due to its cytotoxic effects, rather than an inhibition of the PEPT2 transporter.

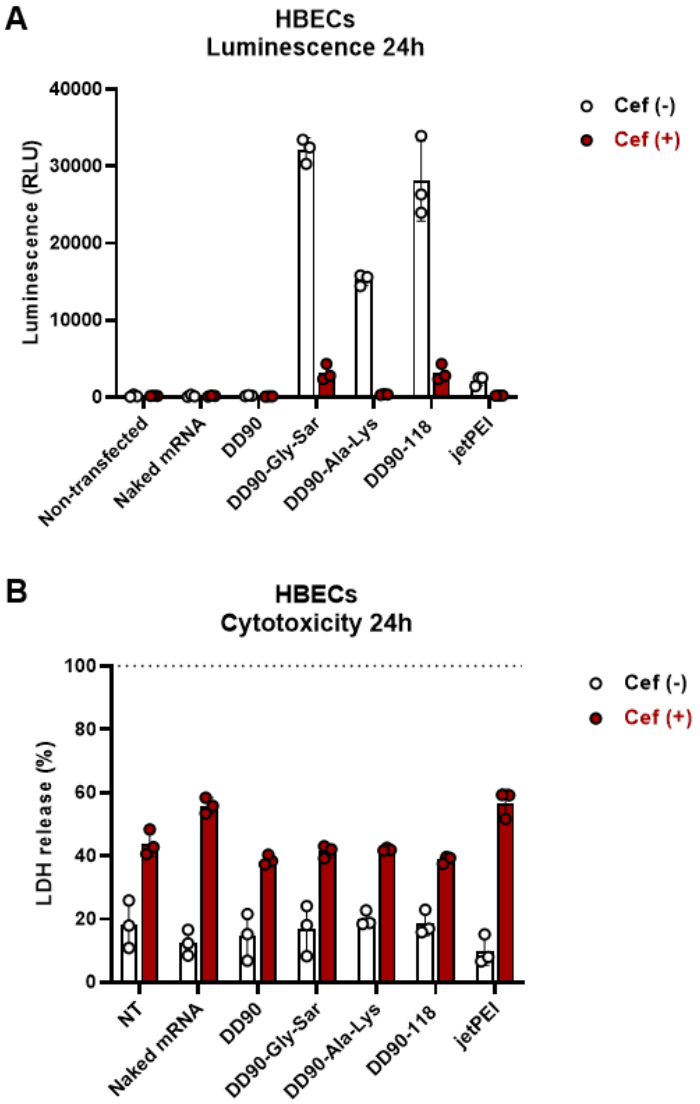


Figure 5.15 Impact of Cefadroxil on transfection efficiency and cytotoxicity in submerged primary bronchial epithelial cells (HBECs) using peptide-modified poly (β-amino esters) (PBAEs).

(A) Transfection efficiency of primary HBECs 24 hours post-transfection with Firefly luciferase (FLuc) mRNA complexed with peptide-modified PBAEs (DD90-Gly-Sar, DD90-Ala-Lys) and control vectors (DD90-118, DD90, jetPEI), either with or without 1 mM Cefadroxil supplementation. (B) Cytotoxicity post-transfection as indicated by lactate dehydrogenase (LDH) release assay. Comparisons were made against no-Cefadroxil control conditions. Dotted line indicates 100% LDH release of positive control cells treated with 1% Triton-X-100 and cytotoxicity was calculated relative to this control. Data are presented as mean ± SD. N = 1 primary cell donor with 3 technical replicates. (Cef: cefadroxil, NT: non-transfected)

5.2.12.4 Impact of pre-transfection with peptide-modified PBAEs on Ala-Lys-AMCA dipeptide uptake by submerged primary HBECs

To elucidate how peptide-modified PBAEs enter cells, a competitive binding assay targeting the PEPT2 transporter was employed. This assay aimed to determine whether these peptide-modified PBAEs use the same transporter as the Ala-Lys-AMCA dipeptide. Primary HBECs were transfected with peptide-modified PBAEs (DD90-Gly-Sar, DD90-Ala-Lys), along with control vectors as detailed in section 5.2.12.2. After allowing 30 minutes for complexes to bind, the Ala-Lys-AMCA dipeptide was introduced, followed by another hour of incubation. The subsequent cellular uptake of the dipeptide was assessed by measuring fluorescence levels. If the PEPT2 transporter acts as the entry route for both the peptide-modified PBAEs and the Ala-Lys-AMCA, competition between them would lead to a lower uptake of the dipeptide in cells transfected with the peptide-modified PBAEs compared to controls.

Figure 5.16 demonstrates a notable decrease in Ala-Lys-AMCA uptake in cells transfected with peptide-modified PBAEs, supporting the theory that PEPT2-mediated endocytosis plays a role in the process. Interestingly, cells transfected with non-peptide-modified polymers also showed decreased uptake of Ala-Lys-AMCA. While these results provided evidence for the role of PEPT2 in the cellular uptake of peptide-modified PBAEs, they do not rule out the possibility that PEPT2 might interact with other polymers as well. Consequently, further investigations are needed to fully understand the specificity of PEPT2 and its potential interactions with various polymeric materials in epithelial cells.

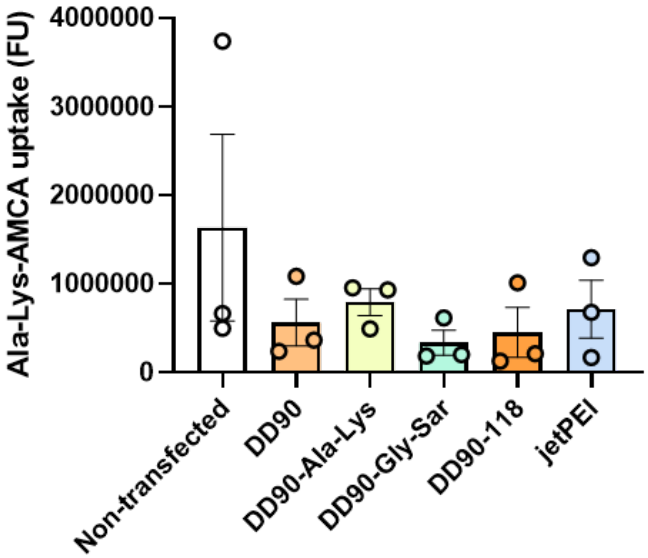


Figure 5.16 Competitive binding assay of PEPT2 transporter with peptide-modified poly (β-amino esters) (PBAEs).

This assay compared the uptake of the fluorescent dipeptide Ala-Lys-AMCA in primary human bronchial epithelial cells (HBECs) after transfection with different transfection reagents: peptide-modified PBAEs (DD90-Gly-Sar, DD90-Ala-Lys), amine end-capped PBAE (DD90-118), non-end-capped PBAE (DD90), jetPEI, and naked Firefly luciferase (FLuc) mRNA. The graph represents the fluorescence intensity measured, which is proportional to the uptake of Ala-Lys-AMCA by the cells. Data are presented as mean ± SD. N = 1 primary cell donor with 3 technical replicates.

5.2.13 Analysis of transfection efficiency and cytotoxicity across two different DD90-Gly-Sar polymer batches

Sections 5.2.9 and 5.2.11 of this chapter highlighted that the peptide-modified PBAE polymer, DD90-Gly-Sar, was the most promising candidate based on transfection data. Building on this, the next objective was to assess the consistency of this polymer's transfection performance across different batches. FLuc mRNA was complexed with two distinct batches of DD90-Gly-Sar polymers and delivered to submerged primary HBECs, alongside a control group transfected with mRNA without any complexing agent ('naked'). Transfection efficiency was quantified by measuring luminescence 24 hours post-transfection.

Figure 5.17A revealed that the two batches of DD90-Gly-Sar performed similarly, as there was no statistically significant difference in luminescence between them. However, variability in luminescence was observed among different donors, indicating that the transfection efficiency might vary depending on the donor. The use of naked mRNA did not result in effective transfection.

Furthermore, the cytotoxicity of the two polymer batches was evaluated using an LDH release assay on cultured supernatants 24 hours post-transfection. As shown in Figure 5.17B, neither batch of the DD90-Gly-Sar polymers, whether complexed with FLuc or used as vector-only controls, caused significant LDH release.

In summary, the data confirmed that both batches of the DD90-Gly-Sar demonstrated comparable transfection efficiencies and maintained a low cytotoxic profile, highlighting their reliability and potential for safe use in primary HBECs.

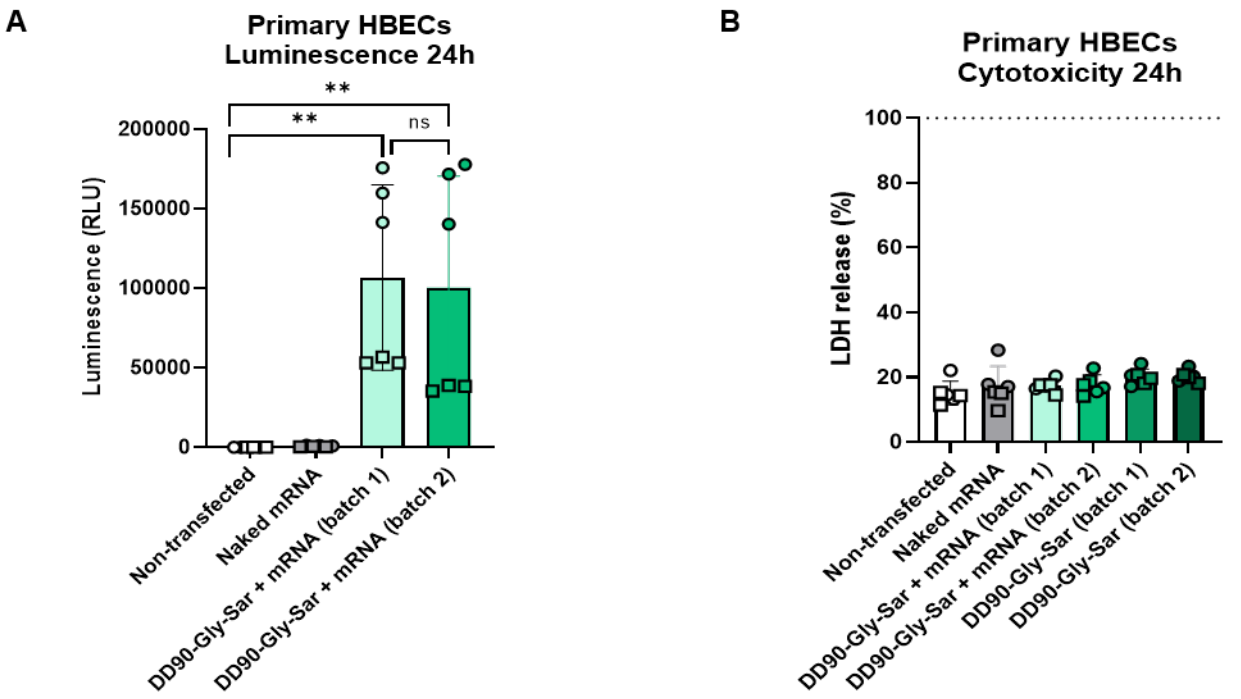


Figure 5.17 Comparison of transfection efficiency and cytotoxicity between two batches of DD90-Gly-Sar polymers in primary human bronchial epithelial cells (HBECs).

(A) Luminescence-based transfection efficiency of Firefly Luciferase (FLuc) mRNA when complexed with two different batches of DD90-Gly-Sar polymers (batch 1 and batch 2) in submerged primary HBECs. Luminescence was assessed 24 hours post-transfection. (B) Lactate dehydrogenase (LDH) release assay to assess the cytotoxicity of the two different batches of DD90-Gly-Sar polymers 24 hours post-transfection. Dotted line indicates 100% LDH release of positive control cells treated with 1% Triton-X-100 and cytotoxicity was calculated relative to this control. Data are presented as mean ± SD. N = 2 primary cell donors with 3 technical replicates each. Each symbol represents a different donor. Statistics: One-way ANOVA followed by Tukey's multiple comparisons test. ** P= 0.003, ns: non-significant P=0.99.

5.2.14 Transfection efficiency of DD90-Gly-Sar in primary HBEC ALI cultures

The previously discussed transfection data highlighted the potential of the peptide-modified polymer DD90-Gly-Sar as a promising agent for reporter mRNA delivery to primary HBECs in submerged cultures. Notably, it was also observed that the expression of the peptide transporter PEPT2 at gene level was higher in HBECs cultured at ALI compared to submerged cultures. This finding led to the hypothesis that DD90-Gly-Sar could enhance mRNA transfection in ALI-cultured HBECs.

In the initial experiments, primary HBECs cultured at ALI for 7 days were transfected with FLuc mRNA (100 ng/well) using DD90-Gly-Sar. This was compared to controls including naked mRNA, a PBAE end-capped with a traditional amine group (DD90-118), and the commercial transfection reagent jetPEI. Luminescence measured 24 hours post-transfection revealed that DD90-Gly-Sar induced a 10-fold increase in luminescence compared to the controls, confirming its effectiveness (Figure 5.18A). However, variability across different donors was noted. Transfection with naked mRNA was ineffective. To evaluate cytotoxicity, LDH release was monitored 24 hours post-transfection. The results, as shown in Figure 5.18D, indicated no significant increase in LDH release in DD90-Gly-Sar transfected compared to controls.

Building on these findings, the study extended to HBECs cultured at ALI for 14 days. In this experiment, the naked mRNA condition was omitted, and the FLuc mRNA dose was increased to 200 ng/well. This aimed to determine if a higher dose could improve transfection efficiency. Transfection efficiency was assessed 24 and 48 hours post-transfection, considering the robust barrier formed by HBECs in ALI culture. Results showed that DD90-Gly-Sar led to a significant increase in luminescence compared to DD90-118 and jetPEI (Figure 5.18B+C). The higher mRNA dose did not enhance transfection efficiency at 24 hours post-transfection (Figure 5.18B) but did result in higher luminescence at 48 hours post-transfection, suggesting a delayed yet enhanced transfection efficiency (Figure 5.18C). Furthermore, the 200 ng mRNA dose outperformed the 100 ng dose at 48 hours. LDH levels remained stable over 48 hours, indicating good tolerance of DD90-Gly-Sar transfection (Figure 5.18E+F).

Overall, these results demonstrated the effectiveness of DD90-Gly-Sar as an mRNA delivery vector for primary HBECs cultured at ALI. DD90-Gly-Sar-mediated transfection resulted in significantly higher luminescence compared to controls at both 24 and 48 hours post-transfection. Furthermore, the DD90-Gly-Sar transfection was well-tolerated by HBECs with no significant increase in LDH release. These findings suggest that DD90-Gly-Sar holds promise as a vector for mRNA delivery in HBEC ALI cultures.

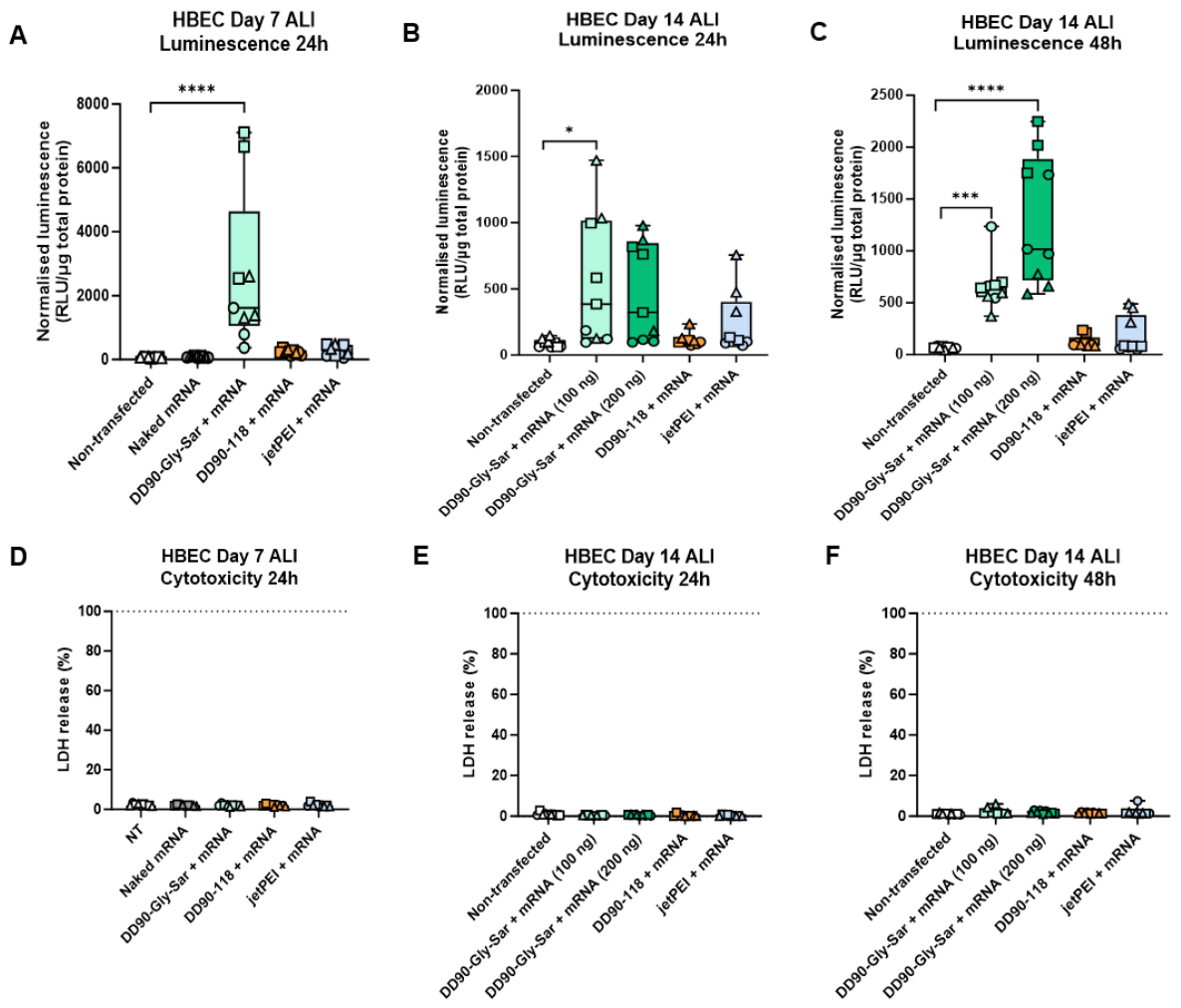


Figure 5.18 Transfection of primary human bronchial epithelial cells (HBECs) grown at air liquid interface (ALI) with peptide-modified poly (β-amino ester) (PBAE) DD-90-Gly-Sar.

(A) HBECs cultured at ALI for 7 days were transfected with Firefly luciferase (FLuc) mRNA (100 ng/well) using DD90-Gly-Sar and compared to control groups including naked mRNA, DD90-118, and jetPEI. The efficiency of transfections was measured by luminescence 24 hours post-transfection. (B) HBECs cultured at ALI for 14 days were transfected with FLuc) mRNA (100 ng/well or 200 ng/well) using DD90-Gly-Sar, DD90-118, and jetPEI. The efficiency of transfections was measured by luminescence 24 hours post-transfection. (C) The same experiment as in (B) was performed, but the transfection efficiency was measured 48 hours post-transfection instead. (D) Cytotoxicity of transfections on HBECs cultured at ALI for 7 days was assessed by measuring lactate dehydrogenase (LDH) release 24 hours post-transfection. (E) Cytotoxicity of transfections on HBECs cultured at ALI for 14 days was assessed by measuring LDH release 24 hours post-transfection. (F) Cytotoxicity of transfections on HBECs cultured at ALI for 14 days was assessed by measuring LDH release 48 hours post-transfection. Dotted line indicates 100% LDH release of positive control cells treated with 1% Triton-X-100 and cytotoxicity was calculated relative to this control. Luminescence data are presented as median and range. Cytotoxicity data are presented as mean ± SD. N = 3 primary cell donors with 3 technical replicates each. Each shape represents a different donor. Statistics: Kruskal-Wallis test followed by Dunn's multiple comparisons test. **P=0015, ***P = 0.0001, ****P<0.0001.

5.3 Discussion

In this chapter, I investigated the impact of PBAE modifications on mRNA transfection efficiency in primary HBECs. I have demonstrated that 1) linear PBAE with shorter chain length (DD90-118 1.2) was effective in transfecting submerged primary HBECs; 2) Expression of PEPT2 was characterised in HBECs, revealing higher gene expression levels in ALI cultured HBECs compared to submerged HBECs. Additionally, the functional activity of PEPT2 was confirmed in submerged and ALI cultured HBECs; 3) Novel peptide-modified PBAEs (DD90-Gly-Sar and DD90-Ala-Lys) facilitated mRNA transfection of submerged primary HBECs; 4) DD90-Gly-Sar polymer effectively transfected day 7 and 14 HBEC ALI cultures, indicating its promising potential for mRNA delivery to HBEC ALI cultures, which have traditionally been challenging to transfect.

This study explored the impact of chain length modification in linear PBAEs on the transfection efficiency of primary HBECs. Two linear PBAEs with distinct chain lengths (DD90-118 1.2, DD90-118 1.05) were synthesised using two different molar ratios of diacrylate to amine monomers (1.2:1 and 1.05:1). The molecular weight and chain length of PBAEs are directly influenced by the diacrylate to amine ratio. PBAEs with molecular weights exceeding 10 kDa are generally considered most effective, which can be achieved using a diacrylate to amine molar ratio of 1.2:1[670]. The findings of this study revealed that DD90-118 1.2 polymer, with an estimated shorter chain length, exhibited enhanced transfection efficiency in primary HBECs compared to DD90-118 1.05 polymer. This observation aligns with previous studies that have reported an inverse relationship between polymer chain length and transfection efficiency[674,708,725]. Polymers with shorter chain lengths may promote improved transfection capabilities due to enhanced mRNA encapsulation efficiency, cellular uptake, endosomal escape, or solubility. Further investigation into the size of polyplexes revealed that both polyplexes exceeded 200 nm. However, the polyplexes formulated with the DD90-118 1.2 polymer were smaller in size than those formulated with the DD90-118 1.05 polymer. This reduction in size might have contributed to their higher transfection efficiency. This aligns with existing literature, which highlights the critical role of nanoparticle size in cellular uptake and gene delivery efficiency[654,684,726]. This finding enhances our understanding of the key design principles for effective gene delivery systems, especially the influence of polymer chain length. Future research should focus on elucidating the relationship between polymer chain length and other cellular processes, such as endosomal escape or degradation, to gain a deeper understanding of the mechanisms underlying transfection efficiency.

One limitation of this study relies on the use of only two primary cell donors for the transfection experiment using DD90-118 1.2 and DD90-118 1.05 polymers. This small sample size restricts the ability to generalise the findings, considering the potential variability in how cells from different donors might react to the transfection process. Furthermore, as reported in the literature, linear PBAEs tend to be larger in size and less stable compared to their branched counterparts[468,727]. Despite these limitations, the use of linear PBAEs in this study was driven by their simpler synthesis and characterisation process.

While acknowledging the limitations of linear PBAEs, their application in this study serves as a valuable foundation for further research into novel peptide-modified PBAEs. These studies aimed to explore the impact of peptide modifications on PBAE transfection efficiency. Given its superior transfection efficiency and smaller polyplex size, the DD90-118 1.2 polymer was selected as the preferred starting point for the design of peptide-modified PBAEs.

This study investigated the expression of PEPT2 in primary HBECs grown under both submerged and ALI culture conditions. The data revealed that PEPT2 mRNA expression was upregulated in HBEC ALI cultures. However, PEPT2 protein expression was only assessed and confirmed in submerged primary HBECs. To evaluate the functional activity of PEPT2 in submerged and ALI-cultured HBECs, the uptake of the fluorescent dipeptide Ala-Lys-AMCA over time was measured. Ala-Lys-AMCA is a well-established substrate for PEPT2 and is extensively used to study its function[723,724]. The data demonstrated that both submerged and ALI-cultured HBECs transported Ala-Lys-AMCA, indicating that PEPT2 is functionally active in these cells. These findings established HBEC ALI cultures as a suitable model for investigating the efficiency of peptide-modified PBAEs for mRNA transfection. It was hypothesised that peptide-modified PBAEs will exhibit enhanced mRNA transfection efficiency in HBEC ALI cultures compared to unmodified PBAEs. The incorporation of peptides into PBAEs that specifically bind to PEPT2 could enhance their cellular uptake, resulting in improved mRNA delivery to HBEC ALI cultures.

Du *et al.* investigated the potential of peptide transporters to enhance drug delivery by examining the role of PEPT1 in the oral absorption of nanoparticles. They modified Poly (lactic-co-glycolic acid) (PLGA) nanoparticles with dipeptide conjugates (L-valine-valine, L-valine-phenylalanine) and polyoxymethylene to deliver docetaxel, a hydrophobic drug with low bioavailability[728]. Their findings demonstrated that dipeptide-modified nanoparticles exhibited enhanced cellular uptake compared to unmodified nanoparticles in stably transfected PEPT1-Hela and Caco-2 cell lines, indicating the involvement of PEPT1 in nanoparticle endocytosis. Additionally, the internalisation of these nanoparticles was proton-dependent, and L-valine-valine modified nanoparticles demonstrated superior intestinal permeability and oral

absorption, significantly improving docetaxel's oral bioavailability. These findings highlight the potential of peptide transporters as targets for enhancing drug delivery to various tissues. Peptide-modified nanoparticles offer a viable strategy for improving the oral delivery of hydrophobic drugs, while targeting PEPT2 could facilitate efficient mRNA transfection to HBEC ALI cultures.

In this study, a series of linear PBAEs end-capped with dipeptides instead of amine groups were synthesised. The selected dipeptides, Gly-Sar, Ala-Lys, Ala-Ala, and Ala-Gly were chosen for their role as PEPT2 substrates[715,716,718–720,729,730]. Initial screening on 16HBE cells identified two promising candidates: DD90-Gly-Sar and DD90-Ala-Lys, exhibiting enhanced luminescence compared to other polymers. Notably, the DD90 polymer without end-cap groups was ineffective for cell transfection, consistent with previous studies[654,684].

Further characterisation using DLS revealed that these two top-performing polymers were large, even exceeding the size of unmodified DD90-118 1.2 polymer. This size increase could be attributed to the additional peptide molecular weight or changes in polymer conformation. Interestingly, despite their larger size, subsequent gel retardation and Ribogreen mRNA encapsulation efficiency assays demonstrated their ability to encapsulate mRNA effectively. This finding suggests that peptides as end-cap groups do not impede mRNA complexation, allowing particles to condense mRNA as efficiently as PBAE end-capped with amine groups (DD90-118 1.2).

Zeta potential measurements indicated a neutral charge for the peptide-modified PBAEs. While a neutral charge can lower cellular uptake compared to positively charged polymers, it can also minimise non-specific interactions with cells, potentially reducing toxicity and enhancing biocompatibility. This is supported by studies demonstrating the transfection efficiency of neutral or slightly negatively charged nanoparticles. For example, Segovia *et al.* reported that complexes derived from mixtures of histidine- and either lysine- or arginine-modified PBAEs, despite their large size (>400 nm) and neutral or slightly negative zeta potential, exhibited efficient transfection of COS-7 cells[684]. Similarly, Green *et al.* demonstrated that neutral nanoparticles self-assembled with anionic peptide coats containing targeting ligands effectively transfected human endothelial cells, outperforming the negative control by an order of magnitude[654]. The neutral charge of nanoparticles can be advantageous in certain applications by mitigating non-specific gene delivery and minimising interactions with serum[731].

Gel electrophoresis and Ribogreen assays yielded inconsistent results, with the former suggesting poor mRNA protection by jetPEI and the latter indicating high mRNA encapsulation efficiency. This discrepancy could arise from the varying sensitivities and detection mechanisms of the two assays. Gel electrophoresis may not be as sensitive as the Ribogreen assay in detecting small quantities of mRNA encapsulated within the polymers. Additionally, the Ribogreen assay measures the total amount of mRNA bound to the polymers, but it cannot determine whether the nucleic acid is degraded. It is possible that the jetPEI/mRNA polyplexes were more susceptible to degradation during the gel electrophoresis process, resulting in an underestimation of mRNA protection.

To further characterise these novel peptide-modified PBAEs, additional assays could be conducted. TEM could unveil the morphology and structural features of nanoparticles, providing insights into their internal organisation and how they interact with encapsulated mRNA[732]. Zeta potential measurements at varying pH conditions could further enhance our understanding of the surface charge properties of the nanoparticles and their potential interactions with cell membranes. Gel permeation chromatography could be utilised to characterise the molecular weight of the peptide-modified PBAEs, offering a more comprehensive profile of the molecular weight distribution[733]. Correlation between the structural aspects of the polymers and their functional outcomes, such as mRNA encapsulation efficiency, cellular uptake, and transfection efficiency, is essential for further development of these gene delivery vectors.

The two top-performing peptide-modified PBAEs identified from the 16HBE screening, DD90-Gly-Sar and DD90-Ala-Lys, were employed to transfect primary HBECs. The DD90-Gly-Sar polymer exhibited superior transfection efficiency, as evidenced by enhanced luminescence compared to unmodified PBAE end-capped with amine groups. This improvement highlights the potential benefits of peptide modification over traditional amine end-capping, particularly in enhancing transfection efficiency. To further elucidate the role of peptides in promoting transfection, it was explored whether the presence of free peptides in the media could facilitate improved transfection using non-end-capped polymers. The findings revealed that the presence of free peptides in the media was not sufficient to enhance transfection, suggesting that chemical conjugation of peptides to the polymers is crucial for their transfection-promoting activity. This observation aligns with previous studies that have demonstrated the importance of peptide-polymer conjugation in achieving efficient gene delivery[734].

To assess the efficiency of mRNA uptake and translation facilitated by peptide-modified PBAEs, Cy5-tagged GFP mRNA was utilised. The percentage of Cy5 expression served as an indicator of successful mRNA uptake mediated by both peptide-modified PBAEs and the commercial transfection reagent jetPEI. It has been reported that larger particles (>400 nm in size), such as the peptide-modified PBAEs investigated here, can undergo sedimentation, leading to increased cellular uptake *in vitro* due to their increased local concentration near the cell surface[735]. However, it is crucial to acknowledge that the unmodified DD90-118 1.2 polymer was not included in this comparison, making it challenging to determine whether the enhanced transfection efficiency observed with the peptide-modified PBAE DD90-Gly-Sar can be attributed solely to its PEPT2-mediated cellular uptake.

Following cellular uptake, PBAE/mRNA polyplexes navigate through the cell's acidic compartments, transitioning from early endosomes (pH 6-6.5) to late-stage endosomes (pH 5-5.5), and ultimately reaching lysosomes (pH 4.5-5). For efficient translation, mRNA requires release from endosomes and lysosomes into the cytoplasm, preventing its enzymatic degradation within the endosome. Introducing pH-buffering polymers or functional groups such as peptides can facilitate endosomal escape of polymer/mRNA complexes. The acid dissociation constant (pKa) of the cationic polymer within the pH range of 6.2-6.5 influences nucleic acid transfection efficiency by regulating endosomal escape[736]. Polymers with superior pH buffering capacity can enhance endosomal escape efficiency through the proton sponge effect, as elaborated in Chapter 1. The final step in mRNA delivery process involves the release of mRNA from the polymer and subsequent translation into protein within the cytoplasm.

The observed differences in GFP expression between the peptide-modified PBAEs and jetPEI control suggest distinct modes of endosomal escape or mRNA release by the two transfection methods. It is possible that the peptide-modified PBAEs promote mRNA release more effectively, potentially due to improved endosomal escape. Furthermore, the transfection differences observed between peptide-modified PBAEs are largely attributed to their differences in mRNA translation. This highlights the impact of a single functional group, in this case a terminal peptide, on endosomal escape and mRNA release into the cytoplasm for translation. A limitation of the Cy5-GFP mRNA transfection experiment lies in its reliance on a single primary cell donor, necessitating repeat in a larger cohort of primary cell donors to ensure the reproducibility of the findings.

Overall, mRNA transfection experiments with submerged primary HBECs demonstrated the potential of peptide-modified PBAEs as effective transfection agents for these cells. The DD90-Gly-Sar polymer demonstrated superior transfection efficiency compared to unmodified PBAE and jetPEI. To investigate the underlying mechanism of enhanced transfection efficiency of peptide-modified PBAEs, various strategies were employed to block PEPT2. Cefadroxil, a well-established PEPT2 inhibitor, was utilised to block PEPT2-mediated uptake of peptide-modified PBAEs[721,722]. However, no significant reduction in transfection efficiency was observed, suggesting that PEPT2 blockage alone might not fully account for the enhanced transfection. Competitive binding assays also did not provide conclusive evidence supporting direct competition between the chemically conjugated peptides and the competitive PEPT2 inhibitor (Ala-Lys-AMCA dipeptide). Nevertheless, we cannot exclude the possibility that PEPT2 may still participate in other aspects of the transfection process, particularly given its presence in primary HBECs. Additionally, the neutral charge of peptide-modified PBAEs might facilitate cellular uptake via non-specific endocytosis, potentially contributing to the enhanced transfection efficiency. This hypothesis is supported by previous studies demonstrating that neutrally charged nanoparticles readily enter cells through non-specific endocytosis[737–739]. While the precise mechanism underlying the transfection-enhancing effects of peptide-modified PBAEs remains to be fully elucidated, the current findings suggest that PEPT2 may play a role, but other mechanisms may also contribute to their enhanced transfection efficiency.

This study delved into the potential of peptide-modified PBAE (DD90-Gly-Sar) for mRNA delivery in HBEC ALI cultures. The findings demonstrated that DD90-Gly-Sar outperformed other vectors tested (DD90-118 and jetPEI) in transfection efficiency at both day 7 and 14 HBEC ALI cultures. To the best of my knowledge, this study is the first to demonstrate successful transfection of HBEC ALI cultures with reporter mRNA using peptide-modified PBAEs. Luciferase mRNA was essential for evaluating transfection efficiency; however, it cannot be used to visualise mRNA distribution and its cellular uptake. To overcome this, future studies could benefit from including Cy5-tagged GFP mRNA. This would provide valuable insights into the uptake and translation of mRNA at single-cell level, thereby further clarifying the mechanism behind the improved ALI transfection observed with DD90-Gly-Sar.

During writing of this thesis, a study by Jiang *et al.* was published, which used ALI cultures to deliver LNPs encapsulated with FLuc mRNA for up to two weeks after airlift[391]. Their findings showed a significant decrease in transfection efficiency over time. This decline is likely due to cellular changes such as differentiation, polarisation, and the formation of tight junctions. These changes hinder uptake through the apical surface and limit access to the cell's more endocytically active basolateral side[647,740].

The observed improvement in transfection efficiency with the DD90-Gly-Sar polymer in day 7 and 14 HBEC ALI cultures is likely due to a combination of factors. The chemical conjugation of the Gly-Sar dipeptide as an end-cap group to the PBAE backbone might have strengthened its interaction with PEPT2, facilitating improved cellular uptake. Although there is an observed increase in PEPT2 gene expression in ALI cultured cells, which suggests its involvement in facilitating DD90-Gly-Sar transfection, it is crucial to note that gene expression does not always correlate with protein expression. Therefore, confirming these findings at protein level through methods such as immunofluorescence staining, or Western blot is essential. Immunofluorescence staining would offer direct evidence of PEPT2 protein expression and its subcellular localisation within HBEC ALI cultures.

Additionally, the DD90-Gly-Sar polymer may promote better endosomal escape of the encapsulated mRNA, enabling its release into the cytoplasm for translation. Previous research has shown that incorporating peptides into polymer-based delivery systems can significantly improve endosomal escape, a crucial step in effective nucleic acid delivery. For instance, Dosta *et al.* demonstrated that altering the terminal oligopeptide can fine-tune the pKa of polyplexes while maintaining effective gene silencing[741]. Polyplexes with lysine-bearing oligopeptides formed particles with positive surface charge, whereas polyplexes prepared with arginine-bearing oligopeptides formed particles with negative surface charge. Moreover, Kato *et al.* developed cationic pH-responsive polymers conjugated to an arginine-rich cell-penetrating peptide, forming stable DNA complexes[742]. These modified polyplexes showed superior cellular uptake, efficient intracellular transport, and enhanced endosomal escape compared to unmodified polyplexes. These findings underscore the effectiveness of polymer peptide modifications in overcoming endosomal barriers and enhancing gene transfection efficiency.

5.4 Conclusion

In conclusion, this chapter presents evidence that PBAE modifications influence mRNA transfection efficiency in primary HBECs. Linear PBAE with shorter chain length exhibited superior transfection efficiency compared to its longer chain counterpart, highlighting the crucial role of polymer architecture in transfection efficiency. Furthermore, novel peptide-modified PBAEs (DD90-Gly-Sar and DD90-Ala-Lys) were synthesised and were effective in transfecting submerged primary HBECs. Importantly, this study demonstrated the successful transfection of day 7 and 14 HBEC ALI cultures using DD90-Gly-Sar polymer, suggesting its potential for mRNA delivery to HBEC ALI cultures, which are notoriously challenging to transfect. While further research is required to elucidate the precise mechanism underlying the enhanced transfection efficiency of DD90-Gly-Sar polymer in HBEC ALI cultures, its demonstrated transfection capabilities hold significant promise for mRNA delivery applications.

6 Final discussion

6.1 Synopsis of thesis outcomes

This thesis had 4 overarching aims: 1) Optimising PBAE formulations to establish efficient reporter mRNA transfection of submerged primary HBECs; 2) Evaluating the impact of reporter mRNA transfection on the differentiation and integrity of HBECs cultured at ALI; 3) Investigating the influence of exogenous FOXJ1 mRNA delivery on the differentiation of HBECs cultured at ALI; and 4) Exploring PBAE modifications to enhance mRNA transfection efficiency in HBEC ALI cultures.

Chapter 3 established a robust transfection protocol for submerged primary HBECs using PBAE. This was achieved by formulating PBAE in NaOAc/PBS buffers at 50:1 PBAE to mRNA mass ratio. This formulation resulted in the formation of stable, positively charged polyplexes, smaller than 200 nm in size. These polyplexes significantly enhanced reporter mRNA transfection efficiency in HBECs without affecting their basal cell phenotype. Moreover, this chapter showed that ALI-cultured HBECs resist reporter mRNA transfection. Importantly, transfecting HBECs with reporter mRNA before air exposure was shown to preserve their differentiation and integrity at ALI, validating the utility of this approach for downstream investigations exploring the impact of physiologically relevant mRNA delivery on epithelial differentiation and integrity.

Chapter 4 demonstrated the efficient transfection and translation of exogenous FOXJ1 mRNA in submerged primary HBECs, leading to activation of downstream genes involved in ciliogenesis. FOXJ1 mRNA transfected cells formed a confluent monolayer and were successfully maintained at ALI for 28 days without compromising epithelial integrity or differentiation into a pseudostratified epithelium composed of club, ciliated, and goblet cells. Furthermore, the cilia ultrastructure of FOXJ1 mRNA transfected HBECs was comparable to that of non-transfected controls. These findings demonstrate the potential of mRNA-encoded TF delivery as a powerful tool for manipulating gene expression in a physiologically relevant model while maintaining HBEC differentiation and integrity.

Chapter 5 investigated novel peptide-modified PBAEs to enhance mRNA transfection efficiency in HBECs grown under ALI conditions. Peptide-modified PBAEs (DD90-Gly-Sar, DD90-Ala-Lys) successfully transfected submerged primary HBECs, and the DD90-Gly-Sar polymer enhanced transfection efficiency in both day 7 and 14 HBEC ALI cultures. This success highlights the promising potential of peptide-modified PBAEs for transfecting HBEC ALI cultures.

6.2 Optimised PBAE formulation enables efficient mRNA transfection of submerged primary HBECs

PBAE has emerged as a promising non-viral platform for mRNA delivery due to its biodegradability, ease of synthesis, and ability to encapsulate mRNA for enhanced cellular uptake and endosomal escape[460–462]. Previous studies have demonstrated the efficacy of branched PBAE for effective mRNA delivery to lung epithelium *in vivo*[445,468]. Building upon these findings, this study aimed to optimise branched PBAE formulations for efficient mRNA delivery to primary HBECs.

The optimisation process focused on buffer formulation and PBAE to mRNA mass ratio. Previous studies have demonstrated that this ratio influences the size and charge of the resulting polyplexes, which in turn affect cellular uptake and endosomal escape – crucial steps for efficient gene deliver[471–475,743]. Smaller, positively charged polyplexes are generally considered more favourable for cellular uptake and endosomal escape, leading to enhanced transfection efficiency[478–483,485]. In this study, NaOAc/PBS buffer formulation at PBAE to mRNA mass ratio of 50:1 emerged as the optimal formulation. This formulation resulted in polyplexes with optimal size and charge characteristics, effectively encapsulating mRNA and improving transfection efficiency in submerged primary HBECs. A possible explanation for the superior performance of NaOAc/PBS formulation at 50:1 PBAE to mRNA mass ratio could be attributed to its ability to form well-defined, compact polyplexes with a positive surface charge that facilitates cellular uptake and endosomal escape. While FLuc mRNA transfection served as a valuable indicator of mRNA translation efficiency, it does not fully capture the mRNA delivery process. To fully understand the mechanisms underlying the superior performance of the optimised branched PBAE formulation (NaOAc/PBS 50:1 PBAE to mRNA mass ratio) compared to other formulations tested, future studies should delve deeper into mRNA uptake, translation, and endosomal escape.

The approximate 20% mRNA translation observed following reporter mRNA transfection might be due to factors including the non-physiological nature of the reporter mRNA, such as GFP. Additionally, the size of the mRNA molecule (e.g. GFP vs FOXJ1) could affect its efficiency of uptake or even cause cytotoxicity. Higher transfection efficiency was observed with the physiologically relevant FOXJ1 mRNA, supporting this hypothesis. Furthermore, the study only investigated the effects of a single reporter mRNA dose. Exploring the impact of different mRNA doses could provide valuable insights into maximising transfection efficiency while minimising cytotoxicity. Moreover, the utilisation of HBECs from only two primary cell donors in this study necessitates cautious interpretation of the results. The conclusions drawn are

specific to the transfection conditions and the cellular characteristics of the two donors tested. To enhance the robustness and applicability of the findings, future studies should incorporate a larger set of donors.

6.3 HBEC integrity and differentiation is unaffected following reporter mRNA transfection

ALI cultures of primary HBECs were established to provide a more accurate model of the human airway epithelium compared to submerged cultures. This allowed evaluation of mRNA delivery and its effects on differentiation and barrier integrity in a more physiologically relevant environment. Histological and ultrastructural analyses confirmed the formation of a well-differentiated pseudostratified epithelium with basal, goblet, and ciliated cells. However, reporter mRNA transfection of HBEC ALI cultures proved to be more challenging compared to submerged cultures. This is in line with published data demonstrating epithelial cells grown at ALI develop a robust barrier with established tight junctions and mucin secretion[647–649]. This highlights the need for tailored mRNA delivery strategies specifically designed for HBEC ALI cultures. Establishing and characterising HBEC ALI cultures laid the groundwork for further investigations into the impact of mRNA delivery on HBEC differentiation and barrier integrity, and for exploring PBAE modification to improve mRNA delivery.

While previous research has evaluated the effects of siRNA transfection on the integrity and differentiation of normal HBEC ALI cultures[497], the impact of mRNA delivery on HBEC differentiation and integrity remains relatively unexplored. This thesis sought to address this knowledge gap by investigating the influence of reporter mRNA transfection on HBEC differentiation and integrity in ALI culture. To assess differentiation, the expression of key differentiation markers was analysed at both gene and protein levels. The findings demonstrated that reporter mRNA transfected HBECs maintained their ability to differentiate at ALI, expressing markers such as *MUC5AC*, *MUC5B*, *SCGBA1*, and *FOXJ1* at levels comparable to non-transfected cells. This finding suggests that mRNA transfection does not compromise HBEC differentiation at ALI.

The integrity of the epithelial barrier is crucial for airway function, as it protects against pathogen invasion and maintains homeostasis. To assess the impact of reporter mRNA transfection on epithelial barrier integrity, epithelial barrier resistance, permeability, and the expression of epithelial integrity markers at both gene and protein levels were evaluated. The findings revealed that reporter mRNA transfection did not compromise epithelial barrier integrity of HBECs cultured at ALI. Neither epithelial barrier resistance nor permeability were altered in mRNA transfected cells compared to controls, and the expression of tight junction

and adherens junction markers remained unaffected. Collectively, these findings indicate that mRNA transfection does not compromise the barrier integrity of the bronchial epithelium.

To the best of my knowledge, the work presented in this thesis represents the first demonstration that reporter mRNA transfection does not hinder HBEC differentiation or epithelial integrity in ALI cultures. This finding provides a robust platform for investigating the effects of mRNA delivery on the function of airway epithelium. Moreover, the optimised mRNA transfection method established in this study holds promise as a tool for exploring modulators of differentiation and function. Importantly, the successful culture of reporter mRNA transfected HBECs at ALI establishes a foundation for future investigations using more physiologically relevant mRNA, such as FOXJ1, to delve deeper into HBEC differentiation.

6.4 mRNA-mediated FOXJ1 protein expression in HBECs induces the expression of downstream genes involved in ciliogenesis

Having confirmed that the mRNA transfection method described in section 6.3 does not compromise HBEC differentiation or integrity at ALI, I sought to investigate the potential of delivering FOXJ1 mRNA to modulate ciliogenesis in HBECs. FOXJ1, a master regulator of ciliogenesis, orchestrates the expression of numerous genes critical for ciliated cell differentiation[585,586]. Manipulating FOXJ1 expression has emerged as a promising approach for deciphering the mechanisms of ciliogenesis and exploring its therapeutic potential[165,215,532,582,583,588,589,744]. However, existing methods, such as viral delivery of plasmid DNA and gene editing, raise concerns about immunogenicity and safety. Studies have shown that FOXJ1 overexpression can stimulate the expression of ciliogenesis-related genes, leading to enhanced cilia growth[215,589]. Conversely, downregulating FOXJ1 suppresses ciliogenesis[744,745]. Additionally, FOXJ1 mutations have been implicated in ciliopathies[159,162,746–748]. Collectively, these findings highlight the critical role of FOXJ1 in cilia formation and function. Despite the expanding knowledge on FOXJ1's function, a gap remained in understanding the impact of manipulating FOXJ1 expression on HBEC differentiation at ALI. This study aimed to address this gap by exploring the influence of mRNA encoded FOXJ1 delivery on the differentiation of HBECs at ALI.

To assess the effectiveness of non-viral delivery of mRNA encoded FOXJ1, I first evaluated transfection efficiency and localisation of the translated protein in submerged primary HBECs. Both the optimised branched PBAE formulation and the commercial transfection reagent JetMessenger successfully delivered FOXJ1 mRNA into submerged HBECs, resulting in its translation and nuclear localisation. Interestingly, FOXJ1 mRNA out-performed Cy5-tagged GFP mRNA transfection discussed in section 6.2. This likely reflects the physiological

relevance of FOXJ1, as HBECs naturally express FOXJ1, while they do not express GFP. Moreover, gene expression analysis revealed that FOXJ1 mRNA transfection induced the expression of FOXJ1 downstream genes involved in ciliogenesis including, *CETN2*, *DNAH11*, *DNALI1*, *RFX3*, *RFX2*, *TUBA1A*, *RSPH9*, *DYN2H1*, *IFT172*. These findings align with previous research demonstrating that plasmid-mediated FOXJ1 overexpression in basal cells induced cilia-associated genes[589]. Additionally, branched PBAE demonstrated superior FOXJ1 transfection efficiency and downstream gene expression changes compared to JetMessenger, making it the preferred choice for further experiments.

While cytotoxicity data suggests that FOXJ1 mRNA transfection is well-tolerated by HBECs, further investigation into potential inflammatory responses is crucial. Measuring the release of pro-inflammatory mediators, such as IL-6 and IL-8, from HBECs following FOXJ1 mRNA transfection would be valuable[749].

This study also provides valuable insights into the relationship between transfection efficiency and functional outcomes. Although approximately 50% FOXJ1 transfection efficiency with branched PBAE was sufficient to activate downstream ciliogenesis-related genes, this level might not be sufficient for other applications. Therefore, determining the optimal transfection efficiency for each specific application is essential, considering factors like the target gene, desired biological response, and cell type.

6.5 FOXJ1 mRNA transfection maintains integrity, differentiation, and cilia ultrastructure of HBEC ALI cultures

Following successful FOXJ1 mRNA delivery in submerged HBECs, its impact on ALI differentiation was investigated. This study represents the first successful manipulation of FOXJ1 expression in HBECs at ALI through mRNA transfection. FOXJ1 mRNA transfected HBECs were able to form a confluent monolayer and were maintained at ALI for 28 days. Before air lift, gene expression analysis confirmed upregulation of FOXJ1 downstream genes involved in ciliogenesis, which are typically upregulated during ALI differentiation. Importantly, expression patterns of basal, club, goblet, and ciliated cell markers, as well as their proportions, remained unchanged compared to non-transfected controls. These findings suggest that while FOXJ1 mRNA transfection induces the expression of ciliogenesis genes prior to air exposure, it does not alter the overall differentiation trajectory of HBECs during ALI.

Histological analysis revealed no differences in epithelial layer morphology or thickness between FOXJ1 mRNA transfected and non-transfected HBECs. Epithelial integrity, assessed by both epithelial integrity marker expression and TEM analysis, remained intact following FOXJ1 mRNA transfection. This demonstrates that FOXJ1 mRNA transfection does not compromise the epithelial integrity of HBECs at ALI, vital for airway barrier function against inhaled pathogens and environmental irritants.

While initial examinations indicate healthy cilia formation and morphology in FOXJ1 mRNA transfected HBECs, further investigation is needed to understand the full functional impact. Histological and ultrastructural analyses revealed well-formed cilia with normal ultrastructure, suggesting no adverse effects on cilia. However, these methods do not directly assess ciliary function, which is crucial for mucociliary clearance. Future studies should incorporate functional assays to evaluate the consequences of FOXJ1 mRNA delivery on HBEC function. Ciliary beat frequency measurements would directly assess ciliary movement[750]. Mucus transport assays and clearance of fluorescently labelled particles would provide insights into mucociliary clearance capabilities[751]. Additionally, quantifying MUC5AC, a key gel-forming mucin, using MUC5AC ELISA would provide valuable insights into the effects of FOXJ1 mRNA transfection on mucus production[752].

While this study focused on specific genes involved in ciliogenesis, delving deeper into the transcriptomic landscape of FOXJ1 mRNA transfected HBECs can provide valuable insights. Employing comprehensive approaches such as RNA-seq and single-cell RNA-seq would provide a broader picture of gene expression changes following transfection[753,754]. These methods offer a broader perspective on gene expression patterns following FOXJ1 mRNA transfection, potentially revealing novel signalling pathways and regulatory mechanisms. Furthermore, they enable the identification of differentially expressed genes between distinct HBEC populations, facilitating a deeper understanding of gene regulation in HBEC differentiation and the identification of targets regulated by FOXJ1.

To understand the long-term effects of FOXJ1 on HBEC differentiation and integrity, repeatedly delivering FOXJ1 mRNA to ALI-cultured HBECs could be insightful. Bartman *et al.* demonstrated the efficacy of repeated siRNA transfections in modulating cellular processes, with transfections performed every three days over a three-week period in normal HBEC ALI cultures[497]. Similarly, delivery of FOXJ1 mRNA at regular intervals to achieve a sustained increase in its expression could be investigated. However, maintaining a balance between transfection efficiency and cell viability is crucial. Repeated transfections may increase the risk of off-target effects and cytotoxicity. Therefore, future studies should carefully determine the

optimal frequency and duration of FOXJ1 mRNA transfections to achieve the desired outcomes without compromising cellular health.

FOXJ1 has emerged as a potential player in cancer biology[755]. However, its role in cancer malignancy remains elusive and controversial, with studies reporting both FOXJ1 overexpression and downregulation across diverse cancer types. For instance, FOXJ1 is overexpressed in hepatocellular carcinoma[756], clear-cell renal cell carcinoma[757], colorectal cancer[758], and bladder cancer[759]. Conversely, FOXJ1 is reduced in gastric cancer[760], ovarian cancer[761], and aggressive ependymoma[762]. The influence of FOXJ1 on cilia and their associated signalling pathways may impact cellular processes crucial that underpin cancer development, such as cell proliferation and migration. However, the underlying mechanisms by which FOXJ1 contributes to oncogenesis remain elusive. Building upon the findings of this study, which successfully induced FOXJ1 downstream ciliogenenic targets through FOXJ1 mRNA transfection without compromising HBEC differentiation and integrity at ALI, future research could aim to manipulate FOXJ1 expression and assess its impact on established oncogenes. This exploration could provide valuable insights into FOXJ1's role in cancer. Additionally, a comprehensive analysis of FOXJ1-induced transcriptomic changes could identify oncogenic pathways that may be inadvertently activated or suppressed by FOXJ1 manipulation.

This study highlights FOXJ1 mRNA transfection as a versatile tool for exploring HBEC differentiation. While further research is essential to fully evaluate its capabilities and address potential limitations, the findings presented in this thesis provide a foundation for future investigations. Future studies, enriched with additional assays, methodologies, and robust statistical analyses, will further elucidate the effects of FOXJ1 mRNA transfection on HBEC function.

6.6 Novel peptide-modified PBAE, DD90-Gly-Sar, enhances reporter mRNA transfection of HBEC ALI cultures

Modifying the terminal groups of PBAEs has proven to be an effective method for improving transfection efficiency[467,681]. Specifically, incorporating oligopeptides as end-cap groups has enhanced their performance in terms of transfection efficiency, target specificity, and biocompatibility[677,684,687,688]. However, the efficacy of peptide-modified PBAEs remains unexplored in the context of transfecting primary HBECs. This thesis investigated the potential of peptide-modified PBAEs to enhance mRNA transfection of HBEC ALI cultures. The strategy of replacing conventional amine terminal groups with dipeptides as end-capping agents was explored. This investigation led to the identification of two promising candidates, DD90-Gly-

Sar and DD90-Ala-Lys, exhibiting superior transfection efficiency in submerged primary HBECs. While these candidates demonstrated effective mRNA encapsulation, limitations such as large size, neutral charge, and instability were observed. These findings highlight the need for further optimisation of particle design to improve their physicochemical properties while maintaining their advantageous transfection efficiency.

Incorporating PEG-lipids into the design of peptide-modified PBAEs presents a promising approach to address their limitations. PEG-lipids, which composed of a hydrophilic PEG moiety and a hydrophobic lipid moiety, offer a powerful tool for modifying the surface properties of nanoparticles and improving their stability763,764. PEG-lipids can create a steric barrier around the nanoparticle. This protective shield minimises protein adsorption and aggregation, consequently enhancing the stability of nanoparticles. Consequently, incorporating PEG-lipids into peptide-modified PBAEs has the potential to improve their physicochemical properties. Further research into the incorporation of PEG-lipids and their impact on the physicochemical properties of these nanoparticles is crucial for optimising their performance as delivery systems.

The DD90-Gly-Sar polymer was effective in delivering mRNA to HBEC ALI cultures. Unlike unmodified PBAE and the commercial transfection reagent jetPEI, which did not achieve transfection, DD90-Gly-Sar successfully transfected these cells, both at day 7 and 14 post-ALI. To get a complete picture of DD90-Gly-Sar's performance, extending the assessment beyond day 14 to days 21 and 28 post-ALI would be valuable. While FLuc mRNA served as an effective reporter gene for assessing transfection efficiency, future experiments could benefit from using Cy5-tagged GFP mRNA. Employing Cy5-tagged GFP mRNA would allow direct visualisation of mRNA localisation and cellular tropism within the HBEC ALI cultures, distinguishing between basal, goblet, and ciliated cells. This would elucidate whether peptide-modified PBAEs exhibit specific cellular uptake preferences, which could have implications for developing targeted mRNA delivery strategies to specific cell types within the bronchial epithelium.

The observed upregulation of PEPT2 gene expression in HBEC ALI cultures compared to submerged cells suggests that this transporter may play a role in the enhanced transfection efficiency of peptide-modified PBAEs. However, the precise mechanism by which the DD90-Gly-Sar polymer leads to superior transfection efficiency in HBEC ALI cultures remains unclear. To unravel the mechanisms underlying the superior transfection efficiency of DD90-Gly-Sar, future studies should explore whether this polymer facilitates efficient endosomal escape, potentially contributing to its enhanced ability to deliver mRNA into HBEC ALI cultures. One approach could involve examining the colocalization of mRNA with endosomal

markers to determine the extent of endosomal entrapment after DD90-Gly-Sar-mediated mRNA transfection[765]. Alternatively, fluorescence microscopy could be used to visualise the morphology and dynamics of endosomes following DD90-Gly-Sar transfection, providing insights into its influence on their maturation process[766]. Furthermore, exploring alternative uptake pathways, such as macropinocytosis and clathrin or caveolin-mediated endocytosis could shed light on the cellular dynamics of peptide-modified PBAE uptake[484,767]. Employing inhibitors specific to these pathways, such as amiloride and chlorpromazine, respectively, could elucidate their potential contribution to DD90-Gly-Sar-mediated mRNA delivery[768].

This study has significantly enhanced mRNA transfection efficiency in HBEC ALI cultures by employing a novel peptide-modified PBAE, DD90-Gly-Sar. While certain limitations remain, and future research is necessary, DD90-Gly-Sar polymer emerges as a promising candidate for mRNA delivery applications.

6.7 Future directions

The findings of this thesis highlight the potential of mRNA encoded TFs as powerful tools for manipulating cellular processes, opening a promising avenue for investigating the role of FOXJ1 and other TFs in HBEC differentiation and ciliogenesis. To enhance the robustness of the findings and address variability, future studies should incorporate a larger cohort of primary cell donors. This expanded sample size would enable a more comprehensive understanding of the effects of FOXJ1 mRNA transfection across a broader population. Additionally, employing power analysis will ensure future studies have sufficient statistical power to detect meaningful differences between groups, enhancing the reliability of the results[769].

This thesis provides evidence that FOXJ1 mRNA transfection induces the expression of FOXJ1 downstream genes in HBECs without compromising their overall differentiation and integrity at ALI. This opens exciting possibilities for using this approach as a versatile tool in various research settings. It could be invaluable for studying *in vitro* differentiation, investigating gene functions, and modelling diseases. While the therapeutic application of FOXJ1 mRNA delivery was beyond the scope of this study, it holds promise for future research, particularly in contexts that more closely resemble disease conditions. For instance, IL-13 stimulated HBECs show decreased FOXJ1 expression and fewer ciliated cells[184,770]. Investigating whether FOXJ1 mRNA delivery can reverse these effects and restore optimal HBEC differentiation and function presents a compelling avenue for further research. Additionally, exploring the impact of FOXJ1 mRNA delivery on HBEC differentiation at ALI, both prophylactically prior to IL-13 stimulation and therapeutically following stimulation, offers another interesting area for future exploration.

To fully assess the potential of novel DD90-Gly-Sar peptide-modified PBAE as a delivery vehicle for physiologically relevant mRNA, future research should characterise its transfection efficiency of FOXJ1 mRNA in HBEC ALI cultures. Building upon the two key findings of this thesis, evaluating the ability of DD90-Gly-Sar polymer to effectively deliver FOXJ1 mRNA and induce the expression of FOXJ1 downstream genes would provide valuable insights into its potential as a tool for modulating differentiation pathways within the ALI system. The demonstrated efficacy of DD90-Gly-Sar in transfecting both day 7 and 14 post-ALI cultures offer a unique opportunity to dissect the temporal dynamics of FOXJ1's contribution to the differentiation process.

6.8 Concluding remarks

The work presented in this thesis provides evidence supporting the efficacy of PBAEs as efficient mRNA delivery vehicles for primary HBECs. Optimising the vector formulation, including buffer and PBAE to mRNA mass ratio, significantly improved polyplex physicochemical properties and transfection efficiency. Notably, HBECs transfected with reporter mRNA were maintained at ALI culture without any adverse effects on their differentiation or epithelial integrity. Additionally, transfection of HBECs with FOXJ1 mRNA induced the expression of downstream genes involved in ciliogenesis. Importantly, FOXJ1 mRNA transfected cells cultured at ALI exhibited normal differentiation, epithelial integrity, and cilia ultrastructure, closely resembling non-transfected controls. These findings highlight the potential of TF-encoded mRNA as a platform technology for modulating HBEC differentiation in ALI, opening new avenues for investigating the function of genes implicated in airway diseases and exploring potential therapeutic interventions. The introduction of novel peptide-modified PBAEs, particularly DD90-Gly-Sar, enhanced mRNA transfection efficiency in HBEC ALI cultures.

In conclusion, this thesis significantly contributes to the evolving field of mRNA technology by establishing PBAEs as a robust and efficient delivery platform for mRNA-encoded TFs to HBECs. This approach enables precise modulation of gene expression while preserving HBEC differentiation and integrity in ALI. Overall, this research provides a powerful tool for manipulating gene expression dynamics and regulating HBEC differentiation, paving the way for novel therapeutic interventions and a deeper understanding of lung biology.

7 References

1. Ross, A. J., Dailey, L. A., Brighton, L. E. & Devlin, R. B. Transcriptional Profiling of Mucociliary Differentiation in Human Airway Epithelial Cells. *https://doi.org/10.1165/rcmb.2006-0466OC* **37**, 169–185 (2012).

2. Parker, D. & Prince, A. Innate Immunity in the Respiratory Epithelium. *Am J Respir Cell Mol Biol* **45**, 189 (2011).

3. Vareille, M., Kieninger, E., Edwards, M. R. & Regamey, N. The Airway Epithelium: Soldier in the Fight against Respiratory Viruses. *Clin Microbiol Rev* **24**, 210 (2011).

4. Gao, N. & Rezaee, F. Airway Epithelial Cell Junctions as Targets for Pathogens and Antimicrobial Therapy. *Pharmaceutics* **14**, (2022).

5. Brune, K., Frank, J., Schwingshackl, A., Finigan, J. & Sidhaye, V. K. Pulmonary epithelial barrier function: some new players and mechanisms. *Am J Physiol Lung Cell Mol Physiol* **308**, L731–L745 (2015).

6. Roche, W. R., Montefort, S., Baker, J. & Holgate, S. T. Cell adhesion molecules and the bronchial epithelium. *Am Rev Respir Dis* **148**, (1993).

7. Schneider, C., O'Leary, C. E. & Locksley, R. M. Regulation of immune responses by tuft cells. *Nat Rev Immunol* **19**, 584–593 (2019).

8. Sha, Q., Truong-Tran, A. Q., Plitt, J. R., Beck, L. A. & Schleimer, R. P. Activation of airway epithelial cells by toll-like receptor agonists. *Am J Respir Cell Mol Biol* **31**, 358–364 (2004).

9. Muir, A. *et al.* Toll-like receptors in normal and cystic fibrosis airway epithelial cells. *Am J Respir Cell Mol Biol* **30**, 777–783 (2004).

10. Lehmann, R. *et al.* Differential regulation of the transcriptomic and secretomic landscape of sensor and effector functions of human airway epithelial cells. *Mucosal Immunology 2018 11:3* **11**, 627–642 (2018).

11. Rehwinkel, J. & Reis E Sousa, C. RIGorous Detection: Exposing Virus Through RNA Sensing. *Science (1979)* **327**, 284–286 (2010).

12. Kato, H. *et al.* Differential roles of MDA5 and RIG-I helicases in the recognition of RNA viruses. *Nature* **441**, 101–105 (2006).

13. Gern, J. E., Vrtis, R., Grindle, K. A., Swenson, C. & Busse, W. W. Relationship of upper and lower airway cytokines to outcome of experimental rhinovirus infection. *Am J Respir Crit Care Med* **162**, 2226–2231 (2000).

14. McNamara, P. S., Flanagan, B. F., Hart, C. A. & Smyth, R. L. Production of chemokines in the lungs of infants with severe respiratory syncytial virus bronchiolitis. *J Infect Dis* **191**, 1225–1232 (2005).

15. McNamara, P. S., Flanagan, B. F., Selby, A. M., Hart, C. A. & Smyth, R. L. Pro- and anti-inflammatory responses in respiratory syncytial virus bronchiolitis. *Eur Respir J* **23**, 106–112 (2004).

16. Message, S. D. & Johnston, S. L. Host defense function of the airway epithelium in health and disease: clinical background. *J Leukoc Biol* **75**, 5–17 (2004).

17. Wark, P. A. B. *et al.* Asthmatic bronchial epithelial cells have a deficient innate immune response to infection with rhinovirus. *J Exp Med* **201**, 937–947 (2005).

18. Sano, H., Nagai, K., Tsutsumi, H. & Kuroki, Y. Lactoferrin and surfactant protein A exhibit distinct binding specificity to F protein and differently modulate respiratory syncytial virus infection. *Eur J Immunol* **33**, 2894–2902 (2003).

19. McCray, P. B. & Bentley, L. Human airway epithelia express a beta-defensin. *Am J Respir Cell Mol Biol* **16**, 343–349 (1997).

20. Van Der Vliet, A., Eiserich, J. P. & Cross, C. E. Nitric oxide: a pro-inflammatory mediator in lung disease? *Respir Res* **1**, 67 (2000).

21. Norden, C. Pseudostratified epithelia - cell biology, diversity and roles in organ formation at a glance. *J Cell Sci* **130**, 1859–1863 (2017).

22. Rock, J. R. *et al.* Basal cells as stem cells of the mouse trachea and human airway epithelium. *Proc Natl Acad Sci U S A* **106**, 12771–12775 (2009).

23. Rock, J. R. *et al.* Notch-Dependent Differentiation of Adult Airway Basal Stem Cells. *Cell Stem Cell* **8**, 639–648 (2011).

24. Tadokoro, T., Gao, X., Hong, C. C., Hotten, D. & Hogan, B. L. M. BMP signaling and cellular dynamics during regeneration of airway epithelium from basal progenitors. *Development (Cambridge)* **143**, 764–773 (2016).

25. Crystal, R. G. Airway basal cells: The 'smoking gun' of chronic obstructive pulmonary disease. *Am J Respir Crit Care Med* **190**, 1355–1362 (2014).

26. Iwasaki, A., Foxman, E. F. & Molony, R. D. Early local immune defences in the respiratory tract. *Nature Reviews Immunology 2016 17:1* **17**, 7–20 (2016).

27. Danopoulos, S., Shiosaki, J. & Al Alam, D. FGF signaling in lung development and disease: Human versus mouse. *Front Genet* **10**, 444859 (2019).

28. Rock, J. R., Randell, S. H. & Hogan, B. L. M. Airway basal stem cells: a perspective on their roles in epithelial homeostasis and remodeling. *Dis Model Mech* **3**, 545 (2010).

29. Boers, J. E., Ambergen, A. W. & Thunnissen, F. B. J. M. Number and Proliferation of Basal and Parabasal Cells in Normal Human Airway Epithelium. *Am J Respir Crit Care Med* **157**, 2000–2006 (2000).

30. Rock, J. R. *et al.* Basal cells as stem cells of the mouse trachea and human airway epithelium. *Proc Natl Acad Sci U S A* **106**, 12771–12775 (2009).

31. Hegab, A. E., Nickerson, D. W., Ha, V. L., Darmawan, D. O. & Gomperts, B. N. Repair and regeneration of tracheal surface epithelium and submucosal glands in a mouse model of hypoxic-ischemic injury. *Respirology* **17**, 1101–1113 (2012).

32. Montoro, D. T. *et al.* A revised airway epithelial hierarchy includes CFTR-expressing ionocytes. *Nature* **560**, 319 (2018).

33. Hong, K. U., Reynolds, S. D., Watkins, S., Fuchs, E. & Stripp, B. R. In vivo differentiation potential of tracheal basal cells: evidence for multipotent and unipotent subpopulations. *Am J Physiol Lung Cell Mol Physiol* **286**, (2004).

34. Rock, J. R. *et al.* Basal cells as stem cells of the mouse trachea and human airway epithelium.

35. Hajj, R. *et al.* Basal cells of the human adult airway surface epithelium retain transit-amplifying cell properties. *Stem Cells* **25**, 139–148 (2007).

36. Travaglini, K. J. *et al.* A molecular cell atlas of the human lung from single cell RNA sequencing. *Nature* **587**, 619 (2020).

37. Watson, J. K. *et al.* Clonal Dynamics Reveal Two Distinct Populations of Basal Cells in Slow-Turnover Airway Epithelium. *Cell Rep* **12**, 90–101 (2015).

38. Boers, J. E., Ambergen, A. W. & Thunnissen, F. B. J. M. Number and Proliferation of Clara Cells in Normal Human Airway Epithelium. *https://doi.org/10.1164/ajrccm.159.5.9806044* **159**, 1585–1591 (2012).

39. Boers, J. E., Ambergen, A. W. & Thunnissen, F. B. J. M. Number and proliferation of clara cells in normal human airway epithelium. *Am J Respir Crit Care Med* **159**, 1585–1591 (1999).

40. Xing, Y. *et al.* Signaling via Alk5 controls the ontogeny of lung Clara cells. *Development* **137**, 825–833 (2010).

41. Hong, K. U., Reynolds, S. D., Giangreco, A., Hurley, C. M. & Stripp, B. R. Clara cell secretory protein-expressing cells of the airway neuroepithelial body microenvironment include a label-retaining subset and are critical for epithelial renewal after progenitor cell depletion. *Am J Respir Cell Mol Biol* **24**, 671–681 (2001).

42. Basil, M. C. *et al.* The Cellular and Physiological Basis for Lung Repair and Regeneration: Past, Present, and Future. *Cell Stem Cell* **26**, 482–502 (2020).

43. Tata, P. R. *et al.* Dedifferentiation of committed epithelial cells into stem cells in vivo. *Nature* **503**, 218–223 (2013).

44. Rawlins, E. L. *et al.* The role of Scgb1a1+ Clara cells in the long-term maintenance and repair of lung airway, but not alveolar, epithelium. *Cell Stem Cell* **4**, 525–534 (2009).

45. Guo, M. *et al.* Single cell RNA analysis identifies cellular heterogeneity and adaptive responses of the lung at birth. *Nature Communications 2019 10:1* **10**, 1–16 (2019).

46. Saglani, S. *et al.* Update in Asthma 2019. *Am J Respir Crit Care Med* **202**, 184–192 (2020).

47. Bustamante-Marin, X. M. & Ostrowski, L. E. Cilia and Mucociliary Clearance. *Cold Spring Harb Perspect Biol* **9**, (2017).

48. Whitsett, J. A. Airway epithelial differentiation and mucociliary clearance. *Ann Am Thorac Soc* **15**, S143–S148 (2018).

49. Morimoto, M., Nishinakamura, R., Saga, Y. & Kopan, R. Different assemblies of Notch receptors coordinate the distribution of the major bronchial Clara, ciliated and neuroendocrine cells. *Development (Cambridge)* **139**, 4365–4373 (2012).

50. Siebel, C. & Lendahl, U. Notch Signaling in Development, Tissue Homeostasis, and Disease. *Physiol Rev* **97**, 1235–1294 (2017).

51. Stubbs, J. L., Vladar, E. K., Axelrod, J. D. & Kintner, C. Multicilin promotes centriole assembly and ciliogenesis during multiciliate cell differentiation. *Nat Cell Biol* **14**, 140 (2012).

52. Morimoto, M. *et al.* Canonical Notch signaling in the developing lung is required for determination of arterial smooth muscle cells and selection of Clara versus ciliated cell fate. *J Cell Sci* **123**, 213–224 (2010).

53. Rock, J. R. *et al.* Notch-dependent differentiation of adult airway basal stem cells. *Cell Stem Cell* **8**, 639 (2011).

54. You, Y. *et al.* Role of f-box factor foxj1 in differentiation of ciliated airway epithelial cells. *Am J Physiol Lung Cell Mol Physiol* **286**, 650–657 (2004).

55. Rajavelu, P. *et al.* Airway epithelial SPDEF integrates goblet cell differentiation and pulmonary Th2 inflammation. *J Clin Invest* **125**, 2021 (2015).

56. Goldfarbmuren, K. C. *et al.* Dissecting the cellular specificity of smoking effects and reconstructing lineages in the human airway epithelium. *Nat Commun* **11**, (2020).

57. Deprez, M. *et al.* A Single-Cell Atlas of the Human Healthy Airways. *Am J Respir Crit Care Med* **202**, 1636–1645 (2020).

58. Hollenhorst, M. I. *et al.* Tracheal brush cells release acetylcholine in response to bitter tastants for paracrine and autocrine signaling. *FASEB J* **34**, 316–332 (2020).

59. O'Leary, C. E., Schneider, C. & Locksley, R. M. Tuft Cells-Systemically Dispersed Sensory Epithelia Integrating Immune and Neural Circuitry. *Annu Rev Immunol* **37**, 47–72 (2019).

60. Von Moltke, J., Ji, M., Liang, H. E. & Locksley, R. M. Tuft-cell-derived IL-25 regulates an intestinal ILC2–epithelial response circuit. *Nature 2015 529:7585* **529**, 221–225 (2015).

61. Lei, L. *et al.* CFTR-rich ionocytes mediate chloride absorption across airway epithelia. *J Clin Invest* **133**, (2023).

62. Montoro, D. T. *et al.* A revised airway epithelial hierarchy includes CFTR-expressing ionocytes. *Nature* **560**, 319–324 (2018).

63. Sui, P. *et al.* Pulmonary neuroendocrine cells amplify allergic asthma responses. *Science* **360**, (2018).

64. Branchfield, K. *et al.* Pulmonary neuroendocrine cells function as airway sensors to control lung immune response. *Science* **351**, 707–710 (2016).

65. Noguchi, M., Furukawa, K. T. & Morimoto, M. Pulmonary neuroendocrine cells: physiology, tissue homeostasis and disease. *Dis Model Mech* **13**, (2020).

66. Shimura, S., Andoh, Y., Haraguchi, M. & Shirato, K. Continuity of airway goblet cells and intraluminal mucus in the airways of patients with bronchial asthma. *Eur Respir J* **9**, 1395–1401 (1996).

67. Ordoñez, C. L. *et al.* Mild and moderate asthma is associated with airway goblet cell hyperplasia and abnormalities in mucin gene expression. *Am J Respir Crit Care Med* **163**, 517–523 (2001).

68. Jeffery, P. K., Wardlaw, A. J., Nelson, F. C., Collins, J. V. & Kay, A. B. Bronchial biopsies in asthma. An ultrastructural, quantitative study and correlation with hyperreactivity. *Am Rev Respir Dis* **140**, 1745–1753 (1989).

69. Wilson, J. W. & Li, X. The measurement of reticular basement membrane and submucosal collagen in the asthmatic airway. *Clinical & Experimental Allergy* **27**, 363–371 (1997).

70. Papi, A., Brightling, C., Pedersen, S. E. & Reddel, H. K. Asthma. *The Lancet* **391**, 783–800 (2018).

71. Hammad, H. & Lambrecht, B. N. The basic immunology of asthma. *Cell* **184**, 1469–1485 (2021).

72. Li, Y. *et al.* Elevated Expression of IL-33 and TSLP in the Airways of Human Asthmatics In Vivo: A Potential Biomarker of Severe Refractory Disease. *J Immunol* **200**, 2253–2262 (2018).

73. Holgate, S. T. *et al.* A new look at the pathogenesis of asthma. *Clin Sci (Lond)* **118**, 439–450 (2009).

74. Xiao, C. *et al.* Defective epithelial barrier function in asthma. *Journal of Allergy and Clinical Immunology* **128**, 549-556.e12 (2011).

75. De Boer, W. I. *et al.* Altered expression of epithelial junctional proteins in atopic asthma: possible role in inflammation. *Can J Physiol Pharmacol* **86**, 105–112 (2008).

76. Chronic obstructive pulmonary disease (COPD). https://www.who.int/news-room/fact-sheets/detail/chronic-obstructive-pulmonary-disease-(copd).

77. Vogelmeier, C. F. *et al.* Global Strategy for the Diagnosis, Management, and Prevention of Chronic Obstructive Lung Disease 2017 Report. GOLD Executive Summary. *Am J Respir Crit Care Med* **195**, 557–582 (2017).

78. Salvi, S. S. & Barnes, P. J. Chronic obstructive pulmonary disease in non-smokers. *Lancet* **374**, 733–743 (2009).

79. Auerbach, O., Stout, A. P., Hammond, E. C. & Garfinkel, L. Changes in bronchial epithelium in relation to cigarette smoking and in relation to lung cancer. *N Engl J Med* **265**, 253–267 (1961).

80. Staudt, M. R. *et al.* Airway basal stem/progenitor cells have diminished capacity to regenerate airway epithelium in chronic obstructive pulmonary disease. *Am J Respir Crit Care Med* **190**, 955–958 (2014).

81. Crystal, R. G. Airway basal cells: The 'smoking gun' of chronic obstructive pulmonary disease. *Am J Respir Crit Care Med* **190**, 1355–1362 (2014).

82. Ghosh, M. *et al.* Exhaustion of airway basal progenitor cells in early and established chronic obstructive pulmonary disease. *Am J Respir Crit Care Med* **197**, 885–896 (2018).

83. Hackett, N. R. *et al.* The Human Airway Epithelial Basal Cell Transcriptome. *PLoS One* **6**, e18378 (2011).

84. Kim, V. *et al.* Small airway mucous metaplasia and inflammation in chronic obstructive pulmonary disease. *COPD* **5**, 329–338 (2008).

85. Gohy, S. *et al.* Altered generation of ciliated cells in chronic obstructive pulmonary disease. *Sci Rep* **9**, (2019).

86. Jeffery, P. K. Comparison of the structural and inflammatory features of COPD and asthma. Giles F. Filley Lecture. *Chest* **117**, 251S-260S (2000).

87. Gohy, S. *et al.* Altered generation of ciliated cells in chronic obstructive pulmonary disease. *Sci Rep* **9**, (2019).

88. Barnes, P. J. Inflammatory mechanisms in patients with chronic obstructive pulmonary disease. *J Allergy Clin Immunol* **138**, 16–27 (2016).

89. Gao, W. *et al.* Bronchial epithelial cells: The key effector cells in the pathogenesis of chronic obstructive pulmonary disease? *Respirology* **20**, 722–729 (2015).

90. Kuschner, W. G., D'Alessandro, A., Wong, H. & Blanc, P. D. Dose-dependent cigarette smoking-related inflammatory responses in healthy adults. *Eur Respir J* **9**, 1989–1994 (1996).

91. Keatings, V. M., Collins, P. D., Scott, D. M. & Barnes, P. J. Differences in interleukin-8 and tumor necrosis factor-alpha in induced sputum from patients with chronic obstructive pulmonary disease or asthma. *Am J Respir Crit Care Med* **153**, 530–534 (1996).

92. Wedzicha, J. A. *et al.* Acute exacerbations of chronic obstructive pulmonary disease are accompanied by elevations of plasma fibrinogen and serum IL-6 levels. *Thromb Haemost* **84**, 210–215 (2000).

93. Heijink, I. H., Noordhoek, J. A., Timens, W., Van Oosterhout, A. J. M. & Postma, D. S. Abnormalities in airway epithelial junction formation in chronic obstructive pulmonary disease. *Am J Respir Crit Care Med* **189**, 1439–1442 (2014).

94. Oldenburger, A. *et al.* A-kinase anchoring proteins contribute to loss of E-cadherin and bronchial epithelial barrier by cigarette smoke. *Am J Physiol Cell Physiol* **306**, (2014).

95. Henke, M. O., Renner, A., Huber, R. M., Seeds, M. C. & Rubin, B. K. MUC5AC and MUC5B Mucins Are Decreased in Cystic Fibrosis Airway Secretions. *Am J Respir Cell Mol Biol* **31**, 86–91 (2004).

96. Ratjen, F. *et al.* Cystic fibrosis. *Nat Rev Dis Primers* **1**, (2015).

97. Lee, T. W. R., Brownlee, K. G., Conway, S. P., Denton, M. & Littlewood, J. M. Evaluation of a new definition for chronic Pseudomonas aeruginosa infection in cystic fibrosis patients. *Journal of Cystic Fibrosis* **2**, 29–34 (2003).

98. Shah, V. S. *et al.* Airway acidification initiates host defense abnormalities in cystic fibrosis mice. *Science* **351**, 503–507 (2016).

99. Leigh, M. W., Kylander, J. E., Yankaskas, J. R. & Boucher, R. C. Cell proliferation in bronchial epithelium and submucosal glands of cystic fibrosis patients. *Am J Respir Cell Mol Biol* **12**, 605–612 (1995).

100. Burgel, P. R., Montani, D., Danel, C., Dusser, D. J. & Nadel, J. A. A morphometric study of mucins and small airway plugging in cystic fibrosis. *Thorax* **62**, 153–161 (2007).

101. Molina, S. A. *et al.* Junctional abnormalities in human airway epithelial cells expressing F508del CFTR. *Am J Physiol Lung Cell Mol Physiol* **309**, L475–L487 (2015).

102. Chanson, M. *et al.* Regulation of gap junctional communication by a pro-inflammatory cytokine in cystic fibrosis transmembrane conductance regulator-expressing but not cystic fibrosis airway cells. *Am J Pathol* **158**, 1775–1784 (2001).

103. Shoemark, A. *et al.* Characterization of Eosinophilic Bronchiectasis: A European Multicohort Study. *Am J Respir Crit Care Med* **205**, 894–902 (2022).

104. Chalmers, J. D., Chang, A. B., Chotirmall, S. H., Dhar, R. & McShane, P. J. Bronchiectasis. *Nat Rev Dis Primers* **4**, (2018).

105. O'Donnell, A. E. Bronchiectasis — A Clinical Review. *New England Journal of Medicine* **387**, 533–545 (2022).

106. Polverino, E. *et al.* The overlap between bronchiectasis and chronic airway diseases: state of the art and future directions. *European Respiratory Journal* **52**, 1800328 (2018).

107. Viegi, G., Maio, S., Fasola, S. & Baldacci, S. Global Burden of Chronic Respiratory Diseases. *J Aerosol Med Pulm Drug Deliv* **33**, 171–177 (2020).

108. Horani, A. & Ferkol, T. W. Advances in the Genetics of Primary Ciliary Dyskinesia: Clinical Implications. *Chest* **154**, 645–652 (2018).

109. Enuka, Y., Hanukoglu, I., Edelheit, O., Vaknine, H. & Hanukoglu, A. Epithelial sodium channels (ENaC) are uniformly distributed on motile cilia in the oviduct and the respiratory airways. *Histochem Cell Biol* **137**, 339–353 (2012).

110. Bloodgood, R. A. Sensory reception is an attribute of both primary cilia and motile cilia. *J Cell Sci* **123**, 505–509 (2010).

111. Yoshiba, S. *et al.* Cilia at the node of mouse embryos sense fluid flow for left-right determination via Pkd2. *Science (1979)* **338**, 226–231 (2012).

112. Panelli, D. M., Phillips, C. H. & Brady, P. C. Incidence, diagnosis and management of tubal and nontubal ectopic pregnancies: a review. *Fertility Research and Practice 2015 1:1* **1**, 1–20 (2015).

113. Desgrange, A., Garrec, J. F. Le & Meilhac, S. M. Left-right asymmetry in heart development and disease: Forming the right loop. *Development (Cambridge)* **145**, (2018).

114. Nonaka, S. *et al.* Randomization of left-right asymmetry due to loss of nodal cilia generating leftward flow of extraembryonic fluid in mice lacking KIF3B motor protein. *Cell* **95**, 829–837 (1998).

115. Prevo, B., Scholey, J. M. & Peterman, E. J. G. Intraflagellar transport: mechanisms of motor action, cooperation, and cargo delivery. *FEBS J* **284**, 2905–2931 (2017).

116. Elliott, K. H. & Brugmann, S. A. Sending mixed signals: Cilia-dependent signaling during development and disease. *Dev Biol* **447**, 28–41 (2019).

117. Singla, V. & Reiter, J. F. The primary cilium as the cell's antenna: signaling at a sensory organelle. *Science* **313**, 629–633 (2006).

118. Patel, M. M. & Tsiokas, L. Insights into the Regulation of Ciliary Disassembly. *Cells 2021, Vol. 10, Page 2977* **10**, 2977 (2021).

119. Brown, J. M. & Witman, G. B. Cilia and Diseases. *Bioscience* **64**, 1126–1137 (2014).

120. Wheway, G., Parry, D. A. & Johnson, C. A. The role of primary cilia in the development and disease of the retina. *Organogenesis* **10**, 69 (2014).

121. Scholey, J. M. Intraflagellar transport motors in cilia: moving along the cell's antenna. *J Cell Biol* **180**, 23 (2008).

122. Rosenbaum, J. L. & Witman, G. B. Intraflagellar transport. *Nature Reviews Molecular Cell Biology 2002 3:11* **3**, 813–825 (2002).

123. Rohatgi, R. & Snell, W. J. The ciliary membrane. *Curr Opin Cell Biol* **22**, 541–546 (2010).

124. Ishikawa, H. & Marshall, W. F. Ciliogenesis: building the cell's antenna. *Nature Reviews Molecular Cell Biology 2011 12:4* **12**, 222–234 (2011).

125. Avasthi, P. & Marshall, W. F. Stages of Ciliogenesis and Regulation of Ciliary Length. *Differentiation* **83**, S30 (2012).

126. Yu, X., Ng, C. P., Habacher, H. & Roy, S. Foxj1 transcription factors are master regulators of the motile ciliogenic program. *Nature Genetics 2008 40:12* **40**, 1445–1453 (2008).

127. Blatt, E. N., Yan, X. H., Wuerffel, M. K., Hamilos, D. L. & Brody, S. L. Forkhead transcription factor HFH-4 expression is temporally related to ciliogenesis. *Am J Respir Cell Mol Biol* **21**, 168–176 (1999).

128. Lim, L., Zhou, H. & Costa, R. H. The winged helix transcription factor HFH-4 is expressed during choroid plexus epithelial development in the mouse embryo. *Proc Natl Acad Sci U S A* **94**, 3094–3099 (1997).

129. Hackett, B. P. *et al.* Primary structure of hepatocyte nuclear factor/forkhead homologue 4 and characterization of gene expression in the developing respiratory and reproductive epithelium. *Proceedings of the National Academy of Sciences* **92**, 4249–4253 (1995).

130. Pelletier, G. J., Brody, S. L., Liapis, H., White, R. A. & Hackett, B. P. A human forkhead/winged-helix transcription factor expressed in developing pulmonary and renal epithelium. *Am J Physiol Lung Cell Mol Physiol* **274**, 351–359 (1998).

131. Stubbs, J. L., Oishi, I., Izpisúa Belmonte, J. C. & Kintner, C. The forkhead protein Foxj1 specifies node-like cilia in Xenopus and zebrafish embryos. *Nat Genet* **40**, 1454–1460 (2008).

132. Yu, X., Ng, C. P., Habacher, H. & Roy, S. Foxj1 transcription factors are master regulators of the motile ciliogenic program. *Nat Genet* **40**, 1445–1453 (2008).

133. Jacquet, B. V. *et al.* FoxJ1-dependent gene expression is required for differentiation of radial glia into ependymal cells and a subset of astrocytes in the postnatal brain. *Development* **136**, 4021–4031 (2009).

134. Hellman, N. E. *et al.* The zebrafish foxj1a transcription factor regulates cilia function in response to injury and epithelial stretch. *Proc Natl Acad Sci U S A* **107**, 18499–18504 (2010).

135. Gomperts, B. N., Gong-Cooper, X. & Hackett, B. P. Foxj1 regulates basal body anchoring to the cytoskeleton of ciliated pulmonary epithelial cells. *J Cell Sci* **117**, 1329–1337 (2004).

136. Cruz, C. *et al.* Foxj1 regulates floor plate cilia architecture and modifies the response of cells to sonic hedgehog signalling. *Development* **137**, 4271–4282 (2010).

137. Pan, J., You, Y., Huang, T. & Brody, S. L. RhoA-mediated apical actin enrichment is required for ciliogenesis and promoted by Foxj1. *J Cell Sci* **120**, 1868–1876 (2007).

138. Brody, S. L., Yan, X. H., Wuerffel, M. K., Song, S. K. & Shapiro, S. D. Ciliogenesis and left-right axis defects in forkhead factor HFH-4-null mice. *Am J Respir Cell Mol Biol* **23**, 45–51 (2000).

139. Chen, J., Knowles, H. J., Hebert, J. L. & Hackett, B. P. Mutation of the mouse hepatocyte nuclear factor/forkhead homologue 4 gene results in an absence of cilia and random left-right asymmetry. *J Clin Invest* **102**, 1077–1082 (1998).

140. Vij, S. *et al.* Evolutionarily Ancient Association of the FoxJ1 Transcription Factor with the Motile Ciliogenic Program. *PLoS Genet* **8**, e1003019 (2012).

141. You, Y. *et al.* Role of f-box factor foxj1 in differentiation of ciliated airway epithelial cells. *Am J Physiol Lung Cell Mol Physiol* **286**, 650–657 (2004).

142. Jain, R. *et al.* Temporal Relationship between Primary and Motile Ciliogenesis in Airway Epithelial Cells. *Am J Respir Cell Mol Biol* **43**, 731 (2010).

143. Marshall, C. B. *et al.* p73 is Required for Multiciliogenesis and Regulates the Foxj1-Associated Gene Network. *Cell Rep* **14**, 2289 (2016).

144. Choksi, S. P., Lauter, G., Swoboda, P. & Roy, S. Switching on cilia: transcriptional networks regulating ciliogenesis. *Development* **141**, 1427–1441 (2014).

145. Fliegauf, M., Benzing, T. & Omran, H. When cilia go bad: cilia defects and ciliopathies. *Nature Reviews Molecular Cell Biology 2007 8:11* **8**, 880–893 (2007).

146. Wallmeier, J. *et al.* Motile ciliopathies. *Nature Reviews Disease Primers 2020 6:1* **6**, 1–29 (2020).

147. Onoufriadis, A. *et al.* Combined exome and whole-genome sequencing identifies mutations in ARMC4 as a cause of primary ciliary dyskinesia with defects in the outer dynein arm. *J Med Genet* **51**, 61–67 (2014).

148. Lucas, J. S. *et al.* Diagnosis and management of primary ciliary dyskinesia. *Arch Dis Child* **99**, 850–856 (2014).

149. Hjeij, R. *et al.* ARMC4 mutations cause primary ciliary dyskinesia with randomization of left/right body asymmetry. *Am J Hum Genet* **93**, 357–367 (2013).

150. Werner, C., Onnebrink, J. G. & Omran, H. Diagnosis and management of primary ciliary dyskinesia. *Cilia* **4**, 1–9 (2015).

151. Arndal, E. *et al.* Primary ciliary dyskinesia patients have the same P. aeruginosa clone in sinuses and lungs. *European Respiratory Journal* **55**, (2020).

152. Irving, S. *et al.* Primary Ciliary Dyskinesia Due to Microtubular Defects is Associated with Worse Lung Clearance Index. *Lung* **196**, 231–238 (2018).

153. Boon, M. *et al.* Lung structure–function correlation in patients with primary ciliary dyskinesia. *Thorax* **70**, 339–345 (2015).

154. Halbeisen, F. S. *et al.* Lung function in patients with primary ciliary dyskinesia: an iPCD Cohort study. *European Respiratory Journal* **52**, (2018).

155. Shah, A. *et al.* A longitudinal study characterising a large adult primary ciliary dyskinesia population. *European Respiratory Journal* **48**, 441–450 (2016).

156. Roden, L. *et al.* A retrospective analysis of the pathogens in the airways of patients with primary ciliary dyskinesia. *Respir Med* **156**, 69–77 (2019).

157. Lucas, J. S., Davis, S. D., Omran, H. & Shoemark, A. Primary ciliary dyskinesia in the genomics age. *Lancet Respir Med* **8**, 202–216 (2020).

158. Brown, D. E., Pittman, J. E., Leigh, M. W., Fordham, L. & Davis, S. D. Early lung disease in young children with primary ciliary dyskinesia. *Pediatr Pulmonol* **43**, 514–516 (2008).

159. Shapiro, A. J., Tolleson-Rinehart, S., Zariwala, M. A., Knowles, M. R. & Leigh, M. W. The prevalence of clinical features associated with primary ciliary dyskinesia in a heterotaxy population: results of a web-based survey. *Cardiol Young* **25**, 752–759 (2015).

160. Shoemark, A. *et al.* Genome sequencing reveals underdiagnosis of primary ciliary dyskinesia in bronchiectasis. *European Respiratory Journal* **60**, (2022).

161. Contarini, M. *et al.* Why, when and how to investigate primary ciliary dyskinesia in adult patients with bronchiectasis. *Multidiscip Respir Med* **13**, 29–38 (2018).

162. Noone, P. G. *et al.* Primary ciliary dyskinesia: diagnostic and phenotypic features. *Am J Respir Crit Care Med* **169**, 459–467 (2004).

163. Muthusamy, N., Vijayakumar, A., Cheng, G. & Ghashghaei, H. T. A Knock-in Foxj1CreERT2::GFP mouse for recombination in epithelial cells with motile cilia. *genesis* **52**, 350–358 (2014).

164. Brody, S. L., Yan, X. H., Wuerffel, M. K., Song, S. K. & Shapiro, S. D. Ciliogenesis and left-right axis defects in forkhead factor HFH-4-null mice. *Am J Respir Cell Mol Biol* **23**, 45–51 (2000).

165. Wallmeier, J. *et al.* De Novo Mutations in FOXJ1 Result in a Motile Ciliopathy with Hydrocephalus and Randomization of Left/Right Body Asymmetry. *Am J Hum Genet* **105**, 1030–1039 (2019).

166. Jin, S. C. *et al.* Exome sequencing implicates genetic disruption of prenatal neuro-gliogenesis in sporadic congenital hydrocephalus. *Nature Medicine 2020 26:11* **26**, 1754–1765 (2020).

167. Shapiro, A. J. *et al.* Autosomal dominant variants in FOXJ1 causing primary ciliary dyskinesia in two patients with obstructive hydrocephalus. *Mol Genet Genomic Med* **9**, (2021).

168. Ehre, C., Ridley, C. & Thornton, D. J. Cystic fibrosis: an inherited disease affecting mucin-producing organs. *Int J Biochem Cell Biol* **52**, 136–145 (2014).

169. Piorunek, T. *et al.* Correlation between the stage of cystic fibrosis and the level of morphological changes in adult patients. *Journal of Physiology and Pharmacology* **59 suppl. 1**, (2008).

170. Look, D. C. *et al.* Effects of paramyxoviral infection on airway epithelial cell Foxj1 expression, ciliogenesis, and mucociliary function. *Am J Pathol* **159**, 2055–2069 (2001).

171. Amitani, R. *et al.* Effects of human neutrophil elastase and Pseudomonas aeruginosa proteinases on human respiratory epithelium. *Am J Respir Cell Mol Biol* **4**, 26–32 (1991).

172. Balder, R., Krunkosky, T. M., Nguyen, C. Q., Feezel, L. & Lafontaine, E. R. Hag mediates adherence of Moraxella catarrhalis to ciliated human airway cells. *Infect Immun* **77**, 4597–4608 (2009).

173. Robinot, R. *et al.* SARS-CoV-2 infection induces the dedifferentiation of multiciliated cells and impairs mucociliary clearance. *Nat Commun* **12**, (2021).

174. Sisson, J. H. *et al.* Smoke and viral infection cause cilia loss detectable by bronchoalveolar lavage cytology and dynein ELISA. *Am J Respir Crit Care Med* **149**, 205–213 (1994).

175. Wistuba, I. I. & Gazdar, A. F. Lung cancer preneoplasia. *Annu Rev Pathol* **1**, 331–348 (2006).

176. Leopold, P. L. *et al.* Smoking Is Associated with Shortened Airway Cilia. *PLoS One* **4**, e8157 (2009).

177. Shaykhiev, R. *et al.* EGF shifts human airway basal cell fate towarda smoking-Associated airway epithelial phenotype. *Proc Natl Acad Sci U S A* **110**, 12102–12107 (2013).

178. Takeyama, K. *et al.* Oxidative stress causes mucin synthesis via transactivation of epidermal growth factor receptor: role of neutrophils. *J Immunol* **164**, 1546–1552 (2000).

179. Casalino-Matsuda, S. M., Monzon, M. E. & Forteza, R. M. Epidermal growth factor receptor activation by epidermal growth factor mediates oxidant-induced goblet cell metaplasia in human airway epithelium. *Am J Respir Cell Mol Biol* **34**, 581–591 (2006).

180. Filosto, S. *et al.* EGF Receptor Exposed to Oxidative Stress Acquires Abnormal Phosphorylation and Aberrant Activated Conformation That Impairs Canonical Dimerization. *PLoS One* **6**, (2011).

181. Hessel, J. *et al.* Intraflagellar transport gene expression associated with short cilia in smoking and COPD. *PLoS One* **9**, (2014).

182. Tilley, A. E., Walters, M. S., Shaykhiev, R. & Crystal, R. G. Cilia Dysfunction in Lung Disease. *Annu Rev Physiol* **77**, 379 (2015).

183. Yaghi, A., Zaman, A., Cox, G. & Dolovich, M. B. Ciliary beating is depressed in nasal cilia from chronic obstructive pulmonary disease subjects. *Respir Med* **106**, 1139–1147 (2012).

184. Ramos, E. M. C. *et al.* Reversibility of impaired nasal mucociliary clearance in smokers following a smoking cessation programme. *Respirology* **16**, 849–855 (2011).

185. Tilley, A. E., Walters, M. S., Shaykhiev, R. & Crystal, R. G. Cilia Dysfunction in Lung Disease. *Annu Rev Physiol* **77**, 379 (2015).

186. Kuyper, L. M. *et al.* Characterization of airway plugging in fatal asthma. *American Journal of Medicine* **115**, 6–11 (2003).

187. Erle, D. J. & Sheppard, D. The cell biology of asthma. *J Cell Biol* **205**, 621–631 (2014).

188. Thomas, B. *et al.* Ciliary dysfunction and ultrastructural abnormalities are features of severe asthma. *J Allergy Clin Immunol* **126**, (2010).

189. Gomperts, B. N., Kim, L. J., Flaherty, S. A. & Hackett, B. P. IL-13 regulates cilia loss and foxj1 expression in human airway epithelium. *Am J Respir Cell Mol Biol* **37**, 339–346 (2007).

190. Bartalesi, B. *et al.* Different lung responses to cigarette smoke in two strains of mice sensitive to oxidants. *Eur Respir J* **25**, 15–22 (2005).

191. Mercer, B., Lemaitre, V., Powell, C. & D'Armiento, J. The Epithelial Cell in Lung Health and Emphysema Pathogenesis. *Curr Respir Med Rev* **2**, 101–142 (2006).

192. Haswell, L. E., Hewitt, K., Thorne, D., Richter, A. & Gaça, M. D. Cigarette smoke total particulate matter increases mucous secreting cell numbers in vitro: a potential model of goblet cell hyperplasia. *Toxicol In Vitro* **24**, 981–987 (2010).

193. Cloonan, S. M., Lam, H. C., Ryter, S. W. & Choi, A. M. 'Ciliophagy': The consumption of cilia components by autophagy. *Autophagy* **10**, 532–534 (2014).

194. Barnes, P. J., Shapiro, S. D. & Pauwels, R. A. Chronic obstructive pulmonary disease: molecular and cellular mechanisms. *Eur Respir J* **22**, 672–688 (2003).

195. Lung Cancer Facts 2023 - Lung Cancer Research Foundation. https://www.lungcancerresearchfoundation.org/lung-cancer-facts/.

196. Higgins, M., Obaidi, I. & McMorrow, T. Primary cilia and their role in cancer. *Oncol Lett* **17**, 3041 (2019).

197. Fukui, T. *et al.* Lung adenocarcinoma subtypes based on expression of human airway basal cell genes. *Eur Respir J* **42**, 1332–1344 (2013).

198. Rock, J. R. *et al.* Notch-dependent differentiation of adult airway basal stem cells. *Cell Stem Cell* **8**, 639–648 (2011).

199. Tsao, P. N. *et al.* Notch signaling controls the balance of ciliated and secretory cell fates in developing airways. *Development* **136**, 2297–2307 (2009).

200. Bray, S. J. Notch signalling in context. *Nature Reviews Molecular Cell Biology 2016 17:11* **17**, 722–735 (2016).

201. McCaw, T. R. *et al.* Gamma Secretase Inhibitors in Cancer: A Current Perspective on Clinical Performance. *Oncologist* **26**, e608–e621 (2021).

202. Bodas, M. *et al.* Cigarette Smoke Activates NOTCH3 to Promote Goblet Cell Differentiation in Human Airway Epithelial Cells. *Am J Respir Cell Mol Biol* **64**, 426–440 (2021).

203. Reid, A. T. *et al.* Blocking Notch3 Signaling Abolishes MUC5AC Production in Airway Epithelial Cells from Individuals with Asthma. *Am J Respir Cell Mol Biol* **62**, 513–523 (2020).

204. Zong, D., Ouyang, R., Li, J., Chen, Y. & Chen, P. Notch signaling in lung diseases: focus on Notch1 and Notch3. *Ther Adv Respir Dis* **10**, 468–484 (2016).

205. Vladar, E. K., Nayak, J. V., Milla, C. E. & Axelrod, J. D. Airway epithelial homeostasis and planar cell polarity signaling depend on multiciliated cell differentiation. *JCI Insight* **1**, 88027 (2016).

206. Vladar, E. K. *et al.* Notch signaling inactivation by small molecule γ-secretase inhibitors restores the multiciliated cell population in the airway epithelium. *Am J Physiol Lung Cell Mol Physiol* **324**, L771–L782 (2023).

207. Whitsett, J. A. & Tichelaar, J. W. Forkhead transcription factor HFH-4 and respiratory epithelial cell differentiation. *Am J Respir Cell Mol Biol* **21**, 153–154 (1999).

208. Pan, J., You, Y., Huang, T. & Brody, S. L. RhoA-mediated apical actin enrichment is required for ciliogenesis and promoted by Foxj1. *J Cell Sci* **120**, 1868–1876 (2007).

209. Zhang, Y. *et al.* A transgenic FOXJ1-Cre system for gene inactivation in ciliated epithelial cells. *Am J Respir Cell Mol Biol* **36**, 515–519 (2007).

210. Love, D. *et al.* Altered Lung Morphogenesis, Epithelial Cell Differentiation and Mechanics in Mice Deficient in the Wnt/β-Catenin Antagonist Chibby. *PLoS One* **5**, e13600 (2010).

211. Huang, T. *et al.* Foxj1 is required for apical localization of ezrin in airway epithelial cells. *J Cell Sci* **116**, 4935–4945 (2003).

212. Hackett, B. P. *et al.* Primary structure of hepatocyte nuclear factor/forkhead homologue 4 and characterization of gene expression in the developing respiratory and reproductive epithelium. *Proc Natl Acad Sci U S A* **92**, 4249–4253 (1995).

213. Rock, J. R., Randell, S. H. & Hogan, B. L. M. Airway basal stem cells: a perspective on their roles in epithelial homeostasis and remodeling. *Dis Model Mech* **3**, 545–556 (2010).

214. Didon, L. *et al.* RFX3 Modulation of FOXJ1 regulation of cilia genes in the human airway epithelium. *Respir Res* **14**, 1–13 (2013).

215. Ma, M. & Jiang, Y. J. Jagged2a-Notch Signaling Mediates Cell Fate Choice in the Zebrafish Pronephric Duct. *PLoS Genet* **3**, e18 (2007).

216. Dubruille, R. *et al.* Drosophila regulatory factor X is necessary for ciliated sensory neuron differentiation. *Development* **129**, 5487–5498 (2002).

217. Chung, M. I. *et al.* RFX2 is broadly required for ciliogenesis during vertebrate development. *Dev Biol* **363**, 155–165 (2012).

218. Bisgrove, B. W., Makova, S., Yost, H. J. & Brueckner, M. RFX2 is essential in the ciliated organ of asymmetry and an RFX2 transgene identifies a population of ciliated cells sufficient for fluid flow. *Dev Biol* **363**, 166–178 (2012).

219. Swoboda, P., Adler, H. T. & Thomas, J. H. The RFX-type transcription factor DAF-19 regulates sensory neuron cilium formation in C. elegans. *Mol Cell* **5**, 411–421 (2000).

220. Brekman, A., Walters, M. S., Tilley, A. E. & Crystal, R. G. FOXJ1 prevents cilia growth inhibition by cigarette smoke in human airway epithelium in vitro. *Am J Respir Cell Mol Biol* **51**, 688–700 (2014).

221. Leopold, P. L. *et al.* Smoking Is Associated with Shortened Airway Cilia. *PLoS One* **4**, e8157 (2009).

222. Tamashiro, E. *et al.* Cigarette smoke exposure impairs respiratory epithelial ciliogenesis. *Am J Rhinol Allergy* **23**, 117–122 (2009).

223. Nagai, A. & Thurlbeck, W. M. Scanning electron microscopic observations of emphysema in humans. A descriptive study. *Am Rev Respir Dis* **144**, 901–908 (1991).

224. Verra, F. *et al.* Ciliary abnormalities in bronchial epithelium of smokers, ex-smokers, and nonsmokers. *Am J Respir Crit Care Med* **151**, 630–634 (1995).

225. Wang, G. *et al.* Smoking-mediated up-regulation of GAD67 expression in the human airway epithelium. *Respir Res* **11**, 1–15 (2010).

226. Rapiteanu, R. *et al.* Highly efficient genome editing in primary human bronchial epithelial cells differentiated at air–liquid interface. *European Respiratory Journal* **55**, (2020).

227. Wolff, J. A. *et al.* Direct Gene Transfer into Mouse Muscle in Vivo. *Science (1979)* **247**, 1465–1468 (1990).

228. Freyn, A. W. *et al.* A Multi-Targeting, Nucleoside-Modified mRNA Influenza Virus Vaccine Provides Broad Protection in Mice. doi:10.1016/j.ymthe.2020.04.018.

229. Gómez, C. E. *et al.* Enhancement of the HIV-1-Specific Immune Response Induced by an mRNA Vaccine through Boosting with a Poxvirus MVA Vector Expressing the Same Antigen. (2021) doi:10.3390/vaccines9090959.

230. Awasthi, S. *et al.* Nucleoside-modified mRNA encoding HSV-2 glycoproteins C, D, and E prevents clinical and subclinical genital herpes. *Sci Immunol* **4**, 7083 (2019).

231. Aliprantis, A. O. *et al.* A phase 1, randomized, placebo-controlled study to evaluate the safety and immunogenicity of an mRNA-based RSV prefusion F protein vaccine in healthy younger and older adults. *Hum Vaccin Immunother* **17**, 1248–1261 (2021).

232. Espeseth, A. S. *et al.* Modified mRNA/lipid nanoparticle-based vaccines expressing respiratory syncytial virus F protein variants are immunogenic and protective in rodent models of RSV infection. doi:10.1038/s41541-020-0163-z.

233. Latourette, P. C. *et al.* Protection against herpes simplex virus type 2 infection in a neonatal murine model using a trivalent nucleoside-modified mRNA in lipid nanoparticle vaccine. doi:10.1016/j.vaccine.2020.09.079.

234. Egan, K. P. *et al.* An HSV-2 nucleoside-modified mRNA genital herpes vaccine containing glycoproteins gC, gD, and gE protects mice against HSV-1 genital lesions and latent infection. (2020) doi:10.1371/journal.ppat.1008795.

235. Awasthi, S. *et al.* Trivalent nucleoside-modified mRNA vaccine yields durable memory B cell protection against genital herpes in preclinical models. *J Clin Invest* **131**, (2021).

236. Monslow, M. A. *et al.* Immunogenicity generated by mRNA vaccine encoding VZV gE antigen is comparable to adjuvanted subunit vaccine and better than live attenuated vaccine in nonhuman primates. *Vaccine* **38**, 5793–5802 (2020).

237. Nelson, C. S. *et al.* Human Cytomegalovirus Glycoprotein B Nucleoside-Modified mRNA Vaccine Elicits Antibody Responses with Greater Durability and Breadth than MF59-Adjuvanted gB Protein Immunization. *J Virol* **94**, (2020).

238. Webster, H. *et al.* Pre-existing immunity to cytomegalovirus in macaques influences human CMV vaccine responses in preclinical models. *Vaccine* **39**, 5358–5367 (2021).

239. Geall, A. J. *et al.* Nonviral delivery of self-amplifying RNA vaccines. *Proc Natl Acad Sci U S A* **109**, 14604–14609 (2012).

240. Hekele, A. *et al.* Rapidly produced SAM® vaccine against H7N9 influenza is immunogenic in mice. *Emerg Microbes Infect* **2**, 52 (2013).

241. Routy, J. P. *et al.* Immunologic activity and safety of autologous HIV RNA-electroporated dendritic cells in HIV-1 infected patients receiving antiretroviral therapy. *Clinical Immunology* **134**, 140–147 (2010).

242. Allard, S. D. *et al.* A phase I/IIa immunotherapy trial of HIV-1-infected patients with Tat, Rev and Nef expressing dendritic cells followed by treatment interruption. *Clinical Immunology* **142**, 252–268 (2012).

243. Van Gulck, E. *et al.* MRNA-based dendritic cell vaccination induces potent antiviral T-cell responses in HIV-1-infected patients. *AIDS* **26**, (2012).

244. Geall, A. J. *et al.* Nonviral delivery of self-amplifying RNA vaccines. *Proc Natl Acad Sci U S A* **109**, 14604–14609 (2012).

245. Polack, F. P. *et al.* Safety and Efficacy of the BNT162b2 mRNA Covid-19 Vaccine. *N Engl J Med* **383**, 2603–2615 (2020).

246. Baden, L. R. *et al.* Efficacy and Safety of the mRNA-1273 SARS-CoV-2 Vaccine. *N Engl J Med* **384**, 403–416 (2021).

247. Weide, B. *et al.* Results of the first phase I/II clinical vaccination trial with direct injection of mRNA. *Journal of Immunotherapy* **31**, 180–188 (2008).

248. Sebastian, M. *et al.* A phase I/IIa study of the mRNA-based cancer immunotherapy CV9201 in patients with stage IIIB/IV non-small cell lung cancer. *Cancer Immunology, Immunotherapy* **68**, 799–812 (2019).

249. Liu, M. A. A Comparison of Plasmid DNA and mRNA as Vaccine Technologies. doi:10.3390/vaccines7020037.

250. Kyte, J. A. *et al.* Immune response and long-term clinical outcome in advanced melanoma patients vaccinated with tumor-mRNA-transfected dendritic cells. (2016) doi:10.1080/2162402X.2016.1232237.

251. Jansen, Y. *et al.* A randomized controlled phase II clinical trial on mRNA electroporated autologous monocyte-derived dendritic cells (TriMixDC-MEL) as adjuvant treatment for stage III/IV melanoma patients who are disease-free following the resection of macrometastases. **69**, 2589–2598 (2020).

252. Boudewijns, S. *et al.* Autologous monocyte-derived DC vaccination combined with cisplatin in stage III and IV melanoma patients: a prospective, randomized phase 2 trial. **69**, 477–488 (2020).

253. Bol, K. F. *et al.* Intranodal vaccination with mRNA-optimized dendritic cells in metastatic melanoma patients. *Oncoimmunology* **4**, (2015).

254. Aarntzen, E. H. J. G. *et al.* Vaccination with mRNA-electroporated dendritic cells induces robust tumor antigen-specific CD4+ and CD8+ T cells responses in stage III and IV melanoma patients. *Clinical Cancer Research* **18**, 5460–5470 (2012).

255. Kranz, L. M. *et al.* Systemic RNA delivery to dendritic cells exploits antiviral defence for cancer immunotherapy. *Nature 2016 534:7607* **534**, 396–401 (2016).

256. Vik-Mo, E. O. *et al.* Therapeutic vaccination against autologous cancer stem cells with mRNA-transfected dendritic cells in patients with glioblastoma. *Cancer Immunology, Immunotherapy* **62**, 1499–1509 (2013).

257. Heiser, A. *et al.* Autologous dendritic cells transfected with prostate-specific antigen RNA stimulate CTL responses against metastatic prostate tumors. *J Clin Invest* **109**, 409 (2002).

258. Nair, S. K. *et al.* Induction of cytotoxic T cell responses and tumor immunity against unrelated tumors using telomerase reverse transcriptase RNA transfected dendritic cells. *Nature Medicine 2000 6:9* **6**, 1011–1017 (2000).

259. Nair, S. K. *et al.* Induction of prin1ary carcinoen1bryonic antigen (CEA)-specific cytotoxic T lyn1phocytes in vitro using hun1an dendritic cells transfected with RNA. (1998).

260. Wilgenhof, S. *et al.* A phase IB study on intravenous synthetic mRNA electroporated dendritic cell immunotherapy in pretreated advanced melanoma patients. *Annals of Oncology* **24**, 2686–2693 (2013).

261. Cisco, R. M. *et al.* Induction of Human Dendritic Cell Maturation Using Transfection with RNA Encoding a Dominant Positive Toll-Like Receptor 4. *The Journal of Immunology* **172**, 7162–7168 (2004).

262. Bonehill, A. *et al.* Enhancing the t-cell stimulatory capacity of human dendritic cells by co-electroporation with CD40L, CD70 and constitutively active TLR4 encoding mRNA. *Molecular Therapy* **16**, 1170–1180 (2008).

263. Calderhead, D. M. *et al.* Cytokine maturation followed by CD40L mRNA electroporation results in a clinically relevant dendritic cell product capable of inducing a potent proinflammatory CTL response. *Journal of Immunotherapy* **31**, 731–741 (2008).

264. Routy, J. P. *et al.* Immunologic activity and safety of autologous HIV RNA-electroporated dendritic cells in HIV-1 infected patients receiving antiretroviral therapy. *Clinical Immunology* **134**, 140–147 (2010).

265. Bontkes, H. J. *et al.* Dendritic cells transfected with interleukin-12 and tumor-associated antigen messenger RNA induce high avidity cytotoxic T cells. *Gene Therapy 2007 14:4* **14**, 366–375 (2006).

266. Aarntzen, E. H. J. G. *et al.* Vaccination with mRNA-electroporated dendritic cells induces robust tumor antigen-specific CD4+ and CD8+ T cells responses in stage III and IV melanoma patients. *Clinical Cancer Research* **18**, 5460–5470 (2012).

267. Fotin-Mleczek, M. *et al.* Messenger RNA-based vaccines with dual activity induce balanced TLR-7 dependent adaptive immune responses and provide antitumor activity. *Journal of Immunotherapy* **34**, 1–15 (2011).

268. Fotin-Mleczek, M. *et al.* Highly potent mRNA based cancer vaccines represent an attractive platform for combination therapies supporting an improved therapeutic effect. *J Gene Med* **14**, 428–439 (2012).

269. Rittig, S. M. *et al.* Intradermal vaccinations with RNA coding for TAA generate CD8 and CD4 immune responses and induce clinical benefit in vaccinated patients. *Molecular Therapy* **19**, 990–999 (2011).

270. Magadum, A., Kaur, K. & Zangi, L. mRNA-Based Protein Replacement Therapy for the Heart. *Molecular Therapy* **27**, 785–793 (2019).

271. Lui, K. O. *et al.* Driving vascular endothelial cell fate of human multipotent Isl1+ heart progenitors with VEGF modified mRNA. *Cell Research 2013 23:10* **23**, 1172–1186 (2013).

272. Anttila, V. *et al.* Synthetic mRNA Encoding VEGF-A in Patients Undergoing Coronary Artery Bypass Grafting: Design of a Phase 2a Clinical Trial. *Mol Ther Methods Clin Dev* **18**, 464–472 (2020).

273. Zangi, L. *et al.* Modified mRNA directs the fate of heart progenitor cells and induces vascular regeneration after myocardial infarction. *Nature Biotechnology 2013 31:10* **31**, 898–907 (2013).

274. Sahu, I., Haque, A. K. M. A., Weidensee, B., Weinmann, P. & Kormann, M. S. D. Recent Developments in mRNA-Based Protein Supplementation Therapy to Target Lung Diseases. doi:10.1016/j.ymthe.2019.02.019.

275. Bangel-Ruland, N. *et al.* Cystic fibrosis transmembrane conductance regulator-mRNA delivery: a novel alternative for cystic fibrosis gene therapy. *J Gene Med* **15**, 414–426 (2013).

276. Robinson, E. *et al.* Lipid Nanoparticle-Delivered Chemically Modified mRNA Restores Chloride Secretion in Cystic Fibrosis. *Molecular Therapy* **26**, 2034–2046 (2018).

277. Kormann, M. S. D. *et al.* expression of therapeutic proteins after delivery of chemically modified mrNA in mice. *Nat Biotechnol* **29**, (2011).

278. Mays, L. E. *et al.* Modified Foxp3 mRNA protects against asthma through an IL-10-dependent mechanism. *J Clin Invest* **123**, (2013).

279. Karikó, K., Muramatsu, H., Keller, J. M. & Weissman, D. Increased erythropoiesis in mice injected with submicrogram quantities of pseudouridine-containing mRNA encoding erythropoietin. *Molecular Therapy* **20**, 948–953 (2012).

280. Russick, J. *et al.* Correction of bleeding in experimental severe hemophilia A by systemic delivery of factor VIII-encoding mRNA. *Haematologica* **105**, 1129–1137 (2020).

281. Ramaswamy, S. *et al.* Systemic delivery of factor IX messenger RNA for protein replacement therapy. doi:10.1073/pnas.1619653114.

282. Berraondo, P., Martini, P. G. V., Avila, M. A. & Fontanellas, A. Messenger RNA therapy for rare genetic metabolic diseases. *Gut* **68**, 1323–1330 (2019).

283. Jiang, L. *et al.* Systemic messenger RNA as an etiological treatment for acute intermittent porphyria. *Nature Medicine 2018 24:12* **24**, 1899–1909 (2018).

284. An, D. *et al.* Systemic Messenger RNA Therapy as a Treatment for Methylmalonic Acidemia. *Cell Rep* **21**, 3548–3558 (2017).

285. Prieve, M. G. *et al.* Targeted mRNA Therapy for Ornithine Transcarbamylase Deficiency. *Molecular Therapy* **26**, 801–813 (2018).

286. Karadagi, A. *et al.* Systemic modified messenger RNA for replacement therapy in alpha 1-antitrypsin deficiency. doi:10.1038/s41598-020-64017-0.

287. Uchida, S. *et al.* In Vivo Messenger RNA Introduction into the Central Nervous System Using Polyplex Nanomicelle. doi:10.1371/journal.pone.0056220.

288. Nabhan, J. F. *et al.* Intrathecal delivery of frataxin mRNA encapsulated in lipid nanoparticles to dorsal root ganglia as a potential therapeutic for Friedreich's ataxia OPEN. (2015) doi:10.1038/srep20019.

289. Doyon, Y. *et al.* Heritable targeted gene disruption in zebrafish using designed zinc-finger nucleases. *Nature Biotechnology 2008 26:6* **26**, 702–708 (2008).

290. Tesson, L. *et al.* Knockout rats generated by embryo microinjection of TALENs. *Nature Publishing Group* (2011) doi:10.1093/nar/gkr188.

291. Wang, H. *et al.* One-step generation of mice carrying mutations in multiple genes by CRISPR/cas-mediated genome engineering. *Cell* **153**, 910–918 (2013).

292. Wefers, B. *et al.* Generation of targeted mouse mutants by embryo microinjection of TALEN mRNA. *Nature Protocols 2013 8:12* **8**, 2355–2379 (2013).

293. Shen, B. *et al.* Cas9/RNA and gene targeting 720 Generation of gene-modified mice via Cas9/RNA-mediated gene targeting. (2013) doi:10.1038/cr.2013.46.

294. Ma, Y. *et al.* Generating conditional knockout rats using CRISPR/Cas9 122 Generating rats with conditional alleles using CRISPR/Cas9. (2014) doi:10.1038/cr.2013.157.

295. Niu, Y. *et al.* Generation of gene-modified cynomolgus monkey via Cas9/RNA-mediated gene targeting in one-cell embryos. *Cell* **156**, 836–843 (2014).

296. Li, B. *et al.* Combinatorial design of nanoparticles for pulmonary mRNA delivery and genome editing. *Nat Biotechnol* **41**, 1410 (2023).

297. Warren, L. *et al.* Cell Stem Cell Article Highly Efficient Reprogramming to Pluripotency and Directed Differentiation of Human Cells with Synthetic Modified mRNA. doi:10.1016/j.stem.2010.08.012.

298. Warren, L., Ni, Y., Wang, J. & Guo, X. Feeder-Free Derivation of Human Induced Pluripotent Stem Cells with Messenger RNA. doi:10.1038/srep00657.

299. Mandal, P. K. & Rossi, D. J. Reprogramming human fibroblasts to pluripotency using modified mRNA. *Nat Protoc* **8**, 568–582 (2013).

300. Yoshioka, N. *et al.* Cell Stem Cell Resource Efficient Generation of Human iPSCs by a Synthetic Self-Replicative RNA. doi:10.1016/j.stem.2013.06.001.

301. Kehler, J. *et al.* RNA-Generated and Gene-Edited Induced Pluripotent Stem Cells for Disease Modeling and Therapy. *J Cell Physiol* **232**, 1262–1269 (2017).

302. Chen, L., Shi, K., Qiu, W., Aagaard, L. & Kassem, M. Generation of Inducible CRISPRi and CRISPRa Human Stromal/Stem Cell Lines for Controlled Target Gene Transcription during Lineage Differentiation. *Stem Cells Int* **2020**, (2020).

303. Abbasi, S. *et al.* Co-encapsulation of Cas9 mRNA and guide RNA in polyplex micelles enables genome editing in mouse brain. *J Control Release* **332**, 260–268 (2021).

304. Sahin, U., Karikó, K. & Türeci, Ö. mRNA-based therapeutics — developing a new class of drugs. (2014) doi:10.1038/nrd4278.

305. Li, Y. & Kiledjian, M. Regulation of mRNA decapping. *Wiley Interdiscip Rev RNA* **1**, 253–265 (2010).

306. Stepinski, J., Waddell, C., Stolarski, R., Darzynkiewicz, E. & Rhoads, R. E. Synthesis and properties of mRNAs containing the novel 'anti-reverse' cap analogs 7-methyl(39-O-methyl)GpppG and 7-methyl(39-deoxy)GpppG. (2001).

307. Jemielity, J. *et al.* Novel 'anti-reverse' cap analogs with superior translational properties. (2003) doi:10.1261/rna.5430403.

308. Mockey, M. *et al.* mRNA transfection of dendritic cells: Synergistic effect of ARCA mRNA capping with Poly(A) chains in cis and in trans for a high protein expression level. *Biochem Biophys Res Commun* **340**, 1062–1068 (2006).

309. Rabinovich, P. M. *et al.* Synthetic Messenger RNA as a Tool for Gene Therapy. *https://home.liebertpub.com/hum* **17**, 1027–1035 (2006).

310. Kuhn, A. N. *et al.* Phosphorothioate cap analogs increase stability and translational efficiency of RNA vaccines in immature dendritic cells and induce superior immune responses in vivo. *Gene Ther* **17**, 961–971 (2010).

311. Gallie, D. R. The cap and poly(A) tail function synergistically to regulate mRNA translational efficiency.

312. Holtkamp, S. *et al.* Modification of antigen-encoding RNA increases stability, translational efficacy, and T-cell stimulatory capacity of dendritic cells. (2006) doi:10.1182/blood-2006-04-015024.

313. Karikó, K., Kuo, A. & Barnathan, E. S. Overexpression of urokinase receptor in mammalian cells following administration of the in vitro transcribed encoding mRNA. *Gene Therapy 1999 6:6* **6**, 1092–1100 (1999).

314. Ross, J. & Sullivan, T. D. Half-lives of beta and gamma globin messenger RNAs and of protein synthetic capacity in cultured human reticulocytes. *Blood* **66**, 1149–1154 (1985).

315. Matoulkova, E., Michalova, E., Vojtesek, B. & Hrstka, R. RNA Biology The role of the 3' untranslated region in post-transcriptional regulation of protein expression in mammalian cells. (2012) doi:10.4161/rna.20231.

316. Jiang, Y., Xu, X.-S. & Russell, J. E. A Nucleolin-Binding 3′ Untranslated Region Element Stabilizes β-Globin mRNA In Vivo. *Mol Cell Biol* **26**, 2419–2429 (2006).

317. Bourquin, C. *et al.* Immunostimulatory RNA oligonucleotides trigger an antigen-specific cytotoxic T-cell and IgG2a response. *Blood* **109**, 2953–2960 (2007).

318. Sander, L. E. *et al.* Detection of prokaryotic mRNA signifies microbial viability and promotes immunity. doi:10.1038/nature10072.

319. Yoneyama, M. *et al.* The RNA helicase RIG-I has an essential function in double-stranded RNA-induced innate antiviral responses. *Nature Immunology 2004 5:7* **5**, 730–737 (2004).

320. Yoneyama, M. *et al.* Shared and Unique Functions of the DExD/H-Box Helicases RIG-I, MDA5, and LGP2 in Antiviral Innate Immunity. *The Journal of Immunology* **175**, 2851–2858 (2005).

321. Karikó, K., Buckstein, M., Ni, H. & Weissman, D. Suppression of RNA recognition by Toll-like receptors: The impact of nucleoside modification and the evolutionary origin of RNA. *Immunity* **23**, 165–175 (2005).

322. Karikó, K. *et al.* Incorporation of pseudouridine into mRNA yields superior nonimmunogenic vector with increased translational capacity and biological stability. *Molecular Therapy* **16**, 1833–1840 (2008).

323. Meet the authors: Katalin Karikó and Drew Weissman. *Immunity* **54**, 2673–2675 (2021).

324. Press release: The Nobel Prize in Physiology or Medicine 2023 - NobelPrize.org. https://www.nobelprize.org/prizes/medicine/2023/press-release/.

325. Gilbert, W. V., Bell, T. A. & Schaening, C. Messenger RNA modifications: Form, distribution, and function. *Science* **352**, 1408–1412 (2016).

326. Lambert, S. A. *et al.* The Human Transcription Factors. *Cell* **172**, 650–665 (2018).

327. Arnit, I. *et al.* Unbiased reconstruction of a mammalian transcriptional network mediating pathogen responses. *Science (1979)* **326**, 257–263 (2009).

328. Ravasi, T. *et al.* An atlas of combinatorial transcriptional regulation in mouse and man. *Cell* **140**, 744–752 (2010).

329. Joung, J. *et al.* A transcription factor atlas of directed differentiation. *Cell* **186**, 209-229.e26 (2023).

330. Weintraub, H. *et al.* Activation of muscle-specific genes in pigment, nerve, fat, liver, and fibroblast cell lines by forced expression of MyoD. *Proc Natl Acad Sci U S A* **86**, 5434–5438 (1989).

331. Zhang, Y. *et al.* Rapid single-step induction of functional neurons from human pluripotent stem cells. *Neuron* **78**, 785–798 (2013).

332. Ng, A. H. M. *et al.* A comprehensive library of human transcription factors for cell fate engineering. *Nature Biotechnology 2020 39:4* **39**, 510–519 (2020).

333. Parekh, U. *et al.* Mapping Cellular Reprogramming via Pooled Overexpression Screens with Paired Fitness and Single-Cell RNA-Sequencing Readout. *Cell Syst* **7**, 548-555.e8 (2018).

334. Pang, Z. P. *et al.* Induction of human neuronal cells by defined transcription factors. *Nature 2011 476:7359* **476**, 220–223 (2011).

335. Perrier, A. L. *et al.* Derivation of midbrain dopamine neurons from human embryonic stem cells. *Proc Natl Acad Sci U S A* **101**, 12543–12548 (2004).

336. Sugimura, R. *et al.* Haematopoietic stem and progenitor cells from human pluripotent stem cells. *Nature 2017 545:7655* **545**, 432–438 (2017).

337. Takahashi, K. *et al.* Induction of Pluripotent Stem Cells from Adult Human Fibroblasts by Defined Factors. *Cell* **131**, 861–872 (2007).

338. Yu, J. *et al.* Induced pluripotent stem cell lines derived from human somatic cells. *Science (1979)* **318**, 1917–1920 (2007).

339. Takahashi, K. & Yamanaka, S. Induction of Pluripotent Stem Cells from Mouse Embryonic and Adult Fibroblast Cultures by Defined Factors. *Cell* **126**, 663–676 (2006).

340. Umebayashi, M., Sumita, Y., Kawai, Y., Watanabe, S. & Asahina, I. Gene-Activated Matrix Comprised of Atelocollagen and Plasmid DNA Encoding BMP4 or Runx2 Promotes Rat Cranial Bone Augmentation. doi:10.1089/biores.2014.0057.

341. Tu, Q. *et al.* Osterix Overexpression in Mesenchymal Stem cells Stimulates Healing of Critical-Sized Defects in Murine Calvarial Bone. doi:10.1089/ten.2006.0406.

342. Tsuchiya, H., Kitoh, H., Sugiura, F. & Ishiguro, N. Chondrogenesis enhanced by overexpression of sox9 gene in mouse bone marrow-derived mesenchymal stem cells. *Biochem Biophys Res Commun* **301**, 338–343 (2003).

343. Zhang, G., Nie, M., Webster, T. J., Zhang, Q. & Fan, W. Ectopic chondrogenesis of nude mouse induced by nano gene delivery enhanced tissue engineering technology . *Int J Nanomedicine* **14**, 4755–4765 (2019).

344. Qian, L. *et al.* In vivo reprogramming of murine cardiac fibroblasts into induced cardiomyocytes. *Nature 2012 485:7400* **485**, 593–598 (2012).

345. Song, K. *et al.* Heart repair by reprogramming non-myocytes with cardiac transcription factors. *Nature 2012 485:7400* **485**, 599–604 (2012).

346. Damase, T. R. *et al.* The Limitless Future of RNA Therapeutics. *Front Bioeng Biotechnol* **9**, 628137 (2021).

347. Chang, C. W. *et al.* Polycistronic Lentiviral Vector for “Hit and Run” Reprogramming of Adult Skin Fibroblasts to Induced Pluripotent Stem Cells. *Stem Cells* **27**, 1042–1049 (2009).

348. Choi, H. W. *et al.* Neural Stem Cells Differentiated From iPS Cells Spontaneously Regain Pluripotency. *Stem Cells* **32**, 2596–2604 (2014).

349. Schott, J. W. *et al.* Improved retroviral episome transfer of transcription factors enables sustained cell fate modification. *Gene Therapy 2014 21:11* **21**, 938–949 (2014).

350. Sridhar, A., Ohlemacher, S. K., Langer, K. B. & Meyer, J. S. Robust Differentiation of mRNA-Reprogrammed Human Induced Pluripotent Stem Cells Toward a Retinal Lineage. *Stem Cells Transl Med* **5**, 417–426 (2016).

351. Deng, X.-Y. *et al.* Non-Viral Methods For Generating Integration-Free, Induced Pluripotent Stem Cells. *Curr Stem Cell Res Ther* **10**, 153 (2015).

352. Li, S. D. & Huang, L. Gene therapy progress and prospects: non-viral gene therapy by systemic delivery. *Gene Therapy 2006 13:18* **13**, 1313–1319 (2006).

353. Yin, H. *et al.* Non-viral vectors for gene-based therapy. *Nature Reviews Genetics 2014 15:8* **15**, 541–555 (2014).

354. Stadtfeld, M., Nagaya, M., Utikal, J., Weir, G. & Hochedlinger, K. Induced pluripotent stem cells generated without viral integration. *Science (1979)* **322**, 945–949 (2008).

355. Cao, X. *et al.* Non-Viral Co-Delivery of the Four Yamanaka Factors for Generation of Human Induced Pluripotent Stem Cells via Calcium Phosphate Nanocomposite Particles. *Adv Funct Mater* **23**, 5403–5411 (2013).

356. Qu, X., Liu, T., Song, K., Li, X. & Ge, D. Induced Pluripotent Stem Cells Generated from Human Adipose-Derived Stem Cells Using a Non-Viral Polycistronic Plasmid in Feeder-Free Conditions. *PLoS One* **7**, e48161 (2012).

357. Chen, F. *et al.* High-efficiency generation of induced pluripotent mesenchymal stem cells from human dermal fibroblasts using recombinant proteins. *Stem Cell Res Ther* **7**, 1–14 (2016).

358. Zhou, H. *et al.* Generation of Induced Pluripotent Stem Cells Using Recombinant Proteins. *Cell Stem Cell* **4**, 381–384 (2009).

359. Preskey, D., Allison, T. F., Jones, M., Mamchaoui, K. & Unger, C. Synthetically modified mRNA for efficient and fast human iPS cell generation and direct transdifferentiation to myoblasts. *Biochem Biophys Res Commun* **473**, 743–751 (2016).

360. Warren, L. *et al.* Highly efficient reprogramming to pluripotency and directed differentiation of human cells with synthetic modified mRNA. *Cell Stem Cell* **7**, 618–630 (2010).

361. Yakubov, E., Rechavi, G., Rozenblatt, S. & Givol, D. Reprogramming of human fibroblasts to pluripotent stem cells using mRNA of four transcription factors. *Biochem Biophys Res Commun* **394**, 189–193 (2010).

362. Poleganov, M. A. *et al.* Efficient Reprogramming of Human Fibroblasts and Blood-Derived Endothelial Progenitor Cells Using Nonmodified RNA for Reprogramming and Immune Evasion. *Hum Gene Ther* **26**, 751–766 (2015).

363. Wang, K. *et al.* Robust differentiation of human pluripotent stem cells into endothelial cells via temporal modulation of ETV2 with modified mRNA. *Sci Adv* **6**, (2020).

364. Hausburg, F. *et al.* Defining Optimized Properties of Modified mRNA to Enhance Virus- and DNA- Independent Protein Expression in Adult Stem Cells and Fibroblasts. *Cellular Physiology and Biochemistry* **35**, 1360–1371 (2015).

365. Lee, K. *et al.* Peptide-enhanced mRNA transfection in cultured mouse cardiac fibroblasts and direct reprogramming towards cardiomyocyte-like cells. *Int J Nanomedicine* **10**, 1841 (2015).

366. Xue, Y. *et al.* Synthetic mRNAs Drive Highly Efficient iPS Cell Differentiation to Dopaminergic Neurons. *Stem Cells Transl Med* **8**, 112 (2019).

367. Medvedev, S. P., Shevchenko, A. I. & Zakian, S. M. Induced Pluripotent Stem Cells: Problems and Advantages when Applying them in Regenerative Medicine. *Acta Naturae* **2**, 18 (2010).

368. Eguizabal, C., Montserrat, N., Veiga, A. & Carlos Izpisua Belmonte, J. Dedifferentiation, Transdifferentiation, and Reprogramming: Future Directions in Regenerative Medicine. (2013) doi:10.1055/s-0032-1331802.

369. Jopling, C., Boue, S. & Belmonte, J. C. I. Dedifferentiation, transdifferentiation and reprogramming: three routes to regeneration. *Nature Reviews Molecular Cell Biology 2011 12:2* **12**, 79–89 (2011).

370. Yoshioka, N. *et al.* Efficient Generation of Human iPS Cells by a Synthetic Self-Replicative RNA. *Cell Stem Cell* **13**, 246–254 (2013).

371. Koblas, T., Leontovyc, I., Loukotova, S., Kosinova, L. & Saudek, F. Reprogramming of Pancreatic Exocrine Cells AR42J Into Insulin-producing Cells Using mRNAs for Pdx1, Ngn3, and MafA Transcription Factors. *Mol Ther Nucleic Acids* **5**, e320 (2016).

372. Corritore, E. *et al.* V-Maf Musculoaponeurotic Fibrosarcoma Oncogene Homolog A Synthetic Modified mRNA Drives Reprogramming of Human Pancreatic Duct-Derived Cells Into Insulin-Secreting Cells. *Stem Cells Transl Med* **5**, 1525–1537 (2016).

373. Van Belle, T. L., Coppieters, K. T. & Von Herrath, M. G. Type 1 diabetes: Etiology, immunology, and therapeutic strategies. *Physiol Rev* **91**, 79–118 (2011).

374. Barton, F. B. *et al.* Improvement in Outcomes of Clinical Islet Transplantation: 1999–2010. *Diabetes Care* **35**, 1436–1445 (2012).

375. Orlando, G. *et al.* Cell Replacement Strategies Aimed at Reconstitution of the β-Cell Compartment in Type 1 Diabetes. *Diabetes* **63**, 1433–1444 (2014).

376. Akinci, E., Banga, A., Greder, L. V., Dutton, J. R. & Slack, J. M. W. Reprogramming of pancreatic exocrine cells towards a beta (β) cell character using Pdx1, Ngn3 and MafA. *Biochemical Journal* **442**, 539 (2012).

377. Rezania, A. *et al.* Maturation of human embryonic stem cell-derived pancreatic progenitors into functional islets capable of treating pre-existing diabetes in mice. *Diabetes* **61**, 2016–2029 (2012).

378. Aini, H. *et al.* Messenger RNA delivery of a cartilage-anabolic transcription factor as a disease-modifying strategy for osteoarthritis treatment OPEN. *Nature Publishing Group* (2015) doi:10.1038/srep18743.

379. Xia, S. *et al.* Coupled CRC 2D and ALI 3D Cultures Express Receptors of Emerging Viruses and Are More Suitable for the Study of Viral Infections Compared to Conventional Cell Lines. *Stem Cells Int* **2020**, (2020).

380. Hiemstra, P. S., Grootaers, G., van der Does, A. M., Krul, C. A. M. & Kooter, I. M. Human lung epithelial cell cultures for analysis of inhaled toxicants: Lessons learned and future directions. *Toxicol In Vitro* **47**, 137–146 (2018).

381. Kicic, A., Sutanto, E. N., Stevens, P. T., Knight, D. A. & Stick, S. M. Intrinsic biochemical and functional differences in bronchial epithelial cells of children with asthma. *Am J Respir Crit Care Med* **174**, 1110–1118 (2006).

382. Martinovich, K. M. *et al.* Conditionally reprogrammed primary airway epithelial cells maintain morphology, lineage and disease specific functional characteristics. *Sci Rep* **7**, (2017).

383. Stewart, C. E., Torr, E. E., Mohd Jamili, N. H., Bosquillon, C. & Sayers, I. Evaluation of differentiated human bronchial epithelial cell culture systems for asthma research. *J Allergy (Cairo)* **2012**, 1–11 (2012).

384. Gray, T. E., Guzman, K., Davis, C. W., Abdullah, L. H. & Nettesheim, P. Mucociliary differentiation of serially passaged normal human tracheobronchial epithelial cells. *Am J Respir Cell Mol Biol* **14**, 104–112 (1996).

385. Zhang, C. *et al.* Long-Term In Vitro Expansion of Epithelial Stem Cells Enabled by Pharmacological Inhibition of PAK1-ROCK-Myosin II and TGF-β Signaling. *Cell Rep* **25**, 598-610.e5 (2018).

386. Fulcher, M. L., Gabriel, S., Burns, K. A., Yankaskas, J. R. & Randell, S. H. Well-differentiated human airway epithelial cell cultures. *Methods Mol Med* **107**, 183–206 (2005).

387. Leung, C., Wadsworth, S. J., Jasemine Yang, S. & Dorscheid, D. R. Structural and functional variations in human bronchial epithelial cells cultured in air-liquid interface using different growth media. *Am J Physiol Lung Cell Mol Physiol* **318**, L1063–L1073 (2020).

388. Pezzulo, A. A. *et al.* The air-liquid interface and use of primary cell cultures are important to recapitulate the transcriptional profile of in vivo airway epithelia. *Am J Physiol Lung Cell Mol Physiol* **300**, 25–31 (2011).

389. Prytherch, Z. *et al.* Tissue-Specific stem cell differentiation in an in vitro airway model. *Macromol Biosci* **11**, 1467–1477 (2011).

390. Dvorak, A., Tilley, A. E., Shaykhiev, R., Wang, R. & Crystal, R. G. Do airway epithelium air-liquid cultures represent the in vivo airway epithelium transcriptome? *Am J Respir Cell Mol Biol* **44**, 465–473 (2011).

391. Palermo, L. M. *et al.* Human Parainfluenza Virus Infection of the Airway Epithelium: Viral Hemagglutinin-Neuraminidase Regulates Fusion Protein Activation and Modulates Infectivity. *J Virol* **83**, 6900 (2009).

392. Krunkosky, T. M., Jordan, J. L., Chambers, E. & Krause, D. C. Mycoplasma pneumoniae host-pathogen studies in an air-liquid culture of differentiated human airway epithelial cells. *Microb Pathog* **42**, 98–103 (2007).

393. Thaikoottathil, J. V. *et al.* Cigarette smoke extract reduces VEGF in primary human airway epithelial cells. *European Respiratory Journal* **33**, 835–843 (2009).

394. Comer, D. M., Kidney, J. C., Ennis, M. & Elborn, J. S. Airway epithelial cell apoptosis and inflammation in COPD, smokers and nonsmokers. *Eur Respir J* **41**, 1058–1067 (2013).

395. Ostrowski, L. E., Stewart, D. & Hazucha, M. Interferon γ Stimulates Accumulation of Gas Phase Nitric Oxide in Differentiated Cultures of Normal and Cystic Fibrosis Airway Epithelial Cells. *Lung* **190**, 563 (2012).

396. Jiang, A. Y. *et al.* Combinatorial development of nebulized mRNA delivery formulations for the lungs. *Nature Nanotechnology 2023* 1–12 (2023) doi:10.1038/s41565-023-01548-3.

397. Lin, H. *et al.* Air-liquid interface (ALI) culture of human bronchial epithelial cell monolayers as an in vitro model for airway drug transport studies. *J Pharm Sci* **96**, 341–350 (2007).

398. Kong, J. *et al.* Lung organoids, useful tools for investigating epithelial repair after lung injury. *Stem Cell Research & Therapy 2021 12:1* **12**, 1–13 (2021).

399. Chen, J. & Na, F. Organoid technology and applications in lung diseases: Models, mechanism research and therapy opportunities. *Front Bioeng Biotechnol* **10**, (2022).

400. Meyer-Berg, H. *et al.* Identification of AAV serotypes for lung gene therapy in human embryonic stem cell-derived lung organoids. *Stem Cell Res Ther* **11**, 1–6 (2020).

401. Tiwari, S. K., Wang, S., Smith, D., Carlin, A. F. & Rana, T. M. Revealing Tissue-Specific SARS-CoV-2 Infection and Host Responses using Human Stem Cell-Derived Lung and Cerebral Organoids. *Stem Cell Reports* **16**, 437–445 (2021).

402. Huh, D. *et al.* Reconstituting organ-level lung functions on a chip. *Science* **328**, 1662–1668 (2010).

403. Nawroth, J. C. *et al.* A Microengineered Airway Lung Chip Models Key Features of Viral-induced Exacerbation of Asthma. *Am J Respir Cell Mol Biol* **63**, 591–600 (2020).

404. Naldini, L. Gene therapy returns to centre stage. *Nature 2015 526:7573* **526**, 351–360 (2015).

405. Bessis, N., GarciaCozar, F. J. & Boissier, M. C. Immune responses to gene therapy vectors: influence on vector function and effector mechanisms. *Gene Therapy 2004 11:1* **11**, S10–S17 (2004).

406. Torchilin, V. P. Recent advances with liposomes as pharmaceutical carriers. *Nature Reviews Drug Discovery 2005 4:2* **4**, 145–160 (2005).

407. Malone, R. W., Felgner, P. L. & Verma, I. M. Cationic liposome-mediated RNA transfection. *Proc Natl Acad Sci U S A* **86**, 6077 (1989).

408. Tenchov, R., Bird, R., Curtze, A. E. & Zhou, Q. Lipid Nanoparticles□From Liposomes to mRNA Vaccine Delivery, a Landscape of Research Diversity and Advancement. (2021) doi:10.1021/acsnano.1c04996.

409. Li, M. *et al.* The nano delivery systems and applications of mRNA. *Eur J Med Chem* **227**, 113910 (2022).

410. Torchilin, V. P. Recent advances with liposomes as pharmaceutical carriers. *Nature Reviews Drug Discovery 2005 4:2* **4**, 145–160 (2005).

411. Landesman-Milo, D. & Peer, D. Toxicity profiling of several common RNAi-based nanomedicines: A comparative study. *Drug Deliv Transl Res* **4**, 96–103 (2014).

412. Ma, Z. *et al.* Cationic lipids enhance siRNA-mediated interferon response in mice. *Biochem Biophys Res Commun* **330**, 755–759 (2005).

413. Lurie, R. H. & Platanias, L. C. MECHANISMS OF TYPE□I□ AND TYPE□II□INTERFERON□MEDIATED SIGNALLING. (2005) doi:10.1038/nri1604.

414. Meng, C., Chen, Z., Li, G., Welte, T. & Shen, H. Nanoplatforms for mRNA Therapeutics. *Adv Ther (Weinh)* **4**, 2000099 (2021).

415. Kim, J., Eygeris, Y., Gupta, M. & Sahay, G. Self-assembled mRNA vaccines. *Adv Drug Deliv Rev* **170**, 83–112 (2021).

416. Hajj, K. A. & Whitehead, K. A. Tools for translation: non-viral materials for therapeutic mRNA delivery. (2017) doi:10.1038/natrevmats.2017.56.

417. Pardi, N., Hogan, M. J., Porter, F. W. & Weissman, D. mRNA vaccines — a new era in vaccinology. *Nature Reviews Drug Discovery 2018 17:4* **17**, 261–279 (2018).

418. Knop, K., Hoogenboom, R., Fischer, D. & Schubert, U. S. Poly(ethylene glycol) in Drug Delivery: Pros and Cons as Well as Potential Alternatives. *Angewandte Chemie International Edition* **49**, 6288–6308 (2010).

419. Akinc, A. *et al.* Development of Lipidoid–siRNA Formulations for Systemic Delivery to the Liver. *Molecular Therapy* **17**, 872–879 (2009).

420. Zhu, X. *et al.* Surface De-PEGylation Controls Nanoparticle-Mediated siRNA Delivery *In Vitro* and *In Vivo*. *Theranostics* **7**, 1990–2002 (2017).

421. Martinez-Pomares, L. The mannose receptor. *J Leukoc Biol* **92**, 1177–1186 (2012).

422. Geijtenbeek, T. B. H. *et al.* Identification of DC-SIGN, a Novel Dendritic Cell-Specific ICAM-3 Receptor that Supports Primary Immune Responses efficient T cell activation (Hernandez-Caselles et al., 1993). Indeed, antibody engagement of ICAM-3 results in elevation of intracellular calcium levels and induction of tyrosine phosphorylation (Juan et al The 2 integrins LFA-1 (L2) and D2 have both. *Cell* **100**, 575–585 (2000).

423. Jiang, W. *et al.* The receptor DEC-205 expressed by dendritic cells and thymic epithelial cells is involved in antigen processing. *Nature 1995 375:6527* **375**, 151–155 (1995).

424. Valladeau, J. *et al.* Langerin, a novel C-type lectin specific to langerhans cells, is an endocytic receptor that induces the formation of Birbeck granules. *Immunity* **12**, 71–81 (2000).

425. Veiga, N. *et al.* Cell specific delivery of modified mRNA expressing therapeutic proteins to leukocytes. *Nature Communications 2018 9:1* **9**, 1–9 (2018).

426. Lokugamage, M. P. *et al.* Optimization of lipid nanoparticles for the delivery of nebulized therapeutic mRNA to the lungs. *Nature Biomedical Engineering 2021 5:9* **5**, 1059–1068 (2021).

427. Sago, C. D., Krupczak, B. R., Lokugamage, M. P., Gan, Z. & Dahlman, J. E. Cell Subtypes Within the Liver Microenvironment Differentially Interact with Lipid Nanoparticles. *Cell Mol Bioeng* **12**, 389 (2019).

428. Adams, D. *et al.* Patisiran, an RNAi Therapeutic, for Hereditary Transthyretin Amyloidosis. *New England Journal of Medicine* **379**, 11–21 (2018).

429. Anderson, E. J. *et al.* Safety and Immunogenicity of SARS-CoV-2 mRNA-1273 Vaccine in Older Adults. *N Engl J Med* **383**, 2427–2438 (2020).

430. Corbett, K. S. *et al.* Evaluation of the mRNA-1273 Vaccine against SARS-CoV-2 in Nonhuman Primates. *New England Journal of Medicine* **383**, 1544–1555 (2020).

431. Corbett, K. S. *et al.* SARS-CoV-2 mRNA vaccine design enabled by prototype pathogen preparedness. *Nature* **586**, 567–571 (2020).

432. Walsh, E. E. *et al.* Safety and Immunogenicity of Two RNA-Based Covid-19 Vaccine Candidates. *N Engl J Med* **383**, 2439–2450 (2020).

433. Schoenmaker, L. *et al.* mRNA-lipid nanoparticle COVID-19 vaccines: Structure and stability. *Int J Pharm* **601**, 120586 (2021).

434. Boussif, O. *et al.* A versatile vector for gene and oligonucleotide transfer into cells in culture and in vivo: polyethylenimine. *Proceedings of the National Academy of Sciences* **92**, 7297–7301 (1995).

435. Lungwitz, U., Breunig, M., Blunk, T. & Göpferich, A. Polyethylenimine-based non-viral gene delivery systems. *European Journal of Pharmaceutics and Biopharmaceutics* **60**, 247–266 (2005).

436. Akinc, A., Thomas, M., Klibanov, A. M. & Langer, R. Exploring polyethylenimine-mediated DNA transfection and the proton sponge hypothesis. *J Gene Med* **7**, 657–663 (2005).

437. Behr, J. P. Gene Transfer with Synthetic Cationic Amphiphiles: Prospects for Gene Therapy. *Bioconjug Chem* **5**, 382–389 (1994).

438. Lv, H., Zhang, S., Wang, B., Cui, S. & Yan, J. Toxicity of cationic lipids and cationic polymers in gene delivery. *Journal of Controlled Release* **114**, 100–109 (2006).

439. Li, M. *et al.* Enhanced intranasal delivery of mRNA vaccine by overcoming the nasal epithelial barrier via intra- and paracellular pathways. *Journal of Controlled Release* **228**, 9–19 (2016).

440. Mahiny, A. J. *et al.* In vivo genome editing using nuclease-encoding mRNA corrects SP-B deficiency. (2015) doi:10.1038/nbt.3241.

441. Derraz, M. *et al.* Extraction and Physicochemical Characterization of an Environmentally Friendly Biopolymer: Chitosan for Composite Matrix Application. *Journal of Composites Science 2023, Vol. 7, Page 260* **7**, 260 (2023).

442. Ardean, C. *et al.* Factors Influencing the Antibacterial Activity of Chitosan and Chitosan Modified by Functionalization. *Int J Mol Sci* **22**, (2021).

443. Galli, G., Laus, M., Angeloni, A. S., Ferruti, P. & Chiellini, E. Thermotropic poly(β-aminoester)s containing azoxy groups. *Die Makromolekulare Chemie, Rapid Communications* **4**, 681–686 (1983).

444. Lynn, D. M. & Langer, R. Degradable Poly(β-amino esters): Synthesis, Characterization, and Self-Assembly with Plasmid DNA. *J Am Chem Soc* **122**, 10761–10768 (2000).

445. Zhang, Y., Satterlee, A. & Huang, L. In vivo gene delivery by nonviral vectors: Overcoming hurdles. *Molecular Therapy* **20**, 1298–1304 (2012).

446. Kaczmarek, J. C. *et al.* Optimization of a Degradable Polymer-Lipid Nanoparticle for Potent Systemic Delivery of mRNA to the Lung Endothelium and Immune Cells. *Nano Lett* **18**, 6449–6454 (2018).

447. Kaczmarek, J. C. *et al.* Systemic delivery of mRNA and DNA to the lung using polymer-lipid nanoparticles. *Biomaterials* **275**, 120966 (2021).

448. Kaczmarek, J. C. *et al.* Polymer–Lipid Nanoparticles for Systemic Delivery of mRNA to the Lungs. *Angewandte Chemie International Edition* **55**, 13808–13812 (2016).

449. Patel, A. K. *et al.* Inhaled Nanoformulated mRNA Polyplexes for Protein Production in Lung Epithelium. *Adv Mater* **31**, e1805116 (2019).

450. Blanchard, E. L., Vanover, D., Subhash Bawage, S. & Munnilal Tiwari, P. Treatment of influenza and SARS-CoV-2 infections via mRNA-encoded Cas13a in rodents. *Nat Biotechnol* doi:10.1038/s41587-021-00822-w.

451. Fields, R. J. *et al.* Surface modified poly(β amino ester)-containing nanoparticles for plasmid DNA delivery. *J Control Release* **164**, 41–48 (2012).

452. Andorko, J. I., Hess, K. L., Pineault, K. G. & Jewell, C. M. Intrinsic immunogenicity of rapidly-degradable polymers evolves during degradation. *Acta Biomater* **32**, 24 (2016).

453. Dold, N. M., Zeng, Q., Zeng, X. & Jewell, C. M. "A poly(beta-amino ester) activates macrophages independent of NF-κB signaling". *Acta Biomater* **68**, 168 (2018).

454. Valadi, H. *et al.* Exosome-mediated transfer of mRNAs and microRNAs is a novel mechanism of genetic exchange between cells. *Nature Cell Biology 2007 9:6* **9**, 654–659 (2007).

455. Skog, J. *et al.* Glioblastoma microvesicles transport RNA and proteins that promote tumour growth and provide diagnostic biomarkers. *Nature Cell Biology 2008 10:12* **10**, 1470–1476 (2008).

456. Bu, T. *et al.* Exosome-mediated delivery of inflammation-responsive *Il-10* mRNA for controlled atherosclerosis treatment. *Theranostics* **11**, 9988–10000 (2021).

457. Yang, J. *et al.* Therapeutic Effects of Simultaneous Delivery of Nerve Growth Factor mRNA and Protein via Exosomes on Cerebral Ischemia. *Mol Ther Nucleic Acids* **21**, 512 (2020).

458. Gómez-Aguado, I. *et al.* Nanomedicines to Deliver mRNA: State of the Art and Future Perspectives. *Nanomaterials 2020, Vol. 10, Page 364* **10**, 364 (2020).

459. Eltoukhy, A. A., Chen, D., Alabi, C. A., Langer, R. & Anderson, D. G. Degradable Terpolymers with Alkyl Side Chains Demonstrate Enhanced Gene Delivery Potency and Nanoparticle Stability. *Advanced Materials* **25**, 1487–1493 (2013).

460. Fornaguera, C. *et al.* In Vivo Retargeting of Poly(beta aminoester) (OM-PBAE) Nanoparticles is Influenced by Protein Corona. *Adv Healthc Mater* **8**, 1900849 (2019).

461. Fornaguera, C. *et al.* mRNA Delivery System for Targeting Antigen-Presenting Cells In Vivo. *Adv Healthc Mater* **7**, 1800335 (2018).

462. Duran-Mota, J. A., Yani, J. Q., Almquist, B. D., Borrós, S. & Oliva, N. Polyplex-Loaded Hydrogels for Local Gene Delivery to Human Dermal Fibroblasts. *ACS Biomater Sci Eng* **7**, 4347–4361 (2021).

463. Patel, A. K. *et al.* Inhaled Nanoformulated mRNA Polyplexes for Protein Production in Lung Epithelium. *Advanced Materials* **31**, 1805116 (2019).

464. Qin, S. *et al.* mRNA-based therapeutics: powerful and versatile tools to combat diseases. *Signal Transduction and Targeted Therapy 2022 7:1* **7**, 1–35 (2022).

465. Weng, Y. *et al.* The challenge and prospect of mRNA therapeutics landscape. *Biotechnol Adv* **40**, (2020).

466. Lynn, D. M. & Langer, R. Degradable poly(β-amino esters): Synthesis, characterization, and self-assembly with plasmid DNA. *J Am Chem Soc* **122**, 10761–10768 (2000).

467. Cordeiro, R. A., Serra, A., Coelho, J. F. J. & Faneca, H. Poly(β-amino ester)-based gene delivery systems: From discovery to therapeutic applications. *J Control Release* **310**, 155–187 (2019).

468. Rui, Y. *et al.* High-throughput and high-content bioassay enables tuning of polyester nanoparticles for cellular uptake, endosomal escape, and systemic in vivo delivery of mRNA. *Sci Adv* **8**, (2022).

469. Kaczmarek, J. C. *et al.* Optimization of a Degradable Polymer−Lipid Nanoparticle for Potent Systemic Delivery of mRNA to the Lung Endothelium and Immune Cells. (2018) doi:10.1021/acs.nanolett.8b02917.

470. Kaczmarek, J. C. *et al.* Polymer–Lipid Nanoparticles for Systemic Delivery of mRNA to the Lungs. *Angewandte Chemie International Edition* **55**, 13808–13812 (2016).

471. Kaczmarek, J. C. *et al.* Systemic delivery of mRNA and DNA to the lung using polymer-lipid nanoparticles. *Biomaterials* **275**, (2021).

472. Karlsson, J., Rhodes, K. R., Green, J. J. & Tzeng, S. Y. Poly(beta-amino ester)s as gene delivery vehicles: challenges and opportunities. *Expert Opin Drug Deliv* **17**, (2020).

473. Green, J. J., Langer, R. & Anderson, D. G. A combinatorial polymer library approach yields insight into nonviral gene delivery. *Acc Chem Res* **41**, 749–759 (2008).

474. Navalón-López, M., Dols-Perez, A., Grijalvo, S., Fornaguera, C. & Borrós, S. Unravelling the role of individual components in pBAE/polynucleotide polyplexes in the synthesis of tailored carriers for specific applications: on the road to rational formulations. *Nanoscale Adv* **5**, 1611–1623 (2023).

475. Schaffer, D. V, Fidelman, N. A., Dan, N. & Lauffenburger, D. A. Vector Unpacking as a Potential Barrier for Receptor-Mediated Polyplex Gene Delivery. (2000) doi:10.1002/(SICI)1097-0290(20000305)67:5.

476. Tsai, S. J., Andorko, J. I., Zeng, X., Gammon, J. M. & Jewell, C. M. Polyplex interaction strength as a driver of potency during cancer immunotherapy. *Nano Res* **11**, 5642–5656 (2018).

477. Wilson, D. R. *et al.* Biodegradable STING agonist nanoparticles for enhanced cancer immunotherapy. *Nanomedicine* **14**, 237–246 (2018).

478. Sunshine, J. C., Peng, D. Y. & Green, J. J. Uptake and transfection with polymeric nanoparticles are dependent on polymer end-group structure, but largely independent of nanoparticle physical and chemical properties. *Mol Pharm* **9**, 3375–3383 (2012).

479. Fornaguera, C., Castells-Sala, C., Lázaro, M. A., Cascante, A. & Borrós, S. Development of an optimized freeze-drying protocol for OM-PBAE nucleic acid polyplexes. *Int J Pharm* **569**, 118612 (2019).

480. Wilson, D. R. *et al.* The role of assembly parameters on polyplex poly (beta-amino ester) nanoparticle transfections. (2019) doi:10.1002/bit.26921.

481. Chivu, A. *et al.* Cellular gene delivery via poly(hexamethylene biguanide)/pDNA self-assembled nanoparticles. *Eur J Pharm Biopharm* **158**, 62–71 (2021).

482. Anderson, D. G., Lynn, D. M. & Langer, R. Semi-automated synthesis and screening of a large library of degradable cationic polymers for gene delivery. *Angew Chem Int Ed Engl* **42**, 3153–3158 (2003).

483. Mosquera, J., García, I. & Liz-Marzán, L. M. Cellular Uptake of Nanoparticles versus Small Molecules: A Matter of Size. *Acc Chem Res* **51**, 2305–2313 (2018).

484. Liu, Q., Guan, J., Qin, L., Zhang, X. & Mao, S. Physicochemical properties affecting the fate of nanoparticles in pulmonary drug delivery. *Drug Discov Today* **25**, 150–159 (2020).

485. Xu, L. & Anchordoquy, T. Drug Delivery Trends in Clinical Trails and Translational Medicine: challenges and opportunities in the delivery of nucleic acid-based therapeutics. *J Pharm Sci* **100**, 38 (2011).

486. Mendes, B. B. *et al.* Nanodelivery of nucleic acids. *Nature Reviews Methods Primers 2022 2:1* **2**, 1–21 (2022).

487. Salatin, S., Maleki Dizaj, S. & Yari Khosroushahi, A. Effect of the surface modification, size, and shape on cellular uptake of nanoparticles. *Cell Biol Int* **39**, 881–890 (2015).

488. Anderson, D. G., Akinc, A., Hossain, N. & Langer, R. Structure/property studies of polymeric gene delivery using a library of poly(beta-amino esters). *Mol Ther* **11**, 426–434 (2005).

489. Sousa De Almeida, M. *et al.* Understanding nanoparticle endocytosis to improve targeting strategies in nanomedicine. *Chem Soc Rev* **50**, 5397–5434 (2021).

490. Mott, L., Akers, C. & Pack, D. W. Effect of polyplex surface charge on cellular internalization and intracellular trafficking. *J Drug Deliv Sci Technol* **84**, 104465 (2023).

491. Karlsson, J., Rhodes, K. R., Green, J. J. & Tzeng, S. Y. Poly(beta-amino ester)s as gene delivery vehicles: challenges and opportunities. *Expert Opin Drug Deliv* **17**, 1395 (2020).

492. Castellani, S., Di Gioia, S., di Toma, L. & Conese, M. Human Cellular Models for the Investigation of Lung Inflammation and Mucus Production in Cystic Fibrosis. *Anal Cell Pathol (Amst)* **2018**, (2018).

493. Ross, A. J., Dailey, L. A., Brighton, L. E. & Devlin, R. B. Transcriptional Profiling of Mucociliary Differentiation in Human Airway Epithelial Cells. *https://doi.org/10.1165/rcmb.2006-0466OC* **37**, 169–185 (2012).

494. Pezzulo, A. A. *et al.* The air-liquid interface and use of primary cell cultures are important to recapitulate the transcriptional profile of in vivo airway epithelia. *Am J Physiol Lung Cell Mol Physiol* **300**, 25–31 (2011).

495. Baldassi, D., Gabold, B. & Merkel, O. M. Air−Liquid Interface Cultures of the Healthy and Diseased Human Respiratory Tract: Promises, Challenges, and Future Directions. *Adv Nanobiomed Res* **1**, 2000111 (2021).

496. Ferrari, S., Geddes, D. M. & Alton, E. W. F. W. Barriers to and new approaches for gene therapy and gene delivery in cystic fibrosis. *Adv Drug Deliv Rev* **54**, 1373 (2002).

497. Zabner, J., Fasbender, A. J., Moninger, T., Poellinger, K. A. & Welsh, M. J. Cellular and molecular barriers to gene transfer by a cationic lipid. *J Biol Chem* **270**, 18997–19007 (1995).

498. Caci, E. *et al.* Epithelial sodium channel inhibition in primary human bronchial epithelia by transfected siRNA. *Am J Respir Cell Mol Biol* **40**, 211–216 (2009).

499. Griesenbach, U. *et al.* Inefficient cationic lipid-mediated siRNA and antisense oligonucleotide transfer to airway epithelial cells in vivo. *Respir Res* **7**, 26–26 (2006).

500. Krishnamurthy, S. *et al.* Manipulation of Cell Physiology Enables Gene Silencing in Well-differentiated Airway Epithelia. *Mol Ther Nucleic Acids* **1**, e41 (2012).

501. Platz, J. *et al.* Application of small interfering RNA (siRNA) for modulation of airway epithelial gene expression. *Oligonucleotides* **15**, 132–138 (2005).

502. Bartman, C. M., Stelzig, K. E., Linden, D. R., Prakash, Y. S. & Chiarella, S. E. Passive siRNA transfection method for gene knockdown in air-liquid interface airway epithelial cell cultures. (2021) doi:10.1152/ajplung.00122.2021.

503. Highly efficient genome editing in primary human bronchial epithelial cells differentiated at air-liquid interface. doi:10.1183/13993003.00950-2019.

504. Kulkarni, J. A. *et al.* The current landscape of nucleic acid therapeutics. *Nature Nanotechnology 2021 16:6* **16**, 630–643 (2021).

505. Patel, A. K. *et al.* CommuniCation 1805116 (1 of 7) Inhaled Nanoformulated mRNA Polyplexes for Protein Production in Lung Epithelium. (2019) doi:10.1002/adma.201805116.

506. Green, J. J., Zugates, G. T., Langer, R. & Anderson, D. G. Poly (β-amino esters): Procedures for Synthesis and Gene Delivery. *Methods Mol Biol* **480**, 53 (2009).

507. Callaghan, P. J., Ferrick, B., Rybakovsky, E., Thomas, S. & Mullin, J. M. Epithelial barrier function properties of the 16HBE14o- human bronchial epithelial cell culture model. *Biosci Rep* **40**, 20201532 (2020).

508. Callaghan, P. J., Rybakovsky, E., Ferrick, B., Thomas, S. & Mullin, J. M. Retinoic acid improves baseline barrier function and attenuates TNF-α-induced barrier leak in human bronchial epithelial cell culture model, 16HBE 14o-. *PLoS One* **15**, e0242536 (2020).

509. Evans, M. J., Van Winkle, L. S., Fanucchi, M. V. & Plopper, C. G. Cellular and molecular characteristics of basal cells in airway epithelium. *Exp Lung Res* **27**, 401–415 (2001).

510. Purkis, P. E. *et al.* Antibody markers of basal cells in complex epithelia. *J Cell Sci* **97 (Pt 1)**, 39–50 (1990).

511. Yan, Y. *et al.* Non-viral vectors for RNA delivery. *Journal of Controlled Release* **342**, 241 (2022).

512. Sang, Y. *et al.* Salt ions and related parameters affect PEI–DNA particle size and transfection efficiency in Chinese hamster ovary cells. *Cytotechnology* **67**, 67 (2015).

513. SY, T., PH, Y., WL, G. & JJ, G. Synthetic poly(ester amine) and poly(amido amine) nanoparticles for efficient DNA and siRNA delivery to human endothelial cells. *Int J Nanomedicine* **6**, 3309 (2011).

514. Maurisse, R. *et al.* Comparative transfection of DNA into primary and transformed mammalian cells from different lineages. *BMC Biotechnol* **10**, 9 (2010).

515. Routkevitch, D. *et al.* Efficiency of Cytosolic Delivery with Poly(beta-amino ester) Nanoparticles is Dependent on the Effective pKa of the Polymer. *ACS Biomater Sci Eng* **6**, 3411 (2020).

516. M. Pavan, G. *et al.* Role of generation, architecture, pH and ionic strength on successful siRNA delivery and transfection by hybrid PPV-PAMAM dendrimers. *Curr Med Chem* **19**, 4929–4941 (2012).

517. Wiethoff, C. M. & Middaugh, C. R. Barriers to nonviral gene delivery. *J Pharm Sci* **92**, 203–217 (2003).

518. Evans, M. J., Van Winkle, L. S., Fanucchi, M. V. & Plopper, C. G. Cellular and molecular characteristics of basal cells in airway epithelium. *Exp Lung Res* **27**, 401–415 (2001).

519. Rock, J. R., Randell, S. H. & Hogan, B. L. M. Airway basal stem cells: a perspective on their roles in epithelial homeostasis and remodeling. *Dis Model Mech* **3**, 545 (2010).

520. Rock, J. R. *et al.* Basal cells as stem cells of the mouse trachea and human airway epithelium. *Proc Natl Acad Sci U S A* **106**, 12771–12775 (2009).

521. Ruysseveldt, E., Martens, K. & Steelant, B. Airway Basal Cells, Protectors of Epithelial Walls in Health and Respiratory Diseases. *Frontiers in Allergy* **2**, 787128 (2021).

522. Purkis, P. E. *et al.* Antibody markers of basal cells in complex epithelia. *J Cell Sci* **97 (Pt 1)**, 39–50 (1990).

523. Baldassi, D., Gabold, B. & Merkel, O. M. Air-liquid interface cultures of the healthy and diseased human respiratory tract: promises, challenges and future directions. *Adv Nanobiomed Res* **1**, 2000111 (2021).

524. Garcıá, S. R. *et al.* Novel dynamics of human mucociliary differentiation revealed by single-cell RNA sequencing of nasal epithelial cultures. *Development (Cambridge)* **146**, (2019).

525. Hovenberg, H. W., Davies, J. R., Herrmann, A., Lindén, C. J. & Carlstedt, I. MUC5AC, but not MUC2, is a prominent mucin in respiratory secretions. *Glycoconj J* **13**, 839–847 (1996).

526. Schamberger, A. C., Staab-Weijnitz, C. A., Mise-Racek, N. & Eickelberg, O. Cigarette smoke alters primary human bronchial epithelial cell differentiation at the air-liquid interface. *Scientific Reports 2015 5:1* **5**, 1–9 (2015).

527. Balda, M. S. & Matter, K. The tight junction protein ZO-1 and an interacting transcription factor regulate ErbB-2 expression. *EMBO J* **19**, 2024 (2000).

528. Srinivasan, B. *et al.* TEER measurement techniques for in vitro barrier model systems. *J Lab Autom* **20**, 107–126 (2015).

529. Glass, K. *et al.* Integrative epigenomic analysis in differentiated human primary bronchial epithelial cells exposed to cigarette smoke. *Sci Rep* **8**, (2018).

530. Rayner, R. E., Makena, P., Prasad, G. L. & Cormet-Boyaka, E. Optimization of Normal Human Bronchial Epithelial (NHBE) Cell 3D Cultures for in vitro Lung Model Studies. *Sci Rep* **9**, (2019).

531. Elbrecht, D. H., Long, C. J. & Hickman, J. J. Transepithelial/endothelial Electrical Resistance (TEER) theory and ap-plications for microfluidic body-on-a-chip devices Keywords TEER Body-on-a-chip Barrier tissue Blood-brain barrier Organ Endothelial cells Epithelial cells Human-on-a-chip. *J Rare Dis Res Treat* **1**, 46–52 (2016).

532. Frost, T. S., Jiang, L. & Zohar, Y. Pharmacokinetic Analysis of Epithelial/Endothelial Cell Barriers in Microfluidic Bilayer Devices with an Air-Liquid Interface. *Micromachines (Basel)* **11**, (2020).

533. Heijink, I. H. *et al.* Characterisation of cell adhesion in airway epithelial cell types using electric cell-substrate impedance sensing. *Eur Respir J* **35**, 894–903 (2010).

534. Buckley, A. G. *et al.* Visualisation of Multiple Tight Junctional Complexes in Human Airway Epithelial Cells. *Biol Proced Online* **20**, 1–9 (2018).

535. Porchet, N. *et al.* Human mucin genes: genomic organization and expression of MUC4, MUC5AC and MUC5B. *Biochem Soc Trans* **23**, 800–805 (1995).

536. Zhu, L. *et al.* The club cell marker SCGB1A1 downstream of FOXA2 is reduced in asthma. *Am J Respir Cell Mol Biol* **60**, 695–704 (2019).

537. You, Y. *et al.* Role of f-box factor foxj1 in differentiation of ciliated airway epithelial cells. *Am J Physiol Lung Cell Mol Physiol* **286**, (2004).

538. Bustamante-Marin, X. M. & Ostrowski, L. E. Cilia and Mucociliary Clearance. doi:10.1101/cshperspect.a028241.

539. Brekman, A., Walters, M. S., Tilley, A. E. & Crystal, R. G. ORIGINAL RESEARCH FOXJ1 Prevents Cilia Growth Inhibition by Cigarette Smoke in Human Airway Epithelium In Vitro. (2014) doi:10.1165/rcmb.2013-0363OC.

540. Salathe, M. Regulation of mammalian ciliary beating. *Annu Rev Physiol* **69**, 401–422 (2007).

541. Ishikawa, T. Axoneme Structure from Motile Cilia. *Cold Spring Harb Perspect Biol* **9**, (2017).

542. Vertii, A., Hung, H. F., Hehnly, H. & Doxsey, S. Human basal body basics. *Cilia* **5**, 1–7 (2016).

543. Stoltz, D. A., Meyerholz, D. K. & Welsh, M. J. Origins of cystic fibrosis lung disease. *N Engl J Med* **372**, 351–362 (2015).

544. Santamaria, F. *et al.* Structural and functional lung disease in primary ciliary dyskinesia. *Chest* **134**, 351–357 (2008).

545. Lobo, L. J., Zariwala, M. A. & Noone, P. G. Primary ciliary dyskinesia. *QJM* **107**, 691–699 (2014).

546. Horani, A., Ferkol, T. W., Dutcher, S. K. & Brody, S. L. Genetics and biology of primary ciliary dyskinesia. *Paediatr Respir Rev* **18**, 18–24 (2016).

547. Ehre, C., Ridley, C. & Thornton, D. J. Cystic fibrosis: an inherited disease affecting mucin-producing organs. *Int J Biochem Cell Biol* **52**, 136–145 (2014).

548. Cutting, G. R. Cystic fibrosis genetics: from molecular understanding to clinical application. *Nat Rev Genet* **16**, 45–56 (2015).

549. Hirst, R. A. *et al.* Culture of Primary Ciliary Dyskinesia Epithelial Cells at Air-Liquid Interface Can Alter Ciliary Phenotype but Remains a Robust and Informative Diagnostic Aid. *PLoS One* **9**, e89675 (2014).

550. Lucas, J. S. *et al.* European Respiratory Society guidelines for the diagnosis of primary ciliary dyskinesia. *European Respiratory Journal* **49**, (2017).

551. Grosse-Onnebrink, J. *et al.* Effect of TH2 cytokines and interferon gamma on beat frequency of human respiratory cilia. *Pediatr Res* **79**, 731–735 (2016).

552. Tamashiro, E. *et al.* Cigarette smoke exposure impairs respiratory epithelial ciliogenesis. *Am J Rhinol Allergy* **23**, 117–122 (2009).

553. Yaghi, A. & Dolovich, M. B. Airway Epithelial Cell Cilia and Obstructive Lung Disease. *Cells* **5**, (2016).

554. Montefort, S., Djukanovic, R., Holgate, S. T. & Roche, W. R. Ciliated cell damage in the bronchial epithelium of asthmatics and non-asthmatics. *Clin Exp Allergy* **23**, 185–189 (1993).

555. S, M., WR, R. & ST, H. Bronchial epithelial shedding in asthmatics and non-asthmatics. *Respir Med* **87 Suppl B**, 9–11 (1993).

556. Thomas, B. *et al.* Ciliary dysfunction and ultrastructural abnormalities are features of severe asthma. *J Allergy Clin Immunol* **126**, (2010).

557. Ancel, J. *et al.* Impaired ciliary beat frequency and ciliogenesis alteration during airway epithelial cell differentiation in COPD. *Diagnostics* **11**, (2021).

558. Que, J., Luo, X., Schwartz, R. J. & Hogan, B. L. M. Multiple roles for Sox2 in the developing and adult mouse trachea. *Development* **136**, 1899 (2009).

559. Hogan, B. L. M. *et al.* Repair and regeneration of the respiratory system: complexity, plasticity, and mechanisms of lung stem cell function. *Cell Stem Cell* **15**, 123 (2014).

560. Daniely, Y. *et al.* Critical role of p63 in the development of a normal esophageal and tracheobronchial epithelium. *Am J Physiol Cell Physiol* **287**, (2004).

561. Rock, J. R. & Hogan, B. L. M. Epithelial progenitor cells in lung development, maintenance, repair, and disease. *Annu Rev Cell Dev Biol* **27**, 493–512 (2011).

562. Rock, J. R. *et al.* Notch-dependent differentiation of adult airway basal stem cells. *Cell Stem Cell* **8**, 639–648 (2011).

563. Morimoto, M., Nishinakamura, R., Saga, Y. & Kopan, R. Different assemblies of Notch receptors coordinate the distribution of the major bronchial Clara, ciliated and neuroendocrine cells. *Development* **139**, 4365–4373 (2012).

564. Arbi, M., Pefani, D. E., Taraviras, S. & Lygerou, Z. Controlling centriole numbers: Geminin family members as master regulators of centriole amplification and multiciliogenesis. *Chromosoma* **127**, 151–174 (2018).

565. Ma, L., Quigley, I., Omran, H. & Kintner, C. Multicilin drives centriole biogenesis via E2f proteins. *Genes Dev* **28**, 1461–1471 (2014).

566. Terré, B. *et al.* GEMC1 is a critical regulator of multiciliated cell differentiation. *EMBO J* **35**, 942–960 (2016).

567. Lu, H. *et al.* Mcidas mutant mice reveal a two-step process for the specification and differentiation of multiciliated cells in mammals. *Development (Cambridge)* **146**, (2019).

568. Lewis, M. & Stracker, T. H. Transcriptional regulation of multiciliated cell differentiation. *Semin Cell Dev Biol* **110**, 51–60 (2021).

569. Marshall, C. B. *et al.* P73 Is Required for Multiciliogenesis and Regulates the Foxj1-Associated Gene Network. *Cell Rep* **14**, 2289–2300 (2016).

570. Nemajerova, A. *et al.* Non-oncogenic roles of TAp73: from multiciliogenesis to metabolism. *Cell Death & Differentiation 2018 25:1* **25**, 144–153 (2017).

571. Brooks, E. R. & Wallingford, J. B. Multiciliated Cells. *Current Biology* **24**, R973–R982 (2014).

572. Tan, F. E. *et al.* Myb promotes centriole amplification and later steps of the multiciliogenesis program. *Development* **140**, 4277–4286 (2013).

573. Wallmeier, J. *et al.* Mutations in CCNO result in congenital mucociliary clearance disorder with reduced generation of multiple motile cilia. *Nature Genetics 2014 46:6* **46**, 646–651 (2014).

574. Boon, M. *et al.* MCIDAS mutations result in a mucociliary clearance disorder with reduced generation of multiple motile cilia. *Nature Communications 2014 5:1* **5**, 1–8 (2014).

575. Didon, L. *et al.* RFX3 Modulation of FOXJ1 regulation of cilia genes in the human airway epithelium. *Respir Res* **14**, 1–13 (2013).

576. Plasschaert, L. W. *et al.* A single-cell atlas of the airway epithelium reveals the CFTR-rich pulmonary ionocyte. *Nature 2018 560:7718* **560**, 377–381 (2018).

577. Zhou, F. *et al.* Gmnc Is a Master Regulator of the Multiciliated Cell Differentiation Program. *Current Biology* **25**, 3267–3273 (2015).

578. Brody, S. L., Yan, X. H., Wuerffel, M. K., Song, S. K. & Shapiro, S. D. Ciliogenesis and Left–Right Axis Defects in Forkhead Factor HFH-4–Null Mice. *https://doi.org/10.1165/ajrcmb.23.1.4070* **23**, 45–51 (2012).

579. Chen, J., Knowles, H. J., Hebert, J. L. & Hackett, B. P. Mutation of the mouse hepatocyte nuclear factor/forkhead homologue 4 gene results in an absence of cilia and random left-right asymmetry. *J Clin Invest* **102**, 1077–1082 (1998).

580. Gomperts, B. N., Gong-Cooper, X. & Hackett, B. P. Foxj1 regulates basal body anchoring to the cytoskeleton of ciliated pulmonary epithelial cells. *J Cell Sci* **117**, 1329–1337 (2004).

581. You, Y. *et al.* Role of f-box factor foxj1 in differentiation of ciliated airway epithelial cells. *Am J Physiol Lung Cell Mol Physiol* **286**, (2004).

582. Stubbs, J. L., Oishi, I., Carlos Izpisú A Belmonte, J. & Kintner, C. The forkhead protein Foxj1 specifies node-like cilia in Xenopus and zebrafish embryos. (2008) doi:10.1038/ng.267.

583. Yu, X., Ng, C. P., Habacher, H. & Roy, S. Foxj1 transcription factors are master regulators of the motile ciliogenic program. *Nature Genetics 2008 40:12* **40**, 1445–1453 (2008).

584. Stubbs, J. L., Oishi, I., Izpisúa Belmonte, J. C. & Kintner, C. The Forkhead protein, FoxJ1, specifies node-like cilia in Xenopus and Zebrafish embryos. *Nat Genet* **40**, 1454 (2008).

585. Blatt, E. N., Yan, X. H., Wuerffel, M. K., Hamilos, D. L. & Brody, S. L. Forkhead Transcription Factor HFH-4 Expression Is Temporally Related to Ciliogenesis. *https://doi.org/10.1165/ajrcmb.21.2.3691* **21**, 168–176 (2012).

586. Look, D. C. *et al.* Effects of paramyxoviral infection on airway epithelial cell foxj1 expression, ciliogenesis, and mucociliary function. *American Journal of Pathology* **159**, 2055–2069 (2001).

587. Tristram, D. A., Hicks, W. & Hard, R. Respiratory Syncytial Virus and Human Bronchial Epithelium. *Arch Otolaryngol Head Neck Surg* **124**, 777–783 (1998).

588. Ostrowski, L. E., Hutchins, J. R., Zakel, K. & O'Neal, W. K. Targeting expression of a transgene to the airway surface epithelium using a ciliated cell-specific promoter. *Molecular Therapy* **8**, 637–645 (2003).

589. Foxj1 regulates floor plate cilia architecture and modifiesthe response of cells to sonic hedgehog signalling. (2010) doi:10.1242/dev.051714.

590. Choksi, S. P., Lauter, G., Swoboda, P. & Roy, S. Switching on cilia: transcriptional networks regulating ciliogenesis. *Development* **141**, 1427–1441 (2014).

591. Mukherjee, I., Roy, S. & Chakrabarti, S. Identification of important effector proteins in the FOXJ1 transcriptional network associated with ciliogenesis and ciliary function. *Front Genet* **10**, 416138 (2019).

592. Rapiteanu, R. *et al.* Highly efficient genome editing in primary human bronchial epithelial cells differentiated at air–liquid interface. *European Respiratory Journal* **55**, (2020).

593. Zahid, M. *et al.* Rapid Ex-Vivo Ciliogenesis and Dose-Dependent Effect of Notch Inhibition on Ciliogenesis of Respiratory Epithelia. *Biomolecules 2020, Vol. 10, Page 1182* **10**, 1182 (2020).

594. Didon, L. *et al.* RFX3 Modulation of FOXJ1 regulation of cilia genes in the human airway epithelium. (2013) doi:10.1186/1465-9921-14-70.

595. Sahin, U., Karikó, K. & Türeci, Ö. mRNA-based therapeutics — developing a new class of drugs. *Nature Publishing Group* (2014) doi:10.1038/nrd4278.

596. Watson, J. K. *et al.* Clonal Dynamics Reveal Two Distinct Populations of Basal Cells in Slow-Turnover Airway Epithelium. *Cell Rep* **12**, 90–101 (2015).

597. Rawlins, E. L. *et al.* The Role of Scgb1a1+ Clara Cells in the Long-Term Maintenance and Repair of Lung Airway, but Not Alveolar, Epithelium. *Cell Stem Cell* **4**, 525–534 (2009).

598. Forbes, B. Human airway epithelial cell lines for in vitro drug transport and metabolism studies. *Pharm Sci Technol Today* **3**, 18–27 (2000).

599. Wang, G. *et al.* Characterization of an immortalized human small airway basal stem/progenitor cell line with airway region-specific differentiation capacity. *Respir Res* **20**, 1–14 (2019).

600. Gray, T. E., Guzman, K., Davis, C. W., Abdullah, L. H. & Nettesheim, P. Mucociliary differentiation of serially passaged normal human tracheobronchial epithelial cells. *Am J Respir Cell Mol Biol* **14**, 104–112 (1996).

601. Garcıá, S. R. *et al.* Novel dynamics of human mucociliary differentiation revealed by single-cell RNA sequencing of nasal epithelial cultures. *Development (Cambridge)* **146**, (2019).

602. Singh, G. & Katyal, S. L. Clara Cell Proteins. *Ann N Y Acad Sci* **923**, 43–58 (2000).

603. Yu, X., Ng, C. P., Habacher, H. & Roy, S. Foxj1 transcription factors are master regulators of the motile ciliogenic program. *Nat Genet* **40**, 1445–1453 (2008).

604. Karikó, K., Buckstein, M., Ni, H. & Weissman, D. Suppression of RNA recognition by Toll-like receptors: the impact of nucleoside modification and the evolutionary origin of RNA. *Immunity* **23**, 165–175 (2005).

605. Karikó, K. *et al.* Incorporation of pseudouridine into mRNA yields superior nonimmunogenic vector with increased translational capacity and biological stability. *Mol Ther* **16**, 1833–1840 (2008).

606. Nicholson, A. L. & Pasquinelli, A. E. Tales of Detailed Poly(A) Tails. *Trends Cell Biol* **29**, 191–200 (2019).

607. Homann, S. *et al.* A novel rapid and reproducible flow cytometric method for optimization of transfection efficiency in cells. *PLoS One* **12**, e0182941 (2017).

608. Marjanovič, I., Kandušer, M., Miklavčič, D., Keber, M. M. & Pavlin, M. Comparison of flow cytometry, fluorescence microscopy and spectrofluorometry for analysis of gene electrotransfer efficiency. *J Membr Biol* **247**, 1259–1267 (2014).

609. Ho, H. Y., Cheng, M. L., Wang, Y. H. & Chiu, D. T. Y. Flow cytometry for assessment of the efficacy of siRNA. *Cytometry A* **69**, 1054–1061 (2006).

610. Putnam, D. Polymers for gene delivery across length scales. *Nat Mater* **5**, 439–451 (2006).

611. Anderson, D. G., Akinc, A., Hossain, N. & Langer, R. Structure/property studies of polymeric gene delivery using a library of poly(β-amino esters). *Molecular Therapy* **11**, 426–434 (2005).

612. Sunshine, J. C., Bishop, C. J. & Green, J. J. Advances in polymeric and inorganic vectors for nonviral nucleic acid delivery. *Ther Deliv* **2**, 493 (2011).

613. van Asbeck, A. H. *et al.* Protein expression correlates linearly with mrna dose over up to five orders of magnitude in vitro and in vivo. *Biomedicines* **9**, (2021).

614. Wang, K. *et al.* Robust differentiation of human pluripotent stem cells into endothelial cells via temporal modulation of ETV2 with modified mRNA. *Sci Adv* **6**, (2020).

615. Ma, S. *et al.* An Efficient and Footprint-Free Protocol for the Transdifferentiation of Hepatocytes Into Insulin-Producing Cells With IVT mRNAs. *Front Genet* **11**, (2020).

616. Qabrati, X. *et al.* Transgene-free direct conversion of murine fibroblasts into functional muscle stem cells. *npj Regenerative Medicine 2023 8:1* **8**, 1–16 (2023).

617. Ledo, A. M. *et al.* mRNA-activated matrices encoding transcription factors as primers of cell differentiation in tissue engineering. *Biomaterials* **247**, 120016 (2020).

618. de Jong, P. M. *et al.* Ciliogenesis in human bronchial epithelial cells cultured at the air-liquid interface. *Am J Respir Cell Mol Biol* **10**, 271–277 (1994).

619. Ostrowski, L. E. & Nettesheim, P. Inhibition of ciliated cell differentiation by fluid submersion. *Exp Lung Res* **21**, 957–970 (1995).

620. Gerovac, B. J. *et al.* Submersion and hypoxia inhibit ciliated cell differentiation in a Notch-dependent manner. *Am J Respir Cell Mol Biol* **51**, 516–525 (2014).

621. Prescott, R. A. *et al.* A comparative study of in vitro air–liquid interface culture models of the human airway epithelium evaluating cellular heterogeneity and gene expression at single cell resolution. *Respir Res* **24**, 1–17 (2023).

622. Prytherch, Z. *et al.* Tissue-Specific Stem Cell Differentiation in an in vitro Airway Model. *Macromol Biosci* **11**, 1467–1477 (2011).

623. Bukowy-Bieryłło, Z. *et al.* In vitro differentiation of ciliated cells in ALI-cultured human airway epithelium – The framework for functional studies on airway differentiation in ciliopathies. *Eur J Cell Biol* **101**, 151189 (2022).

624. Tam, A., Wadsworth, S., Dorscheid, D., Man, S. f. P. & Sin, D. D. The airway epithelium: more than just a structural barrier. *Ther Adv Respir Dis* **5**, 255–273 (2011).

625. Cohen, L. *et al.* Epithelial cell proliferation contributes to airway remodeling in severe asthma. *Am J Respir Crit Care Med* **176**, 138–145 (2007).

626. Ganesan, S., Comstock, A. T. & Sajjan, U. S. Barrier function of airway tract epithelium. *Tissue Barriers* **1**, e24997 (2013).

627. Shaykhiev, R. *et al.* Cigarette smoking reprograms apical junctional complex molecular architecture in the human airway epithelium in vivo. *Cell Mol Life Sci* **68**, 877–892 (2011).

628. Ivanov, A. I., Parkos, C. A. & Nusrat, A. Cytoskeletal regulation of epithelial barrier function during inflammation. *Am J Pathol* **177**, 512–524 (2010).

629. Buckley, A. G. *et al.* Visualisation of Multiple Tight Junctional Complexes in Human Airway Epithelial Cells. *Biol Proced Online* **20**, (2018).

630. Rezaee, F. & Georas, S. N. Breaking barriers. New insights into airway epithelial barrier function in health and disease. *Am J Respir Cell Mol Biol* **50**, 857–869 (2014).

631. Georas, S. N. & Rezaee, F. Epithelial barrier function: at the front line of asthma immunology and allergic airway inflammation. *J Allergy Clin Immunol* **134**, 509–520 (2014).

632. Davies, D. E. Epithelial barrier function and immunity in asthma. *Ann Am Thorac Soc* **11 Suppl 5**, S244–S255 (2014).

633. Garrod, D. & Chidgey, M. Desmosome structure, composition and function. *Biochim Biophys Acta* **1778**, 572–587 (2008).

634. Shebani, E., Shahana, S., Janson, C. & Roomans, G. M. Attachment of columnar airway epithelial cells in asthma. *Tissue Cell* **37**, 145–152 (2005).

635. Rackley, C. R. & Stripp, B. R. Building and maintaining the epithelium of the lung. *J Clin Invest* **122**, 2724–2730 (2012).

636. Bukowy-Bieryłło, Z. *et al.* In vitro differentiation of ciliated cells in ALI-cultured human airway epithelium – The framework for functional studies on airway differentiation in ciliopathies. *Eur J Cell Biol* **101**, 151189 (2022).

637. Zugibe, F. T. Positive periodic acid-Schiff staining of acid mucopolysaccharides. *Histochem J* **2**, 191–197 (1970).

638. Ross, A. J., Dailey, L. A., Brighton, L. E. & Devlin, R. B. Transcriptional profiling of mucociliary differentiation in human airway epithelial cells. *Am J Respir Cell Mol Biol* **37**, 169–185 (2007).

639. Clarus Leung, X., Wadsworth, S. J., Jasemine Yang, S. & Dorscheid, D. R. Structural and functional variations in human bronchial epithelial cells cultured in air-liquid interface using different growth media. *Am J Physiol Lung Cell Mol Physiol* **318**, 1063–1073 (2020).

640. Rhodin, J. A. The ciliated cell. Ultrastructure and function of the human tracheal mucosa. *Am Rev Respir Dis* **93**, (1966).

641. Thaler, M. *et al.* Impact of changes in human airway epithelial cellular composition and differentiation on SARS-CoV-2 infection biology. *J Innate Immun* **15**, 562–580 (2023).

642. Hoh, R. A., Stowe, T. R., Turk, E. & Stearns, T. Transcriptional program of ciliated epithelial cells reveals new cilium and centrosome components and links to human disease. *PLoS One* **7**, (2012).

643. Brooks, E. R. & Wallingford, J. B. Multiciliated cells. *Curr Biol* **24**, R973–R982 (2014).

644. Chen, Q. *et al.* Host Antiviral Response Suppresses Ciliogenesis and Motile Ciliary Functions in the Nasal Epithelium. *Front Cell Dev Biol* **8**, 581340 (2020).

645. Bukowy-Bieryłło, Z. *et al.* In vitro differentiation of ciliated cells in ALI-cultured human airway epithelium – The framework for functional studies on airway differentiation in ciliopathies. *Eur J Cell Biol* **101**, 151189 (2022).

646. Legebeke, J. *et al.* Temporal Whole-Transcriptomic Analysis of Characterized In Vitro and Ex Vivo Primary Nasal Epithelia. *Front Cell Dev Biol* **10**, 907511 (2022).

647. Zietkiewicz, E. *et al.* CFAP300: Mutations in slavic patients with primary ciliary dyskinesia and a role in ciliary dynein arms trafficking. *Am J Respir Cell Mol Biol* **61**, 400–449 (2019).

648. Saint-Criq, V. *et al.* Choice of Differentiation Media Significantly Impacts Cell Lineage and Response to CFTR Modulators in Fully Differentiated Primary Cultures of Cystic Fibrosis Human Airway Epithelial Cells. *Cells 2020, Vol. 9, Page 2137* **9**, 2137 (2020).

649. Sorokin, S. P. Reconstructions of centriole formation and ciliogenesis in mammalian lungs. *J Cell Sci* **3**, 207–230 (1968).

650. Pezzulo, A. A. *et al.* The air-liquid interface and use of primary cell cultures are important to recapitulate the transcriptional profile of in vivo airway epithelia. *Am J Physiol Lung Cell Mol Physiol* **300**, L25 (2011).

651. Karp, P. H. *et al.* Human Airway Epithelia 115 An In Vitro Model of Differentiated Human Airway Epithelia Methods for Establishing Primary Cultures. *From: Methods in Molecular Biology* **188**,.

652. Krishnamurthy, S. *et al.* Manipulation of cell physiology enables gene silencing in well-differentiated airway epithelia. *Mol Ther Nucleic Acids* **1**, e41 (2012).

653. Ramachandran, S. *et al.* Efficient delivery of RNA interference oligonucleotides to polarized airway epithelia in vitro. *Am J Physiol Lung Cell Mol Physiol* **305**, L23 (2013).

654. Hill, D. B. & Button, B. Establishment of respiratory air-liquid interface cultures and their use in studying mucin production, secretion, and function. *Methods in Molecular Biology* **842**, 245–258 (2012).

655. Farmen, S. L. *et al.* Gene transfer of CFTR to airway epithelia: low levels of expression are sufficient to correct Cl transport and overexpression can generate basolateral CFTR. *Am J Physiol Lung Cell Mol Physiol* **289**, (2005).

656. Liu, X., Yan, Z., Luo, M. & Engelhardt, J. F. Species-Specific Differences in Mouse and Human Airway Epithelial Biology of Recombinant Adeno-Associated Virus Transduction. *Am J Respir Cell Mol Biol* **34**, 56 (2006).

657. Zhang, L. *et al.* CFTR Delivery to 25% of Surface Epithelial Cells Restores Normal Rates of Mucus Transport to Human Cystic Fibrosis Airway Epithelium. doi:10.1371/journal.pbio.1000155.

658. Nayerossadat, N., Maedeh, T. & Ali, P. A. Viral and nonviral delivery systems for gene delivery. *Adv Biomed Res* **1**, 27 (2012).

659. Green, J. J., Langer, R. & Anderson, D. G. A Combinatorial Polymer Library Approach Yields Insight into Nonviral Gene Delivery. *Acc Chem Res* **41**, 749 (2008).

660. Cordeiro, R. A., Serra, A., Coelho, J. F. J. & Faneca, H. Poly(β-amino ester)-based gene delivery systems: From discovery to therapeutic applications. *Journal of Controlled Release* **310**, 155–187 (2019).

661. Anderson, D. G., Akinc, A., Hossain, N. & Langer, R. Structure/Property Studies of Polymeric Gene Delivery Using a Library of Poly(B-amino esters). (2004) doi:10.1016/j.ymthe.2004.11.015.

662. Wu, D. *et al.* Evaluation of Hyperbranched Poly(amino ester)s of Amine Constitutions Similar to Polyethylenimine for DNA Delivery. *Biomacromolecules* **6**, 3166–3173 (2005).

663. Cutlar, L. *et al.* Highly Branched Poly(β-Amino Esters): Synthesis and Application in Gene Delivery. *Biomacromolecules* **16**, 2609–2617 (2015).

664. Lynn, D. M., Anderson, D. G., Putnam, D. & Langer, R. Accelerated discovery of synthetic transfection vectors: Parallel synthesis and screening of a degradable polymer library [20]. *J Am Chem Soc* **123**, 8155–8156 (2001).

665. Akinc, A., Lynn, D. M., Anderson, D. G. & Langer, R. Parallel Synthesis and Biophysical Characterization of a Degradable Polymer Library for Gene Delivery. (2003) doi:10.1021/ja034429c.

666. Anderson, D. G., Lynn, D. M. & Langer, R. Semi-Automated Synthesis and Screening of a Large Library of Degradable Cationic Polymers for Gene Delivery. *Angewandte Chemie International Edition* **42**, 3153–3158 (2003).

667. Anderson, D. G. *et al.* A polymer library approach to suicide gene therapy for cancer Optimal gene therapy for cancer must (i) deliver DNA to tumor cells with high efficiency, (ii) induce minimal toxicity. (2004).

668. Van De Wetering, P., Cherng, J. Y., Talsma, H., Crommelin, D. J. A. & Hennink, W. E. 2-(dimethylamino)ethyl methacrylate based (co)polymers as gene transfer agents. *Journal of Controlled Release* **53**, 145–153 (1998).

669. Layman, J. M., Ramirez, S. M., Green, M. D. & Long, T. E. Influence of Polycation Molecular Weight on Poly(2-dimethylaminoethyl methacrylate)-Mediated DNA Delivery In Vitro. doi:10.1021/bm9000124.

670. Gao, Y. *et al.* Highly Branched Poly(β-amino esters) for Non-Viral Gene Delivery: High Transfection Efficiency and Low Toxicity Achieved by Increasing Molecular Weight. *Biomacromolecules* **17**, 3640–3647 (2016).

671. Brey, D. M., Erickson, I. & Burdick, J. A. Influence of Macromer Molecular Weight and Chemistry on Poly(β-amino ester) Network Properties and Initial Cell Interactions. *J Biomed Mater Res A* **85**, 731 (2008).

672. Eltoukhy, A. A. *et al.* Effect of molecular weight of amine end-modified poly(β-amino ester)s on gene delivery efficiency and toxicity. *Biomaterials* **33**, 3594 (2012).

673. Cordeiro, R. A. *et al.* High transfection efficiency promoted by tailor-made cationic tri-block copolymer-based nanoparticles. *Acta Biomater* **47**, 113–123 (2017).

674. Iqbal, S. *et al.* Poly (β-amino esters) based potential drug delivery and targeting polymer; an overview and perspectives (review). *Eur Polym J* **141**, 110097 (2020).

675. Anderson, D. G., Akinc, A., Hossain, N. & Langer, R. Structure/property studies of polymeric gene delivery using a library of poly(beta-amino esters). *Mol Ther* **11**, 426–434 (2005).

676. Akinc, A., Anderson, D. G., Lynn, D. M. & Langer, R. Synthesis of poly(beta-amino ester)s optimized for highly effective gene delivery. *Bioconjug Chem* **14**, 979–988 (2003).

677. Chen, J., Ouyang, J., Kong, J., Zhong, W. & Xing, M. M. Photo-cross-linked and pH-sensitive biodegradable micelles for doxorubicin delivery. *ACS Appl Mater Interfaces* **5**, 3108–3117 (2013).

678. Chen, J. *et al.* Reducible self-assembled micelles for enhanced intracellular delivery of doxorubicin. *J Mater Chem* **22**, 7121–7129 (2012).

679. Sunshine, J. C., Peng, D. Y. & Green, J. J. Uptake and transfection with polymeric nanoparticles are dependent on polymer end-group structure, but largely independent of nanoparticle physical and chemical properties. *Mol Pharm* **9**, 3375 (2012).

680. Sunshine, J. *et al.* Small Molecule End Group of Linear Polymer Determines Cell-type Gene Delivery Efficacy. *Adv Mater* **21**, 4947 (2009).

681. Green, J. J. *et al.* Combinatorial Modification of Degradable Polymers Enables Transfection of Human Cells Comparable to Adenovirus. *Advanced Materials* **19**, 2836–2842 (2007).

682. Zugates, G. T. *et al.* Gene delivery properties of end-modified poly(β-amino ester)s. *Bioconjug Chem* **18**, 1887–1896 (2007).

683. Riera, R. *et al.* Complex pBAE Nanoparticle Cell Trafficking: Tracking Both Position and Composition Using Super Resolution Microscopy. *ChemMedChem* **17**, (2022).

684. Sunshine, J. C., Akanda, M. I., Li, D., Kozielski, K. L. & Green, J. J. Effects of Base Polymer Hydrophobicity and End-Group Modification on Polymeric Gene Delivery. (2011) doi:10.1021/bm200807s.

685. Zugates, G. T. *et al.* Rapid Optimization of Gene Delivery by Parallel End-modification of Poly(β-amino ester)s. *Molecular Therapy* **15**, 1306–1312 (2007).

686. Loecher, A., Bruyns-Haylett, M., Ballester, P. J., Borros, S. & Oliva, N. A machine learning approach to predict cellular uptake of pBAE polyplexes. *Biomater Sci* **11**, 5797–5808 (2023).

687. Segovia, N., Dosta, P., Cascante, A., Ramos, V. & Borrós, S. Oligopeptide-terminated poly(β-amino ester)s for highly efficient gene delivery and intracellular localization. *Acta Biomater* **10**, 2147–2158 (2014).

688. Dosta, P., Segovia, N., Cascante, A., Ramos, V. & Borrós, S. Surface charge tunability as a powerful strategy to control electrostatic interaction for high efficiency silencing, using tailored oligopeptide-modified poly(beta-amino ester)s (PBAEs). *Acta Biomater* **20**, 82–93 (2015).

689. Segovia, N., Dosta, P., Cascante, A., Ramos, V. & Borrós, S. Oligopeptide-terminated poly(β-amino ester)s for highly efficient gene delivery and intracellular localization. *Acta Biomater* **10**, 2147–2158 (2014).

690. Thapa, R. K. & Sullivan, M. O. Gene delivery by peptide-assisted transport. *Curr Opin Biomed Eng* **7**, 71–82 (2018).

691. Urello, M., Hsu, W. H. & Christie, R. J. Peptides as a material platform for gene delivery: Emerging concepts and converging technologies. *Acta Biomater* **117**, 40–59 (2020).

692. Fornaguera, C. *et al.* In Vivo Retargeting of Poly(beta aminoester) (OM-PBAE) Nanoparticles is Influenced by Protein Corona. *Adv Healthc Mater* **8**, 1900849 (2019).

693. Núñez-Toldrà, R. *et al.* Improvement of osteogenesis in dental pulp pluripotent-like stem cells by oligopeptide-modified poly(β-amino ester)s. *Acta Biomater* **53**, 152–164 (2017).

694. Rodriguez-Garcia, M. *et al.* Formation of oligopeptides in high yield under simple programmable conditions. *Nat Commun* **6**, (2015).

695. Roth, M., Obaidat, A. & Hagenbuch, B. OATPs, OATs and OCTs: the organic anion and cation transporters of the SLCO and SLC22A gene superfamilies. *Br J Pharmacol* **165**, 1260 (2012).

696. Zhou, F. & You, G. Molecular insights into the structure-function relationship of organic anion transporters OATs. *Pharm Res* **24**, 28–36 (2007).

697. Smith, D. E., Clémençon, B. & Hediger, M. A. Proton-coupled oligopeptide transporter family SLC15: Physiological, pharmacological and pathological implications. *Mol Aspects Med* **34**, 323 (2013).

698. Lu, H. & Klaassen, C. Tissue distribution and thyroid hormone regulation of Pept1 and Pept2 mRNA in rodents. *Peptides (N.Y.)* **27**, 850–857 (2006).

699. Bahadduri, P. M. *et al.* Functional characterization of the peptide transporter PEPT2 in primary cultures of human upper airway epithelium. *Am J Respir Cell Mol Biol* **32**, 319–325 (2005).

700. Liu, W. *et al.* Molecular cloning of PEPT 2, a new member of the H+/peptide cotransporter family, from human kidney. *Biochimica et Biophysica Acta (BBA) - Biomembranes* **1235**, 461–466 (1995).

701. Shu, C. *et al.* Role of PEPT2 in peptide/mimetic trafficking at the blood-cerebrospinal fluid barrier: studies in rat choroid plexus epithelial cells in primary culture. *J Pharmacol Exp Ther* **301**, 820–829 (2002).

702. Van Aubel, R. A. M. H., Masereeuw, R. & Russel, F. G. M. Molecular pharmacology of renal organic anion transporters. *Am J Physiol Renal Physiol* **279**, (2000).

703. Lu, X. *et al.* Human oligopeptide transporter 2 (PEPT2) mediates cellular uptake of polymyxins. *Journal of Antimicrobial Chemotherapy* **71**, 403–412 (2016).

704. Sala-Rabanal, M., Loo, D. D. F., Hirayama, B. A. & Wright, E. M. Molecular mechanism of dipeptide and drug transport by the human renal H+/oligopeptide cotransporter hPEPT2. *Am J Physiol Renal Physiol* **294**, 1422–1432 (2008).

705. Agarwal, S. *et al.* Peptide Prodrugs: Improved Oral Absorption of Lopinavir, a HIV Protease Inhibitor. doi:10.1016/j.ijpharm.2008.03.031.

706. Groneberg, D. A., Fischer, A., Chung, K. F. & Daniel, H. Molecular Mechanisms of Pulmonary Peptidomimetic Drug and Peptide Transport. *https://doi.org/10.1165/rcmb.2003-0315TR* **30**, 251–260 (2012).

707. Groneberg, D. A. *et al.* Localization of the Peptide Transporter PEPT2 in the Lung : Implications for Pulmonary Oligopeptide Uptake. *Am J Pathol* **158**, 707 (2001).

708. Cynthia, B. Drug transporters in the lung--do they play a role in the biopharmaceutics of inhaled drugs? *J Pharm Sci* **99**, 2240–2255 (2010).

709. Salomon, J. J. & Ehrhardt, C. Organic cation transporters in the blood-air barrier: expression and implications for pulmonary drug delivery. *Ther Deliv* **3**, 735–747 (2012).

710. Nickel, S., Clerkin, C. G., Selo, M. A. & Ehrhardt, C. Transport mechanisms at the pulmonary mucosa: implications for drug delivery. *Expert Opin Drug Deliv* **13**, 667–690 (2016).

711. Giacomini, K. M. *et al.* Membrane transporters in drug development. *Nat Rev Drug Discov* **9**, 215–236 (2010).

712. Liang, Y., Li, S. & Chen, L. The physiological role of drug transporters. *Protein Cell* **6**, 334 (2015).

713. Eltoukhy, A. A., Chen, D., Alabi, C. A., Langer, R. & Anderson, D. G. Degradable terpolymers with alkyl side chains demonstrate enhanced gene delivery potency and nanoparticle stability. *Adv Mater* **25**, 1487–1493 (2013).

714. Kaczmarek, J. C. *et al.* Polymer-Lipid Nanoparticles for Systemic Delivery of mRNA to the Lungs HHS Public Access. *Angew Chem Int Ed Engl* **55**, 13808–13812 (2016).

715. Prabha, S., Arya, G., Chandra, R., Ahmed, B. & Nimesh, S. Effect of size on biological properties of nanoparticles employed in gene delivery. *Artif Cells Nanomed Biotechnol* **44**, 83–91 (2016).

716. Groneberg, D. A. *et al.* Direct visualization of peptide uptake activity in the central nervous system of the rat. *Neurosci Lett* **364**, 32–36 (2004).

717. Guo, X. *et al.* Construction, identification and application of HeLa cells stably transfected with human PEPT1 and PEPT2. *Peptides (N.Y.)* **34**, 395–403 (2012).

718. Rühl, A., Hoppe, S., Frey, I., Daniel, H. & Schemann, M. Functional expression of the peptide transporter PEPT2 in the mammalian enteric nervous system. *Journal of Comparative Neurology* **490**, 1–11 (2005).

719. Ito, K. *et al.* ARTICLE Analysing the substrate multispecificity of a proton-coupled oligopeptide transporter using a dipeptide library. *Nat Commun* (2013) doi:10.1038/ncomms3502.

720. Martinez Molledo, M., Quistgaard, E. M., Flayhan, A., Pieprzyk, J. & Löw, C. Multispecific Substrate Recognition in a Proton-Dependent Oligopeptide Transporter. *Structure* **26**, 467-476.e4 (2018).

721. Song, F., Hu, Y., Jiang, H. & Smith, D. E. Species Differences in Human and Rodent PEPT2-Mediated Transport of Glycylsarcosine and Cefadroxil in Pichia Pastoris Transformants. *Drug Metabolism and Disposition* **45**, 130–136 (2017).

722. Groneberg, D. A. *et al.* Distribution and function of the peptide transporter PEPT2 in normal and cystic fibrosis human lung. doi:10.1136/thorax.57.1.55.

723. Takano, M., Sugimoto, N., Ehrhardt, C. & Yumoto, R. Functional Expression of PEPT2 in the Human Distal Lung Epithelial Cell Line NCI-H441. *Pharm Res* **32**, 3916–3926 (2015).

724. Rühl, A., Hoppe, S., Frey, I., Daniel, H. & Schemann, M. Functional expression of the peptide transporter PEPT2 in the mammalian enteric nervous system. *J Comp Neurol* **490**, 1–11 (2005).

725. Takano, M. *et al.* Expression and function of PEPT2 during transdifferentiation of alveolar epithelial cells. *Life Sci* **93**, 630–636 (2013).

726. Chisholm, D. R., Deregis, R. G. & Behr, D. A. Therapeutic Efficacy of Cefadroxil and Cephalexin for Pneumonia in a Rat Test Model. *Antimicrob Agents Chemother* 105–109 (1986).

727. Boll, M. *et al.* Expression cloning and functional characterization of the kidney cortex high-affinity proton-coupled peptide transporter (13-lactam antibiotics/di-and tripeptides/Xenopus laevis oocytes/two-electrode voltage clamp). *Physiology* **93**, 284–289 (1996).

728. Alghamdi, O. A., King, N., Jones, G. L. & Moens, P. D. J. A new use of β-Ala-Lys (AMCA) as a transport reporter for PEPT1 and PEPT2 in renal brush border membrane vesicles from the outer cortex and outer medulla. *Biochim Biophys Acta Biomembr* **1860**, 960–964 (2018).

729. Sun, D. *et al.* Functional and Molecular Expression of the Proton-Coupled Oligopeptide Transporters in Spleen and Macrophages from Mouse and Human. *Mol Pharm* **10**, 1409 (2013).

730. Green, J. J. *et al.* Biodegradable polymeric vectors for gene delivery to human endothelial cells. *Bioconjug Chem* **17**, 1162–1169 (2006).

731. Foroozandeh, P. & Aziz, A. A. Insight into Cellular Uptake and Intracellular Trafficking of Nanoparticles. *Nanoscale Res Lett* **13**, (2018).

732. Wang, W. *et al.* The transition from linear to highly branched poly(β-amino ester)s: Branching matters for gene delivery. *Sci Adv* **2**, (2016).

733. Du, Y. *et al.* Dipeptide-modified nanoparticles to facilitate oral docetaxel delivery: new insights into PepT1-mediated targeting strategy. *Drug Deliv* **25**, 1403 (2018).

734. Groneberg, D. A. *et al.* Distribution and function of the peptide transporter PEPT2 in normal and cystic fibrosis human lung. doi:10.1136/thorax.57.1.55.

735. Bahadduri, P. M. *et al.* Functional Characterization of the Peptide Transporter PEPT2 in Primary Cultures of Human Upper Airway Epithelium. *Am J Respir Cell Mol Biol* **32**, 319–325 (2005).

736. Trubetskoy, V. S. *et al.* Recharging cationic DNA complexes with highly charged polyanions for in vitro and in vivo gene delivery. *Gene Ther* **10**, 261–271 (2003).

737. Keeney, M. *et al.* Development of Poly (β-amino esters)-Based Biodegradable Nanoparticles for Non-Viral Delivery of Minicircle DNA. *ACS Nano* **7**, 7241 (2013).

738. Iqbal, S. *et al.* Synthesis and Characterization of Poly (β-amino Ester) and Applied PEGylated and Non-PEGylated Poly (β-amino ester)/Plasmid DNA Nanoparticles for Efficient Gene Delivery. *Front Pharmacol* **13**, (2022).

739. Zhang, B., Zhang, H., Dai, S. & Bi, J. Cell-penetrating peptide–labelled smart polymers for enhanced gene delivery. *Eng Life Sci* **17**, 193 (2017).

740. Cho, E. C., Zhang, Q. & Xia, Y. The effect of sedimentation and diffusion on cellular uptake of gold nanoparticles. *Nat Nanotechnol* **6**, 385–391 (2011).

741. Jayaraman, M. *et al.* Maximizing the Potency of siRNA Lipid Nanoparticles for Hepatic Gene Silencing In Vivo. *Angew Chem Int Ed Engl* **51**, 8529 (2012).

742. Decuzzi, P. & Ferrari, M. The role of specific and non-specific interactions in receptor-mediated endocytosis of nanoparticles. *Biomaterials* **28**, 2915–2922 (2007).

743. Chu, Z., Huang, Y., Tao, Q. & Li, Q. Cellular uptake, evolution, and excretion of silica nanoparticles in human cells. *Nanoscale* **3**, 3291–3299 (2011).

744. Conner, S. D. & Schmid, S. L. Regulated portals of entry into the cell. *Nature* **422**, 37–44 (2003).

745. Coyne, C. B., Kelly, M. M., Boucher, R. C. & Johnson, L. G. Enhanced epithelial gene transfer by modulation of tight junctions with sodium caprate. *Am J Respir Cell Mol Biol* **23**, 602–609 (2000).

746. Dosta, P., Segovia, N., Cascante, A., Ramos, V. & Borrós, S. Surface charge tunability as a powerful strategy to control electrostatic interaction for high efficiency silencing, using tailored oligopeptide-modified poly(beta-amino ester)s (PBAEs). *Acta Biomater* **20**, 82–93 (2015).

747. Kato, T. *et al.* Plasmid DNA delivery by arginine-rich cell-penetrating peptides containing unnatural amino acids. *Bioorg Med Chem* **24**, 2681–2687 (2016).

748. Schaffer, D., Fidelman, N., Dan, N. & Lauffenburger, D. Vector unpacking as a potential barrier for receptor-mediated polyplex gene delivery. *Biotechnol Bioeng* (2000) doi:10.1002/(SICI)1097-0290(20000305)67:5.

749. Rapiteanu, R. *et al.* Highly efficient genome editing in primary bronchial epithelial cells establishes FOXJ1 as essential for ciliation in human airways. *bioRxiv* 533869 (2019) doi:10.1101/533869.

750. Zaragosi, L. E. *et al.* Combination of CRISPR-Cas9-RNP and Single-Cell RNAseq to Identify Cell State-Specific FOXJ1 Functions in the Human Airway Epithelium. *Methods Mol Biol* **2725**, 1–25 (2024).

751. Shapiro, A. J. *et al.* Autosomal dominant variants in FOXJ1 causing primary ciliary dyskinesia in two patients with obstructive hydrocephalus. *Mol Genet Genomic Med* **9**, 1726 (2021).

752. Gao, S. *et al.* A novel heterozygous variant of FOXJ1 in a Chinese female with primary ciliary dyskinesia and hydrocephalus: A case report and literature review. *Mol Genet Genomic Med* **11**, 2235 (2023).

753. Ito, M. *et al.* FOXJ1 Variants Causing Primary Ciliary Dyskinesia with Hydrocephalus: A Case Report from Japan. *Intern Med* (2023) doi:10.2169/INTERNALMEDICINE.2565-23.

754. Hou, C. C. *et al.* Heterozygous FOXJ1 Mutations Cause Incomplete Ependymal Cell Differentiation and Communicating Hydrocephalus. *Cell Mol Neurobiol* **43**, (2023).

755. Mills, P. R., Davies, R. J. & Devalia, J. L. Airway Epithelial Cells, Cytokines, and Pollutants. *https://doi.org/10.1164/ajrccm.160.supplement_1.11* **160**, 38–43 (2012).

756. Chilvers, M. A. & O'Callaghan, C. Analysis of ciliary beat pattern and beat frequency using digital high speed imaging: comparison with the photomultiplier and photodiode methods. *Thorax* **55**, 314–317 (2000).

757. Sears, P. R., Yin, W. N. & Ostrowski, L. E. Continuous mucociliary transport by primary human airway epithelial cells in vitro. *Am J Physiol Lung Cell Mol Physiol* **309**, L99 (2015).

758. Abdullah, L. H., Wolber, C., Kesimer, M., Sheehan, J. K. & Davis, C. W. Studying Mucin Secretion from Human Bronchial Epithelial Cell Primary Cultures. *Methods Mol Biol* **842**, 259 (2012).

759. Wang, Z., Gerstein, M. & Snyder, M. RNA-Seq: a revolutionary tool for transcriptomics. *Nat Rev Genet* **10**, 57 (2009).

760. Hwang, B., Lee, J. H. & Bang, D. Single-cell RNA sequencing technologies and bioinformatics pipelines. *Experimental & Molecular Medicine 2018 50:8* **50**, 1–14 (2018).

761. Library, W. O. & Walentek, P. Ciliary transcription factors in cancer – how understanding ciliogenesis can promote the detection and prognosis of cancer types. *J Pathol* **239**, 6–9 (2016).

762. Chen, H. W. *et al.* Expression of FOXJ1 in hepatocellular carcinoma: correlation with patients' prognosis and tumor cell proliferation. *Mol Carcinog* **52**, 647–659 (2013).

763. Zhu, P., Piao, Y., Dong, X. & Jin, Z. Forkhead box J1 expression is upregulated and correlated with prognosis in patients with clear cell renal cell carcinoma. *Oncol Lett* **10**, 1487–1494 (2015).

764. Liu, K., Fan, J. & Wu, J. Forkhead Box Protein J1 (FOXJ1) is Overexpressed in Colorectal Cancer and Promotes Nuclear Translocation of β-Catenin in SW620 Cells. *Med Sci Monit* **23**, 856 (2017).

765. Xian, S., Shang, D., Kong, G. & Tian, Y. FOXJ1 promotes bladder cancer cell growth and regulates Warburg effect. *Biochem Biophys Res Commun* **495**, 988–994 (2018).

766. Wang, J. *et al.* Decreased expression of FOXJ1 is a potential prognostic predictor for progression and poor survival of gastric cancer. *Ann Surg Oncol* **22**, 685–692 (2015).

767. Siu, M. K. Y. *et al.* Stem cell transcription factor NANOG controls cell migration and invasion via dysregulation of E-cadherin and FoxJ1 and contributes to adverse clinical outcome in ovarian cancers. *Oncogene* **32**, 3500–3509 (2013).

768. Abedalthagafi, M. S. *et al.* Decrease in FOXJ1 expression and its ciliogenesis program in aggressive ependymoma and choroid plexus tumours. *J Pathol* **238**, 584 (2016).

769. Kaczmarek, J. C. *et al.* Polymer-Lipid Nanoparticles for Systemic Delivery of mRNA to the Lungs. *Angewandte Chemie* **128**, 14012–14016 (2016).

770. Kaczmarek, J. C. *et al.* Optimization of a Degradable Polymer−Lipid Nanoparticle for Potent Systemic Delivery of mRNA to the Lung Endothelium and Immune Cells. (2018) doi:10.1021/acs.nanolett.8b02917.

771. Paramasivam, P. *et al.* Endosomal escape of delivered mRNA from endosomal recycling tubules visualized at the nanoscale. *J Cell Biol* **221**, (2022).

772. Podinovskaia, M., Prescianotto-Baschong, C., Buser, D. P. & Spang, A. A novel live-cell imaging assay reveals regulation of endosome maturation. *Elife* **10**, (2021).

773. Behzadi, S. *et al.* Cellular Uptake of Nanoparticles: Journey Inside the Cell. *Chem Soc Rev* **46**, 4218 (2017).

774. Sousa De Almeida, M. *et al.* Understanding nanoparticle endocytosis to improve targeting strategies in nanomedicine. *Chem Soc Rev* **50**, 5397–5434 (2021).

775. Java applets for power and sample size. https://homepage.divms.uiowa.edu/~rlenth/Power/.

776. Jackson, N. D. *et al.* Single-Cell and Population Transcriptomics Reveal Pan-epithelial Remodeling in Type 2-High Asthma. *Cell Rep* **32**, 107872 (2020).

8 Appendix I: FOXJ1 sequence

atggcggagagctggctgcgcctctcgggagccgggccggcggaggaggccgggccggagggcggcct
ggaggagcccgacgccctggatgacagcctgaccagcctgcagtggctgcaggaattctccattctca
acgccaaggcccccgccctgccccccgggggcaccgacccccacggctaccaccaggtgccaggttca
gcggcgcccgggtccccccctggcggccgaccccgcctgcctggggcagccacacacgccgggcaagcc
cacgtcgtcgtgcacgtcgcggagcgcgcccccggggctgcaggccccacccccccgacgacgtggact
acgccaccaatccgcacgtgaagcctccctactcgtatgccacgctcatctgcatggccatgcaggcc
agcaaggccaccaagatcaccctgtcggccatctacaagtggatcacggacaacttctgctacttccg
ccacgcagatcccacctggcagaattcaatccgccacaacctgtctctgaacaagtgcttcatcaaag
tgcctcgggagaaggacgaaccaggcaagggggcttctggcgcattgacccccagtacgcggagcgg
ctactgagcggcgctttcaagaagcggcgactgccccctgtccacatccacccagcctttgcccgcca
ggccgcgcaggagcccagcgctgtcccccgggccgggccgctgacggtgaataccgaggcccagcagc
tgctgcgggagttcgaggaggccaccggggaggcgggctggggtgcaggcgagggcaggctggggcat
aagcgcaaacagccgctgcccaagcgggtggccaaggtcccgcggccccccagcaccctgctgcccac
cccggaggagcagggtgagctggaacccctcaaaggcaactttgactgggaggccatcttcgacgccg
gcactctgggcggggagctgggtgcactggaggccctggagctgagcccgcctctgagccccgcctca
cacgtggacgtggacctcaccatccacggccgccacatcgactgccctgccacctgggggccttcggt
ggagcaggctgccgacagcctggacttcgatgagaccttcctggccacatccttcctgcagcacccct
gggacgagagcggcagtggctgcctgcccccggagcccctctttgaggctggggatgccaccctggcc
tccgacctgcaggactgggccagcgtgggggccttcttgtaa

9 Appendix II: Conference presentations arising from this thesis

Poster presentation at the European Society of Gene and Cell Therapy Annual Congress, October 2022, Edinburgh, UK

Investigating the influence of mRNA encoded transcription factor delivery on human bronchial epithelial cell differentiation

R Konstantinidi [1], L L Yates [1], S Saglani [1], C M Lloyd [1], A K Patel [1]

[1]: Inflammation Repair and Development, National Heart and Lung Institute, Imperial College London, London, SW7 2BX, United Kingdom

Synthetic messenger RNA (mRNA) represents a promising tool for transient, dose-dependent expression of any protein of interest, when efficiently delivered to target cells. Culture of primary human bronchial epithelial cells (HBECs) at air-liquid interface (ALI) facilitates differentiation towards a polarised, pseudostratified epithelium containing basal, ciliated and goblet cells. This model provides a powerful tool for studying the function of HBECs and for manipulating genes to modulate differentiation. mRNA-based therapeutics are being evaluated in clinical trials, however, the impact of delivery and translation of synthetic mRNA on epithelial cell differentiation and barrier integrity remains unclear. To determine how non-viral mRNA delivery impacts the ability of primary HBECs to form a differentiated epithelium at ALI, histological analysis, immunostaining and qPCR was conducted on transfected and non-transfected cells, together with an assessment of barrier integrity using paracellular permeability and tight junction protein expression. Reporter protein expression was observed in HBECs 12 to 48 hours post transfection, with epithelial cell differentiation and barrier integrity unaffected. Cilia dysfunction is observed in several lung diseases, including cystic fibrosis and primary ciliary dyskinesia. Therefore, we aimed to manipulate mucociliary differentiation and subsequent ciliogenesis by transfecting HBECs with an mRNA encoding a key transcription factor involved in ciliogenesis, Forkhead box J1 (FOXJ1). Preliminary data shows expression of FOXJ1 protein following transfection, and upregulation of several downstream genes including *CETN2* and *DNAH11*. Ongoing studies will utilise HBEC ALI as a model to understand how the exogenous delivery of mRNA encoded transcription factors can control differentiation and function of HBECs.

10 Appendix III: Validation of immunofluorescence staining with secondary antibody only controls

